

# CPIMS 12

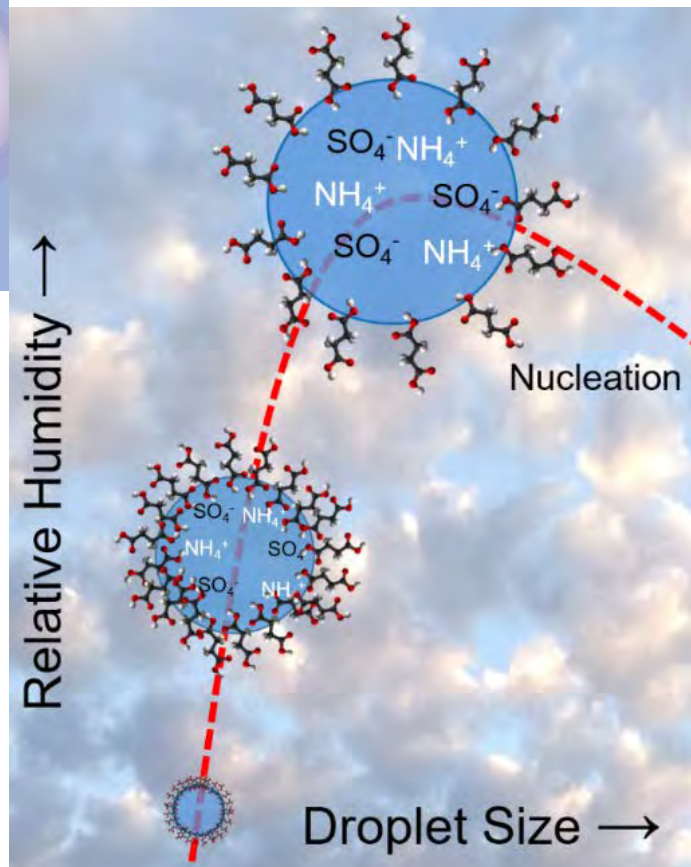
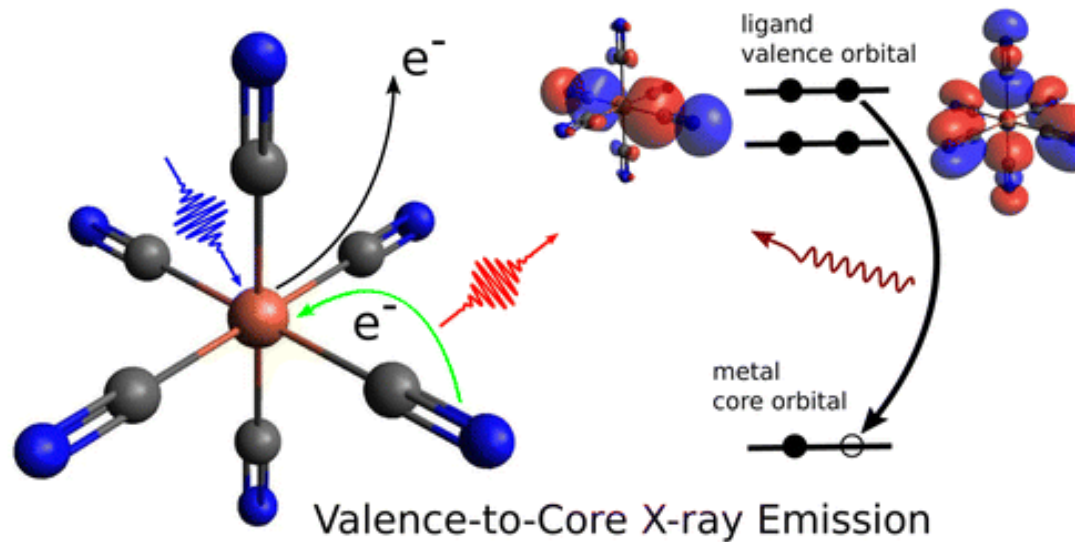
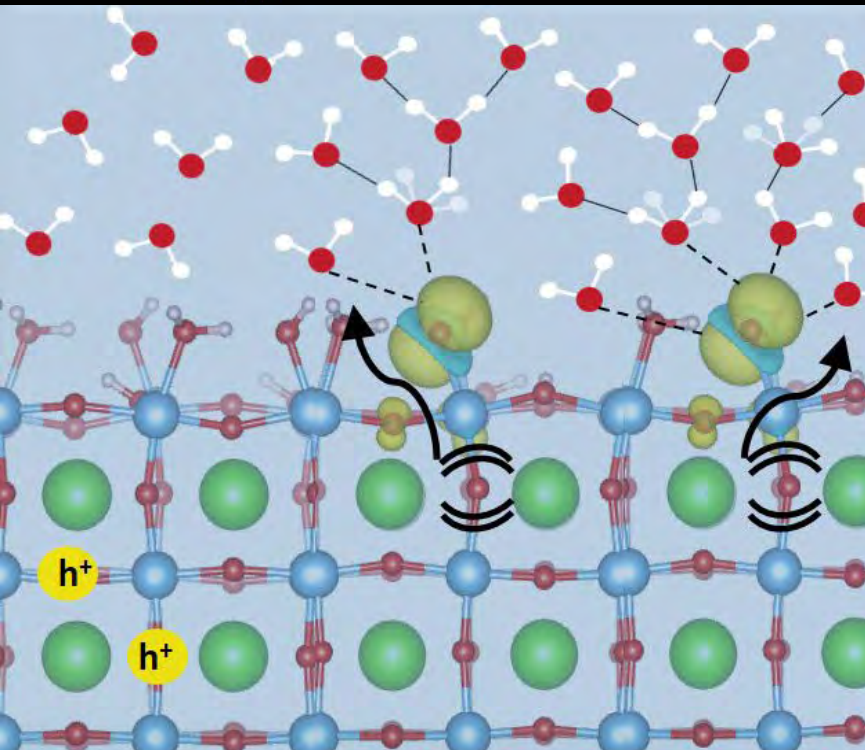
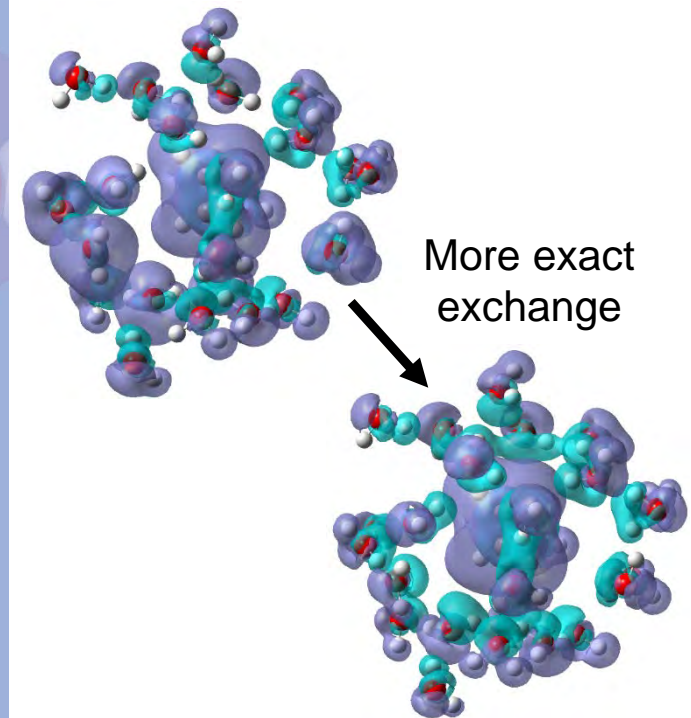
Twelfth Condensed Phase and Interfacial Molecular Science (CPIMS) Research Meeting

Gaithersburg Marriott  
Washingtonian Center  
Gaithersburg, MD  
November 1-4, 2016



U.S. DEPARTMENT OF  
**ENERGY**

Office of  
Science



# CPIMS 12

## ABOUT THE COVER GRAPHICS

### Submitted by Shawn Kathmann (Pacific Northwest National Laboratory)

For more information, see J.A. Fournier, C.T. Wolke, M.A. Johnson, T.T. Odbadrakh, K.D. Jordan, S.M. Kathmann, and S.S. Xantheas, "Snapshots of proton accommodation at a microscopic water Surface: Understanding the vibrational spectral signatures of the charge defect in cryogenically cooled  $H+(H_2O)_n$ ,  $n=2-28$  clusters," *Journal of Physical Chemistry A* **119**, 9425 (2015). DOI: 10.1021/acs.jpca.5b04355

### Submitted by Tanja Cuk (Lawrence Berkeley National Laboratory)

For more information, see D.M. Herlihy, M. M. Waegele, X. Chen, C.D. Pemmaraju, D. Prendergast, and T. Cuk, "Detecting the oxyl radical of photocatalytic water oxidation at an n-SrTiO<sub>3</sub>/aqueous interface through its subsurface vibration," *Nature Chemistry* **8**, 549 (2016). DOI: 10.1038/nchem.2497

See also H. Q. Doana, K. L. Pollocka, and T. Cuk, "Transient optical diffraction of GaN/aqueous interfaces: Interfacial carrier mobility dependence on surface reactivity," *Chemical Physics Letters* **649**, 1 (2016). DOI: 10.1016/j.cplett.2016.02.018

### Submitted by Andrei Tokmakoff (University of Chicago )

For more information, see M. Thämer, L. De Marco, K. Ramasesha, A. Mandal, and A. Tokmakoff, "Ultrafast 2D IR spectroscopy of the excess proton in liquid water," *Science* **350**, 78 (2015). DOI: 10.1126/science.aab3908

### Submitted by Munira Khalil (University of Washington)

For more information, see Y. Zhang, S. Mukamel, M. Khalil, and N. Govind, "Simulating valence-to-core x-ray emission spectroscopy of transition metal complexes with time-dependent density functional theory," *Journal of Chemical Theory and Computation* **11**, 5804 (2015). DOI: 10.1021/acs.jctc.5b00763

### Submitted by Christine Isborn (University of California, Merced)

For more information, see X.A. Sosa Vazquez and C.M. Isborn, "Size-dependent error of the density functional theory ionization potential in vacuum and solution," *Journal of Chemical Physics* **143**, 244105 (2015). DOI: 10.1063/1.4937417

### Submitted by Kevin Wilson (Lawrence Berkeley National Laboratory)

For more information, see C.R. Ruehl, J.F. Davies, and K.R. Wilson, "An interfacial mechanism for cloud droplet formation on organic aerosols," *Science* **351**, 1447 (2016). DOI: 10.1126/science.aad4889

Program and Abstracts for

# CPIMS 12

Twelfth Research Meeting of the Condensed  
Phase and Interfacial Molecular Science  
(CPIMS) Program

Gaithersburg Marriott Washingtonian Center  
Gaithersburg, Maryland  
November 1-4, 2016



U.S. DEPARTMENT OF

**ENERGY**

Office of  
Science

Office of Basic Energy Sciences

Chemical Sciences, Geosciences & Biosciences Division

The research grants and contracts described in this document are supported by the U.S. DOE Office of Science, Office of Basic Energy Sciences, Chemical Sciences, Geosciences and Biosciences Division.

# FOREWORD

This volume summarizes the scientific content of the Twelfth Research Meeting on Condensed Phase and Interfacial Molecular Science (CPIMS) sponsored by the U. S. Department of Energy (DOE), Office of Basic Energy Sciences (BES). The research meeting is held for the DOE laboratory and university principal investigators within the BES CPIMS Program to facilitate scientific interchange among the PIs and to promote a sense of program awareness and identity.

This year's speakers are gratefully acknowledged for their investment of time and for their willingness to share their ideas with the meeting participants.

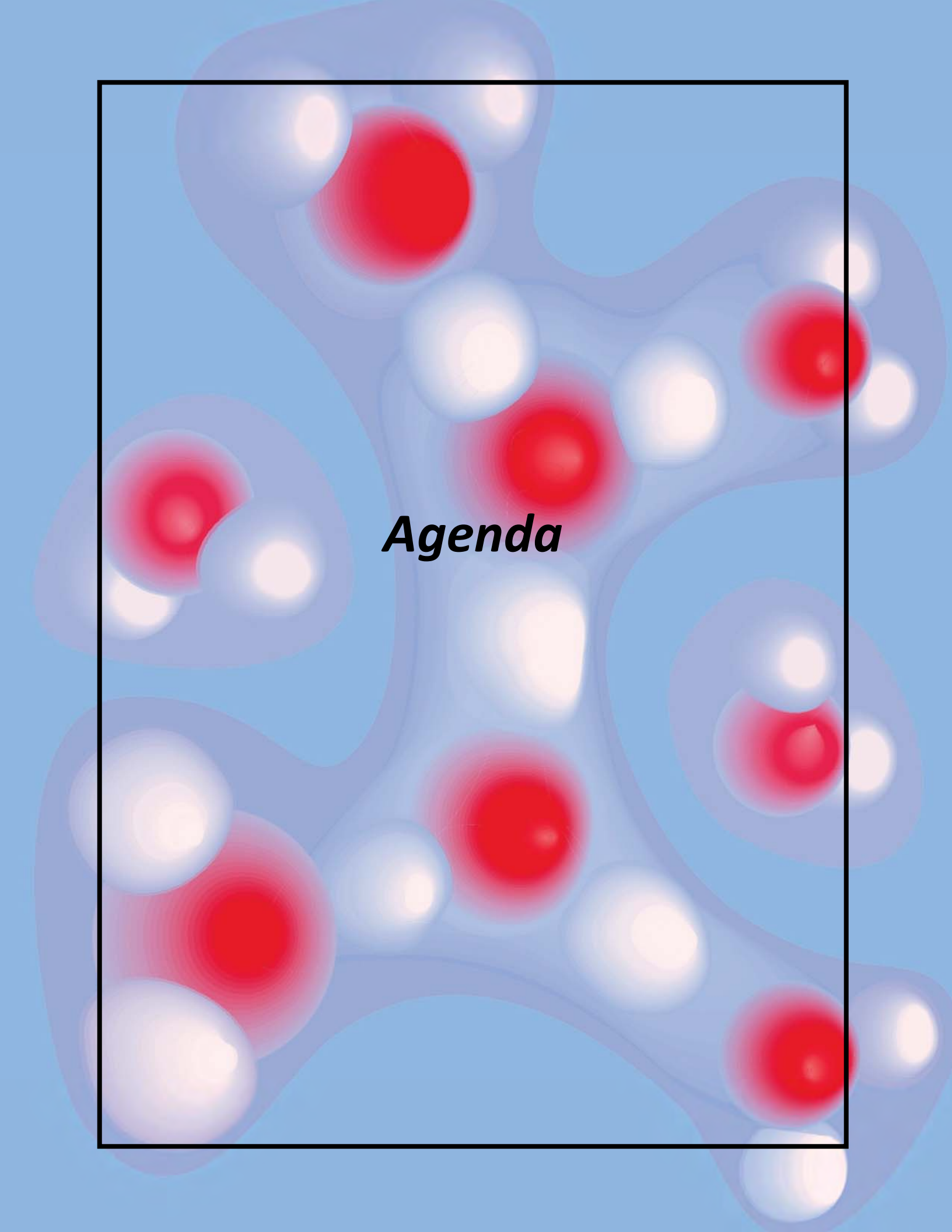
The abstracts in this book represent progress reports for each of the projects that receive support from the CPIMS program. Therefore, the book represents a snapshot in time of the scope of CPIMS-supported research. The CPIMS 12 agenda also features two speakers who receive support for their research from the BES Computational and Theoretical Chemistry (CTC) Program: Mark Gordon and Adam Wasserman, whose presentations will take place on Friday, November 4, and whose abstracts are contained in a special, CTC section of this book. Moreover, several speakers receive co-funding for their work from both the CPIMS and CTC programs, including Christine Isborn (who speaks on Wednesday, November 2), Aurora Clark (who speaks on Thursday, November 3), and Sapna Sarupria (who speaks on Friday, November 4). Finally, several speakers in radiation chemistry receive support from the Solar Photochemistry program, including Sylwia Ptasinska (who speaks on Wednesday, November 2), and Andrew Cook and Jay LaVerne (who both speak on Thursday, November 3); their abstracts are contained in a Solar Photochemistry section of the book.

A recent tradition is the use of the cover of this book to display research highlights from CPIMS investigators. This year, we have included six research highlights on the cover. These images were selected from highlights and abstracts submitted by CPIMS investigators during the past two years. We thank the investigators for allowing us to place their images on the cover of this book, and we thank all CPIMS investigators who submitted research highlights. CPIMS Investigators are encouraged to submit highlight of their results; we will continue to receive these stories of success with great pride. We thank Joshua Haines for his creative advice during assembly of this volume, and his tireless efforts in assembling and editing highlights for the program.

We are deeply indebted to the members of the scientific community who have contributed valuable time toward the review of proposals and programs. These thorough and thoughtful reviews are central to the continued vitality of the CPIMS Program. We appreciate the privilege of serving in the management of this research program. In carrying out these tasks, we learn from the achievements and share the excitement of the research of the many sponsored scientists and students whose work is summarized in the abstracts published on the following pages.

Special thanks are reserved for the staff of the Oak Ridge Institute for Science and Education, in particular, Connie Lansdon and Tim Ledford. We also thank Diane Marceau, Michaelena Kyler-Leon, and Gwen Johnson in the Chemical Sciences, Geosciences, and Biosciences Division for their indispensable behind-the-scenes efforts in support of the CPIMS program. Finally, we thank Gail McLean, who has served as Acting Director for the Chemical Sciences, Geosciences, and Biosciences Division for the past several months; her dedication while she has continued to serve her existing role as Team Lead for the Photo- and Bio-Chemistry Team has been remarkable.

Gregory J. Fiechtner, Mark R. Pederson, and Jeffrey L. Krause  
Chemical Sciences, Geosciences and Biosciences Division  
Office of Basic Energy Sciences

An abstract graphic featuring a light blue background with a central, darker blue, irregularly shaped area. This central area is filled with several glowing red spheres of varying sizes, each surrounded by a white, ethereal glow. The overall composition is symmetrical and has a soft, ethereal quality.

***Agenda***

# CPIMS 12



U.S. DEPARTMENT OF  
**ENERGY**

Office of  
Science

Office of Basic Energy Sciences  
Chemical Sciences, Geosciences & Biosciences Division

## Twelfth Condensed Phase and Interfacial Molecular Science (CPIMS) Research Meeting Gaithersburg Marriott Washingtonian Center, Gaithersburg, Maryland

---

### Tuesday, November 1

3:00-6:00 pm      \*\*\*\* Registration \*\*\*\*  
6:00 pm            \*\*\*\* Reception (No Host, Lobby Lounge) \*\*\*\*  
6:30 pm            \*\*\*\* Dinner (on your own) \*\*\*\*

### Wednesday, November 2

7:30 am            \*\*\*\* Breakfast (Salon A-C) \*\*\*\*

#### All Presentations Held in Salon D-F

8:30 am            *Introductory Remarks and Program Update*  
**Gregory Fiechtner**, DOE Basic Energy Sciences

**Session I**        Chair: **Greg Kimmel**, Pacific Northwest National Laboratory

9:00 am            *Spectroscopic Imaging of Molecular Functions at Surfaces*  
**Wilson Ho**, University of California, Irvine

9:30 am            *A Single Atom Alloy Approach to Selective Dehydrogenations*  
**E. Charles H. Sykes**, Tufts University

10:00 am            \*\*\*\* Break \*\*\*\*

**Session II**        Chair: **L. Robert Baker**, Ohio State University

10:30 am            *Observing the Molecular Dynamics of Catalysis at Solid-Liquid Interfaces*  
**Tanja Cuk**, Lawrence Berkeley National Laboratory

11:00 am            *Charge Transfer Processes at Water/Semiconductor Interfaces*  
**Sylwia Ptasinska**, Notre Dame Radiation Laboratory/University of Notre Dame

11:30 am            *The Interfacial Chemistry of Droplets and Nanoparticles*  
**Kevin Wilson**, Lawrence Berkeley National Laboratory

12:00 pm            \*\*\*\* Lunch (Salon A-C) \*\*\*\*

1:30 pm-4:00 pm      Free/Discussion Time

- Session III** Chair: **Andrei Tokmakoff**, University of Chicago
- 4:00 pm *Exploring Electron Delocalization on the Femtosecond Timescale: Experiment*  
**Munira Khalil**, University of Washington
- 4:30 pm *Exploring Electron Delocalization on the Femtosecond Timescale: Theory*  
**Niranjan Govind**, Pacific Northwest National Laboratory
- 5:00 pm *Modeling Excited States in the Condensed Phase*  
**Christine M. Isborn**, University of California, Merced
- 5:30 pm \*\*\*\*\* Reception (No Host, Lobby Lounge) \*\*\*\*\*
- 6:00 pm \*\*\*\*\* Dinner (Salon A-C) \*\*\*\*\*

## Thursday, November 3

- 7:30 am \*\*\*\*\* Breakfast (Salon A-C) \*\*\*\*\*

- Session IV** Chair: **Christopher Mundy**, Pacific Northwest National Laboratory
- 8:30 am *Graph Theory Strategies for Interrogating Intermolecular Interactions and Reaction Coordinates Within Quantum Dynamics Data*  
**Aurora Clark**, Washington State University
- 9:00 am *Intermolecular Interactions of Water in the Gas and the Condensed Phase*  
**Sotiris Xantheas**, Pacific Northwest National Laboratory
- 9:30 am *Theoretical Studies of Ionic Hydrogen Bonds: The Role of Electric Field Effects*  
**Kenneth Jordan**, University of Pittsburgh

- 10:00 am \*\*\*\*\* Break \*\*\*\*\*

- Session V** Chair: **Caroline Chick Jarrold**, Indiana University
- 10:30 am *Spectroscopic Properties of Ionic H-Bonds: From Ionic liquids to the Grotthuss Mechanism in Water*  
**Mark Johnson**, Yale University
- 11:00 am *Formation and Spectroscopy of Weakly-Bound Clusters: Electronic Couplings and Solvation Effects*  
**Etienne Garand**, University of Wisconsin-Madison
- 11:30 am *Probing Molecular Growth Processes and Solvation with Mass Spectrometry and Photoelectron Spectroscopy*  
**Musahid Ahmed**, Lawrence Berkeley National Laboratory
- 12:00 pm \*\*\*\*\* Lunch (Salon A-C) \*\*\*\*\*
- 12:30 pm–3:30 pm Free/Discussion Time

- Session VI** Chair: **James Wishart**, Brookhaven National Laboratory
- 4:00 pm *CO<sub>2</sub> in Room Temperature Ionic Liquids and Supported Ionic Liquid Membranes*  
**Michael Fayer**, Stanford University
- 4:30 pm *Exceptionally Rapid Capture of Radical Cations Made by Pulse Radiolysis*  
**Andrew R. Cook**, Brookhaven National Laboratory
- 5:00 pm *Radiolysis of Water-Metal Oxide Interfaces*  
**Jay LaVerne**, Notre Dame Radiation Laboratory
- 5:30 pm \*\*\*\*\* Reception (No Host, Lobby Lounge) \*\*\*\*\*
- 6:00 pm \*\*\*\*\* Dinner (Salon A-C) \*\*\*\*\*

## Friday, November 4

- 7:30 am \*\*\*\*\* Breakfast (Salon A-C) \*\*\*\*\*

- Session VII** Chair: **Shawn Kathmann**, Pacific Northwest National Laboratory
- 8:30 am *Accurate Calculations on Large Species: Theory and Applications.*  
**Mark Gordon**, Iowa State University and Ames Laboratory
- 9:00 am *Fixing delocalization and static-correlation errors with Partition Density Functional Theory*  
**Adam Wasserman**, Purdue University
- 9:30 am *Sampling Rare Events in Aqueous Systems Using Molecular Simulations*  
**Sapna Sarupria**, Clemson University
- 9:55 am \*\*\*\*\* Break \*\*\*\*\*

- Session VIII** Chair: **Amber Krummel**, Colorado State University
- 10:25 am *Selective Adsorption of Ions to Aqueous Interfaces: Air/Water vs. Graphene*  
**Richard Saykally**, Lawrence Berkeley National Laboratory
- 10:55 am *Role of Dispersion on Water Ordering about Ions and Hydrophobic Solutes at High Pressure*  
**John Fulton**, Pacific Northwest National Laboratory
- 11:25 am *Closing Remarks*  
**Gregory Fiechtner**, DOE Basic Energy Sciences
- 12:00 noon \*\*\*\*\* Meeting Adjourns \*\*\*\*\*



***Table of Contents***

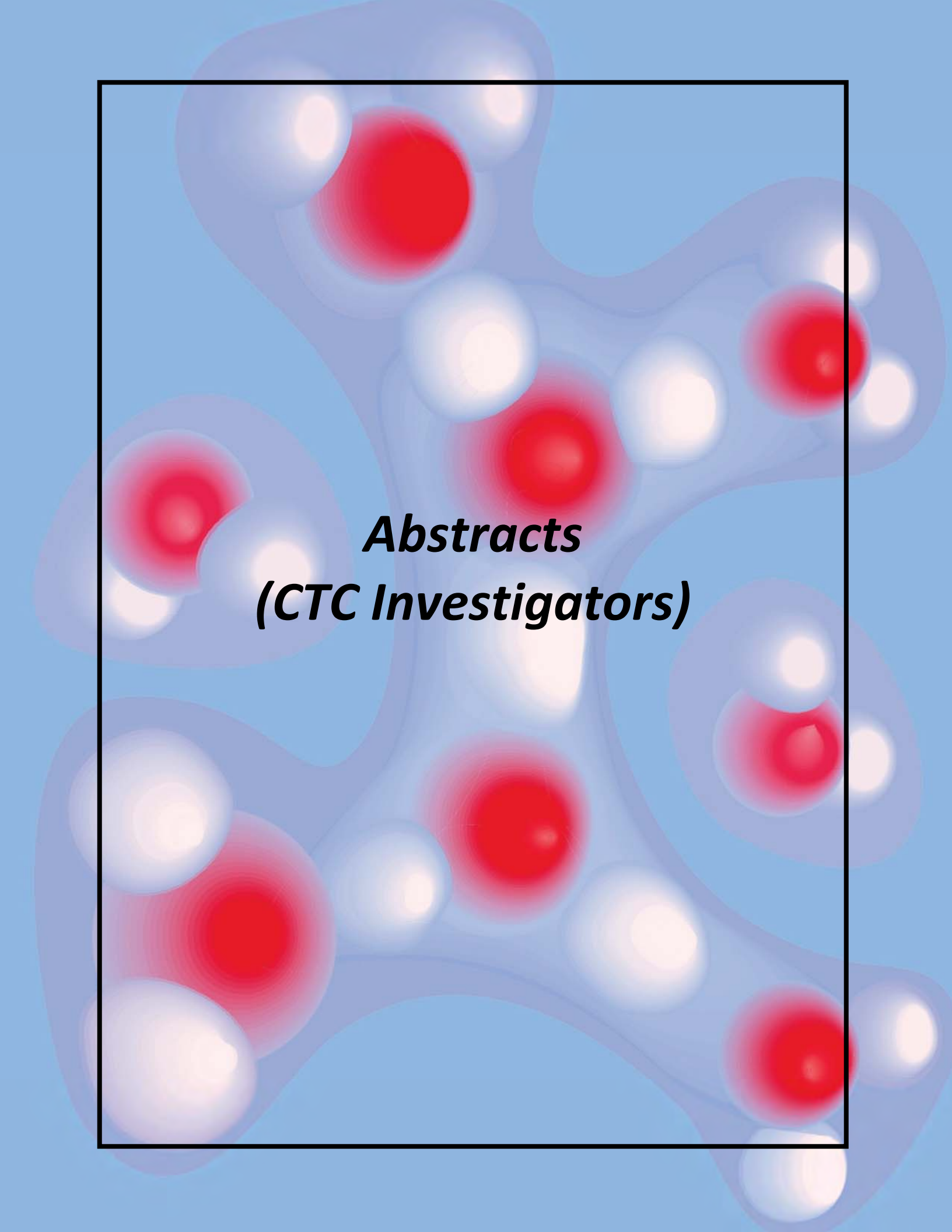
# TABLE OF CONTENTS

FOREWORD.....	ii
AGENDA .....	iii
TABLE OF CONTENTS .....	vi
ABSTRACTS .....	1
<b><u>CTC Principal Investigator Abstracts</u></b>	
<i>Theoretical Developments and Applications to Surface Science, Heterogeneous Catalysis, Heavy Elements, and Intermolecular Interactions</i>	
Mark S. Gordon (Ames Laboratory).....	1
<i>Fixing Delocalization and Static-Correlation Errors with Partition Density Functional Theory</i>	
Adam Wasserman (Purdue University) .....	5
<b><u>CPIMS Principal Investigator Abstracts</u></b>	
<i>Controlling Aqueous Interfacial Phenomena of Redox-Active Ions with External Electric Fields</i>	
Heather C. Allen (The Ohio State University) .....	6
<i>Visible Light Photo-Catalysis in Charged Micro-Droplets</i>	
Abraham Badu-Tawiah (The Ohio State University).....	8
<i>Probing Ion Solvation and Charge Transfer at Electrochemical Interfaces Using Nonlinear Soft X Ray Spectroscopy</i>	
L. Robert Baker (The Ohio State University).....	12
<i>Chemistry at the Advanced Light Source Using Soft X-ray Spectroscopy and Microscopy</i>	
Hendrik Bluhm, Mary K. Gilles, David K. Shuh, Musahid Ahmed (Lawrence Berkeley National Laboratory) .....	16
<i>Surface Chemical Dynamics</i>	
Nicholas Camillone III and Michael G. White (Brookhaven National Laboratory) .....	20
<i>Charge and Molecular Dynamics at Heterogeneous Interfaces</i>	
Tanja Cuk, Charles Harris, and David Chandler (Lawrence Berkeley National Laboratory) .....	24
<i>Rate Theory of Solvent Exchange around Lithium Ions and the Thermodynamics and Kinetics of Ion Pairs in Condensed Phase</i>	
Liem X. Dang (Pacific Northwest National Laboratory) .....	28
<i>Confinement, Interfaces, and Ions: Dynamics and Interactions in Water, Proton Transfer, and Room Temperature Ionic Liquid Systems</i>	
Michael D. Fayer (Stanford University).....	32

<i>Fundamentals of Solvation under Extreme Conditions</i> John L. Fulton (Pacific Northwest National Laboratory).....	36
<i>Probing Chromophore Energetics and Couplings for Singlet Fission in Solar Cell Applications</i> Etienne Garand (University of Wisconsin).....	40
<i>Reactions and Transformations</i> Phillip L. Geissler, Musahid Ahmed, David Chandler, Teresa Head-Gordon and Rich Saykally (Lawrence Berkeley National Laboratory).....	44
<i>Laser Induced Reactions in Solids and at Surfaces</i> Wayne P. Hess (PI) Alan G. Joly and Patrick Z. El-Khoury (Pacific Northwest National Laboratory).....	48
<i>Spectroscopic Imaging of Molecular Functions at Surfaces</i> Wilson Ho (University of California, Irvine).....	52
<i>Development of Approaches to Model Excited State Charge and Energy Transfer in Solution</i> Christine Isborn (University of California Merced), Aurora Clark (Washington State University) and Thomas Markland (Stanford University).....	56
<i>Probing Catalytic Activity in Defect Sites in Transition Metal Oxides and Sulfides using Cluster Models: A Combined Experimental and Theoretical Approach</i> Caroline Chick Jarrold and Krishnan Raghavachari (Indiana University).....	60
<i>Critical Evaluation of Theoretical Models for Aqueous Chemistry and CO<sub>2</sub> Activation in the Temperature-Controlled Cluster Regime</i> Kenneth D. Jordan (University of Pittsburgh) and Mark A. Johnson (Yale University).....	64
<i>Nucleation Chemical Physics</i> Shawn M. Kathmann (Pacific Northwest National Laboratory).....	68
<i>Structure and Reactivity of Ices, Oxides, and Amorphous Materials</i> Bruce D. Kay, R. Scott Smith, and Zdenek Dohnálek (Pacific Northwest National Laboratory).....	72
<i>Probing Ultrafast Electron (De)localization Dynamics in Mixed Valence Complexes Using Femtosecond X-ray Spectroscopy</i> Munira Khalil (University of Washington, Seattle), Niranjan Govind (Pacific Northwest National Laboratory), Shaul Mukamel (University of California, Irvine) and Robert Schoenlein (SLAC National Accelerator Laboratory).....	76
<i>Non-Thermal Reactions at Surfaces and Interfaces</i> Greg A. Kimmel and Nikolay G. Petrik (Pacific Northwest National Laboratory).....	80
<i>2D IR Microscopy—Technology for Visualizing Chemical Dynamics in Heterogeneous Environments</i> Amber T. Krummel (Colorado State University).....	84

<i>Electrochemical Control of Plasmonic Nanomaterial Surface Chemistry</i> Christy F. Landes and Stephan Link (Rice University) .....	86
<i>Single-Molecule Interfacial Electron Transfer</i> H. Peter Lu (Bowling Green State University) .....	90
<i>Ab Initio Approach to Interfacial Processes in Hydrogen Bonded Fluids</i> Christopher J. Mundy (Pacific Northwest National Laboratory) .....	94
<i>Dynamic Studies of Photo- and Electron-Induced Reactions on Nanostructured Surfaces</i> Richard Osgood (Columbia University) .....	98
<i>Studies of Surface Adsorbate Electronic Structure and Femtochemistry at the Fundamental Length and Time Scales</i> Hrvoje Petek (University of Pittsburgh) .....	103
<i>Molecular Structure, Bonding and Assembly at Nanoemulsion and Liposome Surfaces</i> Geraldine Richmond (University of Oregon) .....	107
<i>Sampling Rare Events in Aqueous Systems Using Molecular Simulations</i> Sapna Sarupria (Clemson University) .....	111
<i>Solvation</i> Richard Saykally, Musahid Ahmed, Phillip L. Geissler and Teresa Head-Gordon (Lawrence Berkeley National Laboratory) .....	113
<i>Development of Statistical Mechanical Techniques for Complex Condensed-Phase Systems</i> Gregory K. Schenter (Pacific Northwest National Laboratory) .....	117
<i>An Atomic-scale Approach for Understanding and Controlling Chemical Reactivity and Selectivity on Metal Alloys</i> E. Charles H. Sykes (Tufts University) .....	121
<i>Solvation Dynamics in Nanoconfined and Interfacial Liquids</i> Ward H. Thompson (University of Kansas) .....	125
<i>Imaging Interfacial Electric Fields on Ultrafast Timescales</i> William A. Tisdale (Massachusetts Institute of Technology) .....	129
<i>Structural Dynamics in Complex Liquids Studied with Multidimensional Vibrational Spectroscopy</i> Andrei Tokmakoff (University of Chicago) .....	133
<i>Chemistry of Ionic Species in Aqueous Systems</i> Marat Valiev (Pacific Northwest National Laboratory) .....	136
<i>Cluster Model Investigation of Condensed Phase Phenomena</i> Xue-Bin Wang (Pacific Northwest National Laboratory) .....	138
<i>Free Radical Reactions of Hydrocarbons at Aqueous Interfaces</i> Kevin R. Wilson (Lawrence Berkeley National Laboratory) .....	142

<i>Non-Empirical and Self-Interaction Corrections for DFTB: Towards Accurate Quantum Simulations for Large Mesoscale Systems</i> Bryan M. Wong (University of California-Riverside).....	146
<i>Intermolecular Interactions in the Gas and Condensed Phases</i> Sotiris S. Xantheas (Pacific Northwest National Laboratory) .....	150
<b><u>Solar Photochemistry Principal Investigator Abstracts</u></b>	
<i>Fundamental Advances in Radiation Chemistry</i> David M. Bartels, Ian Carmichael, Ireneusz Janik, Jay A. LaVerne, and Sylwia Ptasińska (Notre Dame Radiation Laboratory) .....	154
<i>Exceptionally Rapid Capture of Radical Cations Made by Pulse Radiolysis</i> Andrew R. Cook and John R. Miller (Brookhaven National Laboratory) .....	158
<i>Interfacial Radiation Sciences</i> Jay A. LaVerne, David M. Bartels, Daniel M. Chipman, and Sylwia Ptasińska (Notre Dame Radiation Laboratory) .....	162
<i>Solution Reactivity and Mechanisms through Pulse Radiolysis</i> Sergei V. Lymar (Brookhaven National Laboratory) .....	166
<i>Ionic Liquids: Radiation Chemistry, Solvation Dynamics and Reactivity Patterns</i> James F. Wishart (Brookhaven National Laboratory) .....	170
<b>LIST OF PARTICIPANTS</b> .....	173

The background of the entire page is a light blue color. Overlaid on this are several large, semi-transparent, light blue shapes that resemble stylized cells or molecular structures. Each of these shapes contains several smaller spheres. Some of these spheres are bright red, while others are bright white. The spheres are arranged in a somewhat symmetrical pattern across the page. In the center of the page, there is a black-bordered rectangular area. Inside this area, the text "Abstracts (CTC Investigators)" is written in a bold, italicized, black font.

***Abstracts  
(CTC Investigators)***

Program Title: Theoretical Developments and Applications to Surface Science, Heterogeneous Catalysis, Heavy Elements, and Intermolecular Interactions

Principal Investigator: Mark S. Gordon, 201 Spedding Hall, Iowa Sate University and Ames Laboratory, Ames, IA 50011; [mark@si.msg.chem.iastate.edu](mailto:mark@si.msg.chem.iastate.edu)

Program Scope. Our research effort combines new theory and code developments with applications to a variety of problems in surface science and heterogeneous catalysis, heavy element chemistry, and the investigation of intermolecular interactions, including solvent effects in ground and excited electronic states and the liquid-surface interface. Many of the surface science studies are in collaboration with Dr. James Evans. Much of the catalysis effort is also in collaboration with Professors Evans, Marek Pruski and Igor Slowing.

Recent Progress. Chemical processes on and with the Si(100) surface have been one research focus. The diffusion of Ga on Si(100) was studied using an embedded cluster model and multi-reference electronic structure methods, including CASSCF explorations of the doublet and quartet potential energy surfaces and improved energies with multi-reference perturbation theory<sup>2</sup>. The details of the potential energy surfaces depend critically on the presence of the bulk that is represented by molecular mechanics (MM). Only when edge effects are minimized by embedding the quantum mechanics (QM) region in a much larger MM region, using our SIMOMM method, does a consistently realistic picture emerge. It appears that Ga can form metal wires on the Si(100) surface. Studies of surface growth are greatly enhanced through collaborations with the Evans group so that the morphology of surface processes can be better understood.

A significant effort involves the development of efficient methods that can be applied to large systems, such as surfaces, nanoparticles and liquids. One such method is the effective fragment potential (EFP) method whose accuracy for intermolecular interactions rivals that of second order perturbation theory (MP2). The EFP method, a highly sophisticated model potential, can be combined with essentially any electronic structure method to, for example, provide insights about solvent effects and liquid behavior. Recently, the EFP method has been combined with nonlinear time-dependent density functional theory to facilitate the investigation of solvent effects on nonlinear optical properties<sup>4</sup>. The EFP method has also been combined with our spin-flip TDDFT method to study solvent effects on the location and energy profile of conical intersections, which have a profound effect on excited states, photochemistry and photobiology. EFP molecular dynamics (MD) simulations have been employed to study the aqueous solvation of the hydronium ion<sup>7</sup> and to predict the melting temperature of ice<sup>9</sup>. In the latter study, the EFP method was shown to outperform density functional theory (DFT) methods.

Another (fully quantum) fragmentation approach is the fragment molecular orbital (FMO) method. The FMO method divides a large species into fragments to facilitate accurate QM calculations on very large systems. The FMO method can be used in concert with any electronic structure method in GAMESS. In order to optimize

geometries using the FMO method, or to perform molecular dynamics (MD) simulations, it is necessary to derive and code fully analytic gradients for each method that is combined with the FMO, such as Hartree-Fock (HF) or DFT. Fully analytic FMO/HF, FMO/DFT, and FMO/MP2 gradients have been derived and implemented in GAMESS, to enable geometry optimizations and MD simulations<sup>11,13</sup>. We have shown previously that one can do FMO/HF MD simulations with periodic boundary conditions and that fully analytic gradients are absolutely essential. An invited review of fragmentation methods has appeared in a high impact journal.<sup>5</sup> The FMO method is also highly scalable, because the calculation for each fragment can be performed on a separate compute node. Advances have also been made in high performance computational chemistry. An INCITE grant has enabled us to have access to the BlueGene /Q at Argonne, where we have demonstrated that the FMO method allows essentially perfect scaling to the petascale (more than 262,000 processors)<sup>13</sup>. The EFP and FMO methods have both been used to study problems related to biomass conversion to useful energy<sup>1</sup>. One bottleneck in the FMO method is that FMO3 calculations with explicit three-body interactions are computationally demanding. This problem has been solved in two ways. The entire FMO code has been made essentially file-less, with virtually no I/O overhead<sup>13</sup>. Also, a new method, the effective fragment molecular orbital (EFMO) method has been developed that replaces the bath potential with the EFP<sup>14</sup>. This incorporates the EFP induction component that includes many body interactions. It has been shown that the EFMO method is both more accurate and faster than the FMO2 method. Fully analytic EFMO gradients have been derived and implemented<sup>14</sup>.

Another approach to making high-level electronic structure calculations is to use localized molecular orbitals (LMOs), because correlation is local. So, one can design LMO domains or subsystems and only perform the correlation calculation within those domains. Carter (Princeton) has developed a multi-configurational (MR) configuration interaction (CI) code called TigerCI to perform such calculations. In collaboration with the Carter group, a preliminary parallel version of TigerCI code has been implemented<sup>6</sup>. The TigerCI code has now been incorporated into GAMESS. A manuscript that describes this effort is in preparation. Another LMO-based fragmentation method, developed by the Piecuch group, called cluster-in-molecule (CIM) has been implemented in GAMESS. The CIM method is primarily intended to work with MP2 and coupled cluster methods, such as CCSD(T) and CR-CC(2,3). The bottleneck in the CIM method is the need to perform a HF calculation on the entire system to obtain the LMOs. This problem has been alleviated by the development of a combined FMO-CIM method, so that only the orbitals on each fragment need to be localized<sup>10</sup>.

Mesoporous silica nanoparticles (MSN) have received increasing attention due to their catalytic capabilities. Because the MSN species are very important for their selective heterogeneous catalytic capability, we have an ongoing effort to model these complex species, in collaboration with the Evans, Pruski and Slowing groups. Electronic structure theory calculations have been combined with the non-equilibrium statistical mechanics methods of the Evans group to provide insights about processes that occur within a MSN<sup>8</sup>. The FMO method has been used to study the formation of carbinolamine, catalyzed by a section of MSN<sup>12</sup>.

A combined experiment/theory study of the Ce atom reaction with ethylene has been completed<sup>15</sup>. The existence of two band systems has been attributed to spin-orbit coupling, and the nature of the bonding has been analyzed.

Current and Future Plans. Having completed an FMO study of the heterogeneous catalysis of carbinolamine formation inside a MSN cage, an examination of the full mechanism for this reaction will be investigated. It was demonstrated that small models of the MSN catalyst do not capture the correct chemistry, so larger cages, with thousands of atoms will be required. These calculations will be made feasible by an existing INCITE grant and by an exascale computing project (ECP) grant that us scheduled to begin in FY17.

An interface between the GAMESS electronic structure program and the FMS program from the Martinez group has been implemented. The combined GAMESS-FMS methodology will now be used to study excited state phenomena, such as conical intersections that are ubiquitous in photochemical processes. In order to fully analyze surface crossings and conical intersections, one needs the ability to calculate non-adiabatic coupling matrix elements (NACME) that couple multiple surfaces when they are in close proximity. For large systems, TDDFT and SF-TDDFT are the most efficient methods for exploring excited state phenomena, so the derivation and implementation of TDDFT and SF-TDDFT NACME are in progress.

A collaboration with the Evans group at the Ames Laboratory on reactions that occur on the Pd surface will combine accurate electronic structure theory with kinetic Monte Carlo studies. These studies are complicated by the existence of several spin states of varying multiplicities, even for large Pd clusters.

The collaboration with the Yang group at the University of Kentucky on the Ce-ethylene reaction will be expanded to other lanthanide elements.

#### References to publications of DOE sponsored research 2013-present

1. A. Devarajan, S. Markutsya, M.H. Lamm, X. Cheng, J.C. Smith, J.Y. Baluyut, Y. Kholod, M.S. Gordon, and T.L. Windus, "Ab Initio Molecular Dynamics Study of Molecular Interactions in a Cellulose I $\alpha$  Microfiber", *J. Phys. Chem. B*, **117**, 10430(2013)
2. D.-J. Liu, D.M. Ackerman, X. Guo, M.A. Albao, L. Roskop, M.S. Gordon, J.W. Evans, Morphological evolution during growth and erosion on vicinal Si(100) surfaces: From electronic structure to atomistic and coarse-grained modeling, *MRS Proc. Symp. EE Fall 2011 (MRS, Pittsburgh, 2012)*.
3. J. Wang, A. Garcia, D.M. Ackerman, M.S. Gordon, I.I. Slowing, T. Kobayashi, M. Pruski, J.W. Evans, Multi-functionalization of nanoporous catalytic materials to enhance reaction yield: Statistical mechanical modeling for conversion reactions with restricted diffusive transport, *MRS Proc. Symp. AA Fall 2013 (MRS, Pittsburgh, 2014)*.
4. F. Zahariev and M.S. Gordon, "Non-linear Response Time-Dependent Density Functional Theory combined with the Effective Fragment Potential Method", *J. Chem. Phys.*, **140**, 18A523 (2014)

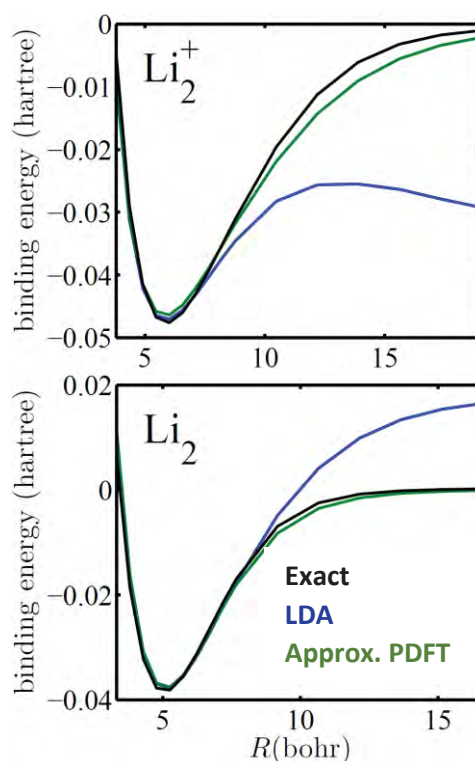
- 5.** S.R. Pruitt, C. Bertoni, K. Brorsen, and M.S. Gordon, “Efficient and Accurate Fragmentation Methods”, *Acc. Chem. Research (INVITED)*, **47**, 2786 (2014)
- 6.** J. Dieterich, D. Krisiloff, A Gaenko, F.Libisch, T. Windus, M. Gordon, E. Carter, “Shared-memory parallelization of a local correlation multi-reference CI program”, *Comp. Phys. Comm.*, **185**, 3175 (2014)
- 7.** K.R. Brorsen, S.R. Pruitt, and M.S. Gordon, “Surface affinity of the hydronium ion: The effective fragment potential and umbrella sampling”, *J. Phys. Chem B.*, **118**, 14382 (2014).
- 8.** J. Wang, A. Garcia, D.M. Ackerman, M.S. Gordon, I.I. Slowing, T. Kobayashi, M. Pruski, and J.W. Evans, “Multi-functionalization of nanoporous catalytic materials to enhance reaction yield: Statistical mechanical modeling for conversion reactions with restricted diffusive transport”, *Mater. Res. Soc. Symp. Proc. Vol. 1641* (2014)
- 9.** K.R. Brorsen, S.Y. Willow, S.S. Xantheas, and M.S. Gordon, “The melting temperature of liquid water with the effective fragment potential”, *J. Phys. Chem. Lett.*, **6**, 3555 (2015).
- 10.** A. Findlater, F. Zahariev, and M.S. Gordon, “A Combined Fragment Molecular Orbital-Cluster in Molecule Approach to Massively Parallel Electron Correlation Calculations for Large Systems”, *J. Phys. Chem. A*, **119**, 3587 (2015)
- 11.** H. Nakata, D.G. Fedorov, F. Zahariev, M.W. Schmidt, M.S. Gordon, and S. Nakamura, “Analytic second derivative of the energy for density functional theory based on the three-body fragment molecular orbital theory”, *J. Chem. Phys.*, **142**, 124101 (2015)
- 12.** Ana P. de Lima Batista, Federico Zahariev, Igor I. Slowing, Ataulpa A. C. Braga, Fernando R. Ornellas, Mark S. Gordon, “Silanol-Assisted Carbinolamine Formation in an Amine-Functionalized Mesoporous Silica Surface: Theoretical Investigation by Fragmentation Methods”, *J. Phys. Chem. B*, **120**, 1660 (2016).
- 13.** S.R. Pruitt, H. Nakata, T. Nagata, M. Mayes, Y. Alexeev, G.D. Fletcher, D.G. Fedorov, K. Kitaura, and M.S. Gordon, “The Importance of Three-Body Interactions in Molecular Dynamics Simulations of Water”, *J. Chem. Theory Comp.*, in press **12**, 1423 (2016)
- 14.** C. Bertoni and M.S. Gordon, “Analytic gradients for the Effective Fragment Molecular Orbital method”, *J. Chem. Theory Comp.*, in press.
- 15.** Y. Zhang, M. W. Schmidt, S. Kumari, M. S. Gordon, and D.-S. Yang, “Threshold Ionization and Spin-Orbit Coupling of Ceracyclopropene Formed by Ethylene Dehydrogenation”, *J. Phys. Chem. A*, in press

## Fixing delocalization and static-correlation errors with Partition Density Functional Theory

Supported by grant DE-FG02-10ER16196: Partition Density Functionals: Theory and Applications

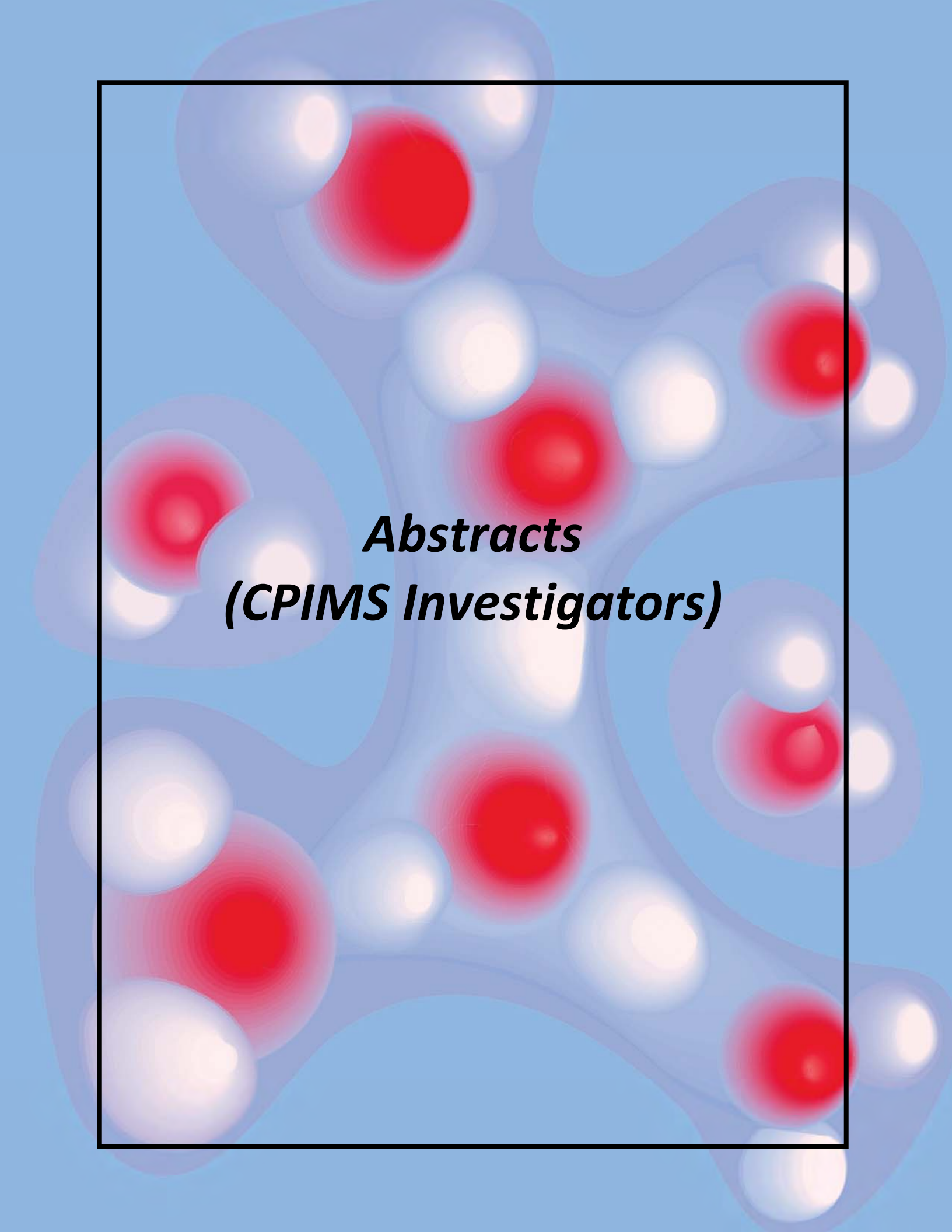
Adam Wasserman\*  
Department of Chemistry  
Purdue University  
560 Oval Dr., West Lafayette, IN 47907  
\*awasser@purdue.edu

Partition Density Functional Theory (PDFT) is a formally-exact method to calculate the ground-state energy and density of molecules via self-consistent calculations on isolated fragments [1]. After a brief introduction to PDFT, I will explain our recent work [2] demonstrating how PDFT can be used to fix the delocalization and static-correlation errors that plague density-functional calculations of stretched molecules. For example, the figure shows the cases of stretched  $\text{Li}_2$  and  $\text{Li}_2^+$ . No existing approximation to the XC-functional can get both of these correctly within standard KS-DFT. The local-density approximation (LDA, in blue) underestimates the binding energy of the ion due to delocalization error and overestimates it in the neutral dimer due to static-correlation. PDFT (in green), with a simple *overlap approximation* for the partition energy and LDA for the fragments, almost entirely corrects both. I will explain why, emphasizing the importance of the ensemble treatment of fragment energies.



I will also discuss our recent efforts to develop a non-decomposable, non-additive, non-interacting kinetic energy functional for use within PDFT [3], and a useful classification of energy errors [4].

1. J. Nafziger and A. Wasserman, *Density-based Partitioning Methods for Ground-state molecular calculations*, J. Phys. Chem. A **118**, 7623 (2014).
2. J. Nafziger and A. Wasserman, *Fragment-based treatment of delocalization and static-correlation errors in Density Functional Theory*, J. Chem. Phys. **143**, 234105 (2015).
3. J. Nafziger, K. Jiang, and A. Wasserman, *Non-decomposable, non-additive, non-interacting kinetic energy for covalent and non-covalent bonds*, to be submitted.
4. A. Wasserman, J. Nafziger, K. Jiang, M.C. Kim, E. Sim, and K. Burke, *The importance of being self-consistent*, Annu. Rev. Phys. Chem., in press (2016).

The background features a light blue field with several clusters of spheres. Each cluster consists of a central red sphere surrounded by several white spheres. The spheres are rendered with a soft, glowing effect, and the overall composition is abstract and symmetrical.

***Abstracts  
(CPIMS Investigators)***

DOE-BES CPIMS  
Condensed Phase and Interfacial Molecular Science  
PI Heather C. Allen  
Ohio State University  
Dept. of Chemistry and Biochemistry  
100 W 18<sup>th</sup> Ave  
Columbus OH 43210

#### Program Scope

*Controlling Aqueous Interfacial Phenomena of Redox-Active Ions with External Electric Fields.* Our central hypothesis, based on literature precedents and our own prior research is that an externally applied electric field will markedly influence ion hydration properties and interfacial water organization at the air/aqueous interface. Redox ions are an important class of ions in which their multivalent states provide the potential for significant interfacial impact, with and without an externally applied field. At the air/aqueous interface of FeCl<sub>2</sub> and FeCl<sub>3</sub> solutions, ions and water are not distributed homogeneously, but current expectation is that these ions will spontaneously form an electric double layer. We expect that multivalent ions will be influenced, and that hydration water and unbound water within the interface will be anomalously perturbed in an externally applied electric field such that our observations could alter currently held assumptions about organization at such interfaces.

Our goal for the proposed research is to show proof of concept experiments for a fundamental understanding of the organization of, and induced by, redox ions Fe(II) and Fe(III) and externally applied electric fields at the hydrophobic air /water interface. These investigations of acidity, co-anion, ionic strength, electric field strength and electrode polarity, as well as the associated perturbations to hydration and organization to these redox ion interfacial systems are imperative in order to develop this knowledge. Methods further developed and employed include vibrational sum frequency generation spectroscopy, glancing angle Raman spectroscopy, surface tension and surface potential instrumentation. Expected outcomes include instrumentation development and advances in surface-sensitive spectroscopy.

#### Recent Progress

As a preliminary surface potential (SP) study, we investigated Fe<sup>2+</sup> and Fe<sup>3+</sup> binding to a lipid to test our current SP instrument sensitivity and for initial training purposes. Previous studies have demonstrated interactions of Na<sup>+</sup>, K<sup>+</sup>, Mg<sup>2+</sup> and Ca<sup>2+</sup> with lipids. However, there is no current understanding of multivalent transition metal interaction with these lipids. Hence, the Fe<sup>2+</sup>/Fe<sup>3+</sup> pair is proposed as cations of interest in the binding interaction with a model lipid. To understand binding between Fe<sup>2+</sup>/Fe<sup>3+</sup> and polar headgroups of phospholipids, it is essential to note the charge, ionic radius, degree of hydration, and orbital geometry as parameters used to evaluate binding. Multivalent cations form stronger complexes than monovalent cations, which have lower charge density. Cations involved in complexation must lose most of their hydration sphere. Therefore, larger, less hydrated metal ions often bind more strongly than do the smaller, more hydrated ones. When considering ions of a given charge type, such as Na<sup>+</sup> vs. K<sup>+</sup> and Mg<sup>2+</sup> vs. Ca<sup>2+</sup>, smaller cations are considerably more strongly hydrated relative to larger cations where charge is dispersed over a larger surface area.

In interaction with lipids, Fe<sup>2+</sup> and Fe<sup>3+</sup> ions are not expected to bind in a manner analogous to Ca<sup>2+</sup> and Mg<sup>2+</sup> respectively due to the potential for d-orbital coordination. However, initial interaction of charge-

charge attraction is expected. It is known that  $Mg^{2+}$  is strongly hydrated and it is energetically unfavorable to remove the surrounding water molecules before making an ionic complex with a negatively-charged headgroup of a phospholipid such as PA. Additionally,  $Ca^{2+}$  has been shown to have a stronger binding affinity than  $Mg^{2+}$ , which is indicated by a large surface excess of  $Ca^{2+}$  at the air/water interface. Compared to  $Fe^{2+}$ ,  $Fe^{3+}$  has a higher charge density and polarizability, and so will be more strongly hydrated, similar to  $Mg^{2+}$ . However, while the  $Fe^{2+}/Fe^{3+}$  interactions with phospholipid headgroups might first appear similar to  $Mg^{2+}/Ca^{2+}$ , it should be noted that Fe has complex relationship with water, which is pH dependent and can result in formation of precipitates, particularly  $Fe(OH)_3$  ( $K_{sp} 2.79 \times 10^{-39}$ , insoluble at pH 7). Given an iron-phospholipid system, pH plays a crucial role. It controls the interfacial charge by protonation/deprotonation of the phosphate group and also determines the types of Fe-complexes in solution. A recent study involving such a system has shown that the calculated percentage of soluble Fe ( $Fe^{3+}$ ,  $Fe(OH)^{2+}$ ) is present below pH  $\sim 2.2$ .

In our first study under this DOE grant, a vibrating plate surface potential was used to quantitatively measure the extent of condensation of the phospholipid by iron. From this, the surface dipole orientation and the surface charge density is also determined. Using dipalmitoylphosphatidylcholine (DPPC) as our model,  $Fe^{2+}$  interaction was studied at three mean molecular areas (m.m.a.) of the lipid. Preliminary surface potential (SP) measurements obtained from the air – aqueous 1mM ferrous chloride interface showed significant SP enhancement (668 mV, 1mM) of the DPPC monolayer at 45 m.m.a., compared to the neat water subphase (569 mV) and those of other divalents, such as  $Mg^{2+}$  (687 mV, 1M) and  $Ca^{2+}$  (734 mV, 1M). Calculated Debye lengths for divalents for two different calculations (1mM: 170.63 Å; 1M: 5.40 Å) show that the impact of  $Fe^{2+}$  SP with a greater Debye length is almost equivalent to  $Mg^{2+}/Ca^{2+}$ .

C. Y. Tang, Z. Huang, H. C. Allen; *J. Phys. Chem. B.* **2011**. 115(1), 34-40

C. Y. Tang, Z. Huang, H. C. Allen; *J. Phys. Chem. B.* **2010**. 114(51), 17068-17076

Stickland, F. G. W. *J. Colloid Interface Sci.* **1973**, 42, 96.

Wang, W.; Park, R. Y.; Meyer, D. H.; Travesset, A; Vaknin, D.; *Langmuir* **2011** 27 (19), 11917-11924

Gaines, G. L., Jr. *Insoluble monolayers at liquid-gas interfaces*; Interscience Publishers, Inc.: New York, 1966; Chapter 4, p 136

## Future Plans

Instrumentation planning is underway for developing a radioactive decay based surface potentiostat to detect bare aqueous Fe solution surfaces. The expected higher sensitivity and increased signal/noise relative to the vibrating plate method currently being used in our laboratory is necessary to achieve reproducible lower intensity air-aqueous salt solution SP data. Our intention is to determine the potential of the double layer of  $Fe^{2+}/Fe^{3+}$  without a lipid monolayer. In addition, for our sum frequency generation (SFG) instrument, a lower groove density compressor grating is scheduled to be installed and tested in mid-November to enable larger spectral region acquisitions for expanded view of the OH stretching region. We are also planning low frequency glancing angle Raman (GAR) testing with a newly order CW Crystalaser 532 laser for this application. The GAR spectroscopy will delineate interfacial iron speciation and low frequency modes of hydrogen bonding. Postdoctoral Associate Lu Lin (start date Nov 1, 2016) will be leading the SFG OH bandwidth expansion and second year graduate student Tehseen Adel is leading the surface potential instrumentation subproject. We plan to begin preliminary SFG OH stretch experiments from the Fe(II, III) solution in January 2017.

Publications. None. (Grant start date: 09/01/2016)

# Visible light photo-catalysis in charged micro-droplets

DE-SC0016044

Abraham Badu-Tawiah

Department of Chemistry and Biochemistry, The Ohio State University. Columbus, OH 43210

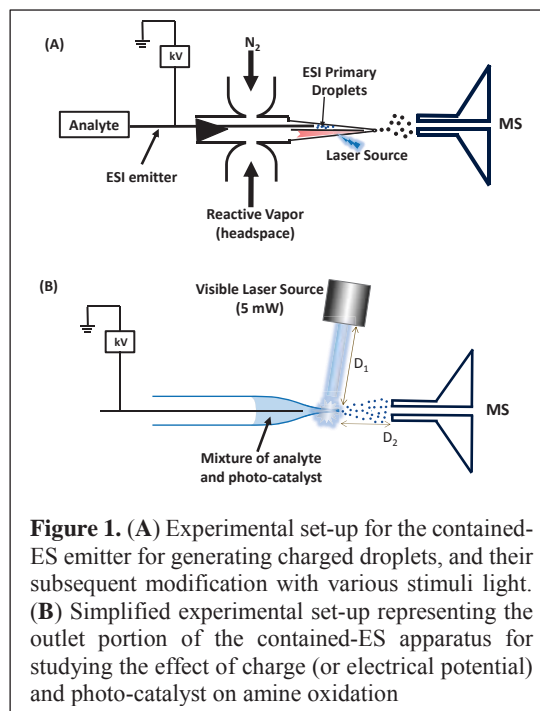
badu-tawiah.1@osu.edu

## Program Scope

This research program seeks to establish the charged micro-droplet environment as a medium for studying photochemical reactions. The confined droplet environment has capacity to accelerate chemical reactions using only picomoles ( $10^{-12}$  mol) of reactants. The hypothesis is that the effect of electric fields used during charged droplet generation, the effect of concentration achieved by solvent evaporation from the resultant charged droplets, and the effect of droplet exposure to a highly intense and coherent visible laser source will enable the production of unique, reactive photo-chemical species for novel pathways that might be difficult to access in traditional bulk, condensed-phase conditions. Unlike traditional gas-phase reactions conducted under reduced pressure, the ionic environment of the charged droplets exists at the interface of solution-phase and the gas-phase, yielding information that is directly transferrable to large scale chemical synthesis. The main focus of our work has been the development of novel devices for charged droplet manipulation and real-time product detection by mass spectrometry (MS). Chemical systems of interest involve the study of interfacial oxidation of amines.

## Recent Progress

We have developed a novel contained-electrospray (ES) ionization device (Figure 1A) that is capable of (i) reactant confinement in charged droplets, and (ii) manipulation of the droplet reaction environment with a variety of stimuli (photons, electrical discharge, and heat). We studied catalytic dehydrogenation of tetrahydroquinolines using a simplified device (Figure 1B) involving nano-electrospray ionization (nESI) that mimicked only the outlet portion of the contained-ES apparatus. By coupling a portable laser source with nESI MS, we have established the first MS-based picomole-scale real-time photoreaction screening platform. This platform can be used for direct and rapid screening of chemical transformations, and results are available within seconds of reaction initiation. With this approach, we discovered an effective photocatalytic pathway involving the dehydrogenation of 1,2,3,4-tetrahydroquinolines to the corresponding



quinolines. The reaction was catalyzed by the common visible-light-harvesting complex  $[\text{Ru}(\text{bpy})_3]\text{Cl}_2$  ( $\text{bpy}=2,2'$ -bipyridine) under ambient conditions. Detailed mechanistic studies revealed that the main active species in the electro spray reaction environment is the superoxide anions ( $\text{O}_2^{\cdot-}$ ) produced during the process of photo-catalyst regeneration (Scheme 1), and that electrochemical effect on reaction yield is minimal.

Using this mechanistic insight, we began a detailed investigation of the new ruthenium-based photoreaction by performing the reaction in bulk solution under the ambient loading conditions of  $[\text{Ru}(\text{bpy})_3]\text{Cl}_2$  photocatalyst; however, the laser light source was replaced with a common energy saving lamp (23 W) and sunlight. The results of these bulk-phase reactions are in agreement with those obtained from the electro spray-based condition. Linear amines were converted into the corresponding imines in high yields >96% when irradiated with the lamp for 1.5 h. For tetrahydroquinolines, the fully dehydrogenated quinolines were formed in >86% yield under sunlight for 2 h at 35 °C. These results are significant because, for the first time, aerobic amine oxidation can be achieved in air at ambient temperature in direct sunlight, or with the aid of an energy-saving lamp using an off-the-shelf  $[\text{Ru}(\text{bpy})_3]\text{Cl}_2 \cdot 6\text{H}_2\text{O}$  photo-catalyst.

The identification of  $\text{O}_2^{\cdot-}$  as the active species suggests that different energy sources (aside from visible light) may be utilized to achieve this industrially important dehydrogenation reaction. For example, ionic wind generated by an electrical discharge has been shown to contain  $\text{O}_2^{\cdot-}$  anions, which are formed by attachment of thermalized electron to oxygen in air. Indeed, complete conversion of tetrahydroquinolines into the corresponding quinolines was achieved in less than 2 min after exposure of droplet present on a hydrophobic paper to corona discharge (Figure 2). In this case, the presence of graphite particles increased reaction efficiency. Although this enhanced reaction rate may be due to reactant confinement and concentration effects resulting from solvent evaporation, we believe the observed catalytic effect is heterogeneous in nature, occurring mostly at the surfaces of the graphite particles. The combined effect is expected to limit the diffusion of the dihydroquinoline intermediates and allow rapid conversion into the final product. This expectation was further investigated by employing linear primary amines ( $\text{R}-\text{CH}_2\text{NH}_2$ ) such as hexylamine and decylamine. Depending on reaction conditions, primary amines can be converted into three possible products: (i) imine ( $\text{R}-\text{CH}=\text{NH}$ ) via the removal of two hydrogen atoms, (ii) nitriles ( $\text{R}-\text{C}\equiv\text{N}$ ) through the removal of four hydrogen atoms, and (iii)  $\text{R}-\text{CH}_2\text{N}=\text{CH}_2-\text{R}$  via the elimination of ammonia in a self-coupling reaction between imine and unreacted amine. Formation of nitriles in aerobic oxidation is rare

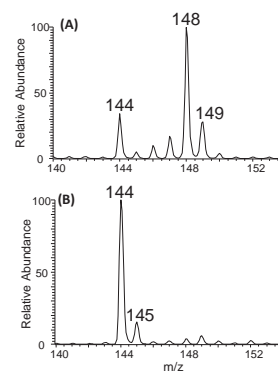
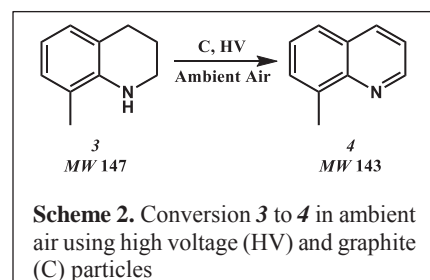
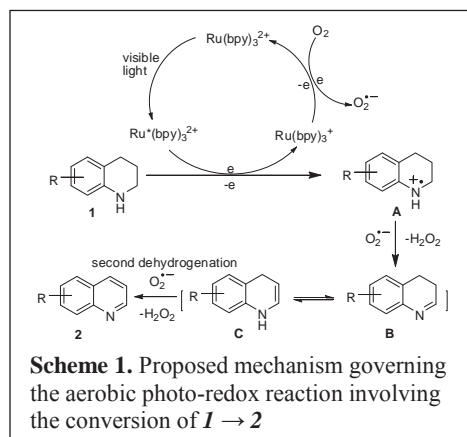


**Figure 2.** Paper spray mass spectra recorded after 2 min exposure to electrical discharge in the (A) absence and (B) presence of graphite particles

because of intrinsic self-coupling properties of primary amine substrates. In our experiments with corona discharge, however, nitriles were formed exclusively suggesting the current reaction condition is energetic and occurs faster compared with the traditional aerobic dehydrogenation reactions which require hours of reaction time.

## Future Plans

The focus of our work will remain (i) the development and refinement of methodologies to “process” ions at atmospheric pressure, where processing includes ion formation, ion stimulation, ion reaction, and product collection, and (ii) attempts to advance understanding of the fundamentals of photo-redox catalysis, and ion chemistry at interfaces and atmospheric pressure, using these new methodologies. Of particular interests are the elucidation of the complete mechanism governing the photo-redox reaction to enable the creation of new pathways for other substrates. For example, a key feature of the current mechanism includes a tautomerization step, yielding secondary amine with  $sp^3$  hybridized orbital in the nitrogen atom for a second round of oxidation. This hypothesis will be investigated further using experiments and density functional theory calculations. Experiments will involve tetrahydroisoquinolines which we predict to resist tautomerization. In this case, we expect the photo-redox reaction to stop after the removal of 2 hydrogen atoms. Accordingly, we will study this hypothesis by utilizing various isomers of dihydroisoquinoline and evaluate their susceptibility to dehydrogenation. We plan to tune the reactivity of tetrahydroisoquinolines by varying the electron density on the nitrogen. We will achieve this objective, for example, by placing electron withdrawing (EW) and donating (ED) groups on an N-substituted phenyl tetrahydroisoquinolines derivative. We will study this induction effect by varying the position (ortho, meta and para) and type [i.e., EW (halides, -CN, -NO<sub>2</sub>) versus ED (-NH<sub>2</sub>, -OH, -OR)] of groups on the phenyl substituent.

Detailed experiments are also needed to fully characterize the source of the O<sub>2</sub><sup>•-</sup> reactive species. To be certain of this reaction direction, we will first study the effect that radical scavengers (e.g., benzoquinone) have on the amine oxidation when using [Ru(bpy)<sub>3</sub>]<sup>2+</sup> with blue visible light. Benzoquinone can trap superoxide anions by an electron transfer mechanism and reduced reaction yield is expected. We will also employ 5,5-Dimethyl-1-Pyrroline-N-Oxide (DMPO) as a spin trapping reagent. In this case, DMPO is expected to react with O- and N- centered radicals present in the reaction system to form stable adducts that can be detected and characterized by MS. These experiments will provide both molecular and kinetic information. This result will encourage the development of novel electrospray-based methods that impose electrical discharge on illumination. The combined effect should make it possible to utilize highly abundant first row transition metal (e.g., copper and iron) complexes as catalyst for amine oxidation.

In particular, we are interested in *in-situ* preparation of active catalysts from simple salts (e.g., CuBr<sub>2</sub>) and free ligands (e.g., 2,2'-bipyridine). For example, a previous report on a systematic investigation of the effect of different components in the Cu salt/bpy catalytic system showed

better performance under basic (e.g., N-methylimidazole (NMI)) and stable radical (e.g., 2,2,6,6-tetramethylpiperidinyloxy (TEMPO)) conditions.<sup>[82]</sup> Spectroscopic investigation suggested the presence of  $[\text{Cu}(\text{bpy})(\text{NMI})\text{O}_2]^+$  and oxygen-bound dimer,  $[\text{Cu}(\text{bpy})(\text{NMI})(\text{O}_2)\text{Cu}(\text{bpy})(\text{NMI})]^{2+}$ , all indicating the importance of reactive oxygen species. Through negative mode electrospray, we will simplify the compositional complexity of this catalytic system. Solvent effects will be studied systematically on-line using the contained-ES apparatus. That novel and highly reactive chemical species can be generated under the charged micro-droplet environment motivates us to screen other first row transition metal salts including those of Ni and Fe. We have unique opportunity to vary a multitude of reaction conditions within a short time period. For this, we will electrospray various selected halides from different solvent compositions. Effects from confinement, photon and electrical discharge is expected to generate different micro-solvated  $[\text{ML}_n]^{n+}$  species (L = halide,  $\text{H}_2\text{O}$ ,  $\text{CH}_3\text{CN}$ ,  $\text{OCH}_3$ ,  $\text{OHCH}_3$ , etc.) with various oxidation states, some of which will be expected to have catalytic activities. Intermediate detection and characterization will be achieved by using a novel transmission-mode desorption electrospray (TM-DESI) ion source, which enables rapidly moving charged droplets, of microseconds lifetimes, to be analyzed by MS.

By selecting appropriate photo-catalyst we will be able to explore the entire visible spectrum. We are particularly interested in the development of metal-free photo-catalytic strategies for dehydrogenation. We will test several off-the-shelf organic dyes to assess their susceptibility toward amine oxidation. Given the major limitations of organic dyes as photo-catalysts (including thermal instabilities, poor efficiencies, and slow reaction rates), we expect the droplet environment to facilitate their reactivity. Evaporative cooling and reagent concentration that results after pure solvent evaporation from the charged droplets are expected to accelerate organic dye photo-catalysis. In principle, excited organic dye can interact directly with amine reactant through an electron transfer reaction. Alternative pathways will include electron transfer reactions involving either water or oxygen molecules to generate oxidized products such as  $\text{OH}^-$ ,  $\text{O}_2^-$ , and  $^1\text{O}_2$ . We recognized that, just like electrical discharge, organic dyes can be combined with organometallic photo-catalysts to provide a cooperative photo-redox pathway through which elusive chemical reactions can be realized. Herein, we will study the effect of each photo-catalyst (organic versus organometallic) on our contained-ES apparatus, and the TM-DESI setup will be used to detect reactive intermediates when using the organic and organometallic photo-catalysts in combination.

### Recent Publications

1. Suming Chen, Qiongqiong Wan and Abraham K. Badu-Tawiah “Picomole-Scale Real-Time Photoreaction Screening: Discovery of the Visible-Light-Promoted Dehydrogenation of Tetrahydroquinolines under Ambient Conditions” *Angew. Chem. Int. Ed.* **2016**, 55, 9345
2. Kathryn M. Davis and Abraham K. Badu-Tawiah “Direct and Efficient Dehydrogenation of Tetrahydroquinolines and Primary Amines using Ionic Wind Generated on Ambient Hydrophobic Paper Substrate” **submitted 2016**

# Probing Ion Solvation and Charge Transfer at Electrochemical Interfaces Using Nonlinear Soft X Ray Spectroscopy

L. Robert Baker

Department of Chemistry and Biochemistry, The Ohio State University, Columbus, OH 43210

[baker.2364@osu.edu](mailto:baker.2364@osu.edu)

## 1. Program Scope

Interfacial charge transfer at the electrode-electrolyte interface is a scientifically and technologically relevant chemical process that underlies the overall efficacy of batteries, photocatalytic systems, fuel cells, and solar-energy technology. To improve the efficiency of these important energy conversion applications requires a fundamental understanding of the interfacial electronic structure and the state-dependent charge transfer kinetics at the electrode–electrolyte interface. In many of these systems, kinetics are limited by the charge separation and injection at the electrode surface as mediated by exciton formation, charge transport, polaron formation and trapping as well as by structural reorganization of the redox-active species (i.e., solvent reorganization, surface restructuring). Additionally, other technologies such as batteries operate via the bias-driven charge transfer of *ions* across the interface between a solid electrode and liquid electrolyte. In these systems ion solvation and desolvation dynamics at the electrode–electrolyte interface largely control the kinetics of energy storage and release. Accordingly, the goal of this project is to probe charge carrier dynamics (i.e. both electrons and ions) with chemical state resolution and interface specificity in order to understand how surface electronic structure mediates interfacial charge transfer and energy conversion efficiency.

Toward this goal, we have constructed a tabletop ultrafast X-ray spectrometer with the capability to perform  $8.1^\circ$  near-grazing angle reflectivity with  $\sim 50$  fs time resolution, and in the near future non-linear, two-wave mixing of an optical and a soft X-ray laser pulse. Our instrument is the first of its kind to perform transient reflectivity measurements, where the strength of grazing angle reflectivity experiments is that it is sensitive to the near-surface region of condensed media. This instrument uses a high-harmonic generation (HHG) light source for the production of soft X-rays within the 30–100 eV range - a spectral window which has been shown to provide elemental, oxidation state, and spin state specificity for transition metal centers.<sup>1</sup> Coupling the chemical state resolution of soft X-rays with the surface specificity of near-grazing incidence reflectivity and (in the near future) second order nonlinear mixing allows us to probe the electronic structure of surface states and the near-surface region with ultrafast time resolution and chemical state resolution in electrochemically relevant systems.

In this progress report we describe the results of recent grazing-angle reflectivity studies we have conducted that show surface charge carrier dynamics in single crystal and polycrystalline hematite ( $\alpha$ -Fe<sub>2</sub>O<sub>3</sub>) films. Thermodynamically, hematite is a promising candidate for photoelectrocatalytic water oxidation due to its high earth abundance, near-optimum bandgap, which exhibits a high absorption cross-section within the visible spectrum, and valence band edge that lies below the oxidation potential of water.<sup>2-5</sup> Kinetically, however, high overpotentials are required to observe appreciable current densities for the water oxidation reaction (Figure 1) due in part to poor charge mobility within the catalyst. This has led to doping of the catalyst, primarily by Ni<sup>2+</sup>, to reduce the overpotential.<sup>2</sup> Spectroscopically, hematite serves as an excellent model system for our initial transient X-ray reflectivity studies as its surface charge carrier dynamics are poorly understood, and a surface-sensitive spectroscopic probe of the intrinsic charge transfer properties will be valuable for understanding how to improve the charge mobility of this system. Furthermore, unlike in recent transmission experiments which probed the *bulk* carrier dynamics of hematite, X-ray reflectivity

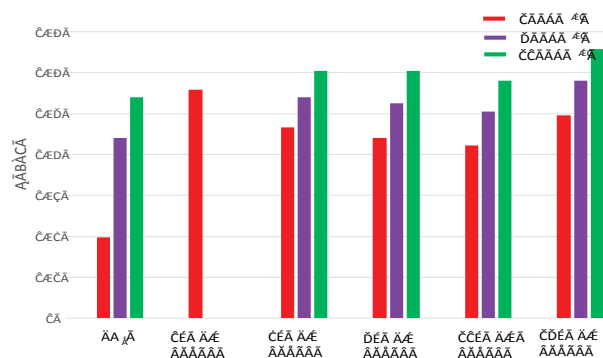


**Figure 1.** Overpotential for water oxidation at various current densities for pure Ni oxide and Ni-doped  $\alpha$ -Fe<sub>2</sub>O<sub>3</sub> at various Ni dopant concentrations

spectroscopy offers the strong advantage of surface sensitivity.<sup>6</sup>

## 2. Recent progress

This past year has seen the completion of the ultrafast X-ray spectrometer, and the successful collection of static and transient soft X-ray reflectivity spectra of hematite at near-grazing incidence angle ( $8.1^\circ$ ). A photograph of the instrument is given in Figure 2. Coherent X-ray pulses are prepared by HHG, whereby a pulsed 800 nm laser is focused onto a flowing stream of noble gas (i.e., argon, neon, or helium). Tunnel ionization of the gas within the intense electric field of the laser pulse leads to generation of a coherent X-ray beam. Two-color generation enables the production of both even and odd laser harmonics for collecting high-resolution spectra. Within our attainable spectral range (30–100 eV), the  $M_{2,3}$ -edge transition of the first row transition metals may be probed with element specificity.

Shown in Figure 3A are static X-ray reflectivity spectra for single crystal (red) and polycrystalline (blue) hematite. The single crystal sample shows two overlapping peaks with centers of 53.8 and 56.2 eV, whereas the polycrystalline sample shows a single well-defined peak at 56.8 eV and a low energy shoulder at  $\sim 53.8$  eV. Contrary to measurements made for transmission spectra, the smoothness of a surface plays a critical role in the overall outcome of the spectroscopic lineshape recorded in reflectivity as the angle-dependent interference between photons upon reflection, and the wavelength-dependent penetration depth of the electromagnetic radiation, can lead to a distortion relative to its transmission spectrum.<sup>7</sup> This distortion inherently arises due to competing effects in simultaneously measuring the real and imaginary parts of the refractive index.

Figures 3B and C show the transient reflectivity spectra for polycrystalline and single crystal hematite, respectively, for select time-points between 0 and 10 ps after photoexcitation with a 400 nm laser pulse. The time resolution in these measurements is 100 fs. In both samples, the initial excited state spectrum reveals a transient bleach observed at 56.6 and 55.8 eV for polycrystalline and single crystal samples, respectively. This transient bleach subsequently blue shifts by approximately 1 eV and a positive transient absorption feature at lower energy rises with a corresponding time constant. Fits of the transient data to a two-step kinetic model shows that the lifetime of the initial state for polycrystalline and single crystal hematite is 480 and 531 fs, respectively, and the lifetime of the second state is greater than the temporal window accessible by our instrument ( $\sim 500$  ps).

The extent to which it is possible to probe core-hole resonances in an X-ray reflection experiment, where the spectrum represents a convolution of both the real and imaginary components of the dielectric function, has been an ongoing question.<sup>8</sup> Of particular importance is to what extent absorptive loss of the reflected beam in the evanescent wave region imposes an absorption-like spectrum on the reflected intensity as well as how to treat line-shape distortions arising from the wavelength-dependent Fresnel factor in reflection. Both of these

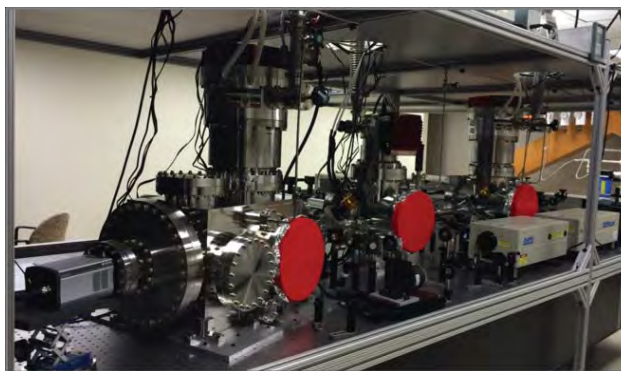


**Figure 2.** Home-built transient X-ray reflectivity spectrometer in the Baker group

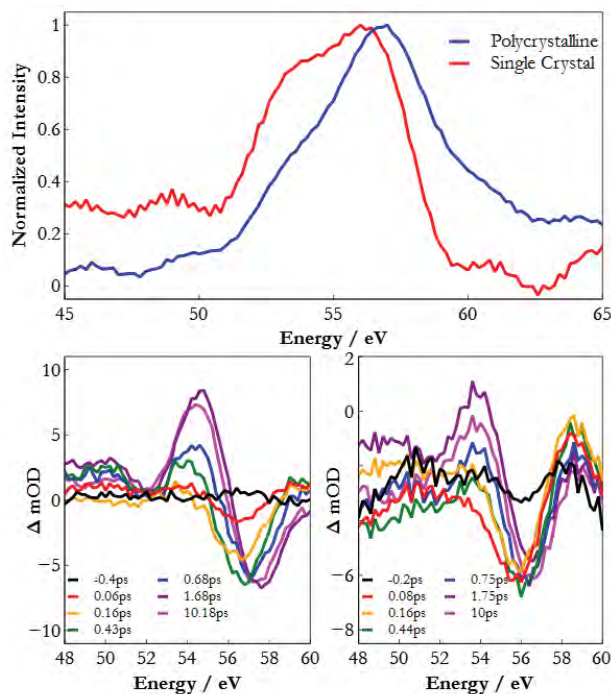


**Figure 3.** (A) Static soft X-ray reflectivity spectra of polycrystalline (blue) and single crystal (red) hematite. The transient reflectivity spectra for polycrystalline (B) and single crystal (C) are shown between 0 and 10 ps.

questions are critical for proper interpretation of ground state and transient spectral features in soft X-ray reflectivity spectroscopy. We have recently demonstrated that Kramers–Kronig transformation of a simulated absorption spectrum can qualitatively reproduce our spectral reflectivity results only when an appropriate term for absorptive loss is included (see Figure 4). These equations show that absorptive loss is significant, indicating that the X-ray reflectivity experiments are directly probing resonant core-hole excitations with interface specificity. Because these element specific core-hole resonances are extremely sensitive to oxidation state and local bonding structure of metal centers, which we now probe with surface specificity by near-grazing incidence reflectivity, full interpretation of these spectral kinetics is expected to provide detailed chemical insight into the charge transfer dynamics at the hematite surface.

One goal of this effort has been to develop a general method to convert the observed resonant absorption, which is nominally measured via the real part of the refractive index ( $n$ ), to a transmission spectrum, which is primarily a measure of the imaginary part of the refractive index ( $k$ ). Figure 4A shows a comparison between the reflectivity spectrum of single crystal hematite with the experimental transmission spectrum of  $\alpha$ -Fe<sub>2</sub>O<sub>3</sub>.<sup>6</sup> The latter can be readily obtained using CTM4XAS, a program which utilizes charge-transfer multiplet theory to simulate core-valence X-ray transitions.<sup>9</sup> Since spectral simulation is readily attainable in the form of a transmission spectrum, we have focused our efforts on the correct conversion of a resonant transmission spectrum into a reflectivity spectrum. In our modeling, we utilize the Kramers-Kronig relations to attain  $n$  and  $k$ . Once obtained, the Fresnel equation can be used to convert the complex refractive indices into a reflection spectrum. However, at a resonant absorption (i.e., a quantized transition), the real and imaginary parts of the refractive index change rapidly with the frequency of radiation (Figure 4B), and thus only approximate expressions for the Fresnel equation are obtained.

$$R = \frac{N^2 \cos(\theta) - \sqrt{N^2 - \sin^2(\theta)}}{N^2 \cos(\theta) + \sqrt{N^2 - \sin^2(\theta)}} \cdot \exp(-\beta d) \bar{A} \quad (1)$$

We find that qualitative agreement with experimental results is obtained upon modeling the spectrum with the Fresnel equation for a damped harmonic oscillator, scaled by the wavelength-dependent fraction of light absorbed (Equation 1). In Equation 1,  $R$  is the Fresnel coefficient,  $N$  is the complex refractive index ( $N = n + ik$ ),  $\theta$  is the incidence angle with respect to the surface normal,  $\beta$  is the attenuation length at  $\theta$ , and  $d$  is the penetration depth of the radiation. Here,  $d$  is our only adjustable parameter for which we empirically find that a value of 3–5 nm must be used to achieve qualitative agreement with the measured spectrum (see Figure 4C). We interpret the value of  $d$  as a measure of the average penetration depth of the X-ray beam in  $\alpha$ -Fe<sub>2</sub>O<sub>3</sub>, an observation, which confirms the near surface-sensitivity of these measurements. These early results confirm that we can selectively probe the charge transfer dynamics within the near-surface region of electrocatalytically relevant materials with oxidation state, coordination environment, and spin-state sensitivity on the femtosecond timescale.

### 3. Future directions

Our current progress has demonstrated that core-hole resonances can be probed with surface sensitivity on the ultrafast time scale using soft X-ray reflectivity in the 30–100 eV energy range. Work is ongoing to finalize the successful conversion of simulated transmission spectra to reflectivity in order to aid in the interpretation of

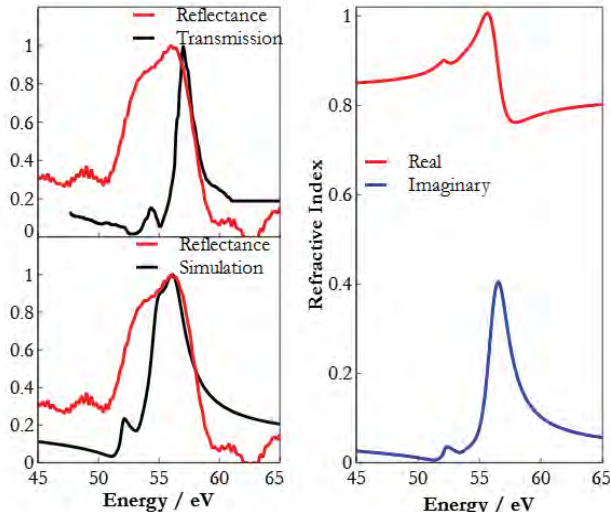


**Figure 4.** Transformation of the simulated transmission spectrum of  $\alpha$ -Fe<sub>2</sub>O<sub>3</sub> into a reflectance spectrum. (A) Comparison between experimental reflectance and transmission highlights the red-shift of the peak maximum measured in reflectance. (B) Kramers-Kronig conversion of a simulated transmission spectrum gives both the real (red) and imaginary (blue) refractive indices of hematite. (C) The reflectance simulation (black) is then obtained from  $n$  and  $k$  by Equation 1.

ground state and transient spectra in solid-state materials. This ability will enable us to utilize ultrafast soft X-ray reflectivity to investigate a number of other catalytically-relevant metal oxides, including NiO and Ni-doped Fe<sub>2</sub>O<sub>3</sub>, which important applications for efficient, low-cost water oxidation catalysis. Continued investigation of single crystalline and polycrystalline metal oxides will allow us to build a library on the reflectivity spectra of metal oxides, which will aid in the future analysis of more complex systems.

As shown above, we are currently probing carrier dynamics within an approximately 3–5 nm region of a surface, which provides us with near-surface sensitivity. However, we note that given the lattice constant for these materials, this probe depth still represents approximately ten or more atomic layers. To further improve surface sensitivity in these time-resolved experiments, we are working to develop soft X-ray SFG as a method for probing core-hole resonances with surface sensitivity. The goal of these experiments is to perform 2-wave mixing of soft X-ray pulse created by high harmonic generation (HHG) with an optical laser pulse and to use this process as a probe of surface electronic structure and charge carrier dynamics at a range of interfaces. This work will extend traditional sum frequency generation (SFG) spectroscopy from the infrared region to the XUV and soft x-ray spectral regions in order to probe core electron resonances with interface specificity. Soft X-ray SFG will provide surface-sensitive visualization of buried interfaces with detailed chemical and electronic state specificity. Using this method, we will extend our studies in surface-sensitive soft X-ray spectroscopy of carrier dynamics in hematite.

We are also currently in the process of fabricating a graphene working electrode deposited onto a spectroscopically transparent silicon nitride membrane. This will enable us to use soft X-ray reflectivity and SFG spectroscopy to probe the solvation dynamics of metal ions in an electrochemical double layer during bias-driven solvation and de-solvation that mediates ion adsorption onto the graphene surface. Using Fe<sup>2+</sup> ions suspended in water, we hypothesize that as we increase the applied negative bias at the graphene working electrode, diffusion of the ion to the electrode and the interfacial adsorption of the ion onto the electrode will both increase. This will lead not only to an increase in signal as a function of applied potential, but ion de-solvation dynamics will be readily apparent in these electrochemical experiments. Reversing the applied bias will lead to restoration of the ground state (i.e., 0 applied bias) of hydrated Fe<sup>2+</sup> and diffusion back into the bulk of the solution. Accordingly, development of this cell will enable *in operando* spectroelectrochemical characterization of ion dynamics in the electrochemical double layer in the soft X-ray spectral region.

#### 4. Publications

N/A

#### 5. References

1. K. Zhang, M.-F. Lin, E.S., Ryland, M.A. Verkamp, K. Benke, F.M.F. de Groot, G.S. Girolami, J. Vura-Weis, *J. Phys. Chem. Lett.*, 2016, 7, 3383-3387
2. D. Friebel, M.W. Louie, M. Bajdich, K.E. Sanwald, Y. Cai, A.M. Wise, M.,-J. Cheng, D. Sokaras, T.-C. Weng, R. Alonso-Mori, R.C. Davis, J.R. Barger, J.K. Nørskov, A. Nilsson, A.T. Bell, *J. Am. Chem. Soc.*, 2015, 137, 1305-1313
3. S. Klaus, M.W. Louie, L. Trotochaud, A.T. Bell, *J. Phys. Chem. C*, 2015, 119, 18303-18316
4. K. Sivula, R. van de Krol, *Nat. Rev. Mater.*, 2016, 1, 1-16
5. O. Zandi, T.W. Hamann, *Nat. Chem.*, 2016, 8, 778-783
6. J. Vura-Weis, C.-M. Jiang, C. Liu, H. Gao, J.M. Lucas, F.M.F. de Groot, P. Yang, A.P. Alivasatos, S.R. Leone, *J. Phys. Chem. Lett.*, 2013, 4, 3667-3671
7. D.L. Allara, A. Baca, C.A. Pryde, *Macromolecules*, 1978, 11, 1215-1220
8. R. Berlasso, C. Dallera, F. Borgatti, C. Vozzi, G. Sansone, S. Stagira, M. Nisoli, G. Ghiringhelli, P. Villorresi, L. Poletto, M. Pascolini, S. Nannarone, S. De Silvestri, L. Braicovich, *Phys. Rev. B*, 2006, 73, 115101-1-115101-5
9. E. Stavitski, F.M.F. de Groot, *Micron*, 2010, 41, 687-694

## Chemistry at the Advanced Light Source Using Soft X-ray Spectroscopy and Microscopy

Hendrik Bluhm, Mary K. Gilles, David K. Shuh, Musahid Ahmed

MS 6R-2100, 1 Cyclotron Rd, Berkeley, CA-94720

[HBluhm@lbl.gov](mailto:HBluhm@lbl.gov), [MKGilles@lbl.gov](mailto:MKGilles@lbl.gov), [DKShuh@lbl.gov](mailto:DKShuh@lbl.gov), [MAhmed@lbl.gov](mailto:MAhmed@lbl.gov)

### Program Scope

This scientific program focuses on the molecular-level investigation of interfaces under operating conditions. This is essential for developing a fundamental understanding of heterogeneous reactions at solid/vapor, solid/liquid, and liquid/vapor interfaces. Soft X-ray based ambient pressure X-ray photoelectron spectroscopy (APXPS) and scanning transmission X-ray microscope (STXM) are the main techniques that are used for these investigations. The high surface sensitivity of APXPS combined with tailored *in situ* cells enables the correlation of the surface chemistry of a solid or liquid with other reaction parameters (e.g., yield, conversion) for a wide variety of pressing problems, such as ion segregation at liquid surfaces, the heterogeneous chemistry of fuel cell electrodes, and ultrafast charge transfer across interfaces. STXM provides spatially-resolved molecular information on materials important for energy sciences and complements the APXPS investigations by expanding the probe depth and pressure range. The unique capabilities in this program enable cutting-edge research in *operando* interfacial chemistry across a wide range of areas of research, from alternative energy devices to aerosol chemistry. The PI's collaborate with scientists from Sandia National Laboratory (X-ray absorption flame measurements), Pacific Northwest National Laboratory (fundamental atmospheric chemistry) and Berkeley Laboratory (chemical catalysis, X-ray spectroscopy of liquids and electrolytes, photosynthetic systems, and time-resolved X-ray spectroscopy).

### Progress Report

**Interface Chemistry Studied With Soft X-ray Spectroscopy.** The program focuses on the investigation of solid/vapor (including ice/vapor) and liquid/vapor interfaces under operating conditions of gas pressure and composition, temperature, electrical bias, and other parameters relevant to heterogeneous catalysis, electrochemistry, energy generation and environmental and atmospheric science. Interfaces of interest are shown in Fig. 1, here illustrated on the example of aqueous interfaces, which are ubiquitous in nature and technology. Processes at aqueous interfaces are paramount to the understanding of the most challenging questions in, e.g., atmospheric science, geochemistry, electrochemistry, and corrosion, yet our knowledge of their fundamental physical chemistry is very limited compared to that of solid surfaces. The program addresses these and related scientific questions and technical challenges through innovative technological approaches and the development of new experimental capabilities and strategies, in collaboration with a diverse range of leaders in interface science, including heterogeneous catalysis (Salmeron), ultrafast charge-transfer processes at interfaces (Gessner, Cuk), physical chemistry of liquid/vapor interfaces (Wilson, Saykally), heterogeneous reactions on model atmospheric aerosols (Wilson), and heterogeneous chemistry of liquid/solid interfaces (Salmeron, Gessner). In the following a specific examples for interface studies are provided.

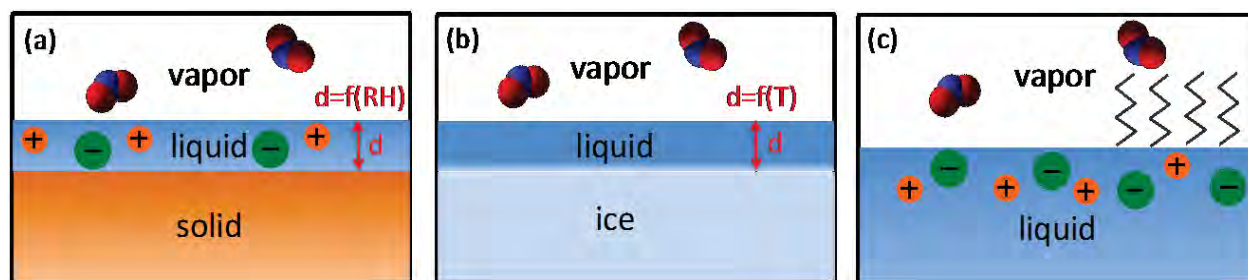


**Figure 1.** Schematic illustrating interfaces explored in this program, ranging from solid/vapor (including ice/vapor) to liquid/vapor.

**Reaction of Water Vapor with Vanadium.** The interaction of water vapor with metals drives atmospheric corrosion reactions and is of great technological importance. We have studied the reaction of water vapor with a polycrystalline vanadium surface using APXPS under isobaric conditions at  $p(\text{H}_2\text{O})$  ranging from 0.01 to 0.50 Torr and temperatures from 625 K to 260 K, i.e. up to a relative humidity (RH) of ~15%. Water vapor exposure leads to oxidation and hydroxylation of the vanadium foil already at a pressure of  $10^{-6}$  Torr at 300 K (RH ~  $4 \times 10^{-6}$  %). The vanadium oxide layer on the surface has a stoichiometry of  $\text{V}_2\text{O}_3$ . Initial adsorption of molecular water on the surface is observed at RH > 0.001%. Above a RH of 0.5% the amount of adsorbed water increases markedly. Experiments at increasing temperatures show that the water adsorption process is reversible. Depth profile measurements show a thickness for the vanadium oxide layer of 3–5 monolayers (ML) and for vanadium hydroxide of 1–1.5 ML over the whole RH range in the isobar experiments. The thickness of the adsorbed water layer was found to be in the sub-ML range for the investigated RH's.

**Adsorption of 2-propanol on Ice.** The interaction of 2-propanol with ice was examined by APXPS to investigate whether the molecule adsorbs intact or dissociates. Isothermal uptake experiments were performed on vapor deposited ice at 227 K in the presence of the equilibrium water vapor pressure of 0.05 Torr and 2-propanol partial pressures ranging from  $5 \times 10^{-5}$  to  $2 \times 10^{-3}$  Torr. The C 1s APXPS spectra of adsorbed 2-propanol show two characteristic peaks associated with the alcohol group and methyl groups in a 1:2 ratio, respectively. Coverage increased with 2-propanol partial pressure and followed first order Langmuir kinetics with a Langmuir constant of  $K = 6300 \text{ Torr}^{-1}$ . The 1:2 ratio of  $\text{C}_{\text{OH}}:\text{C}_{\text{Me}}$  remained constant with increasing coverage, indicating that there is no chemical reaction upon adsorption. The observed Langmuir kinetics using APXPS is consistent with previous observations of other small chain alcohols via indirect adsorption methods using, e.g., Knudsen cell and coated wall flow tube reactors.

**Proxies for Sea Salt Aerosol Aging.** Chloride displacement reactions occur in sea salt aerosol produced by wave action in the ocean when strong atmospheric acids (i.e. nitric & sulfuric acid) condense onto particles during transport. Previously, we reported that much weaker organic acids can also result in chloride depletion via hydration/dehydration cycling. To explore the impact of phase, these experiments were extended to quantify the reactions of liquid-like and semi-solid secondary organic carbon (SOC) generated from ozonolysis of limonene (LSOC) and  $\alpha$ -pinene (PSOC) with NaCl. Micro-spectroscopic analyses showed chloride depletion in the condensed phase, release of gaseous HCl, and formation of organic salts. Analogous reactions also occur in mixed SOC/ $\text{NaNO}_3$  particles. An increase in the organic mass fraction in the internally mixed SOC/NaCl particles leads to higher chloride depletion. The reaction extent depends on SOC composition, particle phase state and viscosity, mixing state, temperature, relative humidity and reaction time. The formation of organic salts from these overlooked reactions can change a particle's physicochemical properties and may affect its reactivity and ability to serve as cloud condensation and ice nuclei. The release and potential recycling of HCl and  $\text{HNO}_3$  from reacted aerosol particles may have important implications for atmospheric chemistry.

**Water Vapor Uptake Effects on Bonding, Viscosity, and Phase.** Atmospheric aerosols can undergo phase transitions including liquid–liquid phase separation as a response to changes in ambient relative humidity. In the atmosphere, mixtures of salts and secondary organics are common and understanding their mixing behavior as a function of relative humidity is essential to predict bulk and surface composition. Laboratory surrogates of ammonium sulfate (AS) mixed with either a) limonene secondary organic carbon (LSOC), b) 4-dihydroxy-3-methoxybenzeneacetic acid (HMMA), or c) polyethylene glycol 400 (PEG 400) aerosols were examined over the RH range of 4%-99%. In situ chemical imaging experiments using STXM showed that all of these mixtures formed core-shell structures. In all cases, the ammonium sulfate dominated the core composition and the lower surface tension component, the organic, was presently largely in the shell at all relative humidities above deliquescence. Chemical imaging with STXM showed that both LSOC/AS and HMMA/AS particles never homogeneously mixed at relative humidities above the deliquescence point. While the majority of the organic component was located in the shell there was also substantial inorganic present in the shell. The shell composition was estimated as

65:35 organic: inorganic in LSOC/AS and as 50:50 organic: inorganic for HMMA/AS. In contrast, PEG-400/AS particles were fully homogeneous mixtures at high relative humidities and phase separated at ~ 90% relative humidity with an estimated 70:30% organic to inorganic mix in the outer phase. These studies indicate the potential for in situ analysis of the hygroscopic behavior, phase separation, and measuring the core and shell composition of aerosol particles.

### **Proposed Work**

***Chemical Reactions at Aqueous Solution/Vapor Interfaces.*** The properties of liquid/vapor interfaces strongly influence the abundance and reactivity of trace gas molecules that are important for many heterogeneous processes in atmospheric and environmental chemistry. To date, little is known about the concentration of solution phase species at the liquid/vapor interface, which can significantly differ from the bulk solution concentration and is an important quantity in the modeling of heterogeneous reactions at liquid/vapor interfaces. These open questions will be addressed by developing new methods to study the surface and subsurface chemistry of liquid/vapor interfaces with the same level of detail and control as in the case for solid/vapor interfaces. At the heart of the experiments is the correlation between bulk chemical composition, surface chemical composition, and gas phase composition under reaction conditions, where some of the reaction parameters are: time, bulk liquid composition at the beginning of the experiment, gas phase composition, UV irradiation, and liquid temperature. The basic concept is to use APXPS and partial electron yield (PEY) NEXAFS for surface measurements, and X-ray emission spectroscopy (XES) as well as fluorescence yield (FY) NEXAFS to investigate the bulk composition. Using droplet trains reactions can be studied on the microsecond time scale, while for slower reactions static droplets will be investigated, either deposited on an unreactive substrate or suspended in an optical or acoustic trap. One of the first experiments will address the uptake of SO<sub>2</sub> by water as a function of pH, an important problem in environmental science.

***Water Vapor Uptake Effects on Bonding, Viscosity and Phase.*** Understanding how bonding and viscosity change as a function of evaporative loss and relative humidity is essential for predicting partitioning of semi-volatile organic compounds in atmospheric aerosols between the aerosol and the surrounding vapor. Historically, models assumed liquid phase aerosols with rapid mass transport. However, recent observations indicate that organic atmospheric aerosols may be liquid, semisolid or even solid under some atmospheric temperatures and relative humidities depending upon the gas phase precursors. Current debate focuses on whether viscosities might be high enough and consequently diffusivities low enough that under some conditions mass transfer shifts from facile to kinetically limited. If aerosols are solid or semi solid the uptake and release rates of semi-volatile organics may be slowed enough to hinder equilibrium on timescales relevant for atmospheric processes. The mass liabilities of films of secondary organic material (representative of atmospheric secondary organic material) generated via oxidation of gas phase precursors will be determined by measurements of evaporation rates and vapor mass concentrations. Changes in chemical composition, with a focus on C:O ratios will be determined using a range of soft x-ray spectroscopies. By probing these as a function of relative humidity, mass loss rates can be determined and resulting changes in effective diffusion rates estimated.

***Metal Ion Coordination Complexes and Clusters: Developing and Exploring the Continuum from Gas-Phase to Bulk Solution Chemistry.*** The fundamental chemistry of metal ions in solution is central to technological, environmental, and biological processes. Efforts to understand solution properties of metal ions suffer from complexities introduced by inner-sphere solvation and coordination, and interactions with outer-sphere molecules and ions. An effective approach for probing interactions in metal ion complexes is soft X-ray absorption spectroscopy (XAS) at core levels of light atoms (C, N, O) in coordinating ligands and of the metal ions. The objective is to explore metal ion coordination chemistry from solution and gas-phase perspectives, using solution XAS and gas-phase VUV/soft X-ray spectroscopies to understand metal ion chemistry in solutions using the special core-level XAS spectromicroscopy at the Molecular Environmental Sciences Beamline at the ALS. This will be accomplished by studying bonding in systems that span a range of complexity from gas-phase systems

that can be modeled, to bulk solutions where a multitude of interactions with solvent molecules, coordinating ligands, and counter-ions need to be considered. Bridging dimensionality from gas-phase to bulk solution, the research will provide new insights into solution chemistry of metal ions based on a bottom-up approach that incrementally introduces complexity, ultimately describing metal ions in realistic solutions. Initial efforts will also conduct simpler, VUV photoionization studies of selected metal ion systems using the capabilities of the Chemical Dynamics Beamline at the ALS. The proposed metal ion solution coordination research program links strongly to LBNL CPIMS size-selected metal ion cluster research and has a future objective to develop and conduct metal ion near-edge X-ray absorption via action spectroscopy with the new ion trap mass spectrometer. This research will incorporate an essential collaborative theoretical component with D. Prendergast (LBNL) and other theorists within the LBNL program. Experimental efforts will complement those of Saykally (UC-Berkeley/LBNL).

### Publications (2015 to date)

1. Arion, T., et al.: Appl. Phys. Lett. **2015**, 106. Artn 121602, Doi 10.1063/1.4916278
2. Björneholm, O., et al.: Chem. Rev. **2016**, 116, 7698. Doi 10.1021/acs.chemrev.6b00045
3. Bonifacio, C.S., et al.: Chemistry of Materials **2016**, 27, 6960. Doi 10.1021/acs.chemmater.5b01862
4. Carencio, S., et al.: J. Phys. Chem. C **2016**, 120, 15354. Doi 10.1021/acs.jpcc.6b06313
5. Carencio, S., et al.: Small **2015**, 11, 3045. Doi 10.1002/sml.201402795
6. Crumlin, E.J., et al.: J. Electr. Spectrosc. Rel. Phenom. **2016**, 200, 264. Doi 10.1016/j.elspec.2015.06.008
7. Dong, A. Y., et al.: Surface Science **2015**, 634, 37. Doi 10.1016/j.susc.2014.10.008
8. Eren, B., et al.: J. Am. Chem. Soc. **2015**, 137, 11186. Doi 10.1021/jacs.5b07451
9. Eren, B., et al.: J. Phys. Chem. C **2015**, 119, 14669. Doi 10.1021/jp512831f
10. Eren, B., et al.: Science **2016**, 351, 475. Doi 10.1126/science.aad8868
11. Head, A.R., et al.: Ref. Mod. in Chem., Mol. Sci. and Chem. Eng. **2016**, Doi 10.1016/B978-0-12-409547-2.10924-2
12. Hiltunen, T., et al.: Phys. Rev. B **2015**, 91. Artn 075301, Doi 10.1103/Physrevb.91.075301
13. Jovic, V., et al.: J. Mater. Chem. A **2016**, 3, 23743. Doi 10.1039/c5ta07898a
14. Karslioglu, O., et al.: Faraday Discuss. **2015**, 180, 35. Doi 10.1039/c5fd00003c
15. Lampimaki, M., et al.: J. Phys. Chem. C **2015**, 119, 7076. Doi 10.1021/jp511340n
16. Laskin, A., et al.: Annu Rev Anal Chem **2016**, 9, 117. 10.1146/annurev-anchem-071015-041521
17. Liu, Z., et al.: In: J. Woicik (Ed.), Hard X-ray Photoelectron Spectroscopy (HAXPES), Springer Series in Surface Sciences, **2016**, Vol. 59, pp. 447. Doi 10.1007/978-3-319-24043-5\_17
18. Mehl, S., et al.: Phys. Rev. B **2015**, 91. Artn 085419, Doi 10.1103/Physrevb.91.085419
19. Mueller, D. N., et al.: Nat. Comm. **2015**, 6. Artn 6097, Doi 10.1038/Ncomms7097
20. Neppel, S., et al.: In: K. Yamanouchi et al. (eds.), Ultrafast Phenomena XIX, Springer Proceedings in Physics **2016**, 162, 325. Doi 10.1007/978-3-319-13242-6\_79
21. Newberg, J.T., et al.: Phys. Chem. Chem. Phys. **2016**, 17, 23554. DOI 10.1039/c5cp03821a
22. Ng, M. L., et al.: ChemPhysChem. **2015**, 16, 923. Doi 10.1002/cphc.201500031
23. Nijem, N., et al.: Cryst. Growth Des. **2015**, 15, 2948. Doi 10.1021/acs.cgd.5b00384
24. Nijem, N., et al.: J. Phys. Chem. C **2016**, 119, 24781. Doi 10.1021/acs.jpcc.5b05716
25. O'Brien, R. E., et al.: Environ. Sci. Technol. **2015**, 49, 4995. Doi 10.1021/acs.est.5b00062
26. Oded, M., et al.: Soft Matter **2016**, 12, 4595. 10.1039/c6sm00381h
27. Oded, M., et al.: Polymer **2016**, *available on line*. DOI: 10.1016/j.polymer.2016.07.016
28. Rameshan, C., et al.: Surface Science **2015**, 641, 141. Doi 10.1016/j.susc.2015.06.004
29. Stoerzinger, K. A., et al.: J. Phys. Chem. C **2015**, 119, 18504. Doi 10.1021/acs.jpcc.5b06621
30. Stoerzinger, K.A., et al.: Acc. Chem. Res. **2016**, 48, 2976. Doi 10.1021/acs.accounts.5b00275
31. Szymanski, C. J., et al.: Biomaterials **2014**, 62, 147. 10.1016/j.biomaterials.2015.05.042
32. Wang, B. B., et al.: J. Phys. Chem. A **2015**, 119, 4498. Doi 10.1021/jp510336q
33. Wei, M. M., et al.: J. Phys. Chem. C **2015**, 119, 13590. Doi 10.1021/acs.jpcc.5b01395
34. Wang, B. B., et al.: J. Phys. Chem. A **2015**, 119, 4498. 10.1021/jp510336q
35. Weatherup, R.S., et al.: J. Phys. Chem. Lett. **2016**, 7, 1622. Doi 10.1021/acs.jpcl.6b00640
36. Yang, Y., et al.: Nano Res. **2015**, 8, 227. Doi 10.1007/s12274-014-0639-0

# Surface Chemical Dynamics

N. Camillone III and M. G. White

Brookhaven National Laboratory, Chemistry Department, Building 555, Upton, NY 11973

([nicholas@bnl.gov](mailto:nicholas@bnl.gov), [mgwhite@bnl.gov](mailto:mgwhite@bnl.gov))

## 1. Program Scope

This program focuses on fundamental investigations of the dynamics, energetics and morphology-dependence of thermal and photoinduced reactions on planar and nanostructured surfaces that play key roles in energy-related catalysis and photocatalysis. Laser pump-probe methods are used to investigate the dynamics of interfacial charge and energy transfer that lead to adsorbate reaction on metal and metal oxide surfaces. State- and energy-resolved measurements of the gas-phase products are used to infer the dynamics of product formation and desorption. Time-resolved correlation techniques follow surface reactions in real time and are used to infer the dynamics of adsorbate–substrate energy transfer. Measurement of the interfacial electronic structure is used to investigate the impact of adsorbate-surface and cluster-support interactions on the activity of thermal and photoinduced reactions. Capabilities to synthesize and investigate the surface chemical dynamics of arrays of supported metal nanoparticles (NPs) on oxide surfaces include the deposition of size-selected gas-phase clusters as well as solution-phase synthesis and deposition of narrow-size-distribution nanometer-scale particles.

## 2. Recent Progress

**Ultrafast Investigations of Interfacial Energy Transfer.** Towards our ultimate goal of following surface chemical transformations in real time, we investigate the dynamics of substrate–adsorbate energy transfer between metal surfaces and simple adsorbates such as CO, O<sub>2</sub>, and O atoms. We use short (~100-fs) near-IR laser pulses, absorbed only by the metal, to inject energy into the system at a well-defined point in time. The short pulses drive a strong electronic excitation of the substrate that in turn can drive adsorbate motion by energy transfer mediated by electrons and phonons.

We are currently working to understand the relationship between surface structure and the energy transfer dynamics. Whereas the structure–function relationship has been long appreciated, very little is known about the underlying structure–dynamics relationship. By varying the adsorbate coverage and composition, we aim to investigate links between structure—viz. adsorption site, proximity to coadsorbates, chemical identity of coadsorbates, and substrate size at the nanoscale—and the dynamics.

Our measurements and simulations of the coverage dependence of energy transfer dynamics in CO desorption from the (111) surface of palladium have revealed both a binding-site dependence and the influence of lateral adsorbate interactions on the energy-transfer timescale. We used coverage as a means for adsorption-site control: with increasing coverage the adsorption-site population shifts from all three-fold hollow (3fh) (up to 0.33 ML), to bridge and near bridge (>0.5–0.6 ML) and finally to mixed 3fh plus top site (at saturation at 0.75 ML). We find that this progression of binding-site motifs is accompanied by two remarkable features in the ultrafast photoinduced desorption:

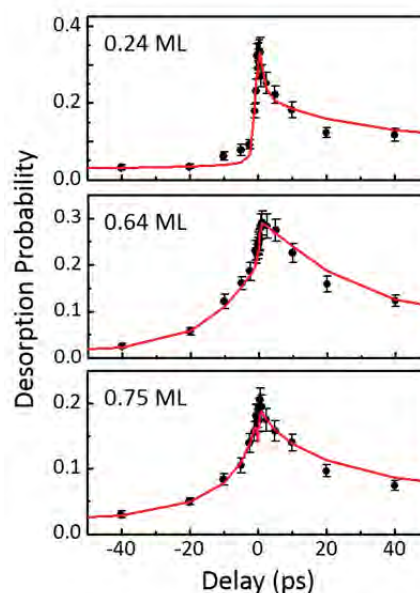


**FIG. 1.** Two-pulse correlation measurements at coverages of 0.24, 0.64 and 0.75 ML. The CO desorption probability was measured as a function of delay between two incident pulses, where positive delay indicates that the more weakly-absorbed (s-polarized) pulse arrives before the more strongly-absorbed (p-polarized) pulse. The lines are simulations using a temperature-dependent electronic friction to describe the energy transfer.

(i) the desorption probability increases roughly two orders magnitude, and (ii) the adsorbate–substrate energy transfer rate observed in two-pulse correlation experiments varies nonmonotonically, having a minimum at intermediate coverages. Frictional-coupling simulations (Fig. 1) indicate that these features are consistent with an adsorption-site dependent electron-mediated energy coupling strength,  $\eta_{el}$ , that decreases with binding site in the order: 3fh > bridge and near bridge > top site. This weakening of  $\eta_{el}$  largely counterbalances the decrease in the desorption activation energy that accompanies this progression of adsorption-site motifs, moderating what would otherwise be a rise of several orders of magnitude in the desorption probability. Significantly, within this framework interadsorbate energy transfer from the copopulation of molecules bound in 3fhs to their top-site neighbors is needed to account for the observed energy transfer rate enhancement at saturation coverage.

In addition, we have found that substituting oxygen atoms for CO at the most tightly-bound sites in the saturation coverage adlayer enhances the desorption probability by an additional factor of 2–3, and also enhances the energy transfer rate by a factor of  $\sim 2$ . Together these enhancements suggest both a static lowering of the potential energy barrier to desorption for the CO at 3fh sites, as well as an interadsorbate energy transfer between the O atoms and CO at both top and 3fh sites. We are developing coupling models to quantify these factors.

In laying the groundwork for the coverage-dependent photoinduced desorption experiments, we surveyed the coverage-dependent structural phases of CO/Pd(111). This led to the discovery of a previously unreported structural phase that has implications for the overall phase diagram of this system. The new phase is a  $c(16\times 2)$  structure comprised of stripes of the saturated  $(2\times 2)$  structure separated by antiphase domain boundaries consisting of top-site vacancies (Fig. 2). DFT calculations in collaboration with P. Liu and Z. Liu (BNL, *Catalysis: Reactivity and Structure* program) show that though the CO prefers high-symmetry sites, the structure incorporates small displacements near the domain boundary of  $\sim 0.2$  Å, approximately 6% the CO–CO nearest neighbor distance, that relieve steric strain. The low-density vacancy-site domain boundary structure is distinct from the high-density  $(1\times 1)$  bridge-site domain boundary structure found at lower coverage, but extrapolation of both of these to the 0.5-ML limit results in a  $c(4\times 2)$  lattice, albeit with distinct bases. These bases have been observed to coexist in real-space imaging at 0.5 ML by other groups.

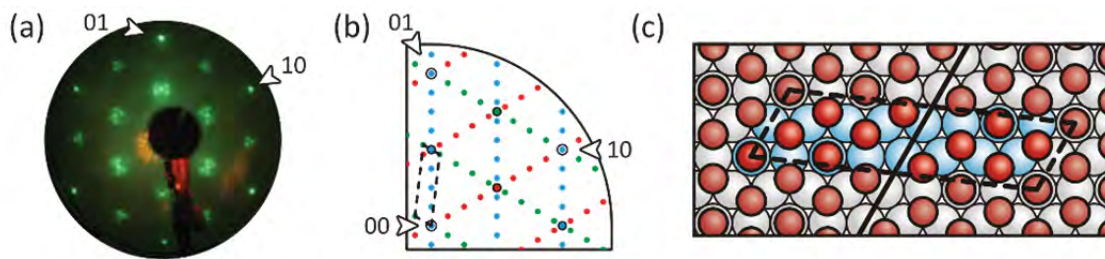


**FIG. 2.** (a) LEED pattern for 0.6875 ML CO/Pd(111). (b) Upper right-hand quadrant of reciprocal space with diffraction spots from the substrate,  $(2\times 2)$  mesh, and all three possible orientations of the  $c(16\times 2)$  mesh. One  $c(16\times 2)$  unit mesh is indicated by dashed lines. (c) Real space  $c(16\times 2)$  adlayer mesh. The primitive unit mesh and the antiphase domain boundary are marked by dashed and solid black lines, respectively.

**Interfacial Electronic Structure of Supported Clusters.** Charge transfer at the metal–support interface can play an important role in determining the chemical properties of supported catalysts, especially for reducible oxides which have the capacity to accept or donate charge through changes in cation oxidation state, e.g.,  $\text{Ti}^{4+} \leftrightarrow \text{Ti}^{3+}$ , and formation of oxygen vacancies. Our recent work has focused on interfacial electron transfer of “inverse” catalysts prepared by size-selected deposition of different transition metal oxide clusters  $\text{M}_x\text{O}_y$  ( $\text{M} = \text{Ti}, \text{Mo}, \text{Nb}, \text{W}$ ) on Cu(111) and  $\text{Cu}_2\text{O}/\text{Cu}(111)$  surfaces. Inverse catalysts involving reducible oxides have been shown to be particularly active for the water-gas-shift reaction, which is important for the production of clean hydrogen ( $\text{CO} + \text{H}_2\text{O} \rightarrow \text{CO}_2 + \text{H}_2$ ). The high activity is

associated with the formation of oxygen vacancies in the oxide which are stabilized by Cu→oxide electron transfer. In our work, electron transfer is probed by two-photon photoemission (2PPE) measurements of the surface work function ( $\Phi$ ) as a function of cluster coverage, from which the surface dipole can be derived. Surface dipoles are characteristic of the specific cluster–support interface and include contributions from electron transfer, as well as cluster structure or surface deformations induced by cluster binding. The results show that electron transfer on both Cu(111) and a Cu<sub>2</sub>O thin film is strongly influenced by cluster stoichiometry and generally follows the order Mo, W > Ti > Nb for both the oxidized and reduced clusters. As illustrated in Fig. 3, the measured work-function shifts are generally much greater on Cu<sub>2</sub>O than on Cu(111). DFT calculations suggest this is largely due to structural deformations of the oxide cluster and the Cu<sub>2</sub>O thin film resulting from the formation of cation-oxygen bonds at the interface. Future studies will investigate the possibility of modifying electron transfer to the cluster by changing the thickness of thin film oxide layer grown on a metal substrate.

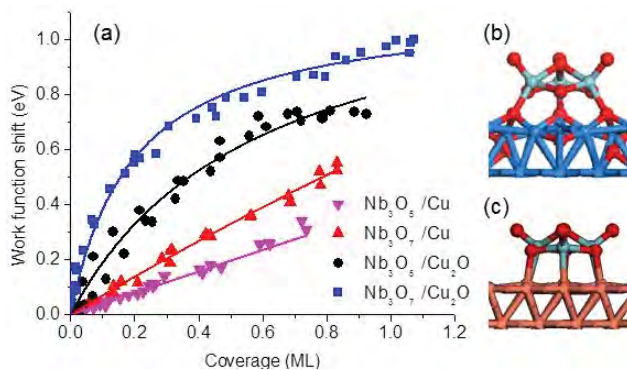


**FIG. 3.** (a) Experimental work function shifts for Nb<sub>3</sub>O<sub>5</sub> and Nb<sub>3</sub>O<sub>7</sub> deposited on Cu(111) and Cu<sub>2</sub>O/Cu(111) surfaces; DFT optimized structures for the Nb<sub>3</sub>O<sub>7</sub> cluster on (b) Cu<sub>2</sub>O/Cu(111) and (c) Cu(111). The measured surface dipoles are -0.84 D and -6.1 D for Nb<sub>3</sub>O<sub>7</sub> on Cu<sub>2</sub>O/Cu(111) and Cu(111) respectively.

**Pump-Probe Studies of Photodesorption and Photooxidation on TiO<sub>2</sub>(110) Surfaces.** A number of studies by Henderson and coworkers (PNNL) have shown that the yields of photoproducts from the UV photooxidation of aldehydes and ketones on TiO<sub>2</sub>(110) are strongly enhanced by the presence of co-adsorbed oxygen. For acetone, the co-adsorbed oxygen leads to the formation of a photoactive acetone-oxygen complex whose existence has been confirmed by a number of experimental and theoretical investigations. The question remains as to why the ketone-oxygen complexes are more photoactive than the adsorbed ketone alone or the surface-bound acetate product that results from the carrier-induced fragmentation process. To address this issue, we recently performed methyl photoyield measurements for a number of ketone molecules—acetaldehyde, acetone, 2-butanone, 2-propanone, acetophenone and trifluoroacetone (TFA)—with and without co-adsorbed oxygen. These molecules are all expected to form oxygen complexes when co-adsorbed with oxygen. As shown in Fig. 4, the measured oxygen

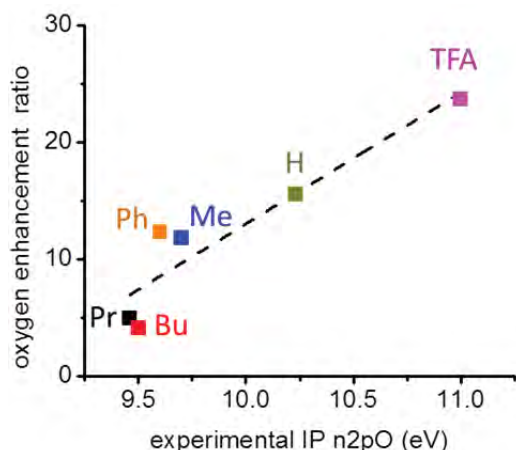


**FIG. 4.** Correlation between the measured oxygen enhancements versus the  $2p_0$  ionization energy of the gas-phase molecules. Pr = 2-pentanone, Bu = 2-butanone, Ph = acetophenone, Me = acetone. H = acetaldehyde, TFA = trifluoroacetic acid.

enhancements of the methyl photoyield varies in a systematic way that correlates with the ionization potentials (IPs) of the  $n(2p_0)$  HOMO of the gas-phase molecules. This correlation suggests that the energy of the HOMO level of the adsorbed molecule relative to the valence band maximum (VBM) of TiO<sub>2</sub> follows the order of the gas-phase IPs, i.e., the TFA HOMO (highest IP) lies furthest below the VBM while butanone and pentanone (lowest IPs) have HOMO levels that lie the closest. Since photoactivity is presumed to involve resonant electron transfer from hybridized HOMO levels of the adsorbate to thermalized holes at the VBM, it would be expected that TFA is the least photoactive as a bare molecule and shows the largest enhancement in photoactivity when converted to the TFA-oxygen complex. The reverse arguments would apply to butanone and pentanone. These results suggest that the main effect of the ketone-diolate formation is to shift

hybridized molecular HOMO levels closer to the VBM, which results in more efficient electron transfer and higher photoactivity. Additional experimental and theoretical work is in progress to more fully explore the orbital-band alignments in these systems.

### 3. Future Plans

Our planned work develops three interlinked themes: (i) the chemistry of supported nanoparticles (NPs) and nanoclusters (NCs), (ii) the exploration of chemical dynamics on ultrafast timescales, and (iii) the photoinduced chemistry of molecular adsorbates. The investigations are motivated by the fundamental need to connect chemical reactivity to chemical dynamics in systems of relevance to catalytic processes—in particular metal and metal-compound NPs and NCs supported on oxide substrates. They are also motivated by fundamental questions of physical changes in the electronic and phononic structure of NPs and their coupling to adsorbates, and to the nonmetallic support, that may alter dynamics associated with energy flow and reactive processes.

Future investigations of interfacial energy transfer will involve oxide-supported metal NP substrates (e.g. Pd/TiO<sub>2</sub>(110)) and focus on NP size-dependent studies of the fundamental changes in surface reaction kinetics and dynamics that accompany reduction in the size of the metal substrate from macroscopic to the nanoscale. Future work in surface photochemistry using pump-probe techniques will continue to explore mechanistic aspects of semiconductor photoreactions, including ultrafast time-resolved studies of photodissociation and photooxidation. New studies in size-selected clusters will focus on oxide nanoclusters deposited onto single crystal (e.g., TiO<sub>2</sub>(110)) and thin film metal oxide (e.g., MgO) supports to explore cluster-support electronic interactions that can provide a basis for understanding and “tuning” interfacial electron transfer and reactivity.

#### DOE-Sponsored Research Publications (2014–2016)

Adlayer Structure Dependent Ultrafast Desorption Dynamics in Carbon Monoxide Adsorbed on Pd(111), S.-Y. Hong, P. Xu, N.R. Camillone, M.G. White, and N. Camillone III, *J. Chem. Phys.* **145**, 014704 (2016).

Understanding the Interactions of CO<sub>2</sub> with Doped and Undoped SrTiO<sub>3</sub>, Q. Wu, J. Cen, K.R. Goodman, M.G. White and A. Orlov, *ChemSusChem*, **9**, 1889–1897 (2016).

Characterization of One-Dimensional Molecular Chains of 4,4'-Biphenyl Diisocyanide on Au(111) by Scanning Tunneling Microscopy, J. Zhou, Y. Li, P. Zahl, P. Sutter, D. J. Stacchiola and M. G. White, *J. Chem. Phys.* **142**, 101901 (2015).

Surface Dipoles and Electron Transfer at the Metal Oxide-Metal Interface: A 2PPE Study of Size-Selected Metal Oxide Clusters Supported on Cu(111), Y. Yang, J. Zhou, M. Nakayama, L. Nie, P. Liu and M. G. White, *J. Phys. Chem. C*, **118**, 13697–13706 (2014).<sup>1</sup>

<sup>1</sup>This paper includes contributions from personnel funded by BES-CSGB-Catalysis Science (FWP-CO-040).

## Charge and Molecular Dynamics at Heterogeneous Interfaces

Tanja Cuk ([TCuk@lbl.gov](mailto:TCuk@lbl.gov)), Charles Harris ([CBHarris@lbl.gov](mailto:CBHarris@lbl.gov)),  
and David Chandler ([chandler@berkeley.edu](mailto:chandler@berkeley.edu))

Lawrence Berkeley National Laboratory, Chemical Sciences Division  
1 Cyclotron Road, Berkeley CA 94720

**Program Scope.** One of the greatest challenges in the design of heterogeneous chemical technologies is the limited fundamental understanding of how interfacial properties at solid-liquid and solid-adsorbate interfaces guide the transfer and reorganization of charge. The central research question is to determine how molecules influence charge dynamics at interfaces, and conversely, how these charge dynamics induce molecular changes. Research often targets separately the delocalized charge in the solid and the localized charge in adsorbates or solvated ions. Experimental and theoretical methodologies that target both actors on the same footing are needed to causally link the two sides of the interface. In this program, a range of transient spectroscopic techniques dynamically follow charge transfer from the perspective of charges leaving the solid side, the rise and decay of intermediate molecular species bound from the liquid/adsorbate side, and the purely interfacial electronic states that cannot be thought of distinctly as one or the other. From the theoretical side, molecular dynamics simulations follow the charge reorganizations that accompany this charge transfer and lead to time scales ranging from picoseconds to microseconds.

### Recent Progress and Future Work.

#### *Observing Molecular Dynamics of Catalysis at Solid-Liquid Interfaces*

The Cuk lab leads an effort in observing the molecular dynamics of catalysis at the solid-liquid interface by merging multi-color, ultrafast transient (optical & mid-infrared) spectroscopy with photo-electrochemistry of the water oxidation reaction. In the last year of the Cuk lab, three advances came to fruition regarding the catalytic intermediates required to form the first bond of the water oxidation cycle (e.g., O-O), or those that are nascent upon charge transformation at the catalytic surface. The first advance is the detection of the oxyl radical ( $\text{Ti-O}^\bullet$ ) by its unique, sub-surface vibration at the n-SrTiO<sub>3</sub>/aqueous interface using ultrafast mid-infrared spectroscopy and theory (in-collaboration). The oxyl's vibration couples to water librations, which means that it excites H-bond breaking events requisite for bond formation; this important, dynamic interaction between a catalytic intermediate and reactants had yet to be observed. The interaction is demonstrated by the analysis of the Fano resonance, which describes a discrete mode coupled to a broad spectral continuum. The resonance provides a distinctive matrix element of a vibration situated at the solid-liquid interface, through the vibration's coupling to both the electronic degrees of freedom in the solid (plasmons) and the vibrational degrees of freedom in water. Current and future work follows the capture of this radical through to the microsecond time scale of bond formation.

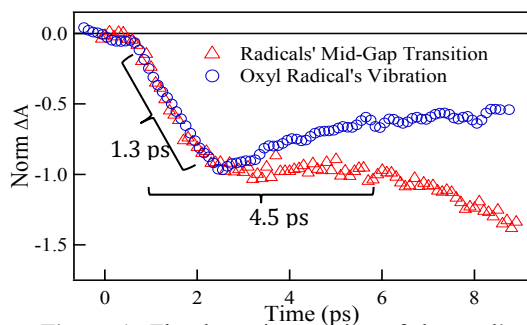


**Figure 1:** The dynamic mapping of the oxyl's sub-surface vibration observed to an electronic mid-gap state with a rising 1.3 ps exponential, and a wait time of 4.5 ps before the next radical forms.

The second advance concerns the rates with which these radicals form at the aqueous interface out of charge carriers in solid-state bands. Nascent catalytic intermediates should appear as localized charge at the solid-liquid interface, creating mid-gap electronic states in semi-conductors. Recently, we discovered that the early time dynamics (1.3 ps) of the sub-surface vibration of the oxyl, where the hole localizes on the terminating oxygen site, maps onto the formation of a mid-gap electronic state (Fig. 1), isolated by a sub-band gap optical probe. This dynamic mapping of an electronic to a vibrational signature of a radical is a unique achievement for the solid-liquid interface. The fact that the two time constants (1.3 ps, 4.5 ps) are exclusively associated

with the reactive, aqueous interface, are otherwise conserved, and reflect vibrational relaxation in interfacial water led to a proposed, non-adiabatic kinetic mechanism for radical formation determined by hydroxyl stretch relaxation in dilute H-bonded water networks. This mechanism highlights the role of water dynamics in creating stable radicals and positions radical creation as a probe of complex water dynamics. The next thrust of the research is to probe the water dynamics directly in the presence of surface radicals—by an ultrafast broadband infrared probe of water librations, bending modes, and hydroxyl stretches.

The third advance concerns the measurement of the interfacial charge mobility at the n-GaN/aqueous interface by transient optical diffraction. A real possibility is that the time scale for bond formation at heterogeneous solid-liquid interfaces is determined by the diffusion of reaction intermediates along the surface. Their diffusion, however, is an elusive quantity since it is guided by hopping between sites at a surface; one has to be able to measure small diffusion coefficients and solely at an interface. We found that, uniquely when reaction intermediates are created by charge transfer between n-GaN and an aqueous electrolyte, interfacial charge carrier diffusion increases markedly (by a factor  $> 2$ ). Essentially, reaction intermediates open a new current pathway for charge carriers. To what extent this inter-dependence of reactivity and transport determines the steady state current evolving from the solid-liquid interface can now be explored by measuring the diffusion coefficient as a function of the current flux.

#### *Ultrafast Excited State Electron Dynamics at Interfaces*

Research in the Harris group concerns the real time behavior of electrons at interfaces. This focus is important on both a fundamental and a technological level. From a fundamental aspect, a material's optoelectrical properties at the interface can deviate substantially from bulk properties as the reduce dimensionality in one direction produces quantum effects. From a technological perspective, the interface between dissimilar materials often dictate a device's performance and efficiency such as the contact resistance at interfaces which play an important role in electronic devices, and organic photovoltaics which rely on charge separation at donor/acceptor interfaces. Furthermore, as the technological advices push devices to the nanometer length scale, it is believed interfacial properties will dominate over bulk properties. Our research utilizes an experimental technique called time- and angle-resolved two-photon photoemission spectroscopy (TPPE) to study the electronic states present at interfaces and the dynamic behavior of excess excited electrons metal/adsorbate interfaces. Briefly, TPPE is an ultrafast pump-probe technique capable of measuring electrons in occupied and unoccupied electronic states with high temporal, momentum, and energy resolution.

Recently, the Harris group has explored the interface between a metal and a highly ionic material, and the behavior of an excess excited electron at these interfaces. We have recently studied the alkali halide/ metal interface, which serves as a model system to explore metal/insulator interfaces relevant to nanoelectronic devices where a thin insulating layer serves as a decoupling layer between a metal electrode and active material. In a recent study, we studied the dynamics of an excess electron at the NaCl/Ag(100) interface. This study was the first to observe an image potential state series of a highly ionic material. We observed that electrons initially excited to free electron states localized to deep trap states assigned to low coordinated sites on the NaCl surface on the hundreds of femtosecond timescale. In follow up study, we observed the emergence of a new distinct trap state low temperatures below ca. 90 K. This study represents the first observation of electron localization through multiple distinct trap states. The emerging trap state observed is assigned to small polaron formation assisted by defect intermediates. Trapped electrons forming small polarons are further stabilized by hundreds of meVs and showed an enhanced relaxation lifetime. This work is currently under edit in our group for resubmission. Future work will seek to expand the behavior of small polaron formation in a different alkali halides and correlate various material properties with the self-trapping energy and lifetime stabilization associated with small polaron formation.

### Molecular Dynamics of Liquid Interfaces and Liquid-Solid Transformations

The Chandler group continued its research on theories and modeling of liquid interfaces and liquid-solid transformations. One project focused on the water-metal interface, and specifically the dynamical pathways by which water molecules adsorb and desorb from Pt(111) and Pt(100) surfaces. This work is the most recent of a series from the Chandler group on water-metal interfaces. Employing the molecular-simulation techniques of rare-event sampling and liquid-interface constructions pioneered by this group, the most recent work shows how the exchange between an adsorbed water and the adjacent liquid involves correlated dynamics of the bulk liquid's fluctuating interface and several neighboring molecules in the underlying adsorbed layer. This correlated dynamics takes place over spatial scales of nanometers, and over time scales of tens of nanoseconds. Any efforts to correctly apply *ab initio* methods to treat catalysis at hydrated metal surfaces will need to account for fluctuations on these scales.

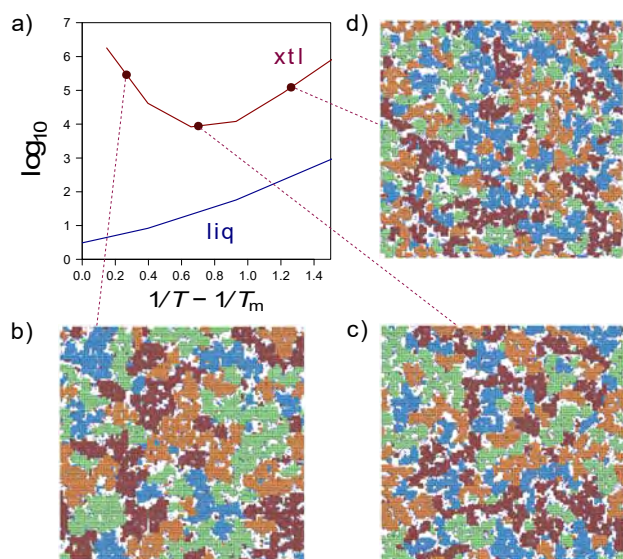


**Figure 2.** Competition between crystallization and vitrification in a  $d=2$  arrow-Potts model after quenching from a liquid to a supercooled temperature  $T$ . (a) Crystal formation time  $\tau_{xtl}$  and liquid relaxation time  $\tau_{liq}$  are plotted as functions of temperature.  $\tau_{liq}$  is the timescale for liquid reorganization and exhibits the super-Arrhenius behavior characteristic of supercooled liquids.  $\tau_{xtl}$  is the time required for 50% of the system to crystallize; it exhibits a non-monotonic dependence on temperature, where at high temperatures, crystallization is limited by the time required to form critical nuclei. At low temperatures, crystallization is limited by slow liquid diffusion. (b)-(d) Snapshots of the system after quenching to different temperatures, as indicated by the dashed lines. Orientations of different crystal domains are represented by different colors (red, orange, green, blue), while disordered domains (liquid or glass) are represented by white space. Quenching to a temperature just below the melting temperature,  $T_m$ , results in relatively large grain sizes, where a single grain consists of crystal in the same orientation. Quenching to slightly lower temperatures results in faster forming crystals. Quenching to very low temperatures leads to many fast-growing smaller crystallites, where subsequent coarsening depends upon the ability of the liquid to reorganize and smooth the grain boundaries.

In another topic of study, the Chandler group has uncovered a mechanism for a generic, powerful force of assembly and mobility for transmembrane proteins in lipid bilayers. This force is a pre-transition (or pre-melting) effect for the first-order transition between ordered and disordered phases in the membrane. Using large-scale molecular simulation, the work shows that a protein with hydrophobic thickness equal to that of the disordered phase embedded in an ordered bilayer stabilizes a microscopic order-disorder interface. The stiffness of that interface is finite. When two such proteins approach each other, they assemble because assembly reduces the net interfacial energy. Analogous to the hydrophobic effect (which similarly leverages the power of the liquid-vapor transition), they refer to this newly appreciated phenomenon as the ‘orderphobic effect’. The effect is mediated by proximity to the order-disorder phase transition and the size and hydrophobic mismatch of the protein.

Finally, the Chandler group has devised a coarse-grained model to treat the competing dynamics of crystal and glass formation. The model is presented on a space-filling lattice, which for the purpose of this discussion, we take to be a cubic in dimension  $d$ . Each lattice site (i.e., microscopic domain) can be in an ordered or disordered state. Each disordered site can be either immobile (i.e., glass-like) or mobile (i.e., liquid-like) with motion in one of  $2^d$  directions. Each ordered site coincides with a local crystal structure oriented in one of  $2^d$  directions. The equivalent symmetry of each ordered direction implies that a  $(1+2^d)$ -state Potts model specifies the energetics of the system. Directional facilitation implies that a  $(1+2^d)$ -state arrow model specifies the stochastic dynamics of the system. This new model, the arrow-

Potts model makes possible simulation studies of emergent polycrystallinity. It predicts that the interfaces between differently oriented crystal domains have a life of their own – glass transitions in  $d-1$  dimensions. The model also successfully predicts non-monotonic time-temperature plots (i.e., crystal formation times as functions of temperature). Non-monotonic time-temperature plots are well known experimentally. The arrow-Potts model provides the first microscopic model for this phenomenon. Figure 2 illustrates a finding of the model.

### **Publications Acknowledging DOE Support:**

D.M. Herlihy, M.M. Waegle, X. Chen, C.D. Pemmaraju, D. Prendergast and T. Cuk, "Uncovering the Oxyl Radical of Photocatalytic Water Oxidation by its Sub-Surface Vibration" *Nature Chemistry* **2016**, 8, 549. (News & Views 8, 527)

X. Chen, S. Choing, D. Aschaffenburg, C.D. Pemmaraju, D. Prendergast and T. Cuk, "The Dynamics of Forming Water Oxidation Radicals at the n-SrTiO<sub>3</sub>/Aqueous Interface " **2016**, *J. Am. Chem. Soc.*, under-review.

H.Q. Doan, K.L. Pollock, and T. Cuk, "Transient Optical Diffraction of an n-GaN/Aqueous interface: interfacial carrier mobility dependent on surface reactivity" *Chemical Physics Letters (Frontiers)* **2016**, 649, 1 (Invited).

A.M. Hibberd, H.Q. Doan, E.N. Glass, F.M.F. de Groot, C.L. Hill, and T. Cuk, "Co Polyoxometalates and a Co<sub>3</sub>O<sub>4</sub> Thin Film Investigated by L-Edge X-ray Absorption Spectroscopy" *J. Phys. Chem. C* **2015**, 119, 4173.

M.M. Waegle, X. Chen, D.M. Herlihy, and T. Cuk, "How Surface Potential Determines the Kinetics of the First Hole Transfer of Photo-catalytic Water Oxidation" *J. Am. Chem. Soc.* **2014**, 136, 10632.

M. Waegle, H. Doan, and T. Cuk, "Long-lived photoexcited carrier dynamics of d-d excitations in spinel ordered Co<sub>3</sub>O<sub>4</sub>," *J. Phys. Chem. C* **2014**, 118, 3426.

Limmer DT, Willard AP, Madden PA, Chandler. **2015**. "Water Exchange at a Hydrated Platinum Electrode is Rare and Collective." *J. Phys. Chem. C* **119**, 24016—24

Katira S, Mandadapu KK, Vaikuntanathan S, Smit B, Chandler D. **2016**. "Pre-transition effects mediate forces of assembly between transmembrane proteins." *eLife* **5**, e13130.1—19.

Schuster KC. **2016**. "Glassy Dynamics on a Lattice and in Nature." Ph.D. Thesis, University of California, Berkeley.  
Shearer, A. J., "Electronic Structure of Novel Materials for Next-Generation Devices" LBNL Thesis, **2016**.

Suich, D. E., "Excited Electronic States and Ultrafast Dynamic Electron Trapping at Alkali Halide / Metal Interfaces" LBNL Thesis, **2015**.

Suich, D. E., Caplins, B. W., Shearer, A. J., Harris, C. B., "Femtosecond Trapping of Free Electrons in Ultrathin Films of NaCl on Ag(100)" *J. Phys. Chem. Lett.*, **2014**, 5, 3073–3077. DOI: 10.1021/jz501572z

Shearer, A. J., Suich, D. E., Caplins, B. W., Harris, C. B., "Impact of Film Thickness and Temperature on Ultrafast Excess Charge Dynamics in Ionic Liquid Films" *J. Phys. Chem. C*, **2015**, 119, 24417–24424. DOI: 10.1021/acs.jpcc.5b07262

Caplins, B.W., Suich, D.E., Shearer, A.J., Harris, C.B., "Quantum Beats at the Metal/Organic Interface" *J. Electron Spectrosc. Relat. Phenom.*, **2015**, 198, 20-25, . DOI: 10.1016/j.elspec.2014.11.006

Caplins, B. W., "Electronic Structure of the Metal/Phthalocyanine Interface Probed by Two-Photon Photoemission" LBNL Thesis, **2014**.

Shearer, A. J., Johns, J. E., Caplins, B. W., Suich, D. E., Harris, C. B., "Electron Dynamics of the Buffer Layer and Bilayer Graphene on SiC" *Appl. Phys. Lett.*, **2014**, 104, 231604. DOI: 10.1063/1.4882236

Caplins, B. W., Suich, D. E., Shearer, A. J., Muller, E. A., Harris, C. B., "Metal/Phthalocyanine Hybrid Interface States on Ag(111)" *J. Phys. Chem. Lett.*, **2014**, 5, 1679-1684. DOI: 10.1021/jz500571z

Caplins, B. W., Shearer, A. J., Suich, D. E., Muller, E. A., Harris, C. B., "Measuring the Electronic Corrugation at the Metal/Organic Interface" *Phys. Rev. B.*, **2014**, 89, 155422. DOI: 10.1103/PhysRevB.89.155422

# Rate Theory of Solvent Exchange around Lithium Ions and the Thermodynamics and Kinetics of Ion Pairs in Condensed Phase

## Recent Progress and Future Plans

Liem X. Dang

Physical Sciences Division

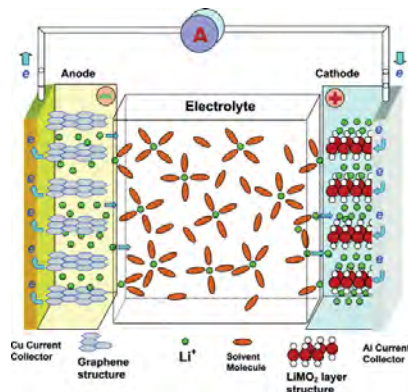
Pacific Northwest National Laboratory

Richland, WA 93352

[liem.dang@pnl.gov](mailto:liem.dang@pnl.gov)

### Background and Significance

Because of their high energy-storage density and high output voltage, rechargeable lithium-ion batteries (LIB) are important for energy-storage applications. The energy and voltage-storage density are determined by the electrode materials used, and various kinds of electrode materials have been investigated. Computer simulations and statistical mechanical methods are useful tools for developing a molecular-level understanding of LIB properties and for designing new LIB materials. Organic solvents such as ethylene carbonate (EC), propylene carbonate, and acetonitrile (ACN) are widely used as liquid electrolytes of these storage systems. Knowledge of free energy profiles and rate theory evaluations are important for understanding a wide range of physical and chemical phenomena for these systems. Information from those sources also provides a challenging test of the accuracy of information derived from force field models. Experimental and theoretical studies have been performed to understand  $\text{Li}^+$  transport and solvation in various carbonate electrolytes. Results from some of those studies indicated a coordination number of 4, in which the  $\text{Li}^+$  ion interacts with the carbonyl oxygen atoms of the carbonate. In mixed carbonate systems such as EC/ACN, both EC and ACN participate in solvating  $\text{Li}^+$ . From the computational perspective, classical potentials sometimes are limited in their transferability and their ability to describe polarizable effects. We also do not know if a quantum-based model is available that can simulate electrolyte phenomena such as electric double layers at the level of complexity of this system. In this work, we made use of accurate electronic structure calculations to construct our polarizable potential models and then explored the consequences of polarizable models.



*Schematic description of a LIB cell that employs graphitic carbon as the anode and a transition-metal oxide as the cathode. The underlying electrochemical process is  $\text{Li}^+$ -ion deintercalation from the graphene structure of the anode and simultaneous intercalation into the layered structure of the metal oxide cathode. For the cell illustrated above, the discharge process shown because the reaction is spontaneous. (Xu K. Chem. Rev. 2004, 104, 4303–4417)*

Our goal was to apply rate theory methods to study solvation of  $\text{Li}^+$  and  $\text{Li}^+$ -ion pairings in LIBs. Additionally, the pressure dependence of the dynamics of ion exchange is examined. Gas formation that has been observed in LIBs can cause an overpressure inside the cells and has been identified as a major problem that negatively impacts their performance. To reduce the internal pressure, a mechanical safety vent can be included. Formation of gases may come from the decomposition of electrolytes or oxygen evolution of certain transition metal oxide cathodes under overvoltage conditions. Thus, it would be useful to examine how pressure affects ionic solvation and possibly the ionic conductivity. We also provide the results of our study of  $\text{Li}^+$ -[BF<sub>4</sub>]/[PF<sub>6</sub>] ion pairing kinetics in ACN to examine the anion effects of lithium salts. Using our polarizable force field parameters and employing classical rate theories of chemical reactions, we examine the ACN solvent exchange process between the first and second solvation shells around  $\text{Li}^+$ . We calculate the exchange rates using transition state theory (TST) and weighted them with transmission coefficients determined by the reactive flux (RF), Grote-Hynes, (GH), and Impey, Madden, and McDonald (IMM) methods. Our results show that, in addition to affecting the free energy of solvation into ACN, the

anion type also should significantly influence the kinetics of ion pairings. These results will increase our understanding of dynamics and kinetics properties of LIB systems.

## Recent Progress

### A. $\text{Li}^+$ in ACN

We begin this section by presenting the results for the exchange dynamics of the ACN molecules around the solvated  $\text{Li}^+$ . Figure 1 shows computed potentials of mean force obtained at 300 K for the three pressures (0, 2, and 4 kbar) normalized to the contact  $\text{Li}^+$ -ACN pair free energy minimum at 0 bar. As expected, the shapes of the computed PMFs are very similar, and the changes are small but noticeable. We observe two effects: 1) increasing the pressure destabilizes the contact ion-ACN pair and 2) the free energy barrier for escaping the first solvation shell decreases from  $1.71 \pm 0.05$  kcal/mol at 0 bar to  $1.48 \pm 0.05$  kcal/mol at 4 kbar. These changes are accompanied by a small change in the transition state distance from  $3.85 \text{ \AA}$  to  $3.95 \text{ \AA}$ . Using the computed PMFs and transition state distances, we computed the rate constant,  $k^{\text{TST}}$ , for the exchange process; the results for  $k^{\text{TST}}$  are 0.55, 0.56, and  $0.74 \text{ ps}^{-1}$  at 0, 2, and 4 kbar, respectively. We found  $k^{\text{TST}}$  increases with increasing pressure, and this trend would be expected by examining at the PMFs and the barrier heights. We computed the activation volume by using the  $k^{\text{TST}}$  values, and a small negative ( $-1.9 \text{ cm}^3/\text{mol}$ ) was obtained. These results establish that an exchange process with increasing pressure and decreasing free energy at the barrier will lead to a negative activation volume (i.e., an associative mechanism).

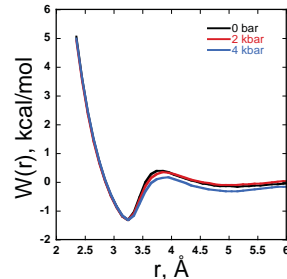


Figure 1 shows the computed PMFs obtained at 300 K for the three pressures.

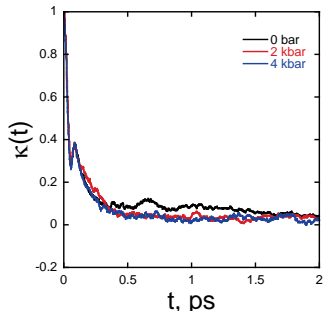


Figure 2 shows the computed time dependent  $\kappa(t)$  at three different pressures.

It is known that TST significantly overestimates the values of rate constants. The RF method and GH theory are well-known and popular corrections to TST that have been reported in the literature. The RF and GH-theory approaches provide a transmission coefficient,  $\kappa$ , to correct TST. In Figure 2, we present the computed time-dependent  $\kappa(t)$  at three different pressures. We observed that rate constants decrease as pressures increase. The transmission coefficients,  $\kappa_{\text{RF}}$ , are  $4.9 \times 10^{-2}$ ,  $3.8 \times 10^{-2}$ , and  $2.7 \times 10^{-2}$ . The activation volume using the computed  $k = \kappa_{\text{RF}} \times k^{\text{TST}}$  is  $1.9 \text{ cm}^3/\text{mol}$ , which is opposite in sign with the value extracted using  $k^{\text{TST}}$ . Thus, we conclude that the pressure dependence of both the barrier height and the transmission coefficient contribute to the activation volume. In addition to the RF method, we also used the IMM method in our study. The IMM method allows the residence time of a solvent molecule in the first solvation shell of another molecule (i.e.,  $\text{Li}^+$ ) to be calculated, and the inversion of the residence time is the rate constant. It is determined from the normalized time-correlation function of the population of solvent molecules in the first solvation shell of the  $\text{Li}^+$ . In Figure 3, we show the values of  $C(t)$  as a function of the pressure obtained using the IMM method. The decay rate of  $C(t)$  is much slower for the ACN system at high pressure than at lower pressure. This would be expected because the fluid is denser at higher pressures. This finding essentially means that the residence time,  $\tau$ , for an ACN in the first solvation shell of the  $\text{Li}^+$  (i.e.,  $\tau$ ) is smaller at lower pressure. This is justified quantitatively by integrating  $C(t)$ , which provides us with  $\tau = 78, 92,$  and  $122 \text{ ps}$  for pressures at 0, 2, and 4 kbar, respectively. In addition, we also have demonstrated that the behavior of  $C(t)$  is equivalent to an exponential decay function (i.e.,  $\exp(-t/t_p)$ ) by plotting  $\ln(C(t))$  vs. time. The inverted slopes of these straight lines provide us with  $\tau = 37, 40,$  and  $60 \text{ ps}$  for pressures of 0, 2, and 4 kbar, respectively. These values are a bit higher than ACN exchange time scales determined using the RF method. The observed trends are very consistent; however, the numerical values obtained using the IMM methods are consistency higher.

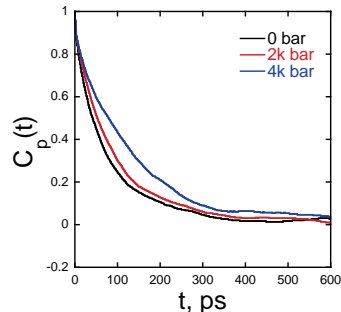


Figure 3 shows the computed time dependent  $C(t)$  at three different pressures.

### B. Kinetics of ion pairing in liquid ACN

We begin this section by presenting results for the kinetics of the  $\text{Li}^+$ - $[\text{BF}_4]/[\text{PF}_6]$  ion pairs in liquid ACN. We start with the PMFs for the  $\text{Li}^+$ - $[\text{BF}_4]/[\text{PF}_6]$  pair, and then continue with the rate theory results determined using the RF and GH methods. We end this section with a comparison of results obtained using the different rate theory methods. In Figure 4, we present PMF plots as a function of center-of-mass separation between the two ions in liquid ACN. It is clear that the PMF for the ion pair containing  $[\text{BF}_4]$  as the anion has a deeper contact ion-pair

minimum compared to the corresponding  $[\text{PF}_6^-]$ -based LIB. This demonstrates that the anion with a small (spherical) shape is more strongly associated with the  $\text{Li}^+$  in ACN. The free energy barriers for the ion-pair dissociation are found to be about  $-5.4$  and  $-3.8$  kcal/mol for  $\text{Li}^+[\text{BF}_4^-]$  and  $\text{Li}^+[\text{PF}_6^-]$ , respectively. Correspondingly, the computed rate constants from the PMFs using TST are determined to be  $5.6 \times 10^{-3}$  and  $3.4 \times 10^{-2}$ . These results clearly indicate that a free energy difference of  $1.6$  kcal/mol can have a noticeable effect on the rate constants. In addition, we also notice that there is no well-defined solvent-separated ion pair as routinely observed for ion pairs in the aqueous solutions. This is probably due to the absence of strong preferred interactions between ion-solvent and solvent-solvent systems.

As mentioned above, we were interested in using the GH theory to compute kinetic properties of ion pairs such as the values for  $\kappa_{\text{GH}}$  and then comparing the values with corresponding results obtained using the RF method. The GH theory transmission coefficient involves the frequency component of the time-dependent friction coefficient,  $\zeta(t)$ , at the Laplace frequency,

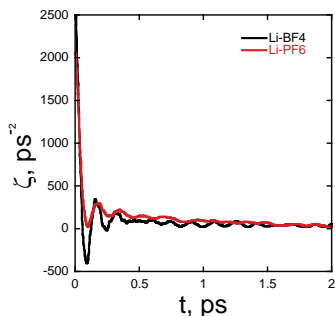


Figure 5. Time-dependent friction kernels, for  $\text{Li}^+[\text{BF}_4^-]$  and  $\text{Li}^+[\text{PF}_6^-]$  ion pairs in ACN computed from GH theory.

$\omega_b \kappa_{\text{GH}}$ , relevant in the barrier region. In Figure 5, we show plots of un-normalized, time-dependent friction kernels of  $\text{Li}^+[\text{BF}_4^-]$  and  $\text{Li}^+[\text{PF}_6^-]$  ion pairs in ACN for comparison. In all cases, there are two distinct decay time scales that show first an initial rapid decay lasting for about  $0.1$  ps and then a longer time decay that lasts for a few picoseconds. We can conclude from these data that the oscillating  $\zeta(t)$  reflects the barrier heights of the computed PMFs. The computed values for  $\kappa_{\text{GH}}$  using these results are  $3.9 \times 10^{-2}$  and  $1.05 \times 10^{-1}$  for  $\text{Li}^+[\text{BF}_4^-]$  and  $\text{Li}^+[\text{PF}_6^-]$ , respectively. We found the relaxation times changed from  $180$  ps to  $4600$  ps and from  $30$  ps to  $280$  ps for  $\text{Li}^+[\text{BF}_4^-]$  and  $\text{Li}^+[\text{PF}_6^-]$  ion pairs, respectively. This result confirms that the solvent response to the kinetics of ion pairing is significant. In Figure 6, we present the computed time-dependent  $\kappa(t)$  for both ion pairs using the RF method. The transmission coefficients,  $\kappa_{\text{RF}}$ , estimated as outlined above are  $6.1 \times 10^{-2}$  and  $1.1 \times 10^{-1}$ . It is clear that the results converted well, and we observed that the rate constants increase from  $\text{Li}^+[\text{BF}_4^-]$  to  $\text{Li}^+[\text{PF}_6^-]$ . Our results show that anion type, in addition to affecting the free energy of solvation into ACN, also should significantly influence the kinetics of ion pairings. The persistence of the ion pair can have important consequence on the dynamical properties of the ions and thus affect the ionic conductivity as observed in previous studies. We found that the relaxation times varied from  $180$  ps to  $2900$  ps and from  $30$  ps to  $270$  ps for the  $\text{Li}^+[\text{BF}_4^-]$  and  $\text{Li}^+[\text{PF}_6^-]$  ion pairs, respectively. These results confirm that the solvent response to the kinetics of ion pairing is significant. These RF results agree qualitatively with the actual transmission coefficients computed using the GH method. In summary, we computed most of the properties associated with the ACN exchange process, such as ion-ACN PMFs, time-dependent transmission coefficients, rate constants, and activation volumes. We found that agreement with experimental results was improved when solvent effects were taken into account. Our results confirm that the solvent response to the kinetics of ion pairing is significant. These GH results qualitatively agree with the actual transmission coefficients computed using the RF method. Our results also show that anion type, in addition to affecting the free energy of solvation into ACN, should also significantly influence the kinetics of ion pairings. Our future research efforts will focus on understanding other organic solvents such as EC and propylene carbonate, which are widely used as liquid electrolytes of these storage systems.

## Future Plans

### Multi-Dimensions PMFs of Ions Transport across Liquid/Vapor and Liquid/Liquid Interfaces

The adsorption and distribution of ions at the liquid/vapor interface of water is a fundamental process encountered in a wide range of biological and chemical systems. In particular, the manner in which water molecules solvate ions is relevant to problems in atmospheric chemistry modeling. In addition, the transport of ions through interfaces is of ubiquitous importance in many fields of chemistry, including separation and extraction, chemical sensors, phase transfer catalysis, membrane transport. While transport phenomena have been extensively treated in a number of disciplines, understanding of microscopic mechanism and kinetics of the interfacial transfer is still far

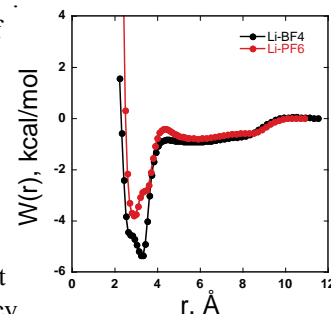


Figure 4. Computed PMFs for  $\text{Li}^+[\text{BF}_4^-]$  and  $\text{Li}^+[\text{PF}_6^-]$  ion pairs in ACN.

from these data that the oscillating  $\zeta(t)$  reflects the barrier heights of the computed PMFs. The computed values for  $\kappa_{\text{GH}}$  using these results are  $3.9 \times 10^{-2}$  and  $1.05 \times 10^{-1}$  for  $\text{Li}^+[\text{BF}_4^-]$  and  $\text{Li}^+[\text{PF}_6^-]$ , respectively. We found the relaxation times changed from  $180$  ps to  $4600$  ps and from  $30$  ps to

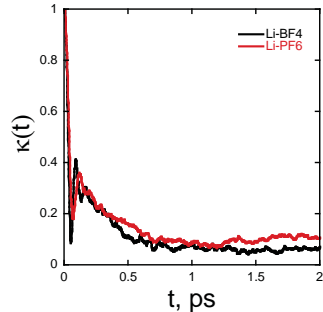


Figure 6. Computed time-dependent transmission coefficients.

from complete. In the past, using a one-dimensional potential of mean force approach, we have demonstrated the molecular mechanism of a polarizable iodide ion binding to the liquid/vapor interface of water. The computed free energy begins to show a major change as the ion approaches the Gibbs dividing surface. The fact that it exhibits a minimum near the Gibbs dividing surface with a well depth of about  $-1.5$  kcal/mol is indicative of the stability of the surface state of the polarizable iodide ion. The results obtained in these studies provide new physical insight into both the free energies and solvent structures as the ions move across the interface. Because the free energy surface is computed with selected coordinates and the choice of the relevant coordinate is crucial. A natural choice is the coordinate of the transferring ion normal to the liquid interface. In performing molecular dynamics simulations of ion transport, we often encounter hysteresis of structure associated to the water finger formation/break as shown in Figure 7, which implies the existence of a stable interface-structure configuration at the same position of  $Z$ . To distinguish the states and possible transition between the configuration, another coordinate relevant to the water finger should be taken into account. Our proposed work includes a proper coordinate of the water finger, which allows us to describe comprehensively two-dimensional free energy surface,  $W(n, z)$  against the ion position and the water finger by using a molecular dynamics simulation. Knowledge we have gained from rate theory of bulk aqueous solutions from our classical molecular dynamics studies easily can be transferred to current systems.

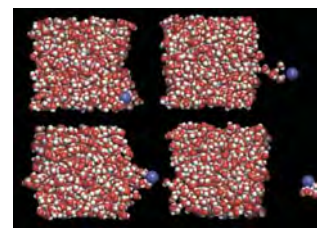


Figure 7. Snapshots taken from molecular dynamics simulations showing the iodide ion leaving the liquid/vapor interface of water.

#### Rate Theory on Ion Pairing at the Liquid/Vapor Interface of Water

There is overwhelming evidence that ions are present close to the vapor–liquid interface of aqueous salt solutions. Despite their importance in many physical phenomena, how ion–ion interactions and the related properties, such as the kinetics and dynamics, are affected by interfaces has not been established. We use molecular simulations to examine the thermodynamics and kinetics between small alkali halides ions in the bulk (Figure 8) and near the water vapor–liquid interface. Using our polarizable force field parameters and employing classical rate theories of chemical reactions, we will calculate the exchange rates using TST, and will weight them with transmission coefficients determined by the RF approach and GH theory. Our results will show that, in addition to affecting the free energy of solvation into solution, the anion type and the interfacial environments (i.e., redistribution of the hydrogen bond network) also should significantly influence the kinetics of ion pairings. These results will increase our understanding of dynamics and kinetics properties of ion pairing in the bulk and near the liquid water interfaces.

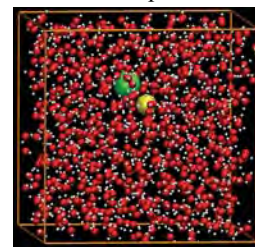


Figure 8. Snapshots taken from molecular dynamics simulations of an ion pair in water.

#### References to publications of DOE sponsored research (2015–Present)

1. Computational Study on the Stability of Nanofluids Containing Metal Organic Frameworks. Harsha V. R. Annapureddy, Satish K. Nune, Radha Kishan Motkuri, Peter B. McGrail and **Liem X. Dang**, *J. Phys. Chem. B*, **119**, 8992 (2015).
2. Nuclear Quantum Effects in Water Exchange around Lithium and Fluoride Ions. David M. Wilkins, David E. Manolopoulos, and **Liem X. Dang**, *J. Chem. Phys.* **142**, 064509 (2015).
3. Water Exchange Dynamics around  $\text{H}_3\text{O}^+$  and  $\text{OH}^-$  Ions. Santanu Roy, **Liem X. Dang**, *Chemical Physics Letters* **628**, 30 (2015).
4. Computational Study of Molecular Structure and Self-Association of Tri-*n*-butyl Phosphates in *n*-Dodecane. Quynh N. Vo, **Liem X. Dang**, M. Nilsson, Hung D. Nguyen, *J. Phys. Chem. B*, **119**, 1588 (2015).
5. **Liem X. Dang** and Gregory K. Schenter, Solvent Exchange in Liquid Methanol and Rate Theory. *Chemical Physics Letters*, **643**, 142 (2016). Frontiers Article, Invited.
6. Computer Simulation of Methanol Exchange Dynamics around Cations and Anions. Roy, Santanu; **Liem X. Dang**, *J. Phys. Chem. B*, **2016**, **120**, 1440-1445.
7. Unexpected Inhibition of  $\text{CO}_2$  Gas Hydrate Formation in Dilute TBAB Solutions and the Critical Role of Interfacial Water Structure. Ngoc N. Nguyen, Anh V. Nguyen, Khoi T. Nguyen, Llew Rintoul, **Liem X. Dang**, *Fuel* **185** (2016) 517–523.
8. Quantifying Dimer and Trimer Formation by Tri-*n*-butyl Phosphates in *n*-Dodecane: Molecular Dynamics Simulations. Quynh N. Vo, **Liem X. Dang**, Mikael Nilsson, and Hung D. Nguyen, *J. Phys. Chem. B*, **2016**, **120** 6985–6994.
9. Rate Theory of Solvent Exchange and Kinetics of  $\text{Li}^+$ - $[\text{BF}_4]^-/[\text{PF}_6]^-$  Ion Pairs in Acetonitrile. **Liem X. Dang** and Tsun-Mei Chang. *J. Chem. Phys.* **145**, 094502 (2016).

## Confinement, Interfaces, and Ions: Dynamics and Interactions in Water, Proton Transfer, and Room Temperature Ionic Liquid Systems (DE-FG03-84ER13251)

Michael D. Fayer  
Department of Chemistry, Stanford University, Stanford, CA 94305  
fayer@stanford.edu

During the last year we have made substantial progress in understanding dynamics of complex systems in interrelated areas using a variety of experimental methods. We studied room temperature ionic liquids (RTILs) with a variety of solutes, including a small anion, carbon dioxide; water, potassium cations, and lithium cations. We have been applying a number of experimental methods, that is, ultrafast 2D IR vibrational echo spectroscopy, polarization selective IR pump-probe experiments, optical heterodyne detected optical Kerr effect measurements, and time dependent fluorescence experiments. In addition, we have made theoretical and experimental advances that are related to the studies.

The dynamics of four 1-alkyl-3-methylimidazolium bis(trifluoromethylsulfonyl)imide room temperature ionic liquids (RTILs) with carbon chain lengths 2, 4, 6, and 10 were studied by measuring the orientational and spectral diffusion dynamics of the vibrational probe  $\text{SeCN}^-$ . Vibrational absorption spectra, two-dimensional infrared (2D IR), and polarization-selective pump-probe (PSPP) experiments were performed on the CN stretch. In addition, optical heterodyne detected optical Kerr effect (OHD-OKE) experiments were performed on the bulk liquids. The PSPP experiments yielded triexponential anisotropy decays, which were analyzed with the wobbling-in-a-cone model. The slowest decay, the complete orientational randomization, slows with increasing chain length in a hydrodynamic trend consistent with the increasing viscosity. The shortest time scale wobbling motions are insensitive to chain length, while the intermediate time scale wobbling slows mildly as the chain length increases. The 2D IR spectra measured in parallel ( $\langle XXXX \rangle$ ) and perpendicular ( $\langle XXYY \rangle$ ) polarization configurations gave different decays, showing that reorientation induced spectral diffusion (RISD) contributes to the dynamics. The spectral diffusion caused by the RTIL structural fluctuations was obtained by removing the RISD contributions. The faster structural fluctuations are relatively insensitive to chain length. The slowest structural fluctuations slow substantially when going from Emim (2 carbon chain) to Bmim (4 carbon chain) and slow further, but more gradually, as the chain length is increased. It was shown that  $\text{K}^+$  causes local ion clustering in the Emim RTIL. The  $\text{K}^+$  effect increases with increasing chain length. The OHD-OKE measured complete structural randomization times slow substantially with increasing chain length and are much slower than the dynamics experienced by the  $\text{SeCN}^-$  located in the ionic regions of the RTILs. The experiments and analysis demonstrate that there is a hierarchy of molecular motions that release structural constraints on different time scale, and that the fastest ones are local and independent of the alkyl chain length, while the slower motions are more global and depend on chain length.

Ionic liquids (ILs) have been proposed as carbon dioxide ( $\text{CO}_2$ ) carbon capture media, and so it is useful to understand the dynamics of both the dissolved gas and its IL environment as well as how altering the IL affects these dynamics. With increasing alkyl chain length, it is well established that ILs obtain a mesoscopic structural feature assigned to polar-apolar segregation, and the change in structure with chain length affects dynamics. The dynamics of  $\text{CO}_2$  in a series of 1-alkyl-3-methylimidazolium bis(trifluoromethylsulfonyl)imide ILs, where alkyl is ethyl, butyl, hexyl, or decyl, were investigated using ultrafast infrared spectroscopy by measuring the reorientation and spectral diffusion of carbon dioxide in the ILs. It was found that

reorientation of the carbon dioxide occurs on 3 timescales, which correspond to 2 different timescales of restricted wobbling-in-a-cone motions and a long time complete diffusive reorientation. The complete reorientation slows with increasing chain length but less than the increases in viscosity of the bulk liquids. Spectral diffusion, measured with 2D IR spectroscopy, is caused by a combination of the liquids' structural fluctuations and reorientation of the CO<sub>2</sub>. The data were analyzed using recent theory that takes into account both contributions to spectral diffusion and extracts the structural spectral diffusion. Different components of the structural fluctuations have distinct dependences on the alkyl chain length. All of the dynamics are fast compared to the complete orientational randomization of the bulk ILs, as measured with optical heterodyne detected optical Kerr effect measurements. The results indicate a hierarchy of constraint releases in the liquids that give rise to increasingly slower dynamics.

Solutions of RTILs and water were studied by observing the reorientational dynamics of the fluorescent probe perylene. Perylene is solvated in the alkyl regions of the RTILs. Its D<sub>2h</sub> symmetry made it possible to extract dynamical information on both in-plane and out-of-plane reorientation from time resolved fluorescence anisotropy measurements. Perylene reorientation reports on its interactions with the alkyl chains. The RTILs were a series of 1-alkyl-3-methylimidazolium tetrafluoroborates (C<sub>n</sub>mimBF<sub>4</sub>, where n is the number of carbons in the alkyl chain), and the effects on perylene's dynamics were observed when varying the alkyl chain length of the cation (n = 4, 6, 8, and 10; butyl, hexyl, octyl, decyl) and varying the water content from pure RTIL to roughly three water molecules per RTIL ion pair. Time correlated single photon counting was used to measure the fluorescence anisotropy decays to determine the orientational dynamics. The friction coefficients for both the in-plane and out-of-plane reorientation were determined to eliminate the influence of changes in viscosity caused by both the addition of water and the different alkyl chain lengths. The friction coefficients provided information on the interactions of the perylene with its alkyl environment and how these interactions changed with chain length and water content. As chain length increased, the addition of water had less of an effect on the local alkyl environment surrounding the perylene. The friction coefficients generally increased with higher water contents; the in-plane orientational motion was hindered significantly more than the out-of-plane motion. The restructuring of the alkyl regions is likely a consequence of a rearrangement of the ionic imidazolium head groups to accommodate partial solvation by water, which results in a change in the arrangement of the alkyl chains. At very high water content, BmimBF<sub>4</sub> broke this general trend, with both in-plane and out-of-plane rotational friction decreasing above a water content of one water per ion pair. This decrease indicates a major reorganization of the overall liquid structure in high water content mixtures. In contrast to BmimBF<sub>4</sub>, the longer chain length RTILs are not infinitely miscible with water, and do not show evidence of a major reorganization before reaching saturation and phase-separating. The results suggest that phase separation in longer chain length BF<sub>4</sub> RTILs is a consequence of their inability to undergo the reorganization of the alkyl regions necessary to accommodate high water concentrations.

Water of hydration plays an important role in minerals, determining their crystal structures and physical properties. Ultrafast nonlinear infrared techniques, 2D IR and PSPP spectroscopies, were used to measure the dynamics and disorder of water of hydration in two minerals, gypsum (CaSO<sub>4</sub>·2H<sub>2</sub>O) and bassanite (CaSO<sub>4</sub>·0.5H<sub>2</sub>O). 2D IR spectra revealed that water arrangement in freshly precipitated gypsum contained a small amount of inhomogeneity. Following annealing at 348 K, water molecules became highly ordered; the 2D IR spectrum became homogeneously broadened (motional narrowed). PSPP measurements observed only inertial orientational relaxation. In contrast, water in bassanite's tubular channels is dynamically disordered. 2D IR spectra showed a significant amount of inhomogeneous broadening caused by a range of water configurations. At 298 K, water dynamics cause spectral diffusion that

sampled a portion of the inhomogeneous linewidth on the timescale of ~30 ps, while the rest of inhomogeneity is static on the time scale of the measurements. At higher temperature, the dynamics become faster. Spectral diffusion accelerates, and a portion of the lower temperature spectral diffusion became motionally narrowed. At sufficiently high temperature, all of the dynamics that produced spectral diffusion at lower temperatures became motionally narrowed and only homogeneous broadening and static inhomogeneity were observed. Water angular motions in bassanite exhibit temperature-dependent diffusive orientational relaxation in a restricted cone of angles. The experiments were made possible by eliminating the vast amount of scattered light produced by the granulated powder samples using phase cycling methods.

Future work is focusing on RTILs, particularly in RTILs in supported ionic liquid membranes (SILMs). SILMs, based mainly on nanoporous polymer membranes, are being developed for CO<sub>2</sub> capture applications. It will be important to understand how nanoconfinement in the SILMs influences the RTIL dynamics compared to the bulk liquid. In addition, proton transfer in polyelectrolyte fuel cell membranes is under investigation using time dependent fluorescence measurements on photoacids embedded in three different fuel cell membranes' water filled nanochannels, one made by DuPont and the other two made by 3M. The aim is to understand how differences in the polymers that make up the membranes affect proton transfer in the water filled nanochannels of the membranes. Ultrafast IR nonlinear experiments will be used to study the water dynamics in the membranes' nanochannels.

### **Publications – Last Two Years**

1. Fayer, M. D., Dynamics and Structure of Room Temperature Ionic Liquids. *Chem. Phys. Lett.* **2014**, 616-617, 259-274.
2. Nishida, J.; Tamimi, A.; Fei, H.; Pullen, S.; Ott, S.; Cohen, S. M.; Fayer, M. D., Structural Dynamics inside a Functionalized Metal–Organic Framework Probed by Ultrafast 2D IR Spectroscopy. *Proceedings of the National Academy of Sciences* **2014**, 111, 18442-18447
3. Kramer, P. L.; Giammanco, C. H.; Fayer, M. D., Dynamics of Water, Methanol, and Ethanol in a Room Temperature Ionic Liquid. *J. Chem. Phys.* **2015**, 142, 212408.
4. Giammanco, C. H.; Kramer, P. L.; Fayer, M. D., Dynamics of Dihydrogen Bonding in Aqueous Solutions of Sodium Borohydride. *J. Phys. Chem. B* **2015**, 119, 3546-3559.
5. Yuan, R.; Yan, C.; Tamimi, A.; Fayer, M. D., Molecular Anion Hydrogen Bonding Dynamics in Aqueous Solution. *J. Phys. Chem. B* **2015**, 119, 13407-13415.
6. Kel, O.; Tamimi, A.; Fayer, M. D., The Influence of Cholesterol on Fast Dynamics inside of Vesicle and Planar Phospholipid Bilayers Measured with 2D IR Spectroscopy. *J. Phys. Chem. B* **2015**, 119, 8852-8862.
7. Lawler, C.; Fayer, M. D., Proton Transfer in Ionic and Neutral Reverse Micelles. *J. Phys. Chem. B* **2015**, 119, 6024-6034.
8. Kramer, P. L.; Nishida, J.; Fayer, M. D., Separation of Experimental 2D IR Frequency-Frequency Correlation Functions into Structural and Reorientation-Induced Contributions. *J. Chem. Phys.* **2015**, 143, 124505.

9. Kramer, P. L.; Nishida, J.; Giammanco, C. H.; Tamimi, A.; Fayer, M. D., Observation and Theory of Reorientation-Induced Spectral Diffusion in Polarization-Selective 2D IR Spectroscopy. *J. Chem. Phys.* **2015**, 142, 184505.
10. Giammanco, C. H.; Kramer, P. L.; Yamada, S. A.; Nishida, J.; Tamimi, A.; Fayer, M. D., Coupling of Carbon Dioxide Stretch and Bend Vibrations Reveals Thermal Population Dynamics in an Ionic Liquid. *J. Phys. Chem.B* **2016**, 120, 549-556.
11. Giammanco, C. H.; Kramer, P. L.; Yamada, S. A.; Nishida, J.; Tamimi, A.; Fayer, M. D., Carbon Dioxide in an Ionic Liquid: Structural and Rotational Dynamics. *J. Chem. Phys.* **2016**, 144, 104506.
12. Kramer, P. L.; Giammanco, C. H.; Tamimi, A.; Hoffman, D. J.; Sokolowsky, K. P.; Fayer, M. D., The Quasi-Rotating Frame: Accurate Line Shape Determination with Increased Efficiency in Non-Collinear 2D Optical Spectroscopy. *J. Opt. Soc. Am. B* **2016**, 33, 1143-1156.
13. "Ionic Liquid Dynamics Measured with 2D IR and IR Pump-probe Experiments on a Linear Anion and the Influence of Potassium Cations," Amr Tamimi and Michael D. Fayer *J. Phys. Chem. B* **2016**, 120, 5842-5854.
14. "The Quasi-Rotating Frame: accurate line shape determination with increased efficiency in non-collinear 2D optical spectroscopy," Patrick L. Kramer, Chiara H. Giammanco, Amr Tamimi, David J. Hoffman, Kathleen P. Sokolowsky, and Michael D. Fayer *J. Opt. Soc. Am. B* **2016**, 33, 1143-1156.
15. "Structural and rotational dynamics of carbon dioxide in 1-alkyl-3-methylimidazolium bis(trifluoromethylsulfonyl)imide ionic liquids: The effect of chain length," Chiara H. Giammanco, Steven A. Yamada, Patrick L. Kramer, Amr Tamimi, and Michael D. Fayer *J. Phys. Chem. B* **2016**, 120, 6698-6711.
16. "Water of Hydration Dynamics in the Minerals Gypsum and Bassanite: Ultrafast 2D IR Spectroscopy of Rocks," Chang Yan, Jun Nishida, Rongfeng Yuan, and Michael D. Fayer *J. Am. Chem. Soc.* **2016**, 138, 9694-9703.
17. "Ionic Liquid vs. Li<sup>+</sup> Aqueous Solutions - Water Dynamics near Bistriflimide Anions," Chiara H. Giammanco, Patrick L. Kramer, and Michael D. Fayer *J. Phys. Chem. B ASAP* **2016**, DOI:10.1021/acs.jpcc.6b07145.
18. "Ionic Liquid Dynamics Measured with 2D IR and IR Pump-probe Experiments on a Linear Anion and the Influence of Potassium Cations," Amr Tamimi and Michael D. Fayer *J. Phys. Chem. B* **2016**, 120, 5842-5854.
19. "The Influence of Water on the Alkyl Region Structure in Variable Chain Length Imidazolium-Based Ionic Liquid/Water Mixtures," Joseph E. Thomaz, Christian M. Lawler, and Michael D. Fayer *J. Phys. Chem. B* **2016**, accepted.
20. "Water Dynamics in 1-Alkyl-3-Methylimidazolium Tetrafluoroborate Ionic Liquids," Chiara H. Giammanco, Patrick L. Kramer, Daryl B. Wong, and Michael D. Fayer *J. Phys. Chem. B* **2016**, accepted.

**Chemical Kinetics and Dynamics at Interfaces**  
*Fundamentals of Solvation under Extreme Conditions*

**John L. Fulton**

Physical Sciences Division  
Pacific Northwest National Laboratory  
902 Battelle Blvd., Mail Stop K2-57  
Richland, WA 99354  
[john.fulton@pnl.gov](mailto:john.fulton@pnl.gov)

Collaborators: G. K. Schenter, C. J. Mundy, N. Govind, M. Galib.

### Program Scope

The primary objective of this project is to describe, on a molecular level, the solvent/solute structure and dynamics in fluids such as water under extremely non-ideal conditions. The scope of studies includes solute–solvent interactions, clustering, ion-pair formation, and hydrogen bonding occurring under extremes of temperature, concentration and pH. The effort entails the use of spectroscopic techniques such as x-ray absorption fine structure (XAFS) spectroscopy, high-energy x-ray scattering, coupled with theoretical methods such as molecular dynamics (MD-XAFS), and electronic structure calculations in order to test and refine structural models of these systems. In total, these methods allow for a comprehensive assessment of solvation and the chemical state of an ion or solute under any condition. The research is answering major scientific questions in areas related to energy, environmental and biological processes including specific areas of relevance to DOE such as mixed hazardous waste processing, power plant chemistry, and geologic carbon dioxide sequestration. This program provides the structural information that is the scientific basis for the chemical thermodynamic data and models in these systems under non-ideal conditions.

### Recent Progress

**Water hydrating neutral, hydrophobic solutes.** The solvation of hydrophobic solutes underlies basic concepts in separations, surface wetting, membrane interactions and protein solvation. Hydrophobic solvation has been the subject of numerous theoretical structural studies and of semi-empirical model development for the prediction of solvation energies. There are almost no direct structural measurements of the water ordering about hydrophobic solutes.

We have measured the hydration structure of Kr dissolved in water. Figure 1 shows a simple conceptual experiment in which we start with an ionic species and then simply “switch off” the charge and thereby measure the water reordering around the neutral species. Such an experiment eliminates the electrostatic interactions that strongly affect the structure about ions and thus creates the opportunity to better probe the weaker factors such as polarizability, dispersion, and H-bonding. These EXAFS studies experimentally determined the water structure around dissolved Kr which is isoelectronic with  $\text{Br}^-$ ,  $\text{Rb}^+$  and  $\text{Sr}^{2+}$  ( $[\text{Ar}] 3d^{10}4s^24p^6$ ).

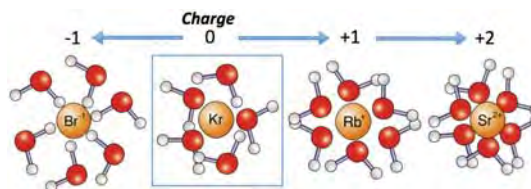


Figure 1. Schematic showing the water ordering around an anion, a neutral solute, and mono- and di-valent cations.

Figure 1 shows schematics of the water ordering around cations ( $\text{Rb}^+$ ,  $\text{Sr}^{2+}$ ), and anions ( $\text{Br}^-$ ) as well as the possible ordering of water around a neutral species (Kr). For both anions and cations the first-shell ordering is mostly a response to alignment of the water dipole moment with the strong local electric field of the ion. These basic structures for ionic species have long been known from early pioneering scattering measurements (especially neutron diffraction (ND)). For a neutral solute such as Kr, an H-bonded, cage-like solvated structure is expected.

Figure 2 shows the predicted pair distribution functions or  $g(r)$ s for Kr dissolved in water from a DFT-MD simulation. The simulation results suggest

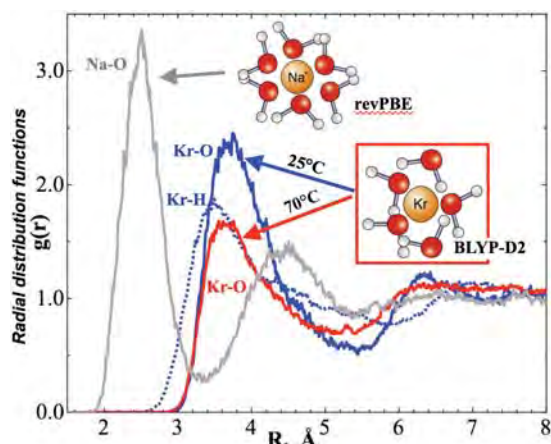


Figure 2. Pair distribution functions, Kr-O and Kr-H, for Kr dissolved in water from DFT-MD simulation using BLYP-D2. Simulation results at 25° and 70°C are shown. For comparison, the Na-O distribution function for aqueous  $\text{Na}^+$  is also shown.

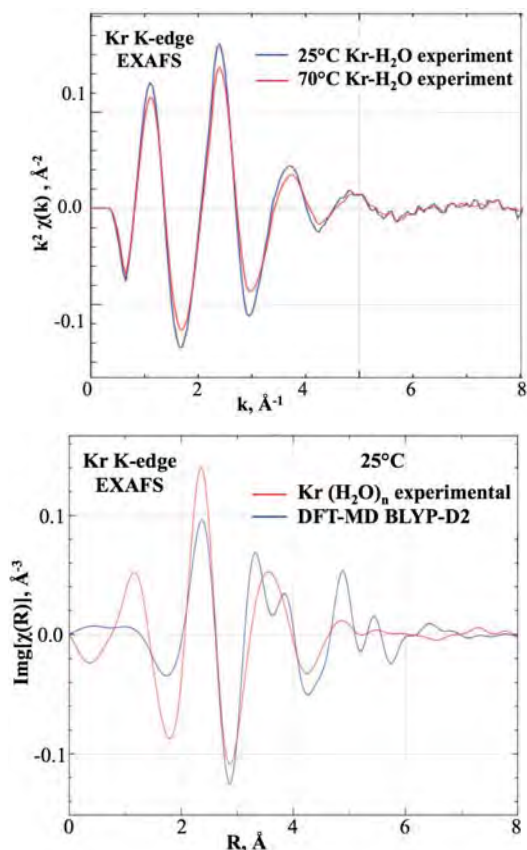


Figure 3. EXAFS  $k^2 \chi(k)$  plots for aqueous 0.03 m Kr (10 bar) at 25° and 75°C (upper panel). EXAFS  $\text{Im}g[\chi(R)]$  plots for aqueous 0.03 m Kr (10 bar) at 25° compared to simulated EXAFS spectrum using DFT-molecular dynamics with BLYP-D2. (lower panel).

that water forms an unexpectedly well-structured “hydration” shell about Kr. In Figure 2, the Kr-O pair distribution function is compared to that of  $\text{Na}^+$ -O. While the Kr-O peak height and width indicate less ordering than for  $\text{Na}^+$ , there is still strong ordering of water that creates a well-defined shell about Kr.

The simulated Kr-H  $g(r)$  shown in Figure 2 indicates that the H’s are located just inside of the O positions of water. This is in agreement with a cage structure in which a H-bonded water network encapsulates the neutral Kr species. Additional ordering or stabilization of this structure may be expected from Kr-water interactions including polarizability and dispersion forces. The simulation results portend a structure around neutral species that is fundamentally different from that of either the anion or cation.

Figure 3 shows the experimental EXAFS spectra for 0.03 m Kr dissolved in water. In the  $\chi(k)$  plot there are strong oscillations from photoelectron backscattering from O’s in the first shell. As temperature is increased to 70°C, the amplitude at low  $k$  is reduced which is consistent with ~10% reduction in the coordination number in the first shell. This agrees with the simulation results for 70°C in Figure 2 although the degree of solvent loss is less in the experimental system. Figure 3 (lower panel) also

compares the experimental radial structure plot to the MD-EXAFS plot for DFT model. The primary features of the Kr-H<sub>2</sub>O distance and CN are faithfully reproduced by the simulation.

**Factors governing cation-anion interactions.** The interaction of anions with cations in aqueous solutions underlies broad areas in separations, catalysis, geochemistry and biochemistry. The electrostatic attractive interactions between counter ions are modulated by a delicate balance of different hydration effects that are not yet fully understood. There is a decades-old problem regarding the question of ion pairing of bicarbonate, HCO<sub>3</sub><sup>-</sup>, with either Mg<sup>2+</sup> or Ca<sup>2+</sup>. The existence of the Mg<sup>2+</sup> / HCO<sub>3</sub><sup>-</sup> ion pair has been the subject of continuing debate for almost 50 years. It is particularly relevant to the chemistry of magnesite, MgCO<sub>3</sub>, that is important for the capture and storage of carbon dioxide in deep geologic formations. The analogous system is amorphous calcium carbonate (ACC), important in geoscience and ocean chemistry, and is the structural framework of many biological systems. One of the routes to formation of ACC involves nucleation and mineralization via liquid-liquid separation. However the liquid phase aqueous speciation is not known, in particular the ion-pairing association of HCO<sub>3</sub><sup>-</sup> with Ca<sup>2+</sup>.

It is not currently known if Ca<sup>2+</sup> (or Mg<sup>2+</sup>) form a CIP or a SSIP with HCO<sub>3</sub><sup>-</sup>. There is some expectation that the CIP may be the dominant species. XANES spectroscopy offers a sensitive method for detection of the ion pair since XANES is sensitive to the disruption of the symmetry and electrostatic fields in both the first and second solvation shell.

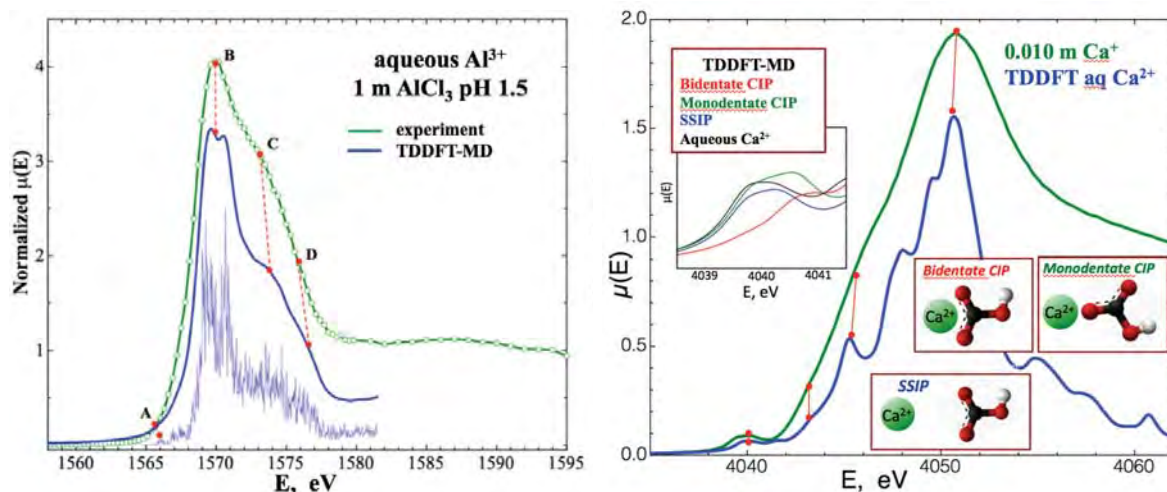


Figure 4. Experimental and theoretical (TDDFT-MD) XANES spectra for aqueous 1 m Al<sup>3+</sup> (left) and 0.010 m Ca<sup>2+</sup> (right). XANES region is sensitive to first and second shell structure about the cation. Coordination numbers, bond distances and symmetry strongly affect the intensity and number of electronic transitions in the XANES region.

As shown in Figure 4 (left) Time-Dependent DFT (TDDFT) has been used to quantitatively predict the XANES spectra of aqueous Al<sup>3+</sup> ions. The strategy involves generating the appropriate MD trajectories and then selecting a large set of simulation snapshots in order to construct the ensemble average MD-XANES spectra. These methods have been used to calculate the XANES spectra for HCO<sub>3</sub><sup>-</sup> ion pairing as either the CIP or SSIP in order to differentiate the two different species experimentally. The overall features of the experimental Ca<sup>2+</sup> spectra are reproduced by the TDDFT simulation. Further, Figure 4 (right) shows that the pre-edge peak at 4040 eV is an especially sensitive feature to detect and differentiate the three different types of ion pair structures. Measurements of 0.01 m Ca<sup>2+</sup>/HCO<sub>3</sub><sup>-</sup> near the phase boundary are ongoing.

## Future Plans

The objective is to gain a fundamental understanding of the molecular structure that provides the basis for understanding ion chemistry and dynamics. We propose exploring ion-water structure for systems in which the local structure has not yet been measured or the structure is not yet fully understood. Our goal is to identify the underlying structural factors that govern the macroscopic properties of ions that have so far eluded a comprehensive theoretical treatment. The proposed work also involves a comprehensive study of ion pairing in concentrated solutions and at high temperatures. The objective is to describe how the ion pair structure is governed by a range of different types of solvent interactions.

## References to publications of DOE sponsored research (2014 - present)

1. "The Aerobic Oxidation of Bromide to Dibromine Catalyzed by Homogeneous Oxidation Catalysts and Initiated by Nitrate in Acetic Acid." Partenheimer W, John L. Fulton, Christine M. Sorensen, Van-Thai Pham, and Yongsheng Chen. **Advanced Synthesis & Catalysis** 387, 130-137, (2014).
2. "Persistent ion pairing in aqueous hydrochloric acid" Marcel D. Baer, John L. Fulton, Mahalingam Balasubramanian, Gregory K. Schenter, and Christopher J. Mundy, **J. Phys. Chem. B**, 118, 7211 (2014) (Feature Article)
3. John C. Linehan, Mahalingam Balasubramanian, John L. Fulton, "Homogeneous catalysis: from metal atoms to small clusters", In "XAFS Techniques for Catalysts, Nanomaterials, and Surfaces", Yasuhiro Iwasawa, Kiyotaka Asakura, and Mizuki Tada, editors, Springer, New York, 2016, in press.
4. Gregory K. Schenter, John L. Fulton, "Molecular Dynamics Simulations and XAFS (MD-XAFS)", In "XAFS Techniques for Catalysts, Nanomaterials, and Surfaces", Yasuhiro Iwasawa, Kiyotaka Asakura, and Mizuki Tada, editors, Springer, New York, 2016 in press.
5. "Electronic and Chemical State of Aluminum from the Single- (K) and Double-Electron Excitation ( $KL_{II\&III}$ ,  $KL_I$ ) X-ray Absorption Near-Edge Spectra of alpha-Alumina, Sodium Aluminate, Aqueous  $Al^{3+}\cdot(H_2O)_6$ , and Aqueous  $Al(OH)_4^-$ ", John L. Fulton, Niranjana Govind, Thomas Huthwelker, Eric J. Bylaska, Aleksei Vjunov, Sonia Pin, Tricia D. Smurthwaite, **J. Phys. Chem. B**, 119, 8380-8388, 2015.
6. "High-resolution Measurement of Contact Ion-pair Structures in Aqueous RbCl Solutions from the Simultaneous Corefinement of their Rb and Cl K-edge XAFS and XRD Spectra", Van-Thai Pham, John L. Fulton, **J. Solution Chem.**, 45, 1061-70, 2016.
7. "The structure of liquid water up to 360 MPa from x-ray diffraction measurements using a high Q-range and from molecular simulation", L. B. Skinner, M. Galib, J. L. Fulton, C. J. Mundy, J. B. Parise, V. -T. Pham, G. K. Schenter, C. J. Benmore, **J. Chem. Phys.**, 144, 134504, 2016.

# Probing Chromophore Energetics and Couplings for Singlet Fission in Solar Cell Applications

DE-FG02-13ER16393

Etienne Garand

Department of Chemistry, University of Wisconsin-Madison, Madison, WI 53706

[egarand@chem.wisc.edu](mailto:egarand@chem.wisc.edu)

## *Program scope*

Our studies aim to provide a molecular-level understanding of processes that can improve efficiencies of alternative sources of energy such as those found in dye-sensitized solar cells. In particular, the mechanisms and molecular requirements for efficient exciton multiplication through singlet fission will be explored using high-resolution anion photoelectron (PE) spectroscopy. More specific aims are (1) to probe the evolution of the electronic structure as a function of cluster size to understand singlet fission in crystals, (2) to explore the relationship between the nature of linkers and the electronic structure in covalently-bonded chromophore dimers, and (3) to highlight the differences, including exciton delocalization and the effects of solvent interactions, between the crystalline species and the isolated covalently-bonded dimers.

The electronic states of organic chromophore clusters and covalently-bonded dimers will be probed via PE spectroscopy of mass-selected anion precursors. Starting from the radical anion with a doublet ground state, all the low-lying singlet and triplet states of the neutral molecule that involve removal of a single electron can be accessed via one-photon photodetachment. Therefore, with the exception of the doubly excited state, all the electronic states relevant to singlet fission are accessible on equal footing in our experiments. This makes PE spectroscopy an ideal method for probing the couplings present between these states. Using anions also provide the added advantage of mass selection, which is crucial for studying the behavior of singlet fission as a function of cluster size. To extract precise information about the electronic state energies and couplings, it is important to obtain well-resolved PE spectra. This can be achieved by using the slow electron velocity-map imaging (SEVI) technique which combines velocity-map imaging (VMI) detection with tunable lasers to yield PE spectrum with sub-meV resolution. Additionally, we can reduce temperature related resolution limitations by collisionally cooling the anions to  $\sim 10$  K in a cryogenic radio-frequency ion trap prior to laser photodetachment. Comparisons of the different chromophore systems can reveal the electronic interactions responsible for the observed differences in their singlet fission efficiency. The results can also be used to benchmark theoretical methods.

## Progress

A schematic of our home-built cryogenic SEVI apparatus is shown in Figure 1. The frontend of the apparatus is highly modular, and can interfaced with an electrospray ionization

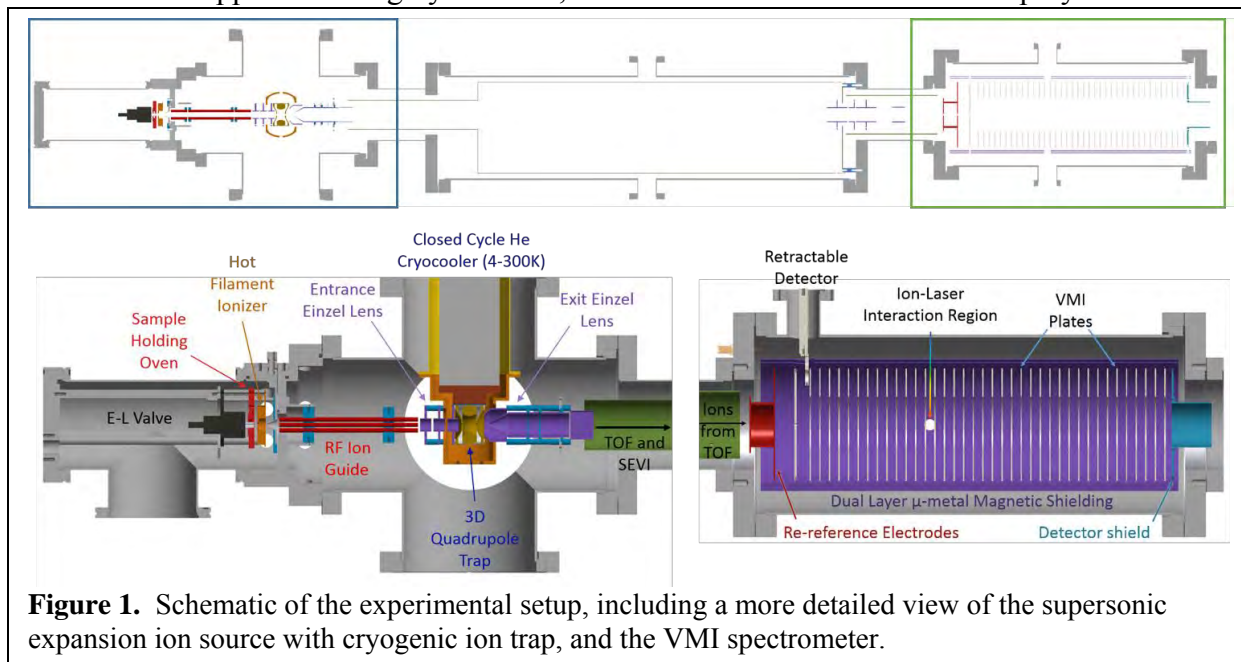
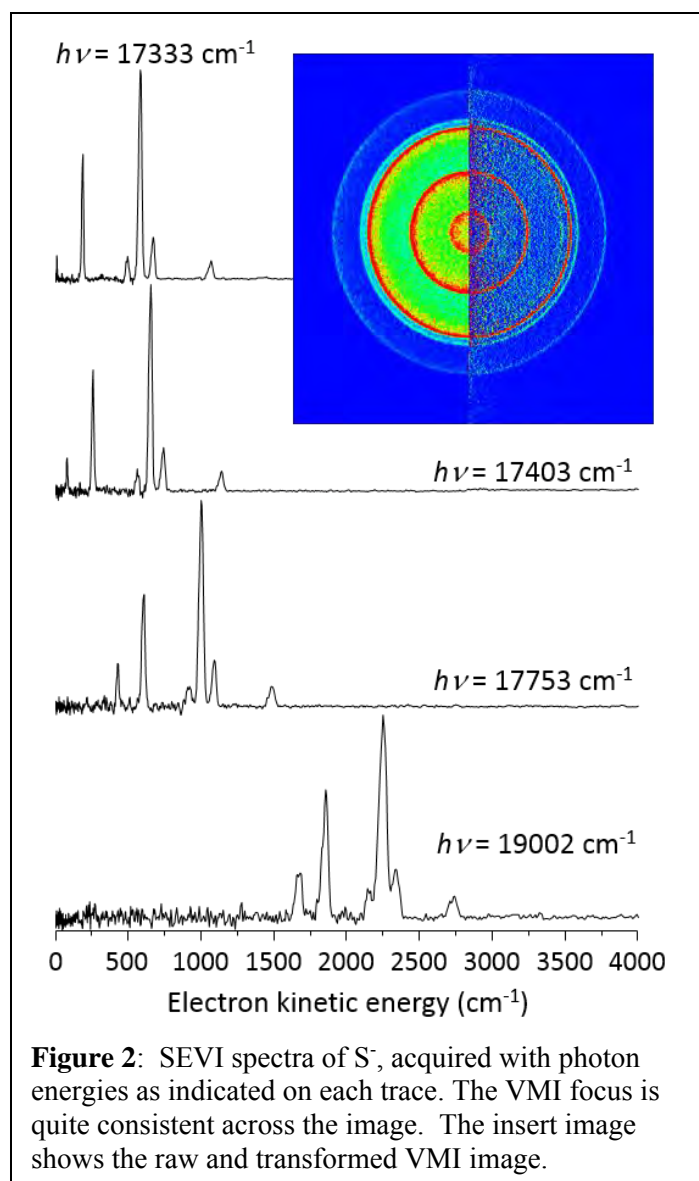


**Figure 1.** Schematic of the experimental setup, including a more detailed view of the supersonic expansion ion source with cryogenic ion trap, and the VMI spectrometer.

source or a heated oven expansion discharge source. We have recently adapted the source to include the use of an Even-Lavie pulsed valve with hot filament ionizer. This source setup is depicted in Figure 1. The anions thusly generated are guided through differential pumping regions into a cryogenic ion trap using a homebuilt RF ion guide. Inside the quadrupole ion trap, the anions are cooled via collisions with helium buffer gas. Residence time inside the trap is typically 50-90 ms to ensure temperature equilibrium before the anions are gently extracted into a linear time-of-flight (TOF) mass spectrometer, which has a resolution of  $m/\Delta m \sim 800$ . A pulsed re-referencing scheme allows only the anions with a specific mass into the VMI region where they are intersected with the gently focused output of a tunable pulsed UV-Vis laser. Photoelectrons, velocity focused by the VMI optics, are mapped onto a detector assembly consisting of imaging quality micro-channel plates and a phosphor screen. The resulting image is captured by a 2048x2048 pixel camera triggered by the time-of-flight timing, providing both the conventional PE spectra via angular integration as well as anisotropy information on the individual vibronic transitions.

To carry out the proposed experiments, we have redesigned the SEVI VMI setup for better focusing and less noise operations. Our VMI includes a series of forty evenly spaced plates extending the entire VMI region, giving us a well-defined electric field environment. Two layers of mu-metal shielding encase the entire electrode stack to provide magnetic shielding. The electrodes are resistively coupled with only three adjustable voltages. One of the voltage remains fixed to define the forward kinetic energy of the electrons. VMI focus is determined by adjusting the other two voltages, where one corrects the energy aberration and the other brings the focal plane onto the detector. Therefore, the day-to-day operation of this VMI is similar to the traditional three-plate VMI while the conditions of operation is more forgiving. We designed our VMI this way for two reasons. First, simulations showed that the best VMI focus across the



are open, minimizing the surface area exposed to stray photons. Minimizing noise electrons are useful when studying the excited states of the polyacene molecules, which typically require photons with energies greater than 4 eV.

Recently, we successfully constructed a dual ion trap setup that allows us to controllably form weakly bound clusters. For example, Figure 3 shows the mass spectrum of  $[\text{Betaine}]^+(\text{H}_2\text{O})_n$  and  $[\text{bmim}]^+(\text{H}_2\text{O})_n$  ( $\text{bmim} = 1\text{-Butyl-3-methylimidazolium}$ ) clusters formed inside a liquid nitrogen cooled octopole reaction trap. The solvated clusters are then further cooled inside the liquid helium quadrupole ion trap before entering the mass spectrometer. This two stage trapping and cooling gives us the flexibility to generate different types of weakly bound clusters, while still maintaining the ability to cool the clusters down to 10 K.

To have a better understanding of the weakly bound clusters formed inside the reaction trap, we acquired the IR predissociation spectra of  $[\text{bmim}]^+(\text{H}_2\text{O})_n$  (ref 2). These spectra have

image is achieved when the photoelectrons are formed on a parabolic electric field line, which is difficult to achieve against a flat repeller plate. Hence, we replaced the repeller plate with a series of open electrodes to give the desired field curvature at the interaction region. Second, because the electrons are formed on a sloping electric field, the VMI focus is also dictated by the physical width of the laser beam. By stretching out the extraction region, the voltage gradient is more gradual, minimizing the blurring effect from the laser beam width. Figure 2 shows an example of the VMI focus we can achieve across an image. This set of SEVI images of  $S^-$  is acquired with photon energy of  $17333\text{ cm}^{-1}$ ,  $17403\text{ cm}^{-1}$ ,  $17753\text{ cm}^{-1}$  and  $19002\text{ cm}^{-1}$ , capturing the expected six transitions originating from the two spin-orbit states of  $S^-$  ( $^2P$ ) going to the three spin-orbit states of  $S$  ( $^3P$ ). Across the  $\sim 3000\text{ cm}^{-1}$  eKE range, the VMI features have the same width in pixels, which yields a square root relationship between the feature width in energy and the eKE. Finally, our design should also minimize the “noise” electrons formed from the electrodes when the laser energy is higher than the work function of stainless steel. Notably the electrodes near the interaction region

full- and partially- resolved features in the C-H and O-H stretch region, indicating that these clusters indeed have low internal energy. Comparisons with calculations indicated that the interaction between  $[\text{BMIM}]^+$  and water is quite weak, with the first water having a binding energy of 9.8 kcal/mol. Furthermore, the  $n \geq 4$  clusters have a structure consisted of a ring of water situated above the imidazolium ring, indicating that water-water interaction is stronger than  $[\text{BMIM}]^+$ -water interaction. This result clearly demonstrates that our reaction trap is capable of forming weakly interacting clusters, such as  $[\text{polyacene}]^-(\text{polyacene})_n$  clusters as well as  $[\text{polyacene}]^-(\text{solvent})_n$  clusters.

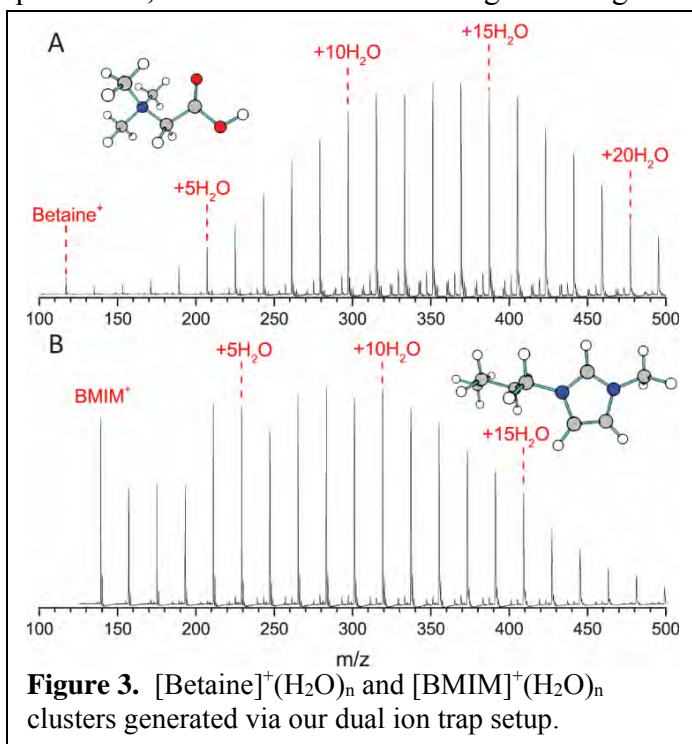
### Future plans

We are preparing a manuscript on the experimental setup of our instrument. The recent success in coupling the Even-Lavie valve to the source region greatly expanded the anions we can produce and preserve. We are currently working on optimizing the conditions for producing the reactive radical anions.

We aim to acquire the well-resolved PE spectra of anthracene and tetracene anions, as well as the dimers of these species in the next year. We will probe the ground states of the neutral species to validate our experimental and theoretical techniques. After which, we will focus our studies on the low-lying excited states that are relevant in the singlet fission process. The analysis of the results will be aided by infrared spectroscopy of the radical anions which can be acquired using our IR predissociation instrument.

### Publications

- 1) B.M. Marsh, J.M. Voss and E. Garand, *A dual cryogenic ion trap spectrometer for the formation and characterization of solvated ionic clusters*, **J. Chem. Phys.**, 143, 204201 (2015)
- 2) J. M. Voss, B. M. Marsh, J. Zhou and E. Garand, *Interaction between ionic liquid cation and water: Infrared predissociation study of  $[\text{bmim}]^+(\text{H}_2\text{O})_n$  clusters*, **Phys. Chem. Chem. Phys.**, 18, 18905-18913 (2016)



## Reactions and Transformations

Phillip L. Geissler (plgeissler@lbl.gov), Musahid Ahmed (mahmed@lbl.gov),  
David Chandler (chandler@berkeley.edu), Teresa Head-Gordon (thg@berkeley.edu), and Rich  
Saykally (saykally@berkeley.edu)

Lawrence Berkeley National Laboratory, Chemical Sciences Division  
1 Cyclotron Road, Berkeley, CA 94720

### Program Scope

A significant gap exists between basic studies of molecular chemical physics and the operation of real devices and natural systems. This program comprises efforts to establish the chemical methods and insight that will enable understanding of systems that are profoundly complex in composition, heterogeneity, preparation, and organization. The problems are multifaceted, and the case studies span a broad range of materials and behaviors. But a long-term unifying theme runs through these efforts: transitioning from the chemical physics of precisely specified model systems to transformations within the disordered and incompletely controlled environments that feature in energy applications.

Ahmed probes chemistry of liquids, surfaces and interfaces under various environments, coupling novel reactors to mass spectrometry, lasers and X-ray spectroscopies. Applying novel methods of theory and numerical simulation, Chandler's research group seeks to understand dynamics at soft interfaces, especially those of water, and the emergent phase behavior of water and other materials, sometimes driven to extreme conditions and far from equilibrium. Head-Gordon's group uses computer simulations to explore how chemical kinetics are sensitive to the fluctuating and inhomogeneous environments presented by enzymes. Saykally's group uses liquid microjet technology to study the details of water evaporation and CO<sub>2</sub> dissolution. Geissler's and Chandler's groups work together on the dynamics of self-assembly, clarifying the time-dependent organization of molecular and nanoscale components into spatial patterns that promote new kinds of chemical reactivity.

### Recent Progress

The dissolution of carbon dioxide in aqueous solutions and the ensuing hydrolysis reactions are of profound importance for understanding the behavior and control of carbon both in the terrestrial environment and in physiological systems, but essential aspects of this chemistry remain poorly understood, particularly those involving aqueous carbonic acid. Using newly developed liquid microjet mixing technology, the first X-ray absorption spectra of aqueous carbonates, including the short-lived carbonic acid species itself, have been measured by Saykally's group as a function of pH to characterize the evolution of electronic structure and the detailed hydration structure of carbonate, bicarbonate, carbonic acid and dissolved CO<sub>2</sub>. Ongoing efforts comprise the investigation of ion pair formation between carbonate and Mg<sup>2+</sup> and Ca<sup>2+</sup> cations in a redesigned liquid jet mixing system, as well as by theoretical modeling. We have also adapted our liquid microjet endstation in order to address the carbonate system via X-ray photoelectron spectroscopy (XPS), in collaboration with LBL beamline scientists. While XAS probes the empty orbitals of a system, XPS probes its filled orbitals, providing complementary details of electronic and geometric structure and hydration. The first results from these experiments indicate a significantly

different interfacial depth for the carbonate and bicarbonate ions, which we are investigating by theoretical calculations.

Clusters are zero-dimensional materials in the sub-nanometer sizes, and have electronic properties in between those of coordination complexes (model systems) and nanoparticles (real catalysts). Ahmed collaborated with Selim Alayoglu (LBNL), Wibe De Jong (LBNL) and Stefan Vajda (ANL), to perform theoretical and experimental X-Ray spectroscopy of size selected Ag metal clusters under reactive gas atmospheres (ethylene+oxygen). Soft X-ray spectroscopy studies of adsorption and reaction of CO in the presence of H<sub>2</sub> over (1) MnO nanoparticles supported on mesoporous Co<sub>3</sub>O<sub>4</sub> and (2) cobalt oxide nanoparticles supported over MgO nanoplates were completed in collaboration with Alayoglu. Self-organization and nano assembly in simple inorganic systems pave a way of understanding dynamical processes typically associated with complex biological systems. Ahmed collaborated with Alayoglu, Destouches (St. Etienne) and Belkacem (LBNL) to investigate the chemical dynamics of nanoparticle grating formation (via laser writing) using imaging mass spectrometry and microprobe X-ray fluorescence spectroscopy.

Head-Gordon performs theoretical studies on chemical transformations. Current computational approaches for de novo enzyme design seek to engineer a small catalytic construct into an accommodating protein scaffold. Two well-studied de novo enzymes for the Kemp elimination reaction are KE07 and KE70, in which very minimal activity was observed in the designed enzymes. Instead laboratory directed evolution (LDE) improved the Michaelis-Menten specificity constant  $k_{cat}/K_M$  by a factor of  $\sim 200$  and  $\sim 400$ , respectively, in the best evolved enzymes. The primary question we have addressed is what is missing in the original computational de novo design that is captured instead during the LDE process to improve the Michaelis-Menten specificity constant  $k_{cat}/K_M$  for KE07 and KE70? We are pursuing the direction that it is the ability to control for protein dynamical motions to rationally design catalysts for new chemical reactions not known to have a natural biocatalyst. The most commonly implied definition of important functional motions for biocatalysis is a thermodynamic one, i.e. statistical fluctuations that are embodied in an entropy change that along with enthalpy contributes to stabilization of the transition state free energy. We showed that the designed KE07 and KE70 enzymes were over-designed for the reactant state, whereas the LDE process created enzymes that preferred the transition state complex instead, in which entropy played a critical stabilizing role. We also found that residues with the highest mutual information entropy proved to be critical for enzyme catalysis, which we tested on the best evolved enzyme for KE07. We showed that amino acids with high mutual information, some of which were far from the active site, were found to diminish or annihilate catalytic activity.

Geissler's group has adapted path sampling techniques to examine how molecular systems can be driven out of equilibrium with low dissipation. Manipulating chemical kinetics in complex environments, which often feature slow relaxation, essentially requires nonequilibrium driving. Doing so without excessive energy waste is a desirable but highly nontrivial goal. We have formulated a statistical ensemble of driving protocols, biased according to their average dissipation, as a way to explore efficient driving routes and also to quantify their diversity. Analogies with conventional equilibrium ensembles, together with symmetries imposed by the fluctuation theorem, allow a very effective numerical survey of protocols, which we demonstrated in an application that inverts the magnetization of an Ising model. From this survey we identify

which features of time-dependent driving are essential for thermodynamic efficiency and which are unimportant.

### **Future Plans**

A major initiative in areas of catalysis, energy, and environmental sciences is to understand chemical kinetics and dynamics when molecules interact in confined geometries, for example, in nano-porous materials, in nanoscale cracks in minerals, and in complex interphase regions. Ahmed seeks to use mass spectrometry, IR and X-Ray spectroscopies coupled to novel reactors to probe model systems which are amenable to theoretical study. Avenues to be pursued by Ahmed are probing aqueous environments within tailor made nanoparticles (chemistry in confined space) via X-Ray Photoelectron spectroscopy in tandem with ambient ionization mass spectrometry and IR spectroscopy. A second direction will be to probe chemical reactions in solution (homogenous catalysis) and gas-surfaces (heterogeneous catalysis) by coupling in-situ and in-operando reactors to mass spectrometry, Raman and IR spectroscopy.

Saykally plans to complete a detailed study of water evaporation rates as a function of pH, comparing solutions of HCl and NaOH, as a means of addressing the controversial interfacial behavior of hydrated protons and hydroxide, respectively. We will further perfect a new planar liquid microjet-based mixing system for generating short lived species, e.g. carbonic acid, in liquid microjets for study by X-ray spectroscopy. We will apply this technology to the study of hydration and hydrolysis of carbon dioxide, nitrogen oxides, and sulfur oxides, including temperature dependence. We also plan to further investigate the nature of the carbonate species by XPS.

Head-Gordon is considering how to improve the calculation of mutual information, and how it can be used to improve alternate de novo designed Kemp eliminases which have not undergone LDE. We are also examining the importance of non-equilibrium effects that may deviate from the standard interpretation of Michaelis-Menten kinetics for biocatalysis. Finally we are considering novel systems that allow for examining accelerated chemical transformations in the condensed phase using advanced DFT functionals.

Chandler's and Geissler's groups are pursuing fundamental studies of self-assembly through new path sampling methods. A range of model systems will be examined in order to develop computational tools, theoretical perspectives, and physical insight for understanding the patterned aggregation of molecularly structured components in strongly fluctuating environments. Landscapes for self-assembly can be explored by exerting biases on trajectory sampling other than, or in addition to, the constraint of successful ordering, focusing attention on dynamics whose statistical weight is negligible in the ensemble of typical aggregation pathways. Geissler will assess the roles of nonequilibrium driving forces in these processes as well, elaborating connections among self-organization, irreversibility, and dissipation.

### **Publications Acknowledging DOE support:**

T.R. Gingrich and P.L. Geissler, "Preserving correlation between trajectories for efficient path sampling," *J. Chem. Phys.* (2015) **142**, 234104, doi: 10.1063/1.4922343

T. R. Gingrich, G. M. Rotskoff, G. E. Crooks, and P. L. Geissler, "Near-optimal protocols in complex nonequilibrium transformations", accepted for publication in *Proc. Natl. Acad. Sci. USA*, doi:10.1073/pnas.1606273113 (2016).

S. Alayoglu, D. Rosenberg & M. Ahmed, "Hydrothermal Synthesis and Characterization under Dynamic Conditions of Cobalt Oxide Nanoparticles Supported over Magnesium Oxide Nanoplates," *Dalton Trans.*, (2016) **45**, 9932, DOI: 10.1039/C6DT00204H

W. T. Ralston, N. Musselwhite, G. Kennedy, K. Ana, Y. Horowitz, A. A. Cordones, B. Rude, M. Ahmed, G. Melaet, & S. Alayoglu, "Soft X-ray Spectroscopy Studies of Adsorption and Reaction of CO in the presence of H<sub>2</sub> over 6 nm MnO Nanoparticles Supported on Mesoporous Co<sub>3</sub>O<sub>4</sub>," *Surface Science* (2016) 648, 14, DOI: 10.1016/j.susc.2015.12.006

Z. Liu, N. Destouches, G. Vitrant, Y. Lefkir, T. Epicier, F. Vocanson, S. Bakhti, Y. Fang, B. Bandyopadhyay, and M. Ahmed, "Understanding the Growth Mechanisms of Ag Nanoparticles Controlled by Plasmon-Induced Charge Transfers in Ag-TiO<sub>2</sub> Films," *J. Phys. Chem. C*, (2015) 119, 9496, DOI: 10.1021/acs.jpcc.5b01350

Willard, A. P., and D. Chandler, "The molecular structure of the interface between water and a hydrophobic substrate is liquid-vapor like," *J. Chem. Phys.* 141, 18C519 (2014).

Limmer, D. T., and D. Chandler, "Premelting, fluctuations and coarse-graining of water-ice interfaces," *J. Chem. Phys.* 141, 18C505 (2014).

Limmer, D. T., and D. Chandler, "Time scales of supercooled water and implications for reversible polyamorphism," *Mol. Phys.* (2015). DOI:10.1080/00268976.2015.1029552

Limmer, D.T., and D. Chandler, "Comment on 'Spontaneous liquid-liquid phase separation of water'," *Phys. Rev. E* 91, 016301 (2015).

Limmer, D.T., and D. Chandler, "Theory of amorphous ices," *Proc. Natl. Acad. Sci. USA.* 111, 9413-9418 (2014).

A. Bhowmick, S. Sharma, T. Head-Gordon, "The role of side chain entropy and mutual information for improving the de novo design of Kemp Eliminases KE07 and KE70," *Phys. Chem. Chem. Phys.* In press (2016).

L. E. Felberg, A. Doshi, G. L. Hura, J. Sly, V. A. Plunova, R. Miller, J. E. Rice, W. C. Swope, T. Head-Gordon, "Controlling the structural transition of polymers with pH using chemical composition and star polymer architecture," *Mol. Phys.* In press. (2016).

Lam, R. K., England, A. H., Smith, J. W., Rizzuto, A. M., Shih, O., Prendergast, D., Saykally, R. J., "The hydration structure of dissolved carbon dioxide from X-ray absorption spectroscopy" *Chem. Phys. Lett.*, 633, 214-217 (2015).

Lam, R. K., England, A. H., Sheardy, A. T., Shih, O., Smith, J. W., Rizzuto, A. M., Prendergast, D., Saykally, R. J., "The hydration structure of aqueous carbonic acid from X-ray absorption spectroscopy" *Chem. Phys. Lett.*, 614, 282-286 (2014).

S. Y. Liu, M. Shawkey, D. Parkinson, T. Troy and M. Ahmed, "*Elucidation of the chemical composition of avian melanin*," *RSC Advances* (2014), **4**, 40396, DOI: 10.1039/C4RA06606E

S. Nepl, A. Shavorskiy, I. Zegkinoglou, M. Fraund, D. S. Slaughter, T. Troy, M. P. Ziemkiewicz, M. Ahmed, S. Gul, B. Rude, J. Z. Zhang, A. S. Termsin, P-A. Glans, Y-S. Liu, C. H. Wu, J. Guo, M. Salmeron, H. Bluhm, and Oliver Gessner, "*Capturing interfacial photo-electrochemical dynamics with picosecond time-resolved X-ray photoelectron spectroscopy*," *Faraday Discuss.* (2014), **171**, 219, DOI: 10.1039/C4FD00036F

H-W. Chang, C-C. Hsu, M. Ahmed, S-Y. Liu, Y. Fang, J. Seog, G. S. Oehrlein, and D. B. Graves, "*Plasma Flux Dependent Lipid A Deactivation*," *J. Phys. D: Appl. Phys.* (2014) **47** 224015

## Chemical Kinetics and Dynamics at Interfaces

*Laser-induced dynamics and reactions at surfaces*

**Wayne P. Hess (PI) Alan G. Joly and Patrick Z. El-Khoury**

Physical Sciences Division  
Pacific Northwest National Laboratory  
P.O. Box 999, Mail Stop K8-88,  
Richland, WA 99352, USA  
[wayne.hess@pnnl.gov](mailto:wayne.hess@pnnl.gov)

Additional collaborators include: Y. Gong, M.T.E. Halliday, D. Hu, R.F. Haglund Jr., A.L. Shluger, P.V. Sushko, V.A. Apkarian, M. Zamkov, A. Tarnovsky, N.D. Browning, P. Abellan, Q. Ramasse, I.V. Novikova, G.E. Johnson, J. Laskin, J.E. Evans, E. Aprà, and N. Govind

### **Program Scope**

The interaction between light, metals and insulators is fundamentally important in photochemistry, microelectronics, sensor technology, and materials processing. The chemistry and physics of electronically excited solids and surfaces is relevant to the fields of photocatalysis, radiation physics, and solar energy conversion. Irradiation of solid surfaces by UV, or higher energy photons, produces energetic transient species such as core holes and free electrons that subsequently relax to form electron-hole pairs, excitons and plasmons. Specifically, the interaction between light and metal nanostructures can lead to intense field enhancement and strong optical absorption through excitation of surface plasmon polaritons. Such plasmon excitation can be used for a variety of purposes such as ultrasensitive chemical detection, solar energy generation, or to drive chemical reactions. Large electric field enhancements can be localized at particular sites by careful design of nanoscale plasmonic structures. Similar to near field optics, field localization below the diffraction limit can be obtained. Through this field enhancement and localization, surface and tip enhanced Raman spectroscopy (SERS and TERS), capable of single molecule sensitivity, becomes possible. Greater understanding of spectroscopic observables is gained using a combined experiment/theory approach. We therefore use *ab initio* calculations to model results from our SERS and TERS studies. The dynamics of plasmonic excitations is complex and we use finite difference time domain calculations to model field enhancements and optical properties of complex structures including substrate couplings or interactions with dielectric materials.

### *Approach:*

We are developing a combined photoemission electron microscopy (PEEM) and femtosecond laser approach to probe plasmonic nanostructures such as solid metal particles or lithographically produced nanostructures such as gratings, trenches, or nanohole arrays. Finite difference time domain (FDTD) calculations are used to interpret field enhancements measured by the electron and optical techniques. The effects of extreme electric field enhancement on Raman spectra is investigated using plasmonic nanostructures constructed from a metal nanoparticles or metal covered atomic force microscopy (AFM) tips on thin film metal/silica substrates. The Raman scattering from molecules positioned between these structures show greatly enhanced scattering and often highly perturbed spectra depending on nanogap dimensions or whether a conductive junction is created between tip and substrate. In photodesorption studies, photon energies are chosen to excite specific surface structural features that lead to particular desorption reactions. The photon energy selective approach takes advantage of energetic differences between

surface and bulk exciton states and probes the surface exciton directly. We measure velocities and state distributions of desorbed atoms or molecules from ionic crystals using resonance enhanced multiphoton ionization and time-of-flight mass spectrometry. We have demonstrated surface-selective excitation and reaction on alkali halides and generalized our exciton model to oxide materials and shown that desorbed atom product states can be selected by careful choice of laser wavelength, pulse duration, and delay between laser pulses.

### **Recent Progress**

We recorded time-resolved PEEM (tr-PEEM) images of propagating surface plasmons launched from lithographically patterned holes and rectangular trenches milled on a flat gold surface. Our tr-PEEM scheme involves a pair of identical, spatially separated, and interferometrically-locked femtosecond laser pulses. Using a combination of tr-PEEM and FDTD simulations, we imaged plasmon propagation properties and including focusing and dispersion. Power dependent PEEM images provide experimental evidence for a sequential coherent nonlinear photoemission process, in which one laser source launches a propagating surface plasmons (PSPs) through a linear interaction, and the second subsequently probes the PSP *via* two-photon photoemission. The recorded time-resolved movies of a PSP allow us to directly measure various properties of the surface-bound wave packet, including its carrier wavelength (783 nm) and group velocity. In addition, tr-PEEM images reveal that the launched PSP may be detected at least 250 microns away from the coupling trench structure. The experimentally measured PSP properties demonstrate that surface plasmons propagating on nominally flat gold surfaces may potentially be harnessed for use in mesoscale plasmonic devices, chiefly incorporated into plasmonic circuits of a several microns in size.

Plasmonic nanocircuits require the ability to launch, focus, and guide PSP waves to specific remote locations. To this end, we study PSP launching asymmetry at a simple symmetric plasmonic trench structure. By selecting polarization, the extent of PSP directional launching can be varied. FDTD calculations confirm experimental results and show that the PSP field intensity is inversely related to the strength of the localized field at the edges of the trench. A square trench structure can be considered an individual element of the toolbox needed for PSP control. The trench structure reveals phenomena that is generally neglected in literature specifically, interplay between LSPs and PSPs. By tuning the polarization of the pump laser, an asymmetry in the intensity of left-side and right-side detected PSPs is observed indicating asymmetric light coupling and plasmon launching from the trench structure. Polarization dependent PSP coupling is a general feature of step edges. For trenches whose edges are separated by a few microns or less, coupling between opposite edges can lead to an increase in PSP launching asymmetry.

Nonlinear PEEM of isolated nanoholes in gold thin films map PSPs launched from the lithographically patterned plasmonic structures. Individual holes constitute an efficient and fundamental light coupling structure in metal substrates that are easily produced and combined into more complex structures such as nanohole arrays lithographically patterned in gold thin films. Again, PEEM was used to map PSPs launched from various array structures. Strong near field photoemission patterns are observed in the PEEM images and recorded photoemission patterns are attributed to constructive and destructive interferences between PSPs launched from the individual nanoholes which comprise the array. In examining the nanohole array geometry-dependent photoemission patterns, we find that once launched, PSPs can be manipulated and focused by changing the separation between the nanoholes. We then demonstrated how varying the array geometry (hole diameter, pitch, and number of rows/columns) leads to intense localized photoemission and identified optimal array geometries for efficient light coupling and interferometric plasmonic lensing. We concluded that the focal lengths of the array-based interferometric plasmonic lenses can be tuned by varying the incidence angle and wavelength of

the driving laser field and that the overall efficiency of the lenses can be controlled by changing the nanohole diameters and by varying the row and column numbers of the nanohole array. With the aid of FDTD simulations, optimal interferometric focusing of propagating SPPs can be achieved. We have also demonstrated a preliminary application of interferometric plasmonic lensing by enhancing the photoemission from the vertex of a gold triangle using a nanohole array coupling and focusing element.

By again using a locked pair of identical femtosecond laser pulses, we imaged propagating surface plasmons, launched from a lithographically patterned rectangular trench, on a flat gold surface. The use of spatially and temporally offset pump and probe pulse pairs allowed the determination of the plasmon group velocity of  $0.95c$ . A series of PEEM images recorded using sequentially delayed probe pulses produces a nearly light speed PSP movie, at 220 attoseconds per frame, and a 50 nm spatial resolution. Using a combination of tr-PEEM and FDTD simulations, we determined that the upper limit for the  $1/e$  decay length of the plasmon field is 88 microns. The recorded time-resolved movies of a PSP allow us to directly measure various properties of the surface-bound wave packet, including its carrier wavelength (783 nm) and group velocity. The experimentally measured PSP properties demonstrate that surface plasmons propagating on nominally flat gold surfaces may potentially be harnessed for use in plasmonic devices.

### **Future Plans**

Prospective efforts include extending time-resolved non-linear PEEM studies which offers both nanometer spatial and fs time resolution. We now have the tools needed to correlate field enhancement with SERS and TERS response and by adding a two-color photoemission scheme to our PEEM set up, the path opens to an entirely new set of measurements capable of correlating structure and dynamics of a variety of designer plasmonic constructs. These developments will eventually enable us to examine photochemical transformations at the ultimate detection limit of a single molecule in ultrasensitive nanoscale chemical imaging experiments or possibly characterize the atomistic nature of SERS hot spots. Such developments could lead to design principles for substrates capable of reproducible single-molecule detection and characterization.

In a similar vein, one of the proposed goals is to extend our prior works to understand the effect of tailored electromagnetic fields on individual molecules and molecular assemblies. Such comparison will provide insights on emergent behavior in the few molecule and single-molecule regime where the 3D structure (vector components) and absolute magnitude of the local electric field can be inferred from the SERS/TERS spectra/images of carefully selected molecular reporters. The first step involves engineering and characterizing plasmonic constructs which support LSPs and/or PSPs. The inclusion of helium ion lithography into our arsenal, now allows sub 10 nm structures to be fabricated enabling correlated femtosecond PEEM with transmission electron microscopy (TEM), tip-enhanced Raman spectroscopy and electron energy loss spectroscopy (EELS). Femtosecond time-resolved PEEM can reveal spatially resolved ultrafast dynamics and is a powerful tool for studying the near-surface electronic state dynamics of nanostructures or plasmonic devices. We have recently developed capabilities to perform energy-resolved two-photon photoemission using a hemispherical analyzer XPS instrument. In combination we expect these two techniques will provide spatially-resolved electronic state dynamics of nanostructured metal and hybrid metal-semiconductor-insulator materials.

## References to publications of DOE BES sponsored research (2014 to present)

1. P. Z. El-Khoury, K. Honkala, W. P. Hess, "Electronic and Vibrational Properties of Meso-Tetraphenylporphyrin on Silver Substrates." *J. Phys. Chem. A* **118**, 8115 (2014).
2. P. Z. El-Khoury and W. P. Hess, "Vibronic Raman Scattering at the Quantum Limit of Plasmons" *Nano Lett.* **14**, 4114 (2014).
3. Y. Gong, A. G. Joly, P. Z. El-Khoury and W. P. Hess, "Nonlinear Photoemission Electron Micrographs of Plasmonic Nanoholes in Gold Thin Films" *J. Phys. Chem. C* **118**, 25671 (2014).
4. P. Z. El-Khoury, T. W. Ueltschi, A. L. Mifflin, D. Hu, and W. P. Hess, "Frequency Resolved "Nanoscale Chemical Imaging of 4,4'-Dimercaptostilbene on Silver" *J. Phys. Chem. C* **118**, 27525 (2014).
5. Y. Gong, A. G. Joly, P. Z. El-Khoury and W. P. Hess,, "Interferometric Plasmonic Lensing with Nanohole Arrays" *J. Phys. Chem. Lett.* **5**, 4243 (2014).
6. P. Z. El-Khoury, E. Khon, Y. Gong, A. G. Joly, P. Abellan, J. E. Evans, N. D. Browning, D. Hu, M. Zamkov and W. P. Hess, "Electric Field Enhancement in a Self-Assembled 2D Array of Silver Nanospheres", *J. Chem. Phys.* **141**, 214308 (2014).
7. Y. Gong, A. G. Joly, P. Z. El-Khoury, L. M. Kong and W. P. Hess "High Brightness Plasmon-Enhanced Nanostructured Gold Photoemitter" *Phys. Rev. Appl.* **2**, 064012 (2014).
8. P. Z. El-Khoury, Y. Gong, P. Abellan, B. W. Arey, A. G. Joly, D. Hu, J. E. Evans, N. D. Browning and W. P. Hess "Tip-Enhanced Raman Nanographs: Mapping Topography and Local Electric Fields" *Nano Lett.* **15**, 2385 (2015).
9. Y. Gong, A. G. Joly, D. Hu, P. Z. El-Khoury and W. P. Hess, "Ultrafast Imaging of Surface Plasmons Propagating on a Gold Surface" *Nano Lett.* **15**, 3472 (2015).
10. R. B. Davidson II, J. I. Ziegler, G. Vargas, S. M. Avanesyan, Y. Gong, W. Hess and R. F. Haglund Jr., "Efficient Forward Second-Harmonic Generation from Planar Archimedean Nanospirals" *Nanophotonics*, **4**, 108 (2015).
11. M. T. E. Halliday, W. P. Hess and A. L. Shluger, "Structure and properties of electronic and hole centers in CsBr from theoretical calculations" *J. Phys. Condens. Matter* **27**, 245501 (2015).
12. P. Z. El-Khoury, G. E. Johnson, I. V. Novikova, Y. Gong, A. G. Joly, J. E. Evans, M. Zamkov, J. Laskin and W. P. Hess "Enhanced Raman Scattering from Aromatic Dithiols Electrosprayed into Plasmonic Nanojunctions" *Faraday Discuss.* **184**, 339-357 (2015).
13. M. T. E. Halliday, A. G. Joly, W. P. Hess and A. L. Shluger, "Photo-Induced Br Desorption From CsBr Thin Films Grown on Cu(100)" *J. Phys. Chem. C* (2015) **119**, 24036
14. M. T. E. Halliday, W. P. Hess and A. L. Shluger, "A mechanism of Cu work function reduction in CsBr/Cu photocathodes" *Phys. Chem. Chem. Phys.* **18**, 7427-7434 (2016).
15. T. Ueltschi, S. Fischer, E. Aprà, A. Tarnovsky, N. Govind, P. Z. El-Khoury, W. P. Hess, "Time-Domain Simulations of Transient Species in Experimentally Relevant Environments" *J. Phys. Chem. A*, **120**, 556 (2016).
16. P. Z. El-Khoury, P. Abellan, R. L. Chantry, Y. Gong, A. G. Joly, I. V. Novikova, J. E. Evans, E. Aprà, D. Hu, Q. M. Ramasse and W. P. Hess, "On the information content in single molecule Raman nanoscopy" *Advances in Physics: X*, **1**, 35 (2016).
17. S. A. Fischer, T. W. Ueltschi, P. Z. El-Khoury, A. L. Mifflin W. P. Hess, H.-F. Wang, C. J. Cramer, and N. Govind, "Molecular Dynamics and Static Normal Mode Analysis: The C-H Region of DMSO as a Case Study" *J. Phys. Chem. B* **120**, 1429 (2016).
18. P. Z. El-Khoury, A. G. Joly and W. P. Hess, Hyperspectral Dark Field Optical Microscopy of Single Silver Nanospheres," *J. Phys. Chem. C*, **120**, 7295 (2016).
19. P. Z. El-Khoury, P. Abellan, Y. Gong, F. S. Hage, J. Cottom, A. G. Joly R. Brydson, Q. M. Ramasse and W. P. Hess, "Visualizing Surface Plasmons with Photons, Photoelectrons, and Electrons", *Analyst* **141**, 3562-3572 (2016).

# Spectroscopic Imaging of Molecular Functions at Surfaces

*Wilson Ho*

Department of Physics & Astronomy and of Chemistry  
University of California, Irvine  
Irvine, CA 92697-4575 USA

[wilsonho@uci.edu](mailto:wilsonho@uci.edu)

## **Program Scope:**

This project focuses on the understanding of the nature of the intramolecular chemical bonds and intermolecular interactions using a unique technique developed in 2014: the inelastic tunneling probe (itProbe) with the scanning tunneling microscope (STM). By operating the STM at  $\sim 600$  mK, high energy resolution of  $\sim 0.6$  meV is achieved, in combination with the inherent sub- $\text{\AA}$  spatial resolution of the STM. Spatially resolved inelastic electron tunneling spectroscopy (IETS) with the STM of single molecule vibrations is the main probe for all the measurements in this program. The range of application of STM-IETS is significantly broadened by lowering the temperature with  $^3\text{He}$  cooling to increase the energy resolution from  $\sim 8$  meV at 10 K. The high energy resolution of  $\sim 0.6$  meV at 600 mK resolves closely separated peaks, brings out low intensity modes, and follows small changes in the intensity, energy, and line shape of the vibrational peaks. The STM-IETS with high energy and spatial resolutions enables itProbe to monitor energy shifts in the CO hindered translational mode as the CO-tip is scanned over an adsorbed molecule. Images are obtained that relate to the two-dimensional slices of the potential energy surface at different chosen heights above the substrate, rendering a tomography of the molecule. Comparison of experimental results to density functional theory (DFT) calculations provides an explanation into the origin of the contrast in itProbe images by relating them to the potential energy surface of the composite CO-tip with the adsorbed molecule. Results from these studies provide information on the electronic, vibrational, and structural properties, as well as how these properties relate to the reactivity, chemical sensing, self-assembly, and other chemical interactions of higher complexity. This project leads to new insights into surface chemistry and catalysis, environmental processes and energy generation, electronic processing and electron transport through molecules as in molecular electronics.

## **Recent Progress:**

Results obtained during the past year are described in this report. The fact that molecules self-assemble into ordered structures that vary in symmetry from the substrate points to intermolecular bonding. Thus features between molecules revealed in itProbe images can be attributed to intermolecular bonding that drives the self-assembly. For isolated single molecules, itProbe images provide visual verification of expected skeletal structures, as shown in Fig. 1 for 6 selected molecules. However, new features have also been discovered for some of these molecules. Intramolecular interactions are revealed in cobalt(II) phthalocyanine among the two hydrogens in C-H bonds and the lone pair of electrons of the nearest N atom. When adsorbed on the surface, cyclooctatetraene assumes a planar structure even though DFT calculations do not

show the required two-electrons charge transfer to the ring to achieve aromaticity. In the case of hexabromobenzene, a ring is present around the molecule, suggesting a potential energy barrier surrounding the molecule. In all the molecules, an outer ring is consistently imaged, suggesting the Van der Waals radius for each molecule.

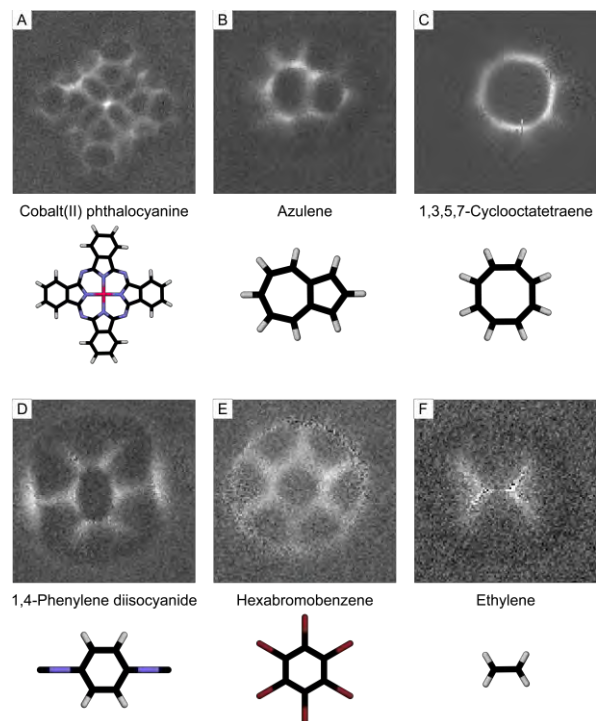


**Fig. 1: itProbe images of single molecules.**

Skeletal structures of isolated single molecules reveal details of the “expected” chemical structure and also features that are new to our understanding of chemical interactions. The technique is best suited to imaging molecules that are close to planar structure when adsorbed on the surface. itprobe can be applied to cyclic and noncyclic molecules. The size of the images varies for the six molecules ranging in size from cobalt(II) phthalocyanine to ethylene. These molecules were adsorbed on Ag(110) and imaged at 600 mK. In addition to imaging the skeletal structure by the itProbe, the CO-tip resolves individual atoms of the underlying substrate, hence revealing the bonding site of the molecules. This information is important to guide theoretical calculations by DFT.

A significant application of the itProbe lies in the imaging of intermolecular interactions. These interactions are responsible for a wide range of hierarchical structures and functions in chemical and biological systems, such as molecular recognition, self-assembly, and folding. The intermolecular interactions are usually weaker than those that lead to bonds between atoms that form molecules. While the skeletal structures depicting molecules largely reflect the nature of the intramolecular covalent bonds, as those shown in Fig. 1, intermolecular interactions lead to complex structures based on weaker Van der Waals forces, hydrogen and halogen bonds, and other types of interactions arising from small rearrangement of the electron density. A comprehensive perspective of chemical bonds requires the understanding of both intramolecular and intermolecular interactions.

As an example, the self-assembly of 1,3,5-trifluorobenzene ( $C_6H_3F_3$ ) poses two interesting questions: 1. How do the molecules self-assemble? 2. How do the hydrogen bond and the halogen bond compete and coordinate to produce the lowest energy state for the self-assembly? For hexafluorobenzene ( $C_6F_6$ ), the halogen bond prevails since it is the only type of bonding that is possible. In 1,3,5-trifluorobenzene, the molecule has more “knobs”. It is not obvious priori how the molecules are coupled to each other. This network could not be revealed by topography alone, either with the bare metal tip or a CO-terminated metal tip. In Fig. 2, the intermolecular interactions are fully resolved and in hindsight, the pattern of intermolecular interactions makes sense but difficult to predict. In 1,3-difluorobenzene ( $C_6H_4F_2$ ), not shown here, the lower symmetry of the molecule leads to dominant hydrogen bond between

H and F and to a lesser degree halogen bond between F's because the molecule has less number of F atoms. While there is translational order, the rotational order is missing.

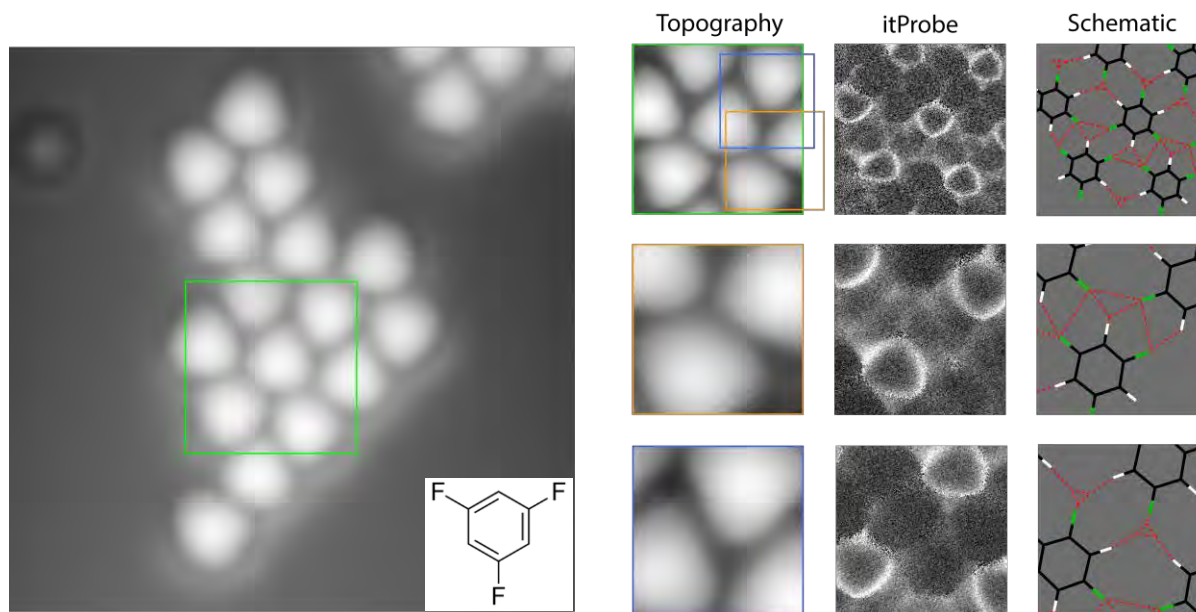


**Fig. 2: Self-assembly for probing nature of intermolecular bonding.** 1,3,5-trifluorobenzene ( $C_6H_3F_3$ ) molecules self-assemble into islands when exposed to Ag(110) at 25 K, followed by cooling down to 600 mK for spectroscopy and imaging. Leftmost panel: One of the islands imaged with a CO-terminated tip formed by transferring a CO molecule to a Ag tip. A zoom-in of the island marked by the green square is imaged and displayed in the topmost row on the right. The three columns are topography, itProbe image, and schematic of the itProbe image. The unit cell is composed of two types of triangular bonding configurations: two adjacent rows held together by one H in C-H bond interacting with two F's in C-F bonds, alternating with two H's in C-H bonds interacting with one F in C-F bond. These two different types of interactions lead to different spacings between two adjacent layers, as can be seen in the topmost itProbe image. These two triangular bonding configurations are imaged in the middle and bottom rows, as noted by zooming in the areas outlined by the blue and orange squares.

The intermolecular interactions have also been imaged in the self-assembly of hexabromobenzene ( $C_6Br_6$ ). Distinct from fluorobenzenes, the larger polarizability, C-Br bond length, and the distinct ring around the molecule provide a deeper understanding into the nature of halogen bonding and intermolecular interactions.

### **Future Plans:**

The relationship among the molecular composition, structure, bonding, and reactivity is one of the central dogmatic principles in chemistry. The itProbe images the structure and bonding in single molecules and interactions between molecules that are responsible for the formation of larger molecular structures. The focus in the coming year lies in elucidating two-dimensional water clusters on surfaces with the aim to understand the nature of the hydrogen bond by imaging the sharing of protons in the bonding. The manipulation of water molecules to

induce interaction with coadsorbed NaCl molecules opens a new avenue for direct visualization of the solvation of single  $\text{Na}^+$  and  $\text{Cl}^-$  ions by water molecules and the nature of the ionic bond in an isolated NaCl molecule. In NaCl clusters, there lies the opportunity to understand the formation of salt. Instead of halogens, molecules containing nitrogen and oxygen atoms also are known to be involved in hydrogen bonds in forming extended molecular structures in chemical and biological systems. In the simplest case of molecular nitrogen ( $\text{N}_2$ ), itProbe can be used to ask the question on the nature of intermolecular interactions between  $\text{N}_2$  in the liquid and solid states. Similarly, the nature of the intermolecular interactions between carbon dioxide molecules ( $\text{CO}_2$ ) can be imaged by the itProbe. These interesting states of matter and the chemical interactions within them require low temperatures for probing them at the fundamental level through fine energy resolution spectroscopy and imaging with sub-Ångström spatial resolution.

### **References to Publications of DOE Sponsored Research:**

- [1] “*Rotational Spectromicroscopy: Imaging the Orbital Interaction between Molecular Hydrogen and an Adsorbed Molecule*”, S. Li, D. Yuan, A. Yu, G. Czap, R. Wu, and W. Ho, Phys. Rev. Lett. **114**, 206101 (2015). Additional support is obtained for S.L. A.Y., and D.Y. from the NSF Center for Chemical Innovation: Chemistry at the Space-Time Limit.
- [2] “*Single-Molecule Rotational and Vibrational Spectroscopy and Microscopy with the Scanning Tunneling Microscope*”, A. Yu, S. Li, G. Czap, and W. Ho, J. Phys. Chem. C **119**, 14737 (2015). Additional support is obtained for A.Y. and S.L. from the NSF Center for Chemical Innovation: Chemistry at the Space-Time Limit.
- [3] “*Trapping and Characterization of a Single Hydrogen Molecule in a Continuously Tunable Nanocavity*”, H. Wang, S. Li, H. He, A. Yu, F. Toledo, Z. Han, W. Ho, and R.Q. Wu, J. Phys. Chem. Lett. **6**, 3453 (2015). Additional support is obtained for H.W., S.L., H.H., and A.Y. from the NSF Center for Chemical Innovation: Chemistry at the Space-Time Limit, and for H.W. and R.W. from the Chinese National Science Foundation.
- [4] “*Nature of Asymmetry in the Vibrational Line Shape of Single-Molecule Inelastic Electron Tunneling Spectroscopy with the STM*”, C. Xu, C.-L. Chiang, Z. Han, and W. Ho, Phys. Rev. Lett. **116**, 166101 (2016). Additional support is obtained for C.C. from the NSF Condensed Matter Physics Program.
- [5] “*Quantitative Understanding of van der Waals Interactions by Analyzing the Adsorption Structure and Low-Frequency Vibrational Modes of Single Benzene Molecules on Silver*”, D. Yuan, Z. Han, G. Czap, C.-L. Chiang, C. Xu, W. Ho, and R.Q. Wu, J. Phys. Chem. Lett. **7**, 2228 (2016). Additional support is obtained for D.Y. from the NSF Center for Chemical Innovation: Chemistry at the Space-Time Limit, and for C.C. from the NSF Condensed Matter Physics Program.
- [6] “*Tunneling-Electron-Induced Light Emission from Single Gold Nanoclusters*”, A. Yu, S. Li, G. Czap, and W. Ho, Nano Lett. DOI: 10.1021/acs.nanolett.6b018245 (2016). Additional support is obtained for A.Y. and S.L. from the NSF Center for Chemical Innovation: Chemistry at the Space-Time Limit.

**DEVELOPMENT OF APPROACHES TO MODEL EXCITED STATE  
CHARGE AND ENERGY TRANSFER IN SOLUTION**

Christine Isborn, [cisborn@ucmerced.edu](mailto:cisborn@ucmerced.edu), University of California Merced

Aurora Clark, [auclark@wsu.edu](mailto:auclark@wsu.edu), Washington State University

Thomas Markland, [tmarkland@stanford.edu](mailto:tmarkland@stanford.edu), Stanford University

### **Program Scope**

The development of next generation energy conversion and catalytic systems requires a fundamental understanding of the interplay between photo-excitation and the resulting proton and electron transfer processes that occur in solution. To address these challenges requires accurate and efficient methods to compute ground and excited states, as well as the ability to treat the dynamics of electrons, protons, and electronic energy transfer in the presence of solvent fluctuations occurring over a range of time-scales.

Our work will develop accurate and efficient theoretical models for solution phase reactions. These developments will be used to create a highly scalable computational approach that allows for the accurate computation of electronic ground and excited states, and treats the dynamics of electrons and protons in the presence of solvent. These techniques will provide an improved understanding of photo-initiated excitations, electron transfer, and proton coupled electron transfer processes, and will also elucidate the key role that hydrogen bonding plays in tuning the energetics, selectivity, and rate of electron, proton, and energy transfer in solution.

The development and combination of these computational approaches will enable the broader computational community to access solution phase reactivity at an unprecedented level of chemical complexity. This in turn will enable the development of true predictive models that aid in experimental interpretation and the rational design of solution-mediated chemical processes.

The goal of the proposed work is to create a computational approach that improves the accuracy of theoretical techniques for modeling excited states and quantum dynamics in solution. In concert with this improved accuracy, the analysis techniques will help to provide a detailed understanding of the key role that hydrogen bonding plays, both internally and from solvents, in tuning the energetics, selectivity, and rate of electron, proton, and energy transfer in the condensed phase. In this report, we describe the progress our team has made towards three main objectives:

- 1) Accurate calculation of electronic excitations and charge transfer in solution
- 2) Development of improved nonadiabatic dynamic algorithms that allows for transitions between multiple excited state surfaces by combining semiclassical and Master equation approaches
- 3) Introduction of a theoretical and computational framework for performing quantum dynamics of large condensed phase systems and analyzing the role of solvent dynamics

Below is described recent progress and future plans with a focus on Objective 1.

### **Recent Progress**

#### **Objective 1: Accurate electronic excitations and charge removal in solution**

In the past year Isborn has focused on developing a better model for computing the energies of electronic excitations in solution. One paper has been published in this area and we anticipate another two manuscripts will be submitted in the next 1-2 months. Using large scale electronic structure calculations that include multiple solvation layers treated fully quantum mechanically (QM), we have determined that:

- (1.) The choice of density functional and the amount of exact exchange is crucial for accurate modeling of ionization and electronic excitation in solution due to overdelocalization of the removed electron and charge transfer errors. These errors increase with amount of explicit solvent.
- (2.) A full solvation layer of QM solvent is required to obtain close to converged excitation energies. Trends are examined for solutes of differing charge and polarity.
- (3.) A polarizable continuum environment must be used with caution when including explicit QM solvent in the calculation. A molecular mechanical (MM) point charge model for the long-range solvent is preferable.
- (4.) Nuclear quantum effects play an important role in determining absorption spectra shape. This appears to be true even when heavy atom movements (such as a C-C bond stretch) are the main determiner of spectral shape. (Isborn-Markland collaborative work)

Below is a summary of progress in each of these topics for this objective.

### **(1.) Size-dependent error in the density functional theory ionization potential in solution**

Density functional theory is often the method of choice for modeling the energetics of large molecules and including explicit solvation effects. Work supported by this grant has been published that shows that when modeling ionization of a solute in aqueous solution, the ionized electron will be incorrectly removed from the surrounding solvent with many standard density functionals (ex: B3LYP, BH&HLYP, LC-BLYP with a range separation parameter smaller than  $0.3 \text{ bohr}^{-1}$ ). The delocalization of the ionized electron throughout the solvent results in a size-dependent lowering of the ionization potential for functionals without enough exact exchange. We demonstrated that increasing the amount of exact exchange changes the character of the polarization of the solvent molecules; for small amounts of exact exchange the solvent molecules contribute a fraction of their electron density to the ionized electron, but for larger amounts of exact exchange they properly polarize in response to the cationic solute. Even long-range corrected hybrid functionals yield unphysical electron densities without the correct polarization response of the solvent when the range-separation parameter is below  $0.4 \text{ bohr}^{-1}$  (Figure 1).

For optimal tuning of range-separated hybrid functionals, The optimal range separation parameter will slowly decrease as explicit solvent is included in the QM region of the calculation, leveling off after approximately two solvation spheres are included. Overall, we recommend to the computational community interested in modeling aqueous charge transfer phenomena to use a long-range separated functional with a range-separation parameter of at least  $0.4 \text{ bohr}^{-1}$  to obtain the correct polarization response of the solvent.

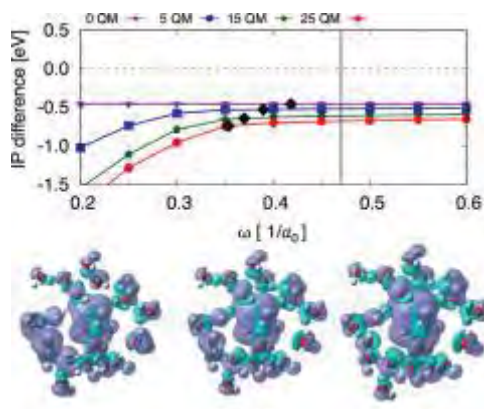


**Figure 1.** The IP difference for a solvated ethene molecule as a function of range separation parameter  $\omega$ . The density difference plot shows the solvent correctly polarizing at  $\omega > 0.4 \text{ bohr}^{-1}$ .

### **(2.) Convergence of excitation energies with QM region size**

We have examined convergence of excited state properties with QM solvation region size for eight different solutes, both neutral and anionic. We systematically varied the polarity of the solutes to see how solute polarity correlates with amount of QM solvent needed to reach a converged result. For example, does an anion require more QM solvent than a nonpolar

hydrocarbon? Our results show that excitation energies are generally converged within 0.05 eV of the large-scale result when approximately one solvation layer of QM solvent is included in the calculation. However, we see marked differences in the convergence behavior using configuration interaction singles (CIS), which has 100% exact exchange for all inter-electronic distances, and time-dependent density functional theory with a long-range corrected functional (100% exact at long-range). The CIS method follows the convergence trends that might be expected based on solute polarity: the excitation energies for anionic solute 1 converge slowest and those for the nonpolar hydrocarbon converge fastest. This is not quite the trend observed for TDDFT, which shows that solutes of intermediate polarity converge more slowly. It is not clear if the difference in the two methods is due to small charge-transfer error artifacts of TDDFT even with a long-range corrected functional, or perhaps correlation effects are important and CIS is not capturing the full polarization response of the solute-solvent interactions.

### **(3.) Polarizable continuum environment with explicit quantum mechanical solvent**

Mixed quantum mechanical (QM)/classical methods provide a computationally efficient approach to modeling both ground and excited state chemical processes in the condensed phase. An ideal approach would combine some amount of the environment in the QM region to account for specific short-range interactions with a computationally affordable classical model for long-range interactions. The best computational protocol for these mixed QM/classical methods can be determined by comparison with converged molecular properties. One decision that must be made is the choice of classical model, i.e. molecular mechanical (MM) fixed point charges or a polarizable continuum model (PCM), when computing electronic excitations in solution. We computed the excitation energy of three pairs of neutral/anionic molecules in aqueous solvent, including up to 250 water molecules in the QM region. Interestingly, the convergence is similar for molecular mechanical point charges and a polarizable continuum model. We also found that while the van der Waals (VDW) definition of the PCM cavity is adequate for molecular structures with small amounts of QM solvent, larger QM solvent layers had gaps in the VDW PCM cavity (see Figure 2), leading to asymptotically incorrect excitation energies. Given that the VDW cavity leads to unphysical solute-solvent interactions, it is advised to instead use a solvent excluded surface (SES) cavity for QM/PCM calculations that include QM solvent. However, given that PCM calculations are more computationally demanding than those with MM charges representing the bulk solvent, and that the rate of excitation energy convergence is similar for the two models, MM water models are preferable over PCM when available.

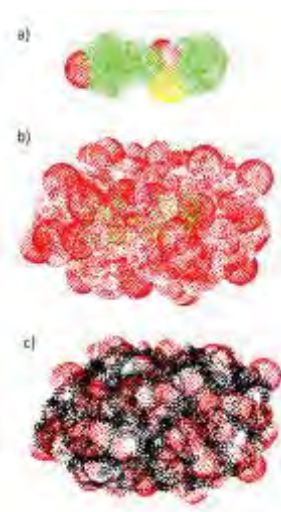


**Figure 2.** Tesserae of the PCM cavity surface using a) VDW surface without QM solvent, b) VDW surface with QM solvent, and c) SES with QM solvent. Color corresponds to origin of the tessera: carbon (green), oxygen (red), sulfur (yellow), hydrogen (white), and added sphere (black).

### **Future Plans**

(1.) Accurate determination of solute/solvent band structure. We noticed large differences in the relative energetics of the solvent/solute valence band with HF and long-range corrected DFT methods, which directly correlated with the convergence trends for the excitation energies. Because of delocalization errors in DFT and the lack of correlation in HF, it isn't clear which theoretical method is more accurate for the band structure calculation for these relative energetics. We are analyzing the band structure of the solute and solvent with various levels of theory, and we hope to compare these results to those obtained by additional methods, such as the Green function and polarization potential (GW) technique, which includes a many-body perturbation correction to the density functional theory quasiparticle energies.

(2.) The role of nuclear quantum effects in determining absorption spectra shape. Our initial studies suggest that even when heavy atom movements (such as a C-C bond stretch) are the main determiner of spectral shape, the nuclear quantum effects are significant in changing the shape and width of the spectrum. The vacuum configurations generated using path integral simulations, which include nuclear quantum effects, give rise to markedly broader absorption spectra in considerably better agreement with experiment. We are starting simulations of the chromophores in solution to see how the nuclear quantum effects that include solute-solvent hydrogen bonding affect the absorption spectra.

(3.) Validation of real-time TDDFT charge transfer for molecular systems. In our previous work we've explored some of the inaccuracies of real-time TDDFT for resonant charge transfer due to the ubiquitous adiabatic approximation. However, these inaccuracies have mainly been explored for small model systems with only two electrons. We plan to use this methodology on larger molecular systems, starting with simple donor-acceptor ethylene systems that are more typical of the dye molecules used in energy applications.

### DOE Sponsored Publications

[1] Size-dependent error of the density functional theory ionization potential in vacuum and solution. X. A. Sosa Vazquez and C. M. Isborn *J. Chem. Phys.* 143, 244105 (2015)

[2] Nonadiabatic dynamics in atomistic environments: harnessing quantum-classical theory with generalized quantum master equations. W. C. Pfalzgraff, A. Kelly and T. E. Markland *J. Phys. Chem. Lett.*, 6, 4743-4748 (2015)[3] Electron Dynamics with Real-Time Time-Dependent Density Functional Theory. M. R. Provorse and C. M. Isborn *Int. J. Quant. Chem.* 116, 739-749 (2016)

[4] Generalized Quantum Master Equations In and Out of Equilibrium: When Can One Win? A. Kelly, A. Montoya-Castillo, L. Wang and T. E. Markland *J. Chem. Phys.* 144, 184105 (2016)

[5] Simulating Nuclear and Electronic Quantum Effects in Enzymes. L. Wang, C. M. Isborn, and T. E. Markland *Methods in Enzymology*, 577, 389-418 (2016)

[6] Unraveling the dynamics and structure of functionalized self-assembled monolayers on gold using 2D IR spectroscopy and MD simulations. C. Yan, R. Yuan, W. C. Pfalzgraff, J. Nishida, L. Wang, T. E. Markland, M. D. Fayer *Proc. Natl. Acad. Sci.*, 113 (18), 4929-4934 (2016)

[7] Nuclear Quantum Effects in Water and Aqueous Systems: Experiment, Theory, and Current Challenges. M. Ceriotti, W. Fang, P. G. Kusalik, R. H. McKenzie, M. A. Morales, A. Michaelides and T. E. Markland *Chem. Rev.*, 116 (13), 7529-7550 (2016)

[8] Ab initio molecular dynamics with nuclear quantum effects at classical cost: ring polymer contraction for density functional theory. O. Marsalek and T. E. Markland *J. Chem. Phys.* 144, 054112 (2016)

# DE-FG02-07ER15889: Probing catalytic activity in defect sites in transition metal oxides and sulfides using cluster models: A combined experimental and theoretical approach

Caroline Chick Jarrold and Krishnan Raghavachari

Indiana University, Department of Chemistry, 800 East Kirkwood Ave.

Bloomington, IN 47405

[cjarrold@indiana.edu](mailto:cjarrold@indiana.edu), [kraghava@indiana.edu](mailto:kraghava@indiana.edu)

## I. Program Scope

Our research program combines experimental and computational methods to study a range of cluster models for heterogeneous catalytic materials. The focus of our studies has been transition metal oxide and sulfide clusters in lower-than-traditional oxidation states, and their chemical and physical interactions with water. More recent efforts have included expanding experimental capabilities for generated isotopically pure metal hyper-sulfide clusters because they have recently emerged as stable solution-phase catalysts for the hydrogen evolution reaction (HER).<sup>i</sup> In addition, we have continued evaluating sacrificial reagents for full-cycle catalysis of H<sub>2</sub> production from water decomposition. The experiments and calculations are designed to probe fundamental, cluster-substrate molecular-scale interactions that are governed by charge state, peculiar oxidation states, and unique molecular structures.

The general strategy of our studies continues to be as follows: (1) Determine how the molecular and electronic structures of transition metal suboxide and subsulfide clusters evolve as a function of oxidation state by reconciling anion photoelectron spectra of the bare clusters with high-level DFT calculations. Anions are of particular interest because of the propensity of metal oxide and sulfides to accumulate electrons in applied systems. (2) Measure and analyze the kinetics of cluster reactivity with water, with and without the inclusion of sacrificial reagents. (3) Dissect possible reaction mechanisms computationally, to determine whether catalytically relevant interactions are involved. (4) Verify these challenging computational studies by spectroscopic investigation [typically, anion photoelectron (PE) spectroscopy] of observed reactive intermediates. (5) Probe the effect of local electronic excitation on bare clusters and cluster complexes, to evaluate photocatalytic processes. The overarching goal of this project is to identify particular defect structures that balance structural stability with electronic activity, both of which are necessary for a site to be simultaneously robust and catalytically active, and to find trends and patterns in activity that can lead to improvement of existing applied catalytic systems, or the discovery of new systems.

## II. Recent Progress

A. Production and characterization of metal sulfide clusters, and computational study of molybdenum hypersulfide cluster as catalysts for H<sub>2</sub> evolution from water. Recently, small molybdenum hyper-sulfide clusters have been found to be active catalysts for the hydrogen evolution reaction, and results of recent computational studies Experimentally, the move from the group 6 transition metal oxides to the sulfides has been complicated by the spontaneous oxidation of the metal sulfides. However, we have had recent success in generating new Mo<sub>x</sub>S<sub>y</sub><sup>-</sup> clusters from newly synthesized MoS<sub>2</sub> using the natural isotopic Mo-metal, as seen in Fig. 1, and are currently extending the high-temperature synthetic methods for the production of isotopically pure <sup>98</sup>Mo<sub>x</sub>S<sub>y</sub> clusters, which will be

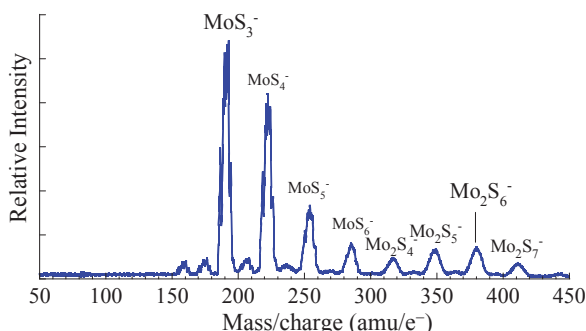


**Figure 1.** Mass distribution of molybdenum sulfide cluster anions generated from ablation of a MoS<sub>2</sub> target.

<sup>i</sup> (a) H.I. Karunadasa *et al.*, *Science* **335**, 698 (2012); (b) Z. Huang, *et al.*, *Angew. Chem. Int. Ed.* **54**, 15181 (2015); (c) J. Kibsgaard *et al.*, *Nat. Chem.* **6**, 248 (2014).

critical for subsequent reactivity studies targeting the HER from water in which cluster masses may change by 1 or 2 amu while undergoing reactions with water.

One of several fundamental difference between molybdenum oxide and molybdenum sulfide is the stoichiometry;  $\text{Mo}_2\text{S}_4^-$ , for example, reflects the bulk stoichiometry of the bulk sulfide, while  $\text{Mo}_2\text{O}_4^-$  is sub-stoichiometric relative to the bulk oxide. The preliminary PE spectra of these congeners shown in Figure 2 exhibit striking differences in the electronic (and therefore, molecular) structures, which we will be following up with computational studies.

To gain insight into the activity of  $\text{MoS}_2$  catalysts for the HER we have conducted studies into the explicit mechanisms of action for systems carrying the  $\text{MoS}_2$  motif. To date computational work on HER catalysis has focused almost solely on the proton binding energies of the catalysts, which may omit

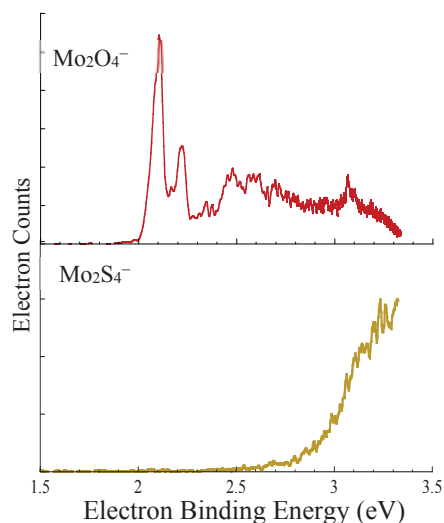


**Figure 2.** PE spectra of  $\text{Mo}_2\text{X}_4^-$  ( $\text{X} = \text{O}, \text{S}$ ) clusters obtained using  $h\nu = 3.49$  eV.

important features of the electronic structure of  $\text{MoS}_2$ . We have therefore investigated the  $[(\text{PY5Me}_2)\text{MoS}_2]^{2+}$  system (Karunadasa *et al.*) which is a noteworthy moiety that mimics the edge sites of bulk  $\text{MoS}_2$ , the abundance of which has been shown to correlate to HER reactivity in  $\text{MoS}_2$  based materials.

The mechanism for hydrogen evolution by  $[(\text{PY5Me}_2)\text{MoS}_2]^{2+}$  was investigated using DFT with the B3LYP functional and the def2-SVP basis set. Production of  $\text{H}_2$  was found to proceed through electrochemical reduction of the starting species at  $-270$  mV to form **2** followed by protonation at the disulfide to generate **3** and a second electrochemical reduction at  $-480$  mV to form the cation **4**. The CV reduction waves observed experimentally were irreversible making it impossible to determine  $E^0$  from the data given. However, the calculated data reports  $E^0$  at slightly more positive than the peak potentials observed for the first and second reduction ( $-340$  mV and  $-530$  mV respectively) which is what is expected. This agreement allows us to confidently state that the calculated data are consistent with experiment even if a direct comparison with the experimental peak potential may not be possible. From **4** dissociation of a

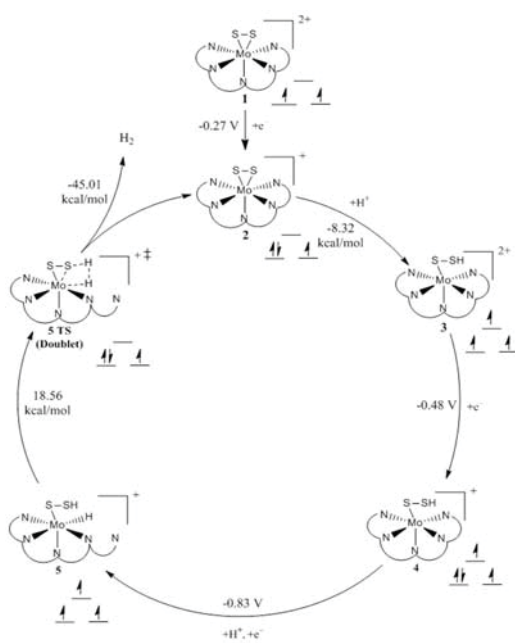


**Figure 3.** Computationally determined mechanism of HER catalyzed by Chang and coworkers Mo-complex.<sup>i(a)</sup> All voltages are reported vs. SHE.

$\text{PY5Me}_2$  ligand arm to open a coordination site combined with proton coupled electron transfer (PCET) to form the hydride containing species **5** produces the potential most consistent with the observed onset of the catalytic wave. Overall the calculated mechanism is very consistent with experimental data.

## B. Theoretical and Experimental studies on potential implementation of sacrificial reagents for full-cycle catalytic HER using the $\text{Mo}_2\text{O}_4^- - \text{Mo}_2\text{O}_5^-$ cluster pair.

Much of the work to date has involved transition metal suboxide reactions with water that generate  $\text{H}_2$ , but then leave the metal oxide cluster in higher and unreactive oxidation states. In the past year, we have

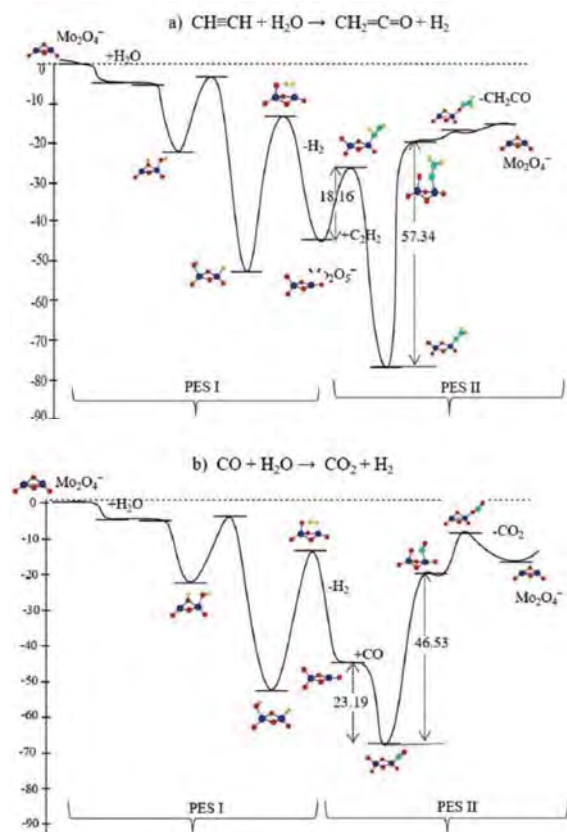
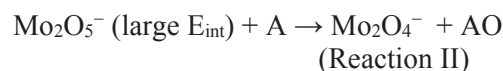


**Figure 4.** Free energy reaction profiles (PES I and PES II) for H<sub>2</sub>O reduction by (a) acetylene and (b) CO in the presence of the Mo<sub>2</sub>O<sub>4</sub><sup>-</sup>/Mo<sub>2</sub>O<sub>5</sub><sup>-</sup> cluster couple. Relative energies (kcal mol<sup>-1</sup>) of the species are calculated from the separated reactants at the entrance channel.

measurements with both Mo<sub>x</sub>O<sub>y</sub><sup>-</sup> and W<sub>x</sub>O<sub>y</sub><sup>-</sup> cluster systems. In both cases, introduction of C<sub>2</sub>H<sub>4</sub> with H<sub>2</sub>O to the cluster reactor suppresses the apparent rate of cluster oxidation, which may be evidence that the rate of Reaction II is becoming competitive with the rate of Reaction I. Figure 5 gives snapshots of the mass spectra in the <sup>98</sup>Mo<sub>2</sub>O<sub>y</sub><sup>-</sup> mass range, showing both nearly identical initial cluster distributions (dotted trace) and post reaction distributions for identical H<sub>2</sub>O concentrations in the reactor. The bottom panel shows the result of adding C<sub>2</sub>H<sub>4</sub> to the reactor: Mo<sub>2</sub>O<sub>4</sub><sup>-</sup> is more abundant, and what we had previously learned to be the terminal water addition product, Mo<sub>2</sub>O<sub>6</sub>H<sub>2</sub><sup>-</sup>, is dramatically suppressed. What is not shown because of space constraints is that the presence of water with C<sub>2</sub>H<sub>4</sub> suppresses the Mo<sub>x</sub>O<sub>y</sub><sup>-</sup> addition product formation. We also observe C<sub>m</sub>H<sub>n</sub>O<sup>-</sup> species in the mass spectrum, giving further evidence that C<sub>2</sub>H<sub>4</sub> is serving as a sacrificial reagent. There are other results, such as a dramatic increase in MoO<sub>2</sub><sup>-</sup> in the mass

continued to explore experimental full-cycle models that implement a sacrificial reagent that reduces the transition metal oxide cluster before it dissipates the internal energy gained from the new M=O bond formation, focusing on the Mo<sub>2</sub>O<sub>4</sub><sup>-</sup>-Mo<sub>2</sub>O<sub>5</sub><sup>-</sup> cluster couple:



Computationally, we determined that the dual-reaction pathway has deeply bound trapped metal carbon-containing products. Figure 4 shows the free energies along Reactions I and II for both A = acetylene and CO. Both molecules provide exothermic pathways for H<sub>2</sub> production accompanied by oxidation of A, but both feature deep wells associated with Mo<sub>2</sub>O<sub>5</sub><sup>-</sup>-A complex formation. The conclusion is therefore that high internal energy must be maintained over the course of the dual reaction in order to achieve catalyst regeneration.

From a practical standpoint, C<sub>2</sub>H<sub>4</sub> has proven to be too reactive toward the transition metal suboxide clusters, (it was the first molecule we have found to react with the inert Mo<sub>3</sub>O<sub>6</sub><sup>-</sup> cluster). We instead have focused on ethene (C<sub>2</sub>H<sub>4</sub>), and have made

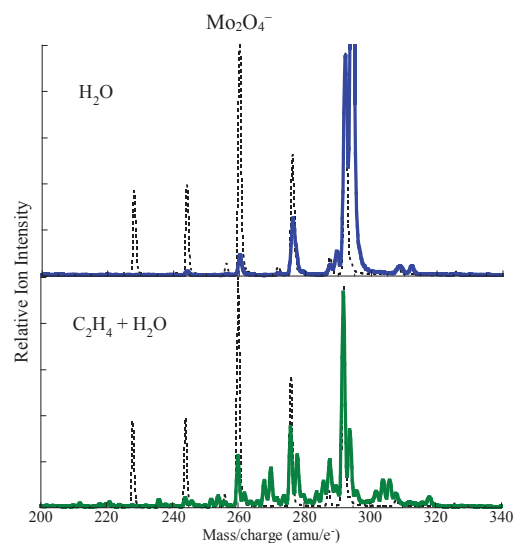


**Figure 5.** Mass spectra of initial reactant (dotted black line) and final product distributions for reactions with H<sub>2</sub>O (blue) and C<sub>2</sub>H<sub>4</sub> combined with H<sub>2</sub>O (green)

spectrum upon any hydrocarbon addition, that indicate cluster fragmentation is occurring. We will be following up on this result, as summarized below.

### III. Future Plans

The enduring strength of the research program is the synergistic interplay between theory and experiment. We will continue to computationally elucidate the HER mechanism for the larger  $\text{Mo}_x\text{S}_y$  hypersulfide clusters, and will begin our mass spectrometric-based reactivity studies on  $^{98}\text{Mo}_x\text{S}_y^-$  ( $y > 2x$ ) clusters with water. Additionally, having recently completed computational studies on heteronuclear  $\text{MoWS}_y$  cluster structures and properties, the logical next step is to measure the spectra of these species with a range of compositions, also following up with reactivity studies. The differences in reducibility and  $M$ -S bond energies is anticipated to result in an interesting electronic and structural environment that will strongly influence interactions with water. Finally, as the reactivity studies implement increasingly complex reaction conditions, we have been designing an ion carpet-based reactor that will allow us to filter out a narrow range of clusters between the cluster source and the reactor. With this new stage in the source/reactor setup, we can more strongly correlate initial cluster distributions with cluster fragment and oxidized sacrificial reagent formation.

### IV. References to publications of DOE sponsored research that have appeared in 2014–present or that have been accepted for publication

1. “Hydrogen evolution from water using Mo-oxide clusters in the gas phase: DFT modeling of a complete catalytic cycle using a  $\text{Mo}_2\text{O}_4^-/\text{Mo}_2\text{O}_5^-$  cluster couple,” Manisha Ray, Arjun Saha, and Krishnan Raghavachari, *Phys. Chem. Chem. Phys.* **18**, 25687-25692 (2016). <http://dx.doi.org/10.1039/c6cp04259g>
2. “Effect of alkyl group on  $\text{M}_x\text{O}_y^- + \text{ROH}$  ( $M = \text{Mo}, \text{W}$ ;  $R = \text{Me}, \text{Et}$ ) reaction rates,” Manisha Ray, Sarah E. Waller, and Caroline Chick Jarrold, *J. Phys. Chem. A* **120**, 1508-1519 (2016). <http://dx.doi.org/10.1021/acs.jpca.6b00102>
3. “Role of weakly-bound complexes in temperature-dependence and relative rates of  $\text{M}_x\text{O}_y^- + \text{H}_2\text{O}$  ( $M = \text{Mo}, \text{W}$ ) reactions,” Jared O. Kafader, Manisha Ray, Krishnan Raghavachari, and Caroline Chick Jarrold, *J. Chem. Phys.* **144**, 074307(1-9) (2016). <http://dx.doi.org/10.1063/1.4941829>
4. “ $\text{H}_2\text{S}$  reactivity on oxygen-deficient heterotrimetallic cores: Cluster fluxionality simulates dynamic aspects of surface chemical reactions,” Debashis Adhikari and Krishnan Raghavachari, *J. Phys. Chem. A* **120**, 447-472 (2016). <http://dx.doi.org/10.1021/acs.jpca.5b10899>
5. “Direct Reduction of Alkyl Halides at Silver in Dimethylformamide: Effects of Position and Identity of the Halogen”, Lauren M. Strawsine, Arkajyoti Sengupta, Krishnan Raghavachari, and Dennis G. Peters, *ChemElectroChem*. **2**, 726–736 (2015). <http://dx.doi.org/10.1002/celec.201402410>
6. “Hydroxyl Migration in Heterotrimetallic Clusters: An Assessment of Fluxionality Pathways”, Debashis Adhikari and Krishnan Raghavachari, *J. Phys. Chem. A* **118**, 11047-11055 (2014). <http://dx.doi.org/10.1021/jp5080835>
7. “Comparative study of water reactions with  $\text{Mo}_2\text{O}_y^-$  and  $\text{W}_2\text{O}_y^-$  clusters: A combined experimental and theoretical investigation,” Manisha Ray, Sarah E. Waller, Arjun Saha, Krishnan Raghavachari, and Caroline Chick Jarrold, *J. Chem. Phys.* **141**, 104310(1-9) (2014) <http://dx.doi.org/10.1063/1.4894760>.
8. “Electronic Structures and Water Reactivity of Mixed Metal Sulfide Cluster Anions,” Arjun Saha and Krishnan Raghavachari, *J. Chem. Phys.* **141**, 074305(1-9) (2014); <http://dx.doi.org/10.1063/1.4892671>.
9. “RH and  $\text{H}_2$  production in reactions between ROH and small molybdenum oxide cluster anions,” Sarah E. Waller and Caroline Chick Jarrold, *J. Phys. Chem. A* **118**, 8493-8504 (2014); <http://dx.doi.org/10.1021/jp502021k>.
10. “Electrochemical Reduction of 2-chloro-N-phenylacetamides at Carbon and Silver Cathodes in Dimethylformamide”, Erick M. Pasciak, Arkajyoti Sengupta, Mohammad S. Mubarak, Krishnan Raghavachari and Dennis G. Peters, *Electrochim. Acta* **127**, 159-166 (2014). <http://dx.doi.org/10.1016/j.electacta.2014.01.133>.

# Critical evaluation of theoretical models for aqueous chemistry and CO<sub>2</sub> activation in the temperature-controlled cluster regime

RE: DE-FG02-00ER15066 and DE-FG02-06ER15800

Program Managers: Dr. Mark Pederson and Dr. Gregory Fiechtner

K. D. Jordan (jordan@pitt.edu), Dept. of Chemistry, University of Pittsburgh, Pittsburgh, PA 15260

M. A. Johnson (mark.johnson@yale.edu), Dept. of Chemistry, Yale University, New Haven, CT 06520

## Program Scope:

Our joint program exploits size-selected clusters as a medium with which to unravel molecular level pictures of key transient species in condensed phase and interfacial chemistry that are relevant to the mediation of radiation damaged systems and the catalytic activation of small molecules (CO<sub>2</sub>, H<sub>2</sub>O). A major advance in the past years has been our successful capture of spectroscopic snapshots of the collective reaction coordinate underlying intermolecular proton transfer in water.[5] This involved first settling a controversy in the literature regarding the structures of the protonated water tetramer and pentamer, which had been called in question based on recent theoretical work employing methods often used to treat the behavior of the excess proton in liquid water. The assignments were clarified by establishing the spectral homogeneity using IR-IR double resonance and following the evolution of the band patterns with isotopic substitution. That work was carried out in collaboration with the Asmis group at the University of Leibniz, which has access to the IR free electron laser at the Fritz Haber Institute in Berlin. We have also extended our work beyond aqueous systems to establish the fundamental interactions at play in a variety of widely used ionic liquids (ILs), with specific emphasis on quantifying the role of hydrogen bonding in EMIM-based ILs, an issue that has proven difficult to resolve with measurements on the bulk systems.

## I. Spectroscopic snapshots of the proton transfer mechanism in water

Proton conduction is known to be anomalously fast in liquid water, but because of the diffuse nature of vibrational bands associated with the excess proton in liquid water, it has not been possible to obtain well defined spectroscopic snapshots of the proton relay process. By

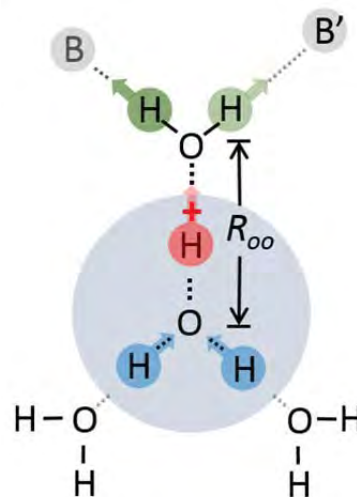
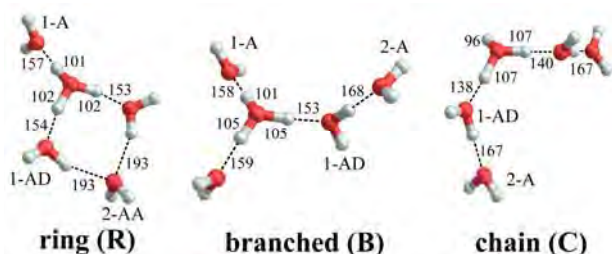


Fig. 1. Schematic of the proton relay mechanism, where the symmetric H<sub>9</sub>O<sub>4</sub><sup>+</sup> Eigen ion is distorted upon addition of different proton acceptors B and B' (B=H<sub>2</sub>, N<sub>2</sub>, CO, H<sub>2</sub>O; B'=H<sub>2</sub>O) to one of the water molecules. The presence of one or more adducts causes a hydrogen atom of the H<sub>3</sub>O<sup>+</sup> core to be attracted toward the tagged H<sub>2</sub>O molecule and reduces the corresponding O-O distance, R<sub>OO</sub>.

using a series of tagged  $D_3O^+(D_2O)_3$  clusters we have been able to obtain the vibrational spectra as the cluster evolves from the Eigen to the Zundel form of the hydrated proton. Figure 1 illustrates the tagging sites and the relay mechanism. The use of the deuterium isotopologue is key to this study in that the deuterium substitution suppresses the strong anharmonicities present in the all-H isotopologue. The most important outcome of this effort is the determination of the *correlations* across the vibrational spectra that are associated with the proton transfer event. Fig. 2 presents the locations of five OD stretching fundamentals at five different locations in the collective reaction coordinate, indexed by the distance between the two oxygen atoms,  $R_{OO}$ , directly involved in the transfer. The paper describing these results is currently under review at Science.[5]

## II. Nuclear Quantum Effects in the Gas Phase Vibrational Spectroscopy of the Protonated Water Pentamer

Cryogenic ion trap vibrational spectroscopy was used to study the structure of the protonated water pentamer,  $H^+(H_2O)_5$ , and its fully deuterated isotopologue,  $D^+(D_2O)_5$ , over nearly the complete infrared spectral range (220-4000  $cm^{-1}$ ) in combination with harmonic and anharmonic electronic structure calculations as well as RRKM modelling. Isomer-selective IR-IR double-resonance measurements on the  $H^+(H_2O)_5$  isotopologue establish that the spectrum is due to a single constitutional isomer B in Fig. 3, thus discounting the recent analysis of the band pattern in the context of two isomers based on AIMD simulations (Kulig and Agmon, *Phys. Chem. Chem. Phys.*, 2014, **16**, 4933-4941). The evolution of the persistent bands in the  $D^+(D_2O)_5$  cluster allowed assignments of the fundamentals in both isotopologues, and the simpler pattern displayed by the heavy isotope is consistent with the calculated spectrum for the branched, Eigen-based structure originally proposed.(J.-C. Jiang, *et al.*, *J. Am. Chem. Soc.*, 2000, **122**, 1398-1410) This pattern persists in the vibrational spectra of both isotopologues in the temperature range from 15 K up to 250 K. Accompanying electronic structure



**Fig. 3.** Of the three isomers recently invoked to explain the spectra of the protonated water pentamer, isotopic substitution and IR-IR double resonance establish that only the branched form (B) is observed experimentally.

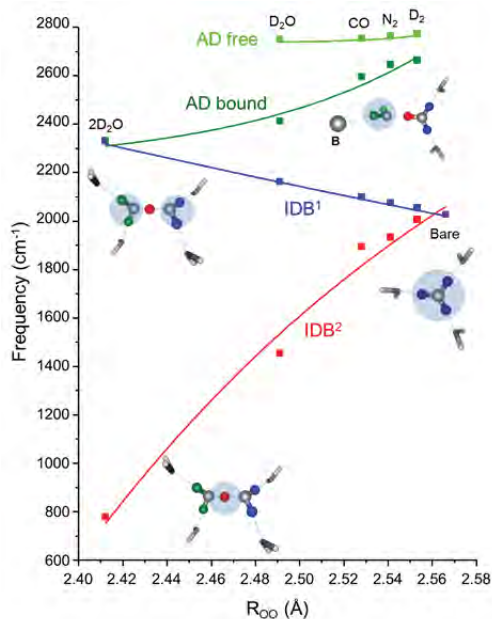


**Fig. 2.** experimental frequencies of the five OD stretches associated with the transfer of a deuteron. The extent of reaction is indexed by the computed O-O distances (MP2/aug-cc-pVDZ) for a series of  $D^+(D_2O)_4$ -B adducts that systematically transform the scaffold between the Eigen and Zundel accommodation motifs.

calculations as well as RRKM modelling. Isomer-selective IR-IR double-resonance measurements on the  $H^+(H_2O)_5$  isotopologue establish that the spectrum is due to a single constitutional isomer B in Fig. 3, thus discounting the recent analysis of the band pattern in the context of two isomers based on AIMD simulations (Kulig and Agmon, *Phys. Chem. Chem. Phys.*, 2014, **16**, 4933-4941). The evolution of the persistent bands in the  $D^+(D_2O)_5$  cluster allowed assignments of the fundamentals in both isotopologues, and the simpler pattern displayed by the heavy isotope is consistent with the calculated spectrum for the branched, Eigen-based structure originally proposed.(J.-C. Jiang, *et al.*, *J. Am. Chem. Soc.*, 2000, **122**, 1398-1410) This pattern persists in the vibrational spectra of both isotopologues in the temperature range from 15 K up to 250 K. Accompanying electronic structure

calculations show that isomer R is more stable than the B isomer in the absence of vibrational zero-point energy (ZPE) but that the relative energies of the two isomers switches upon the inclusion of ZPE. The results of this study are reported in a paper which has been accepted for the *Journal of Chemical Physics*.<sup>[7]</sup>

### III. Characterization of the primary hydration shell of the hydroxide ion with H<sub>2</sub> tagging vibrational spectroscopy of the OH<sup>-</sup>(H<sub>2</sub>O)<sub>n=2,3</sub> and OD<sup>-</sup>(D<sub>2</sub>O)<sub>n=2,3</sub> clusters

The hydroxide ion is among the strongest Brønsted bases, and its interaction with water is complicated by the fact that the binary complex, OH<sup>-</sup>·(H<sub>2</sub>O), is a covalently bound, quasi-symmetrical species. This intrinsic behavior underlies the profound changes that occur upon incremental completion of the hydration shell at the trihydrate. We have obtained isotope-dependent vibrational predissociation spectra of the H<sub>2</sub>-tagged OH<sup>-</sup>·(H<sub>2</sub>O)<sub>n=2 and 3</sub> clusters, from which it has been possible to determine the strongly coordination-dependent energies of the fundamentals due to the OH groups bound to the ion. The experimental spectra for these clusters are compared with those corresponding to completion of the hydration shell around the hydronium ion in Fig. 2, which reveals the close connection between the anomalously large mobilities of positively and negatively charged proton defects in water. These results are described in a paper that has been accepted for publication in the *Journal of Chemical Physics*.<sup>[6]</sup> This study was carried out with support from both DOE (Jordan) and NSF (Johnson).

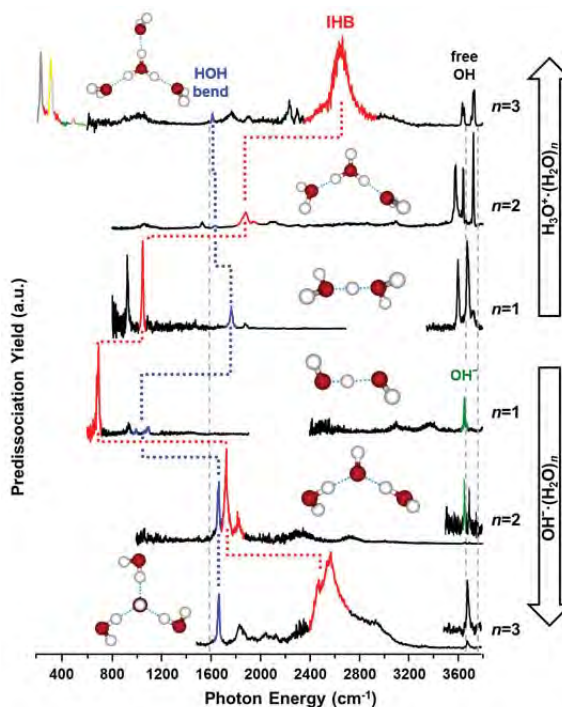


**Fig. 4.** Comparison of the vibrational spectra displayed by the OH<sup>-</sup>·(H<sub>2</sub>O)<sub>n</sub> and H<sub>3</sub>O<sup>+</sup>·(H<sub>2</sub>O)<sub>n</sub> clusters, indicating the surprising similarities in the stepwise hydration of hydroxide and hydronium leading to completion of their hydration shells.

### IV. Proton-coupled electron transfer

We extended our initial study of the [pyridine·(H<sub>2</sub>O)<sub>n</sub>]<sup>-</sup> clusters with a more sophisticated theoretical approach<sup>8</sup> to demonstrate that even in its vibrational zero-point level, the [pyridine·(H<sub>2</sub>O)<sub>3</sub>]<sup>-</sup> cluster samples both pyridine-H(OH)<sup>-</sup>·(H<sub>2</sub>O)<sub>2</sub> and pyridine·(H<sub>2</sub>O)<sub>3</sub><sup>-</sup> diabatic structures. In the former, both an electron and a positron have transferred to the pyridine, and, in the latter, the excess electron is dipole bound. In contrast, for the n = 4 cluster, the extra water molecule preferentially stabilizes the former diabatic structure.

### V. Plans for the next year

We will determine the barriers to proton migration in well-defined water networks. This will be accomplished by analyzing spectroscopic measurements of the temperature dependence of isotopomer-selective vibrational spectra of isotopically labelled as a function of cluster temperature. In parallel with the experimental studies, we will carry out calculations of the pathways for proton migration in the clusters to be studied experimentally. We will also quantify the role of hydrogen bonding in the interactions at play in EMIM-based ionic liquids with a systematic study of the  $(\text{EMIM}^+) \cdot \text{X}^-$ , ( $\text{X}=\text{Cl}, \text{Br}, \text{I}, \text{Tf}_{2n}, \text{BF}_4$ ) clusters. This will be accomplished by studying the correlations between the intensities and red-shifts of the C-D stretches with selective isotopic labeling in the key  $\text{C}_{(2)}$  position of EMIM.

### Papers in the past two years under this grant

1. “Snapshots of Proton Accommodation at a Microscopic Water Surface: Understanding the Vibrational Spectral Signatures of the Charge Defect in Cryogenically Cooled  $\text{H}^+(\text{H}_2\text{O})_{n=2-28}$  Clusters”, J. A. Fournier, C. T. Wolke, M. A. Johnson, T. T. Odbadrakh, K. D. Jordan, S. M. Kathmann, and S. S. Xantheas, *J. Phys. Chem. A*, 119, 9425-9440 (2015) (Feature Article).
2. “Comparison of the Local Binding Motifs in the Imidazolium-based Ionic Liquids  $[\text{EMIM}][\text{BF}_4]$  and  $[\text{EMMIM}][\text{BF}_4]$  through Cryogenic Ion Vibrational Predissociation Spectroscopy: Unraveling the Roles of Anharmonicity and Intermolecular Interactions,” J. A. Fournier, C. T. Wolke, C. J. Johnson, A. B. McCoy, and M. A. Johnson, *J. Chem. Phys.*, 17, 8518-8529 (2015).
3. “Understanding the Ionic Liquid  $[\text{NC}_{4111}][\text{Tf}_{2N}]$  from Individual Building Blocks: An IR-Spectroscopic Study,” K. Hanke, M. Kaufmann, G. Schwaab, M. Havenith, C. T. Wolke, O. Gorlova, M. A. Johnson, B. Kar, W. Sander, E. Sanchez-Garcia, *Phys. Chem. Chem. Phys.*, 17, 8518 (2015).
4. “Water Network-Mediated Electron-Induced Proton Transfer in Anionic  $[\text{C}_5\text{H}_5\text{N}^-(\text{H}_2\text{O})_n]$  Clusters: Size-Dependent Formation of the Pyridinium Radical for  $n > 3$ ”, A. F. DeBlase, C. T. Wolke, G. H. Weddle, K. A. Archer, K. D. Jordan, J. T. Kelly, G. S. Tschumper, N. I. Hammer, and M. A. Johnson, *J. Chem. Phys.* 143, 144305:1-5 (2015).
5. “Spectroscopic Snapshots of the Proton Transfer Mechanism in Water”, C. T. Wolke, J. A. Fournier, L. C. Dzugan, M. R. Fagiani, T. T. Odbadrakh, H. Knorke, K. D. Jordan, A. B. McCoy, K. R. Asmis, and M. A. Johnson, *Science*, submitted.
6. “Characterization of the Primary Hydration Shell of the Hydroxide Ion with  $\text{H}_2$  Tagging Vibrational Spectroscopy of the  $\text{OH}^-(\text{H}_2\text{O})_{n=2,3}$  and  $\text{OD}^-(\text{D}_2\text{O})_{n=2,3}$  Clusters”, O. Gorlova, J. W. DePalma, C. T. Wolke, A. Brathwaite, T. T. Odbadrakh, K. D. Jordan, A. B. McCoy, and M. A. Johnson, *J. Chem. Phys.*, in press.
7. “Nuclear Quantum Effects in the Gas Phase Vibrational Spectroscopy of the Protonated Water Pentamer”, M. R. Fagiani, H. Knorke, T. Esser, N. Heine, C. T. Wolke, S. Gewinner, W. Schöllkopf, M.-P. Gaigeot, R. Spezia, M.A. Johnson, and K.R. Asmis, *J. Chem. Phys.*, in press.
8. “Proton-coupled Electron Transfer in  $[\text{Pyridine}^+(\text{H}_2\text{O})_n]^-$ ,  $n = 3, 4$ , Clusters”, K. A. Archer, and K. D. Jordan, *Chem. Phys. Lett.*, in press.
9. “Theoretical Studies of Charged and Neutral Water Clusters”, K. Sen and K. D. Jordan, *Specialist Periodic Reports on Computational Chemistry*, RSC, in press.

## Nucleation Chemical Physics

Shawn M. Kathmann  
Physical Sciences Division  
Pacific Northwest National Laboratory  
902 Battelle Blvd.  
Mail Stop K1-83  
Richland, WA 99352  
[shawn.kathmann@pnl.gov](mailto:shawn.kathmann@pnl.gov)

### Program Scope

The objective of this work is to develop an understanding of the chemical physics governing nucleation. The thermodynamics and kinetics of the embryos of the nucleating phase are important because they have a strong dependence on size, shape and composition and differ significantly from bulk or isolated molecules. The technological need in these areas is to control chemical transformations to produce specific atomic or molecular nanoparticles with specific properties. Computing reaction barriers and understanding condensed phase mechanisms is much more complicated than those in the gas phase because the reactants are surrounded by solvent molecules and the configurations, energy flow, quantum and classical electric fields and potentials, and ground and excited state electronic structure of the entire statistical assembly must be considered.

### Recent Progress and Future Directions

#### *Voltage Fluctuations in Small NaCl Clusters*

The observations of luminescence during crystallization as well as electric field induced crystallization suggest that the process of crystallization may not be purely classical but also involves an essential electronic structure component. Strong electric field and/or voltage fluctuations may play an important role in this process by providing the necessary driving force for the observed electronic structure changes. The importance of electric field fluctuations driving electron transfer has been a topic of intense research since the seminal work of Marcus. The main objective of this work is to provide basic understanding of the fluctuations in charge, electric potentials, and electric fields, both classically and quantum mechanically, for concentrated aqueous NaCl electrolytes.

The stability of each ion in a finite cluster depends upon the Madelung voltages of the individual ions, each sensitive to its own environment – see Figure 1. As the salt clusters approach their ultimate crystal cubic symmetry, they pass through various non-cubic distorted or amorphous configurations, including the presence of trapped water molecules. Thus, the Madelung voltages for each ion within a salt cluster can be used as an order parameter (in addition to other order parameters e.g., the distance between ions, the angle between ion triplets, and electric fields at the ion sites) characterizing their progress along various nucleation pathways. Figure 1 shows the progression of voltages experienced by a central Cl<sup>-</sup> ion due to all other charges within the cubic clusters. The green squares denote voltages from classical  $\pm 1$  point charges and blue triangles denote quantum mechanical voltages. The dotted green line represents

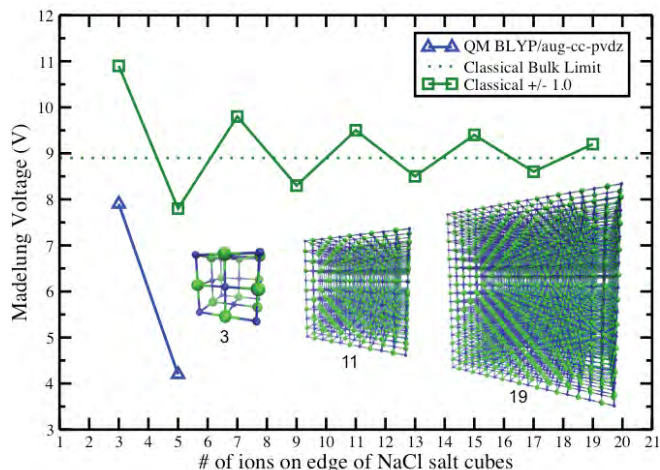


**Figure 1.** Classical and quantum Madelung voltage variations experienced by a central Cl<sup>-</sup> ion in NaCl clusters as a function of cluster size.

the bulk limit of the Madelung voltage for an infinite classical crystal composed of these  $\pm 1$  point charges. However, these classical voltages do not include important quantum effects due to the delocalized nature of electron densities nor electronic excited states of the ions. The variations in voltages, shown in Fig. 1, for both classical and quantum descriptions show large changes with the size of the salt cluster. This is significant because the voltages govern the interaction energy between the ions making up the salt clusters and hence their thermodynamic stability. Furthermore, note the large discrepancy between the classical and quantum voltages. Our previous classical molecular dynamics studies of concentrated aqueous NaCl electrolytes showed that the distribution of voltages for all the ions in the solution, including those ions trapped within salt clusters, spanned a broad range that included the bulk Madelung voltages ( $\pm 8.9\text{V}$ ), however, in that study we did not separate the voltage distributions between solvated ions and those ions involved in salt clusters. Our calculations and analyses provide the first steps toward understanding the magnitude and fluctuations of charge, classical point charge sources of electric potentials and fields in aqueous electrolytes and what role these fields may play in driving charge redistribution/transfer during crystallization as well as inducing crystal formation itself.

### Vibrational Spectroscopy and Electric Fields

The influence of electric fields on the vibrational response of molecules has a long history and is relevant to many chemical processes in condensed phases and their interfaces. The central concept is the use of a particular vibrational mode as a kind of antenna or probe capable of sensing the *effective* electric field fluctuations due to its surrounding environment. Early work in this area employed continuum descriptions of electrostatics while more recent work utilized electric fields arising from classical point charges. A joint CPIMS experimental-theoretical study explored the influence of electric fields on the vibrational response of molecules in a  $\text{Cs}^+(\text{H}_2\text{O})_6$  cluster. This work stands as distinct from previous studies in that we are approaching the electric field coupling to vibrational shifts from an *ab initio* perspective yielding more “exact” electric field strengths in the absolute sense as there is much uncertainty in these fields from continuum, point charges, or polarizable sources. Here we explored the

electric fields arising from quantum mechanical charge distributions for the “4+2”  $\text{Cs}^+(\text{H}_2\text{O})_6$  minimum energy cluster. Specifically, the electric fields on the Hydrogen atom sites are calculated as those arising from the quantum mechanical charge densities of all the other atoms in the system excluding only those atoms with the water molecule for which the field is being evaluated – see Fig. 2. It is in this sense that these fields must be considered as *effective* electric fields arising from the surrounding atoms as this construction formally neglects the electric fields arising from the atoms within the molecule for which the field is being probed as well as the response of the surrounding environment to this probe’s charge distribution. Specifically, the electric fields on the hydrogen atom sites are calculated as those arising from the quantum mechanical charge densities of all the other atoms in the system, excluding only those

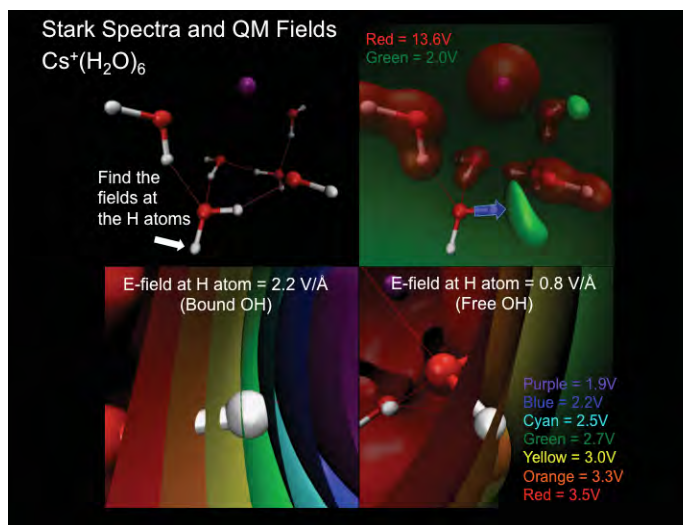


**Figure 2.** (upper left) Schematic showing the H atoms where the projected electric fields are evaluated in the  $\text{Cs}^+(\text{H}_2\text{O})_6$  cluster. (upper right) Quantum voltage isosurfaces (green) represent lone pairs of the adjacent  $\text{H}_2\text{O}$  and the projected electric field for an H-atom is shown by the blue arrow. (lower left) The quantum voltage isosurfaces bathing a hydrogen bonded water yielding a  $2.2\text{V}/\text{\AA}$  projected field. (lower right) The quantum voltage isosurfaces bathing the water molecule’s free OH yielding a  $0.8\text{V}/\text{\AA}$  projected field.

atoms within the water molecule for which the field is being evaluated. These electric fields are then projected onto the OH bond vectors corresponding to each vibrational antenna.

The resulting projected electric fields are shown in Figure 3 as a function of H-atom index (shown in the inset). First, note that the fields can be grouped into two sets: (1) those H atoms involved in hydrogen bonding – denoted as ‘Bound OH’, and (2) those H atoms not hydrogen bonded – denoted as ‘Free OH’. Second, the electric fields at these sites are extremely large! So large that, in fact, they should break the OH bond within the water molecule since it takes only a field of 0.6 V/Å to do so. Thus, there is an inconsistency between the fields evaluated at atomic sites when the water molecule being probed is not included in the quantum mechanical calculation and the field evaluated including the probe water molecule. In the latter case, the electric field at the hydrogen atom must be zero since we are evaluating a cluster at the global energy minimum. Said differently, if the electric field were nonzero, then there would be a nonzero Lorentz force on the H atom, in contradiction to it being at a global minimum energy. Resolving these inconsistencies is the focus of our ongoing research. Using this approach we are able to make spectral assignments as presented in Figure 4, noting that the electric field-to-frequency mapping spectrum (blue curve) provides a remarkably good description of the experimental vibrational spectra (red curve). It is important to note that the electric fields are very sensitive to the bonding structural patterns and hence provide good order parameters for specific cluster configurations.

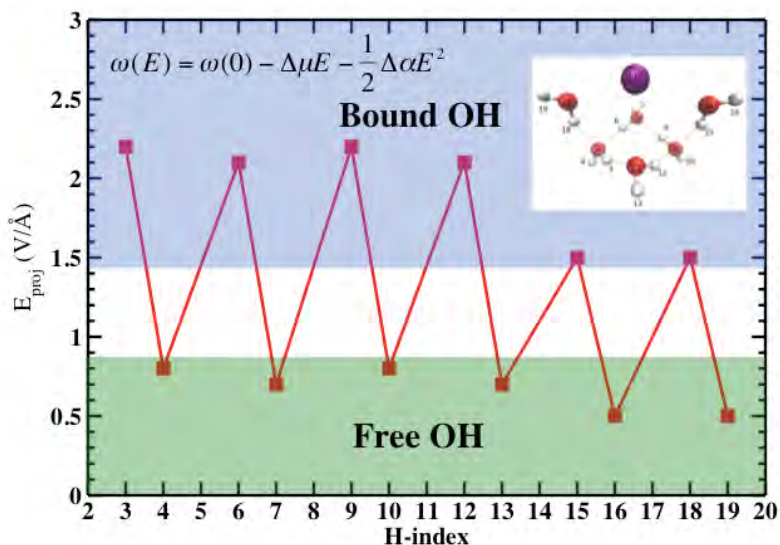


**Figure 3.** Plot of the projected electric fields for all H-atoms in the  $\text{Cs}^+(\text{H}_2\text{O})_6$  cluster.

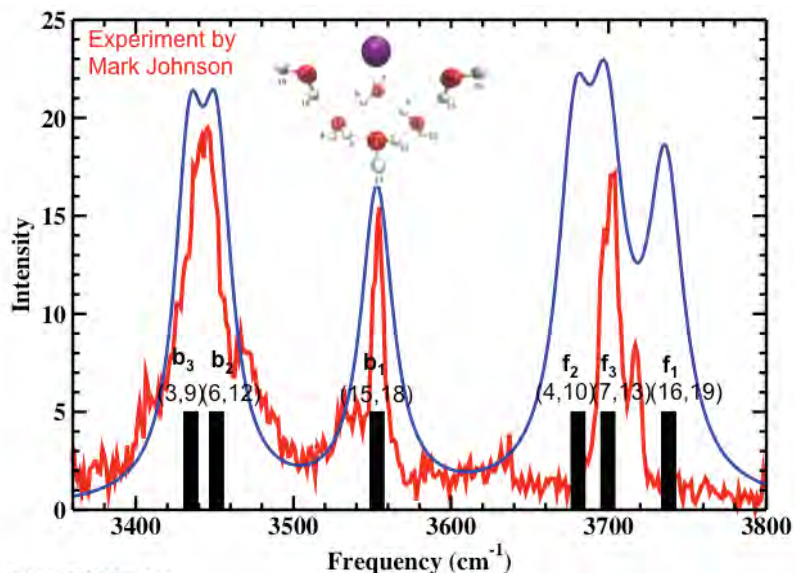


**Figure 4.** Experimental IR spectra (red) and the quadratic field-to-frequency mapping (blue) for the  $\text{Cs}^+\text{W}_6$  cluster. The black sticks denote the 6 doublet electric fields corresponding to the “free” (f) and “hydrogen-bonded” (b) OH stretches.

Direct PNNL collaborators on this project include G.K. Schenter, C.J. Mundy, S.S. Xantheas, M. Valiev, X. Wang, J. Fulton, L. Dang, and M. Baer and Postdoctoral Fellow Bernhard Sellner. Outside collaborations with the University College London include Stephen Cox and Angelos Michaelides on ice nucleation (Chemistry), Jake Stinson and Ian Ford on sulfuric acid-water nucleation as well as Mark Johnson at Yale on connections between electric fields and vibrational spectroscopy have been beneficial.

*Acknowledgement:* This research was performed in part using the DOE NERSC facility. Battelle operates PNNL for DOE.

### **Publications of DOE Sponsored Research (2014-present)**

J.L. Stinson, **S.M. Kathmann**, and I.J. Ford, "Dynamical consequences of a constraint on the Langevin thermostat in molecular cluster simulation", *Molecular Physics*, DOI:10.1080/00268976.2014.917732 (2014).

J.L. Stinson, **S.M. Kathmann**, and I.J. Ford, "Investigating the significance of zero-point motion in small molecular clusters of sulphuric acid and water", *Journal of Chemical Physics*, **140**, 024306 (2014).

B. Sellner and **S.M. Kathmann**, "A Matter of Quantum Voltages", **Invited - Special Issue** of *Journal of Chemical Physics*, **141**, 18C534 (2014).

S.J. Cox, **S.M. Kathmann**, B. Slater, and A. Michaelides, "Molecular simulations of heterogeneous ice nucleation. I. Controlling ice nucleation through surface hydrophilicity", *Journal of Chemical Physics*, **142**, 184704 (2015).

S.J. Cox, **S.M. Kathmann**, B. Slater, and A. Michaelides, "Molecular Simulations of Heterogeneous Ice Nucleation. II. Peeling back the Layers", *Journal of Chemical Physics*, **142**, 184705 (2015).

**Feature Cover Article** - J.A. Fournier, C.T. Wolke, M.A. Johnson, T.T. Odbadrakh, K.D. Jordan, **S.M. Kathmann** and S.S. Xantheas, "Snapshots of Proton Accommodation at a Microscopic Water Surface: Understanding the Vibrational Spectral Signatures of the Charge Defect in Cryogenically Cooled  $H^+(H_2O)_{n=2-28}$  Clusters", *Journal of Physical Chemistry A*, **119**, 9425 (2015).

J.L. Stinson, **S.M. Kathmann**, and I.J. Ford, "A classical reactive potential for molecular clusters of sulphuric acid and water", *Molecular Physics*, DOI:10.1080/00268976.2015.1090027 (2015).

C.T. Wolke, J.A. Fournier, E. Miliordos, **S.M. Kathmann**, S.S. Xantheas, and M.A. Johnson, "Isotopomer-selective spectra of a single intact H<sub>2</sub>O molecule in the Cs+(D<sub>2</sub>O)<sub>5</sub>H<sub>2</sub>O isotopologue: Going beyond pattern recognition to harvest the structural information encoded in vibrational spectra", *Journal of Chemical Physics*, **144**, 074305 (2016).

## Chemical Kinetics and Dynamics at Interfaces

*Structure and Reactivity of Ices, Oxides, and Amorphous Materials*

**Bruce D. Kay (PI), R. Scott Smith, and Zdenek Dohnálek**

Physical Sciences Division  
Pacific Northwest National Laboratory  
P.O. Box 999, Mail Stop K8-88  
Richland, Washington 99352  
bruce.kay@pnnl.gov

Collaborators include: CJ Dibble, GA Kimmel, RA May, NG Petrik, Yuntao Xu, and C. Yuan

### **Program Scope**

The objective of this program is to examine physiochemical phenomena occurring at the surface and within the bulk of ices, oxides, and amorphous materials. The microscopic details of physisorption, chemisorption, and reactivity of these materials are important to unravel the kinetics and dynamic mechanisms involved in heterogeneous (i.e., gas/liquid) processes. This fundamental research is relevant to solvation and liquid solutions, glasses and deeply supercooled liquids, heterogeneous catalysis, environmental chemistry, and astrochemistry. Our research provides a quantitative understanding of elementary kinetic processes in these complex systems. For example, the reactivity and solvation of polar molecules on ice surfaces play an important role in complicated reaction processes that occur in the environment. These same molecular processes are germane to understanding dissolution, precipitation, and crystallization kinetics in multiphase, multicomponent, complex systems. Amorphous solid water (ASW) is of special importance for many reasons, including the open question over its applicability as a model for liquid water, and fundamental interest in the properties of glassy materials. In addition to the properties of ASW itself, understanding the intermolecular interactions between ASW and an adsorbate is important in such diverse areas as solvation in aqueous solutions, cryobiology, and desorption phenomena in cometary and interstellar ices. Metal oxides are often used as catalysts or as supports for catalysts, making the interaction of adsorbates with their surfaces of much interest. Additionally, oxide interfaces are important in the subsurface environment; specifically, molecular-level interactions at mineral surfaces are responsible for the transport and reactivity of subsurface contaminants. Thus, detailed molecular-level studies are germane to DOE programs in environmental restoration, waste processing, and contaminant fate/transport.

Our approach is to use molecular beams to synthesize “chemically tailored” nanoscale films as model systems to study ices, amorphous materials, supercooled liquids, and metal oxides. In addition to their utility as a synthetic tool, molecular beams are ideally suited for investigating the heterogeneous chemical properties of these novel films. Modulated molecular beam techniques enable us to determine the adsorption, diffusion, sequestration, reaction, and desorption kinetics in real-time. In support of the experimental studies, kinetic modeling and simulation techniques are used to analyze and interpret the experimental data.

Recently, in collaboration with Greg Kimmel, we have developed a pulsed laser heating method that will allow us to investigate deeply supercooled liquids by producing transiently heated films, which become liquids that last for approximately 10 ns per laser pulse. Subsequent rapid cooling due to the dissipation of the heat pulse into the metal substrate effectively quenches the liquid dynamics until the next laser heating pulse arrives. The rapid heating and cooling allows the system to reach previously unattainable supercooled liquid temperatures and return to the amorphous state before significant crystallization can occur.

## Recent Progress and Future Directions

***Desorption Kinetics of Ar, Kr, Xe, N<sub>2</sub>, O<sub>2</sub>, CO, Methane, Ethane, and Propane from Graphene and Amorphous Solid Water Surfaces*** The desorption kinetics for a wide range of molecules are needed to develop models to determine the present and historical composition of astrophysical bodies such as comets, interplanetary ices, interplanetary dust, and planetary surfaces. These bodies often consist of carbonaceous materials and/or have deposits of amorphous solid water (ASW). ASW is a kinetically metastable form of water, which is created when water vapor impinges on a substrate at low temperatures. While it does not exist naturally on earth, it is thought to be the predominant form of water in the extremely cold temperatures of many interstellar and planetary environments.

Laboratory-based desorption measurements are currently used to mimic the desorption behavior of astrophysically relevant adsorbates. Researchers have used amorphous carbon and highly oriented pyrolytic graphite (HOPG) as analogs for carbonaceous surfaces. Similarly, ASW analogous can be created in the laboratory by depositing water vapor onto a low temperature substrate (typically <130 K).

In a recent paper (#8), we studied the desorption kinetics of Ar, Kr, Xe, N<sub>2</sub>, O<sub>2</sub>, CO, methane, ethane, and propane from two astrophysically relevant substrates, graphene and ASW. The experimental results clearly show that, for the nine adsorbates studied here, desorption from a graphene covered Pt(111) substrate occurs with zero-order desorption kinetics. Well-resolved first, second, third, and multilayer desorption peaks are observed for all of the adsorbates desorbing from the graphene substrate. The alignment of the TPD leading edges is consistent with zero-order desorption kinetics. Zero-order desorption kinetics in the submonolayer coverage regime are indicative of two-phase coexistence between a high-density condensed phase and a low-density gas phase in two dimensions. This two-dimensional, two-phase coexistence arises from attractive adsorbate–adsorbate interactions.

In contrast, desorption of the same adsorbates (for coverages < 2 ML) from ASW are markedly non-zero order. Alignment of the desorption leading edges on a single curve was not observed for any of the nine adsorbates for coverages up to 2 ML. Also, none of the adsorbates had clearly resolved first and second layer desorption features. The TPD results suggested that the ASW surface has a distribution of binding site energies. In this case, the coverage dependent binding energies were determined using an inversion analysis procedure. The monolayer TPD peaks for a given adsorbate on ASW occur at markedly lower temperatures than they do on graphene. This clearly indicates that the interaction of the adsorbates with ASW is noticeably weaker than their interaction with graphene.

The contrasting desorption mechanisms from these two substrates is an important consideration for kinetic models for adsorbate desorption from astrophysical bodies. The results show that the desorption kinetics from these two astrophysically important substrates need to be analyzed differently. The specific desorption order and mechanism are required to extract adsorbate binding energies needed for accurate models of evaporation from interstellar and planetary ices. Future work will focus on how adsorbate co-adsorption affects the desorption kinetics.

***Surface and Bulk Crystallization of Amorphous Solid Water Films: Confirmation of “Top-Down” Crystallization Kinetics*** As described above, amorphous solid water (ASW) is a metastable glassy phase form of water that can be created in the laboratory by vapor deposition onto a cold substrate. The properties of ASW are of interest for a variety of reasons including its use as a model for liquid and supercooled liquid water, its use as a model for studying the

properties of amorphous solids, and because it is believed to be the predominant form of water in astrophysical and planetary environments.

It has been previously shown that inert adsorbates trapped underneath or within ASW films desorb in an episodic release that occurs in concert with ASW crystallization, a phenomenon called the “molecular volcano”. When heated, or allowed to sit for a fantastically long time, ASW converts to thermodynamically stable crystalline ice. Crystallization of ASW can result in structural changes in the film. For example, when an inert gas ( $\text{CCl}_4$ , Ar,  $\text{CO}_2$ , Kr, Xe, CO,  $\text{N}_2$ ,  $\text{O}_2$ , and others) is deposited underneath an ASW overlayer, the inert gas desorption is delayed until crystallization of the ASW overlayer. The observed abrupt desorption is due to the formation of cracks that accompany the crystallization kinetics and form a connected release pathway.

To date, most studies either report or assume that ASW crystallization proceeds via a random bulk nucleation and growth mechanism. In some recent work, the volcano peak was used to determine the crystallization-induced crack propagation mechanism. In these experiments an inert gas layer was deposited at various elevations in the ASW film. The results showed that the closer to the top of the film the layer was deposited, the earlier in temperature (time) the volcano desorption peak occurred. Through a series of experiments we were able to show conclusively that crack formation begins at the ASW/vacuum interface and moves downward into the film.

Given the link between crystallization and crack formation, the results suggested that ASW crystallization may also begin at the ASW/vacuum interface and proceed into the bulk. In a recent paper (#11), we investigated the crystallization kinetics of nanoscale ASW films using temperature programmed desorption (TPD) and reflection absorption infrared spectroscopy (RAIRS). The TPD measurements were used to probe surface crystallization and the RAIRS measurements were used to probe bulk crystallization. The isothermal TPD results showed that surface crystallization was independent of the film thickness (from 100 to 1000 ML). Conversely, the RAIRS measurements showed that the bulk crystallization time increases linearly with increasing film thickness. These observations suggest that nucleation and crystallization begin at the ASW/vacuum interface and then the crystallization growth front propagates linearly into the bulk. Further evidence for this mechanism was given by experiments where an isotopic layer (5%  $\text{D}_2\text{O}$  in  $\text{H}_2\text{O}$ ) was selectively placed at various elevations in a 1000 ML ASW ( $\text{H}_2\text{O}$ ) film. In this case, the closer the isotopic layer was to the vacuum interface, the earlier the isotopic layer crystallized. These experiments provided direct evidence to confirm that ASW crystallization in vacuum proceeds by a “top-down” crystallization mechanism.

The preference for nucleation at the vacuum interface is likely due to the higher mobility that surface molecules have compared to those in the bulk. Our results mean that prior work using only surface sensitive techniques, such as desorption and adsorbate physisorption, likely do not provide information relevant to bulk nucleation. Surface sensitive experiments may provide information relevant to processes in the environment or in astrophysical ices but it is the bulk nucleation rate that is relevant to processes in supercooled liquid water. Future work will focus on varying the isothermal temperatures to further quantify the ASW kinetics. In addition, experiments where the effects of the vacuum-surface nucleation are eliminated will be conducted. For example, ASW films deposited between two hydrocarbon layers should eliminate the surface nucleation. Quantitative information on bulk nucleation and growth crystallization kinetics of ASW films is needed to increase our understanding of liquid and supercooled liquid water.

***Chemical Dynamics and Kinetics of Tailored Nanoscale Liquids and Liquid/Solid Interfaces Far from Equilibrium*** We have developed an experimental approach to probe fundamental processes in liquids, supercooled liquids and glasses, and at liquid/solid interfaces in temperature regimes that are experimentally challenging. Our approach is to transiently heat compositionally tailored nanoscale films using a nanosecond pulsed laser-heating system. The film is rapidly heated to the temperature of interest for a brief time (nanoseconds) and then it rapidly cools back to the pre-laser pulse temperature. Processes that occur at these elevated temperatures are followed via a post-mortem analysis using surface spectroscopic techniques. This work is a collaborative effort between Collin Dibble (Postdoc), Yuntao Xu (Postdoc), Nikolay G. Petrik, R. Scott Smith, Bruce D. Kay, and Greg A. Kimmel. Initial reports of this work are given in references #9 and #10 and the experimental details are discussed in the CPIMS abstract by Greg Kimmel. Future experiments will focus on exploring diffusion, crystallization, and isotope exchange kinetics of supercooled water in the temperature range 180-273K.

#### **References to Publications of DOE sponsored Research (2014 - present)**

1. G. A. Kimmel, T. Zubkov, R. S. Smith, N. G. Petrik and B. D. Kay, "*Turning things downside up: Adsorbate induced water flipping on Pt(111)*", J. Chem. Phys. **141**, 18C515 (2014).
2. V. Molinero and B. D. Kay, "*Preface: Special topic on interfacial and confined water*", J. Chem. Phys. **141**, 18C101 (2014).
3. R. S. Smith, Z. J. Li, L. Chen, Z. Dohnalek and B. D. Kay, "*Adsorption, desorption, and displacement kinetics of H<sub>2</sub>O and CO<sub>2</sub> on TiO<sub>2</sub>(110)*", J. Phys. Chem. B **118**, 8054-8061 (2014).
4. R. S. Smith, Z. J. Li, Z. Dohnalek and B. D. Kay, "*Adsorption, desorption, and displacement kinetics of H<sub>2</sub>O and CO<sub>2</sub> on forsterite, Mg<sub>2</sub>SiO<sub>4</sub>(011)*", J. Phys. Chem. C **118**, 29091-29100 (2014).
5. R. S. Smith, J. Matthiesen and B. D. Kay, "*Desorption kinetics of methanol, ethanol, and water from graphene*", J. Phys. Chem. A **118**, 8242-8250 (2014).
6. R. S. Smith, R. A. May and B. D. Kay, "*Probing toluene and ethylbenzene stable glass formation using inert gas permeation*", Journal of Physical Chemistry Letters (2015).
7. K. Thürmer, C. Yuan, G. A. Kimmel, B. D. Kay and R. S. Smith, "*Weak interactions between water and clathrate-forming gases at low pressures*", Surface Science **641**, 216-223 (2015).
8. R. S. Smith, R. A. May and B. D. Kay, "*Desorption kinetics of Ar, Kr, Xe, N<sub>2</sub>, O<sub>2</sub>, CO, methane, ethane, and propane from graphene and amorphous solid water surfaces*", J. Phys. Chem. B **120**, 1979-1987 (2016).
9. Y. T. Xu, C. J. Dibble, N. G. Petrik, R. S. Smith, A. G. Joly, R. G. Tonkyn, B. D. Kay and G. A. Kimmel, "*A nanosecond pulsed laser heating system for studying liquid and supercooled liquid films in ultrahigh vacuum*", J. Chem. Phys. **144**, 164201 (2016).
10. Y. T. Xu, C. J. Dibble, N. G. Petrik, R. S. Smith, B. D. Kay and G. A. Kimmel, "*Complete wetting of Pt(111) by nanoscale liquid water films*", Journal of Physical Chemistry Letters **7**, 541-547 (2016).
11. C. Yuan, R. S. Smith and B. D. Kay, "*Surface and bulk crystallization of amorphous solid water films: Confirmation of "top-down" crystallization*", Surface Science **652**, 350-354 (2016).

## Probing Ultrafast Electron (De)localization Dynamics in Mixed Valence Complexes Using Femtosecond X-ray Spectroscopy

**Lead PI:** Munira Khalil, University of Washington, Seattle, WA

**PI:** Niranjan Govind, EMSL, Pacific Northwest National Laboratory, Richland, WA

**PI:** Shaul Mukamel, University of California, Irvine, CA

**PI:** Robert Schoenlein, SLAC, Menlo Park, CA

### Project Goals

The overall goal of this project is to understand valence electron and vibrational motion following metal-to-metal charge transfer (MMCT) excitation in the following mixed valence complexes dissolved in aqueous solution:  $[(\text{NH}_3)_5\text{Ru}^{\text{III}}\text{NCFe}^{\text{II}}(\text{CN})_5]$  (**1**, FeRu), *trans*- $[(\text{NC})_5\text{Fe}^{\text{II}}\text{CNPt}^{\text{IV}}(\text{NH}_3)_4\text{NCFe}^{\text{II}}(\text{CN})_5]^{4-}$  (**2**, FePtFe) and *trans*- $[(\text{NC})_5\text{Fe}^{\text{III}}\text{CNRu}^{\text{II}}(\text{L})_4\text{NCFe}^{\text{III}}(\text{CN})_5]^{4-}$  (**3**, FeRuFe, L=pyridine). The project objectives are (i) to observe the time-dependent re-arrangement of *d* electrons across two transition metal sites and the bridging ligand following photoinduced MMCT excitation on a sub-50 fs timescale using femtosecond X-ray pulses generated at LCLS (ii) to simulate femtosecond X-ray absorption and emission spectra of solvated, photo-excited, transition metal mixed valence complexes using a realistic treatment of multi-electron correlations/transitions, spin-orbit coupling and final state lifetime effects and to propose and study the feasibility of nonlinear X-ray experiments on solvated transition metal mixed valence systems using future X-FEL light sources and (iii) to determine the role of coupled electronic and vibrational motions during ultrafast photoinduced charge transfer.

### Recent Progress

- ***Development of Two-Dimensional Vibrational-Electronic (2D VE) Spectroscopy.*** We have developed a Fourier transform (FT) 2D vibrational-electronic (2D VE) spectroscopy employing a novel mid-IR and optical pulse sequence. This new femtosecond third-order nonlinear spectroscopy provides the high time and frequency resolutions of existing 2D FT techniques, but is sensitive to cross-peaks containing IR and electronic dipole moment cross terms. We have detailed the experimental layout of 2D VE spectroscopy with two examples in two publications.
- ***Equilibrium X-ray Absorption and X-ray Emission Spectroscopy of Transition Metal Mixed Valence Complexes in Solution.*** In order to understand the electronic configuration in the ground state of the transition metal complexes, we have obtained equilibrium X-ray absorption (XA) and X-ray emission (XE) spectra in water for the mixed valence complex complexes and model complexes  $\text{Fe}(\text{II})\text{CN}_6$  and  $\text{Fe}(\text{III})\text{CN}_6$  at the Fe L-edge and the Fe K-edge. The spectra reveal that the oxidation state of the iron atoms in the FeRu and FePtFe complexes is Fe(II) and that of FeRuFe is Fe(III) in the ground electronic state. The successful collection of equilibrium spectra has allowed us to validate parameters in the simulation/computational codes for correctly modelling the electronic structure of the solvated mixed valence complexes. These spectra were obtained at APS 11 ID during August 2015 and at ALS BL 10.3.2 during January 2015 and January 2016.

- Femtosecond X-ray Absorption and X-ray Emission Spectroscopy of Transition Metal Mixed Valence Complexes in Solution.*** We were awarded beam time at LCLS under proposal LJ67 for five shifts in October 2015. Experiments were performed at the X-ray pump probe (XPP) instrument at LCLS using 800 nm laser light to photo excite the sample preceding X-ray measurements. Femtosecond XA and XE spectroscopies are used at the Fe K-edge to directly monitor transient oxidation states and orbital occupancy during charge transfer in a series of solvated mixed-valence complexes. Static XE spectra for  $[\text{Fe}^x(\text{CN})_6]$  compounds ( $x = \text{II}$  and  $\text{III}$ ) were used as a model to determine the expected shift upon MMCT in FeRu and FeRuFe. A transition from  $\text{Fe}^{\text{II}}$  to  $\text{Fe}^{\text{III}}$  (as in FeRu) would result in a blue peak shift of  $\sim 0.2$  eV and broadening of the  $\text{K}\alpha_1$  peak consistent with the experimental transient XE result for FeRu. Transient XE spectra for FeRuFe exhibit the opposite, a red peak shift with spectral narrowing consistent with an  $\text{Fe}^{\text{III}}$  to  $\text{Fe}^{\text{II}}$  transition. Fits of the kinetic traces reveal that the initial MMCT from  $\text{Fe}^{\text{II}}\text{Ru}^{\text{III}}$  to  $\text{Fe}^{\text{III}}\text{Ru}^{\text{II}}$  and  $\text{Fe}^{\text{III}}\text{Ru}^{\text{II}}\text{Fe}^{\text{III}}$  to  $\text{Fe}^{\text{II}}\text{Ru}^{\text{III}}\text{Fe}^{\text{III}}$  occurs within the response of the instrument (50 fs) and the BET occurs within 100 fs for each compound. In the difference XA signal for FeRu, we see the growth of a transient feature upon MMCT which indicates that a hole is created in the  $t_{2g}$  orbital. The other XANES peaks undergo shifts to the blue upon photoexcitation and a change in the linewidth indicating the adjustments of the metal d orbitals following the initial MMCT. We are currently analyzing the data and simulating the experimental observables with theory. In a related effort, the Schoenlein group (in collaboration with Prof. T.-K. Kim, U. Pusan) has focused on the CN- bridged mixed valence transition-metal complex  $\text{Ru}^{\text{II}}\text{-CN-Cr}^{\text{III}}\text{-CN-Ru}^{\text{II}}$  complex as a prototypical model system. Compared to the typical CN-bridged model complex ( $\text{Ru}^{\text{II}}\text{-CN-Ru}^{\text{III}}$ ), the use of the covalently linked  $\text{Cr}^{\text{III}}$  electron acceptor leads to remarkably long-lived charge-separated intermediates, attributed to the existence of electronic states of different spin multiplicity that effectively inhibit BET. The first time-resolved X-ray spectroscopy studies of this complex have recently been conducted at Advanced Photon Source. Transient XAS and XES at the Cr K-edge monitors changes in the local coordination geometry, changes in the spin multiplicity and electronic structure revealed by growth/disappearance of pre-edge features. The experimental results are now being analyzed via ab initio calculations to understand electron delocalization dynamics.

- Simulating Valence-to-Core X-ray Emission Spectroscopy.*** Valence-to-Core X-ray Emission Spectroscopy (VtC-XES) is a sensitive tool to identify ligands and characterize ligand valence orbitals in transition metal complexes. In the past year we studied how linear-response time-dependent density functional theory (LR-TDDFT) can be extended to simulate K-edge VtC-XES reliably. LR-TDDFT allows one to go beyond the single-particle picture. Specifically, we developed a “black box” protocol in NWChem to simulate these spectra. A systematic study of the K-edge VtC-XES spectra of a series of low- and high-spin model Fe-, Mn- and Cr-complexes was performed and compared with experiment. Our results are in good agreement with experiment. The study also revealed that our method has advantages over the conventional single-particle DFT approach in describing VtC-XES features that have multi-configuration character. These results have been published in the Journal of Chemical Theory and Computation in November 2015. We are in the process of calculating of simulating the VtC-XES for the dimer (FeRu) and

trimer (FeRuFe) complexes. VtC-XES for transient species is also possible with our protocol.

- ***Ab Initio Molecular Dynamics/Molecular Mechanics (AIMD/MM), XA, UV/Vis and IR Spectroscopies of Model Complexes [Fe(CN)<sub>6</sub><sup>4-</sup> & Fe(CN)<sub>6</sub><sup>3-</sup>] in Water.*** In order to study solvated model Fe(CN)<sub>6</sub><sup>4-</sup> and Fe(CN)<sub>6</sub><sup>3-</sup> complexes in water, we have performed extensive hybrid AIMD/MM based molecular dynamics simulations with NWChem. We have updated and extended our simulation protocol for all transition metal complexes from what was reported last year to include hybrid exchange-correlation functionals (for example, B3LYP, PBE0) in the QM region. Following the AIMD/MM runs, we extracted snapshots of the complex with an explicit solvation environment water molecules from the trajectory to perform the XANES, UV/Vis, IR, EXAFS spectra calculations. The Fe K-edge XANES and UV/Vis spectra were calculated with our implementation of restricted excitation window (REW) TDDFT. We have extended our TDDFT code to capture the quadrupole transitions in the Fe K-edge XANES.

- ***AIMD/MM, XA, UV/Vis and IR Spectroscopy of Transition Mixed Valence Complexes in Water on the Ground and Photo-excited States.*** The FeRu dimer complex QM/MM model involved the solvation in a simulation box containing the dimer complex with 5000 water molecules to give a density close to 1 g/cm<sup>3</sup>. The FeRuFe and FePtFe complexes contained 7919 and 5842 water molecules respectively to give a density close to 1 g/cm<sup>3</sup>. The details of the AIMD/MM simulations are the same as that for the model complexes. We have completed our AIMD/MM calculations of the dimer complex in water. The XANES, UV/Vis and IR spectra have been calculated. For the Fe(III)Ru(II)Fe(III) complex, we find that both the triplet and open-shell singlet spin configurations on the two Fe(III) centers are degenerate as expected. Both states result in identical Fe K-edge XANES spectra. For the FeRu and FeRuFe complexes, we have developed a new theoretical approach to tackle the transient-XAS to probe the x-ray absorption response of the UV-Vis excited transition metal complex. The goal of this study is to elucidate the structural, spectroscopic changes of the dimer complex in a solvent environment both in the ground and excited states. Our calculations, so far, are in good agreement with experiment. For FePtFe, our extensive ground state calculations reveal that the closed-shell singlet configuration is the lowest energy state compared with the triplet configuration in agreement with experiment. This is in contrast to published theoretical work on this system that reported a lower triplet state. We attribute this to the description of the solvent environment. In our calculations, the solvent environment is treated explicitly which results in systems of approx. 300 atoms. VtC-XES calculations using the ground and excited-state geometries for all three complexes are also planned.

- ***Enhancements and protocols in NWChem.*** The following enhancements have been implemented in the NWChem code over the course of this project:

1. Extensions to the TDDFT code in NWChem to capture quadrupole transitions (1s→3d) which are relevant for transition metal K-edge XANES.
2. TDDFT restart capabilities that will allow a user to systematically increase the number of excitations from previously saved calculations.
3. Parallelization enhancements for TDDFT calculations up to 3000 basis functions.
4. “Black Box” valence-to-core x-ray emission spectroscopy (VtC-XES) protocol.
5. New QM/MM protocols for simulations of the model, dimer and trimer complexes in different solvents.

6. New transient XAS protocol to tackle simulations of pump (optical)-probe (X-ray) spectroscopy.

The enhancements described above (2 and 3) are especially relevant for response calculations on the trimer systems where the transition metal complex (solute) plus the explicit water molecules (solvent) can result in system sizes of ~300 atoms or more

### **Future Plans**

We plan to accomplish the following in the near future. (i) We were awarded beam time at the SXR Instrument at LCLS to perform femtosecond Fe L-edge XA spectroscopy on transition metal mixed valence complexes in December 2016. Following the experiment we will work on data analysis. (ii) We are in the process of preparing several manuscripts combining experimental and computational data on the IR, electronic and core-hole spectroscopies on solvated mixed valence complexes. (iii) We will be performing further benchmark studies on our new transient XAS approach. (iv) We will focus on the development of theoretical approaches for the calculation of L-edge and transient L-edge spectra.

### **DOE Supported Publications**

1. B. E. Van Kuiken, H. Cho, K. Hong, M. Khalil, R. W. Schoenlein, T. K. Kim, and N. Huse, "Time-resolved x-ray spectroscopy in the water window: Elucidating transient valence charge distributions in an aqueous Fe(II) complex", *The Journal of Physical Chemistry Letters* **7** (2016) 465-470.
2. K. M. Slenkamp, M. S. Lynch, J. F. Brookes, C. C. Bannan, S. L. Daifuku, and M. Khalil, "Investigating vibrational relaxation in cyanide-bridged transition metal mixed-valence complexes using two-dimensional infrared and infrared pump-probe spectroscopies", *Structural Dynamics* **3** (2016) 023609.
3. Y. Zhang, S. Mukamel, M. Khalil, and N. Govind, "Simulating valence-to-core x-ray emission spectroscopy of transition metal complexes with time-dependent density functional theory", *Journal of Chemical Theory and Computation* **11** (2015) 5804-5809.
4. T. L. Courtney, Z. W. Fox, K. M. Slenkamp, and M. Khalil, "Two-dimensional vibrational-electronic spectroscopy", *The Journal of Chemical Physics* **143** (2015) 154201.
5. T. L. Courtney, Z. W. Fox, L. Estergreen, and M. Khalil, "Measuring coherently coupled intramolecular vibrational and charge-transfer dynamics with two-dimensional vibrational-electronic spectroscopy", *The Journal of Physical Chemistry Letters* **6** (2015) 1286-1292.

## Chemical Kinetics and Dynamics at Interfaces

### *Non-Thermal Reactions at Surfaces and Interfaces*

**Greg A. Kimmel (PI) and Nikolay G. Petrik**

Physical Sciences Division  
Pacific Northwest National Laboratory  
P.O. Box 999, Mail Stop K8-88  
Richland, WA 99352  
[gregory.kimmel@pnnl.gov](mailto:gregory.kimmel@pnnl.gov)

Collaborators include: CJ Dibble, BD Kay, RS Smith, and Y Xu

### **Program Scope**

The objectives of this program are to investigate 1) thermal and non-thermal reactions at surfaces and interfaces, and 2) the structure of thin adsorbate films and how this influences the thermal and non-thermal chemistry. Energetic processes at surfaces and interfaces are important in fields such as photocatalysis, radiation chemistry, radiation biology, waste processing, and advanced materials synthesis. Low-energy excitations (e.g. excitons, electrons, and holes) frequently play a dominant role in these energetic processes. For example, in radiation-induced processes, the high energy primary particles produce numerous, chemically active, secondary electrons with energies that are typically less than ~100 eV. In photocatalysis, non-thermal reactions are often initiated by holes or (conduction band) electrons produced by the absorption of visible and/or UV photons in the substrate. In addition, the presence of surfaces or interfaces modifies the physics and chemistry compared to what occurs in the bulk.

We use quadrupole mass spectroscopy, infrared reflection-absorption spectroscopy (IRAS), and other ultra-high vacuum (UHV) surface science techniques to investigate thermal, electron-stimulated, and photon-stimulated reactions at surfaces and interfaces, in nanoscale materials, and in thin molecular solids. Since the structure of water near interface plays a crucial role in the thermal and non-thermal chemistry occurring there, a significant component of our work involves investigating the structure of aqueous interfaces. A key element of our approach is the use of well-characterized model systems to unravel the complex non-thermal chemistry occurring at surfaces and interfaces. This work addresses several important issues, including understanding how the various types of low-energy excitations initiate reactions at interfaces, the relationship between the water structure near an interface and the non-thermal reactions, energy transfer at surfaces and interfaces, and new reaction pathways at surfaces.

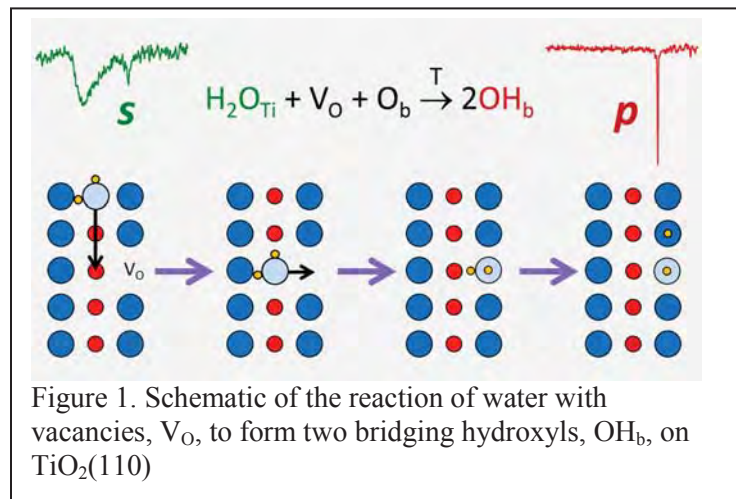
### **Recent Progress**

#### ***Reaction Kinetics of Water Molecules with Oxygen Vacancies on Rutile TiO<sub>2</sub>(110)***

The structure and reactivity of water on various TiO<sub>2</sub> surfaces have been extensively studied. The motivation for developing a detailed understanding of these reactions is derived from both technological and scientific considerations. Since reactions occurring on TiO<sub>2</sub> in contact with aqueous solutions are important for a variety of applications such as the photo-oxidation of organic pollutants and self-cleaning surfaces, a better understanding of the underlying mechanisms can potentially lead to improvements in existing applications or the development of new ones.

As part of an ongoing effort to understand the interactions of water with TiO<sub>2</sub>, we investigated the reactions of water molecules with bridging oxygen vacancies on reduced TiO<sub>2</sub>(110) at low coverages (see Figure 1). We used infrared reflection-absorption spectroscopy (IRAS) to obtain the characteristic IR spectrum of the bridging hydroxyl with narrow peaks at ~2737 (3711) cm<sup>-1</sup> for stretching vibrations of OD<sub>b</sub> (OH<sub>b</sub>). IR measurements with polarized light demonstrated that the OD (OH) bond of the bridging

hydroxyls is normal to the (110) surface. IRAS measurements of the OD<sub>b</sub> peak versus the annealing temperature of a small amount of D<sub>2</sub>O on TiO<sub>2</sub>(110) were used to investigate the kinetics of water molecules dissociating in the bridging oxygen vacancies. In separate experiments, we also measured the loss of molecular water and the bridging oxygen vacancies versus the annealing temperature. The electron-stimulated desorption (ESD) of water and the photooxidation of CO were used to monitor the water and vacancy concentrations, respectively. All three techniques (OD<sub>b</sub> IRAS, water ESD and CO photooxidation) showed that the water-vacancy reaction rate is low for T < 150 K, while the reactions proceed quickly for T > 250 K. The rate limiting step for the reaction has a distribution of activation energies (centered around ~0.55 eV) which is consistent with previous measurements and calculations of the diffusion barrier for water monomers along the Ti<sub>5c</sub> rows of TiO<sub>2</sub>(110). Further details of this work can be found in reference 8.



#### ***A nanosecond pulsed laser heating system for studying liquid and supercooled liquid films in ultrahigh vacuum***

We have developed a pulsed laser heating system that enables investigations of the dynamics and kinetics of nanoscale liquid films and liquid/solid interfaces on the nanosecond timescale in ultrahigh vacuum (UHV). With this approach, nanosecond pulses from a Nd:YAG laser are used to rapidly heat thin films of adsorbed water or other volatile materials on a clean, well-characterized Pt(111) crystal in ultrahigh vacuum (UHV). Heating rates of ~10<sup>10</sup> K/s for temperature increases of ~100 – 200 K are obtained. The short penetration depth of the IR light in the metal substrate (a few nm) leads to initial heating of only a thin layer of the metal near the surface and the adsorbate layer. Subsequent rapid heat transfer deeper into the metal substrate leads to rapid cooling (~5 × 10<sup>9</sup> K/s) of the adsorbed films to cryogenic temperatures. This quenches the film, permitting *in-situ*, post-heating analysis using a variety of surface science techniques. Lateral variations in the laser pulse energy are ~ ± 2.7% leading to a temperature uncertainty of ~ ± 4.4 K for a temperature jump of 200 K. Initial experiments with the apparatus demonstrate that crystalline ice films initially held at 90 K can be rapidly transformed into liquid water films with T > 273 K. No discernable recrystallization occurs during the rapid cooling back to cryogenic temperatures. In contrast, amorphous solid water films heated below the melting point rapidly crystallize. The nanosecond pulsed laser heating system can prepare nanoscale liquid and supercooled liquid films that persist for nanoseconds per heat pulse in an UHV environment, enabling experimental studies of a wide range of phenomena in liquids and at liquid/solid interfaces. For example, we are currently using this technique to investigate the nucleation and growth of crystalline ice in deeply supercooled water.

This work was done in collaboration with B. D. Kay, R. S. Smith, and two postdoctoral fellows – Drs. Yuntao Xu and Collin J. Dibble, and is published in reference 11.

#### ***Complete Wetting of Pt(111) by Nanoscale Liquid Water Films***

Wetting is one of the most basic aspects of water’s interaction with a surface, representing a balance between adhesive and cohesive forces. Typically the wettability of a surface is measured via the contact angle,  $\theta_c$ , of a macroscopic liquid drop on that surface. Thermodynamic considerations lead to Young’s equation for the contact angle:  $\gamma_{sl} + \gamma_{lv} \cos\theta_c = \gamma_{sv}$ , where  $\gamma_{sl}$ ,  $\gamma_{lv}$  and  $\gamma_{sv}$  are the surface tensions of the

solid-liquid, liquid-vapor and solid-vapor interfaces, respectively. A surface is considered to be hydrophobic (hydrophilic) if  $\theta_c > 90^\circ$  ( $\theta_c < 90^\circ$ ). For complete wetting,  $\theta_c = 0^\circ$ .

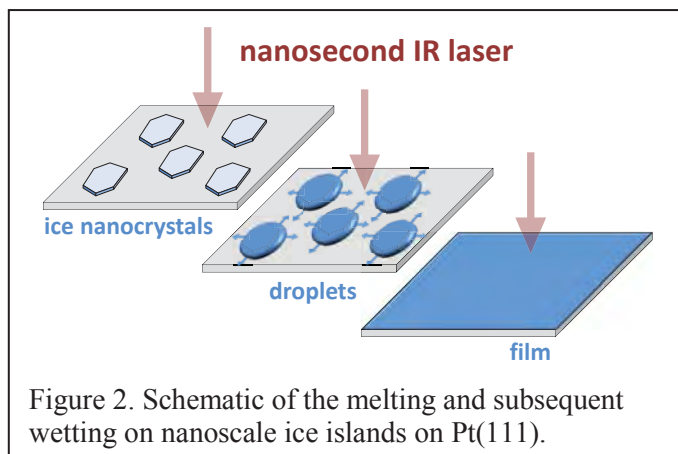


Figure 2. Schematic of the melting and subsequent wetting on nanoscale ice islands on Pt(111).

nanoscale ice crystallites embedded in a hydrophobic water monolayer. Upon heating, these crystallites melt to form nanoscale droplets of liquid water. Rapid cooling after each pulse quenches the films, allowing them to be interrogated with UHV surface science techniques. With each successive heat pulse, these liquid drops spread across the surface until it is entirely covered with multilayer water films. Figure 2 shows a schematic of the melting and wetting process. These results, which show that nanoscale water films completely wet Pt(111), are in contrast to molecular dynamics simulations predicting partial wetting of water drops on a hydrophobic water monolayer. The results provide valuable insights into the wetting characteristics of nanoscale water films on a clean, well-characterized single crystal surface.

This work was done in collaboration with B. D. Kay, R. S. Smith, and two postdoctoral fellows – Drs. Yuntao Xu and Collin J. Dibble, and is published in reference 9.

### Future Directions:

Important questions remain concerning the factors that determine the structure of thin water films on various substrates. We plan to continue investigating the structure of thin water films on non-metal surfaces, such as oxides, and on metals where the first layer of water does not wet the substrate. For the non-thermal reactions in water films, we will use IRAS to characterize the electron-stimulated reaction products and precursors. We will also continue our investigations into the photochemistry of small molecules on TiO<sub>2</sub>(110). The pulsed laser heating experiments will focus on exploring diffusion, crystallization, and isotope exchange kinetics of supercooled water in the temperature range 180-273K.

### References to publications of DOE-sponsored research (FY 2014 – present)

- [1] Nikolay G. Petrik and Greg A. Kimmel, “Probing the photochemistry of chemisorbed oxygen on TiO<sub>2</sub>(110) with Kr and other co-adsorbates,” *Phys. Chem. Chem. Phys.* **16**, 2338 – 2346 (2014) (DOI: 10.1039/c3cp54195a).
- [2] Nikolay G. Petrik, Rhiannon J. Monckton, Sven P. K. Koehler and Greg A. Kimmel, “Electron-stimulated reactions in layered CO/H<sub>2</sub>O films: Hydrogen atom diffusion and the sequential hydrogenation of CO to methanol,” *J. Chem. Phys.* **140**, 204710 (2014) (DOI: 10.1063/1.4878658).
- [3] Nikolay G. Petrik, Rhiannon J. Monckton, Sven P. K. Koehler and Greg A. Kimmel, “Distance-dependent radiation chemistry: Oxidation versus hydrogenation of CO in electron-irradiated H<sub>2</sub>O/CO/H<sub>2</sub>O ices,” *J. Phys. Chem.*, **118**, 27483 (2014). (DOI: 10.1021/jp509785d).

- [4] Greg A. Kimmel, Tykhon Zubkov, R. Scott Smith, Nikolay G. Petrik and Bruce D. Kay, "Turning things downside up: Adsorbate induced water flipping on Pt(111)," *J. Chem. Phys.*, **141**, 18C515 (2014) (DOI: 10.1063.4896226).
- [5] Nikolay G. Petrik, Michael A. Henderson, and Greg A. Kimmel, "Insights into Acetone Photochemistry on Rutile TiO<sub>2</sub>(110). 1. Off-Normal CH<sub>3</sub> Ejection from Acetone Diolate," *J. Phys. Chem. C.*, **119**, 12262 (2015). (DOI: 10.1021/acs.jpcc.5b02477).
- [6] Nikolay G. Petrik, Michael A. Henderson, and Greg A. Kimmel, "Insights into Acetone Photochemistry on Rutile TiO<sub>2</sub>(110). 2. New Photodesorption Channel with CH<sub>3</sub> Ejection along the Surface Normal," *J. Phys. Chem. C.*, **119**, 12273 (2015). (DOI: 10.1021/acs.jpcc.5b02478).
- [7] Konrad Thürmer, Chunqing Yuan, Greg A. Kimmel, Bruce D. Kay, R. Scott Smith, "Weak interactions between water and clathrate-forming gases at low pressures," *Surf. Sci.* **641**, 216-223 (2015). (DOI: 10.1016/j.susc.2015.07.013).
- [8] Nikolay G. Petrik and Greg A. Kimmel, "Reaction Kinetics of Water Molecules with Oxygen Vacancies on Rutile TiO<sub>2</sub>(110)," *J. Phys. Chem.* **119**, 23059 (2015) (DOI: 10.1021/acs.jpcc.5b07526).
- [9] Yuntao Xu, Collin J. Dibble, Nikolay G. Petrik, R. Scott Smith, Bruce D. Kay, and Greg A. Kimmel, "Complete Wetting of Pt(111) by Nanoscale Liquid Water Films," *J. Phys. Chem. Lett.* **7**, 541 (2016). (DOI: 10.1021/acs.jpcclett.5b02748).
- [10] Nikolay G. Petrik, Greg A. Kimmel, Mingmin Shen, Michael A. Henderson, "Quenching of Electron Transfer Reactions Through Coadsorption: A Study of Oxygen Photodesorption from TiO<sub>2</sub>(110)," *Surf. Sci.* **562** (2016) 183 (DOI: 10.1016/j.susc.2015.12.038).
- [11] Yuntao Xu, Collin J. Dibble, Nikolay G. Petrik, R. Scott Smith, Alan G. Joly, Russel G. Tonkyn, Bruce D. Kay, and Greg A. Kimmel, "A Nanosecond Pulsed Laser Heating System for Studying Liquid and Supercooled Liquid Films in Ultrahigh Vacuum," *J. Chem. Phys.* **144** (2016) 164201 (DOI: 10.1063/1.4947304).

# 2D IR Microscopy—Technology for Visualizing Chemical Dynamics in Heterogeneous Environments

PI: Amber T. Krummel

Colorado State University, 200 W. Lake Street, Fort Collins, CO 80525

[amber.krummel@colostate.edu](mailto:amber.krummel@colostate.edu)

## 1. Program Scope

Chemistries crucial for energy technologies including battery technology, fuel cell technology, and enhanced oil recovery take place in heterogeneous environments. Understanding and predicting chemical dynamics, including solute-solvent interactions, adsorption processes, and transport processes, to name a few, requires the ability to probe these events directly and ultimately visualizing these processes via microscopy. The overarching goal of this project is to develop two-dimensional infrared (2D IR) imaging tools to directly probe chemical interactions in heterogeneous environments, with geochemical systems being our primary target in this project. A combination of experiments directed toward technology development, the exploration of fundamental chemical physics of large macrocycles and acidic oils, and culminating with the direct visualization of chemical interactions in model pore structures. This project builds from our expertise in fabricating IR compatible microfluidic structures, in developing a 100 kHz 2D IR spectrometer, and in probing the nanoaggregates of large macrocycles.

The large number of observables offered by 2D IR spectroscopy allows us to disentangle and quantify complex chemical interactions in ways that were not previously feasible. These observables include the direct measurement of the frequency-frequency correlation function, which is a direct measure of the homogeneous and inhomogeneous contributions to the vibrational lifetime; and the peak positions (both diagonal peaks and cross peaks) and intensities, which are a direct measure of molecular structure. Each of these observables can be spatially resolved. We will interface a microscope with a high-speed 2D IR spectrometer, thus we will be able to perform 2D IR imaging at acquisition rates suitable for probing length scales beyond the micrometer length scale, resulting in connections being made between molecular length scale interactions to mesoscale phenomena.

## 2. Recent Progress & Current Efforts

The start date of this project was July 15, 2016. In the past two months we have focused on the initial steps of integrating a microscope head on our high-repetition rate 2D IR spectrometer. The design of the microscope head, the acquisition of optical components, and the first generation layout of the microscope head was completed in the past two months. In order to gain the full utility of our 100 kHz laser system, the microscope head was built as a point scanning microscope, rather than operating in a wide-field configuration with a mid-IR camera. The sample positioning for the microscope utilizes a combination of nanopositioners and micropositioners. Nanopositioners are used in X-Y-Z in order to navigate 200  $\mu\text{m}$  in each dimension with high precision and speed. The three-axis nanopositioners are integrated on a X-Y micropositioner with 25 mm of travel in each dimension. This combination of stages affords the potential of performing linear IR and 2D IR microspectroscopy across multiple length scales. The initial objectives that have been purchased are long working distance objectives with 2x and 5x magnifications; these



**Figure 1.** Photograph of microscope head to be integrated with a 100 kHz 2D IR spectrometer.

objectives were chosen based on the anticipated beam diameters at the image plane. In addition, a CMOS camera has been incorporated into the system in order to capture bright field images along with chemical maps generated from linear IR and 2D IR spectral acquisitions. Sufficient advances have been made in the design and build of the microscope head such that we are prepared to collect the initial images on this system in the next few months. The microscope head discussed here is shown in Figure 1 and will be integrated with our 100 kHz 2D IR spectrometer detailed in Figure 2. Initial experiments will be performed using known microparticle structures that are decorated with pseudohalide moieties as vibrational probes; polystyrene microspheres are available with coatings containing  $-OCN$  chemical groups. NIST standard microscopy targets will be used to calibrate the spatial resolution of our instrument.

microspheres are available with coatings containing  $-OCN$  chemical groups. NIST standard microscopy targets will be used to calibrate the spatial resolution of our instrument.

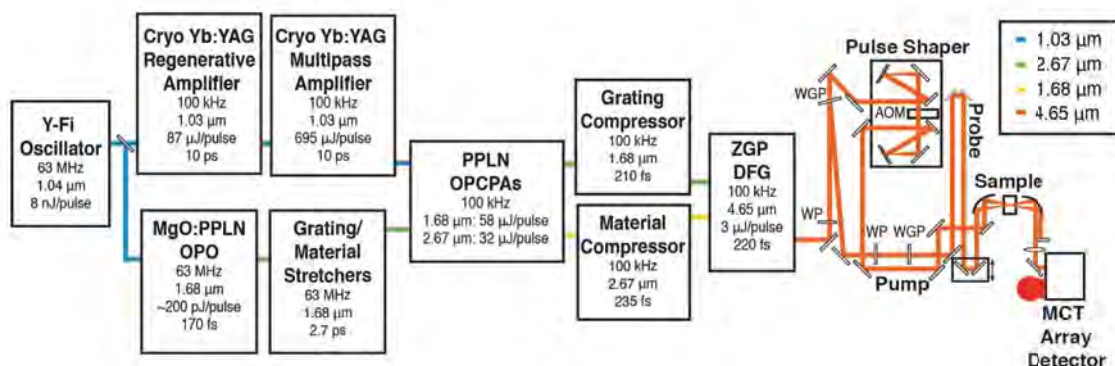


**Figure 2.** Box diagram of our 100 kHz 2D IR spectrometer.

### 3. Future Plans

The first year of this project is focused on designing, building, and calibrating our 2D IR microscope. As part of these efforts we will also improve the tunability of the 100 kHz midIR OPCPA that drives these 2D IR spectroscopy and microscopy experiments. Our approach to add more tunability to this system will be to generate continuum in a YAG crystal and use the continuum to seed our existing ZGP OPA. It is expected that this approach will yield tunable midIR light that spans the 3.0  $\mu\text{m}$  to 8.0  $\mu\text{m}$  wavelength region. Thus, opening the ability to use this 2D IR spectrometer and microscope to probe macrocyclic molecules and acids directly. In parallel with this effort we will perform preliminary IR microscopy experiments of representative fluids in pore structures fabricated in IR compatible materials.

### 4. Publications

Given the July 15, 2016 start date of this project, no publications have been produced under this award.

## Electrochemical control of plasmonic nanomaterial surface chemistry

Christy F. Landes

Department of Chemistry, Department of Electrical and Computer Engineering  
Rice University, Houston, TX 77005 USA  
[cflandes@rice.edu](mailto:cflandes@rice.edu)

Stephan Link

Department of Chemistry, Department of Electrical and Computer Engineering  
Rice University, Houston, TX 77005 USA  
[slink@rice.edu](mailto:slink@rice.edu)

12<sup>th</sup> Condensed Phase and Interfacial Molecular Science Research PI Meeting  
US Department of Energy, Basic Energy Sciences  
Nov. 1-4, 2016.

### 1. Program Scope

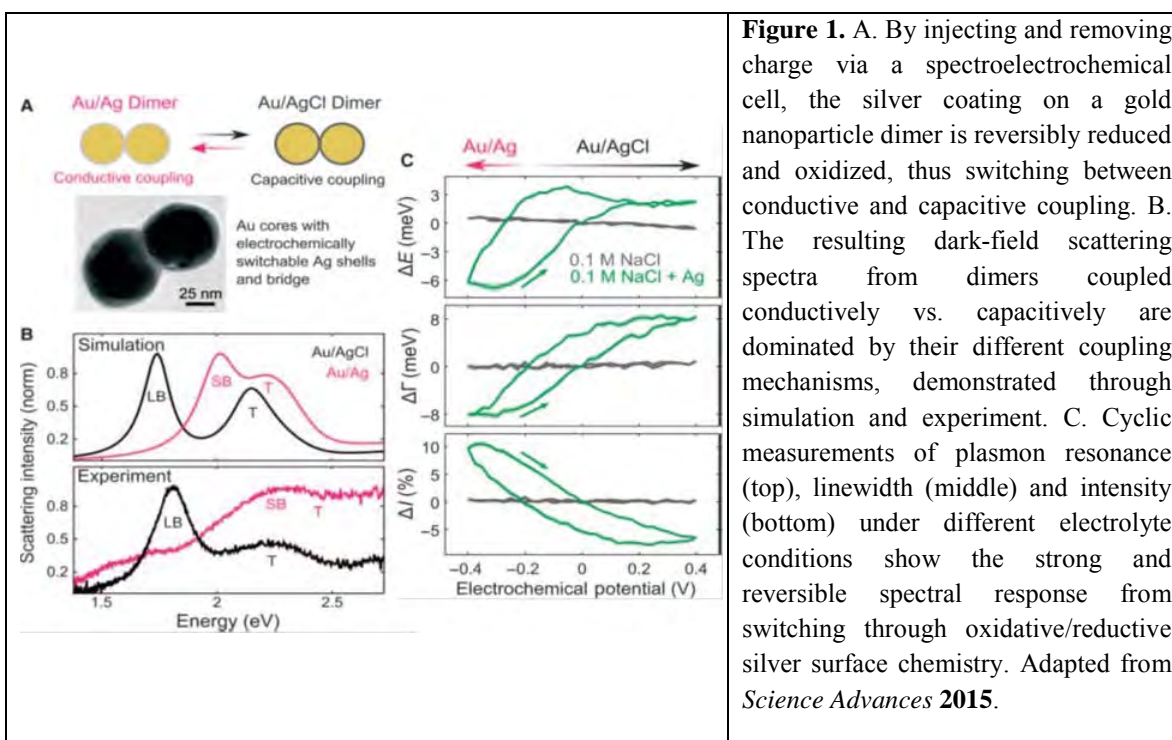
One of the keys to developing compact, robust, and affordable power sources is the identification of novel catalytic supports and reactions. Nanoparticles are of increasing interest because they provide a larger surface-to-volume ratio compared to flat surfaces. Additionally, new selectivities and activities are achievable with nanoparticle-based electrocatalysts compared to single crystalline metal electrodes. For example, 'noble metal' Au nanoparticles with diameters of 5 - 100 nm, initially considered inert and not suited for catalysis, show a significant catalytic activity for many reactions including methanol oxidation, oxygen reduction, hydrogen peroxide reduction, etc. Furthermore, plasmonic nanoparticles offer the possibility for photocatalysis via 'hot' electrons. However, it still remains controversial how nanoscale properties determine the catalytic activity because most previous studies measured innately heterogeneous distributions of nanoparticles. It is therefore not known if the average catalytic activity arises from an almost equal contribution of all nanoparticles or if only a few, 'super-active' nanoparticles dominate the signal.

To resolve this and other issues and to be able to optimize electrocatalysts, it is thus necessary to characterize the catalytic activity at the single nanoparticle level. ***The goal of this project is to correlate the activity of plasmonic electrocatalysts with nanoparticle morphology, surface chemistry, and 'hot' carrier physics using single particle spectro-electrochemical microscopy.***

The aims are to: (1) Determine the catalytic activities of single nanoelectrocatalysts and correlate them with their structural morphologies. (2) Investigate the effects of plasmon enhancement on the electrocatalytic activities of single metal nanoparticles and demonstrate feasibility of super-resolution mapping of catalytic activity.

## 2. Recent Progress

Novel chemical and physical processes occur at nanoparticle surfaces, both aided and reported by the broad tunability of their plasmonic properties. Electrochemical tuning is one way to control both plasmon resonance shifts and underlying morphology, composition, and surface chemistry. We approach this challenge with electrochemical redox tuning of metallic nanoparticles and assembled structures. Our method allows us, for example, to electrodeposit silver and/or its salts on the surface of gold nanostructures and selectively grow silver metal on the surface of these structures. We demonstrate repeatable spectro-electrochemical tuning of single nanoparticles and dimers (Figure 1). Potential applications include novel heterogeneous catalysis routes, experimental tests of charge transfer plasmonics, and nanoscopic plasmonic switches.



### Reference:

1. Byers, C.P.; Zhang, H.; Swearer, D.F.; Yorulmaz, M.; Hoener, B.S.; Huang, D.; Hoggard, A.; Chang, W.S.; Mulvaney, P.; Ringe, E.; Halas, N.J.; Nordlander, P.; Link, S.; Landes, C.F. "From tunable core-shell nanoparticles to plasmonic drawbridges: Active control of nanoparticle optical properties" *Science Advances* **2015**, 1, e1500988.

While single-particle spectroscopy is a powerful method to characterize nanoparticle heterogeneity, most experiments are performed in sequence, one nanoparticle at a time. Chemical reactions occurring at the surface of metal nanoparticle catalysts can however change the nanoparticle geometry as well. The problem therefore arises that while one nanoparticle is monitored all others are subjected to potential irreversible changes at the same time. It is therefore necessary to develop spectroscopic methods that allow one to monitor the spectral response of many nanoparticles in parallel with fast time resolution in order to fully characterize how charge transfer reactions at the surface of metal nanoelectrodes depend on their size and shape.

We have established a novel approach that facilitates a simultaneous readout of the 0 and 1st order diffraction of the dark-field scattering from over 60 individual plasmonic nanoparticles at the same time in order to extract their respective spectra. The high-intensity evanescent wave excitation of the particles enables signal to noise ratios greater than 90 with 1 ms time resolution when using a white light continuum laser source (Figure 2). The spatial throughput of the imaging technique is further increased by using of a highly ordered nanoparticle matrix. We have also developed an alternative excitation approach that utilizes a combination of a supercontinuum laser and a reflecting objective for polarization controlled snapshot hyperspectral imaging. Our measurement strategy can reveal the influence of particle heterogeneity on the kinetics of irreversible plasmon-mediated processes, impacting research fields such as sustainable energy and electrochemistry. With this instrument we have taken an important step forward in our aim to resolve reactions on metal nanoparticles because ‘looking’ one nanoparticle at a time as done in conventional methods is simply not feasible for irreversible reactions.

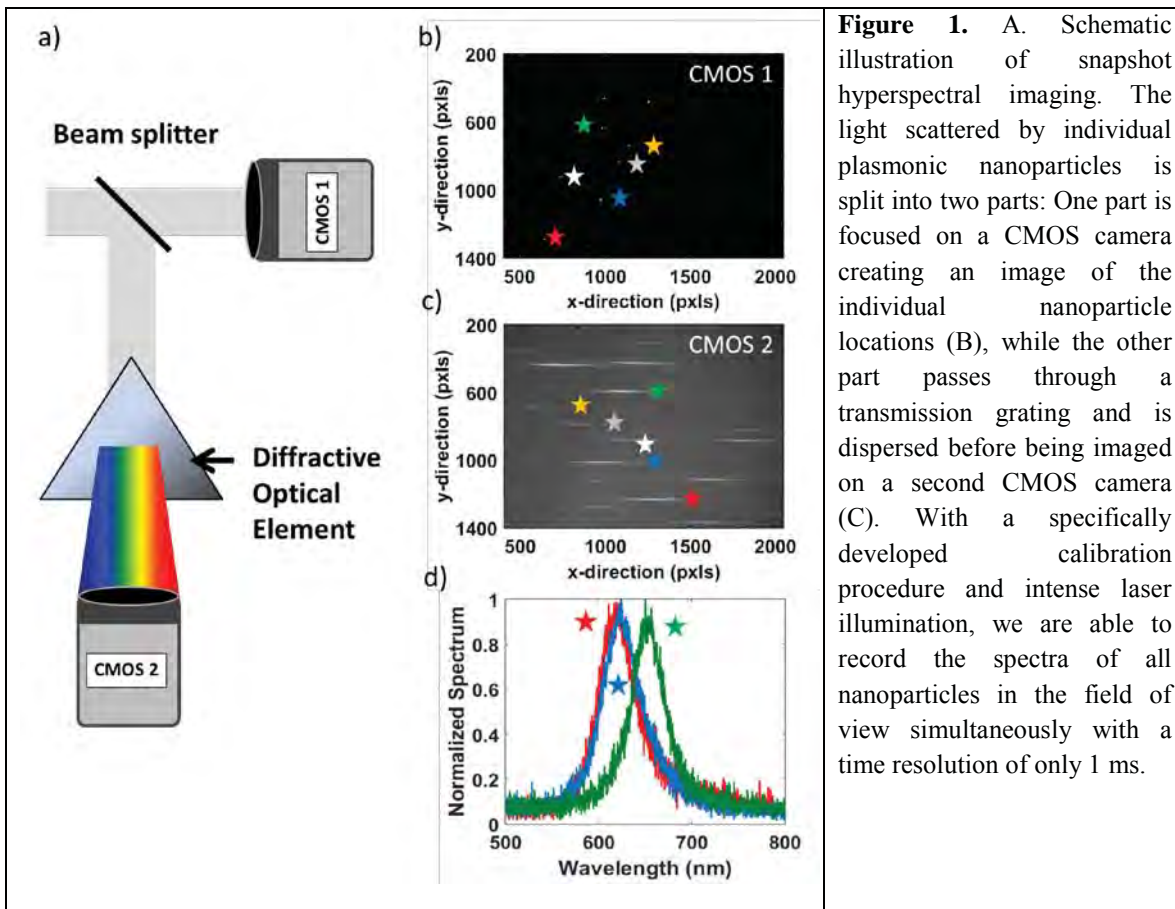


**Figure 1.** A. Schematic illustration of snapshot hyperspectral imaging. The light scattered by individual plasmonic nanoparticles is split into two parts: One part is focused on a CMOS camera creating an image of the individual nanoparticle locations (B), while the other part passes through a transmission grating and is dispersed before being imaged on a second CMOS camera (C). With a specifically developed calibration procedure and intense laser illumination, we are able to record the spectra of all nanoparticles in the field of view simultaneously with a time resolution of only 1 ms.

# Single-Molecule Interfacial Electron Transfer

H. Peter Lu

Bowling Green State University  
Department of Chemistry and Center for Photochemical Sciences  
Bowling Green, OH 43403  
[hplu@bgsu.edu](mailto:hplu@bgsu.edu)

## Program Scope

We develop and apply single-molecule high spatial and temporal resolved techniques to study molecular dynamics in condensed phase and at interfaces, especially, the complex reaction dynamics associated with electron and energy transfer rate processes. The complexity and inhomogeneity of the interfacial ET dynamics often present a major challenge for a molecular level comprehension of the intrinsically complex systems, which calls for both higher spatial and temporal resolutions at ultimate single-molecule and single-particle sensitivities. Combined single-molecule spectroscopy and electrochemical atomic force microscopy (E-Chem AFM) approaches are unique for heterogeneous and complex interfacial electron transfer systems because the static and dynamic inhomogeneities can be identified and characterized by studying one molecule at a specific nanoscale surface site at a time. Single-molecule spectroscopy reveals statistical distributions correlated with microscopic parameters and their fluctuations, which are often hidden in ensemble-averaged measurements. The goal of our project is to integrate and apply these spectroscopic imaging and topographic scanning techniques to measure the energy flow and electron flow between molecules and substrate surfaces as a function of surface site geometry and molecular structure. We have been primarily focusing on studying interfacial electron transfer under ambient condition and electrolyte solution involving both single crystal and colloidal TiO<sub>2</sub> and related substrates. The resulting molecular level understanding of the fundamental interfacial electron transfer processes will be important for developing efficient light harvesting systems and broadly applicable to problems in fundamental chemistry and physics.

## Recent Progress

### *Simultaneous Imaging of Single-Molecule Interfacial Electron Transfer Reactivity and Local Nanoscale Environment.*

The fundamental information related to the charge and energy flow between molecules and substrate surfaces as a function of surface site geometry and molecular structure are critical for understanding interfacial electron transfer (ET) mechanism and dynamics. The inhomogeneous nanoscale molecule-surface and molecule-molecule interactions are presumably the origins of the complexity in interfacial ET dynamics. Therefore, identifying the environment of molecules at nanoscale is critical to our understanding of the molecule-substrate interaction. We have developed a new AFM tip-enhanced single-molecules fluorescence intensity/lifetime imaging microscopy to investigate each single-molecule heterogeneously distributed across the surface to obtain nanoscale topology as well as interfacial ET dynamics at single-molecules level (Fig. 1)<sup>1</sup>. This correlated imaging technique provides a mean to distinguish and characterize each single-molecule distributed across the surface at the nanometer spatial

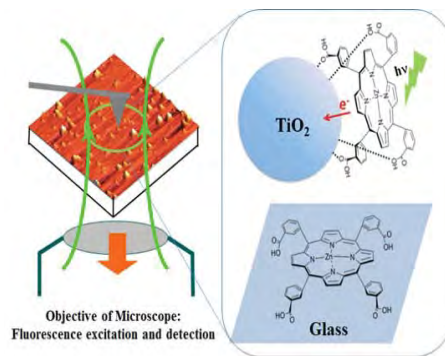


**Figure 1.** Left: Scheme of correlated AFM-fluorescence microscopy; Right: Scheme of the sample, single *m*-ZnTCPP molecule coupled with TiO<sub>2</sub> NPs and single *m*-ZnTCPP molecule adsorbed on glass surface.

scale. The observed fluorescence blinking behavior of each dye molecule and its lifetime in combination with the topography of the local environment at nanoscale provides the location of each dye on the surface (on top of ET active TiO<sub>2</sub> surface or on ET non-active glass surface) at nanoscale as well as the coupling strength of each dye with TiO<sub>2</sub> nanoparticles (Fig. 2).

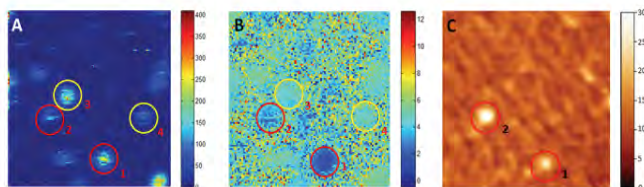


**Figure 2.** Correlated AFM-fluorescence intensity and lifetime data: Fluorescence intensity image (A) and Fluorescence lifetime image (B) of (*m*-ZnTCPP/TiO<sub>2</sub> + *m*-ZnTCPP)/Cover Glass, the image is 4 μm × 4μm and 100×100 pixel with each pixel 20ms and Correlated AFM image (4 μm × 4μm) (C).

**Single-molecule femtosecond pump-probe stimulate emission spectroscopic detection and analysis of molecule excited state dynamics.** We have recently developed and demonstrated a state-of-the-art single-molecule femtosecond ultrafast spectroscopy station capable of detecting single-molecule excited state involving in charge transfer and other non-radiative relaxation dynamics by pump-probe stimulate emission spectroscopic microscopy. The preliminary applications of ultrafast spectroscopy at single-molecular level provide a direct measurement of the inhomogeneity with respect to the electronic and chemical properties of the molecules at dye-solid interfaces,<sup>3</sup> including dye-TiO<sub>2</sub> nanoparticles (electron transfer) and dye-glass surfaces (no electron transfer). Here, we present the experimental setup for the time-resolved pump-probe single molecule spectroscopy that we have developed in our laboratory. We demonstrated detections of the excited-state dynamics of electron transfer in interactions of dye molecules with TiO<sub>2</sub> nanoparticles at ambient conditions (Fig. 3).

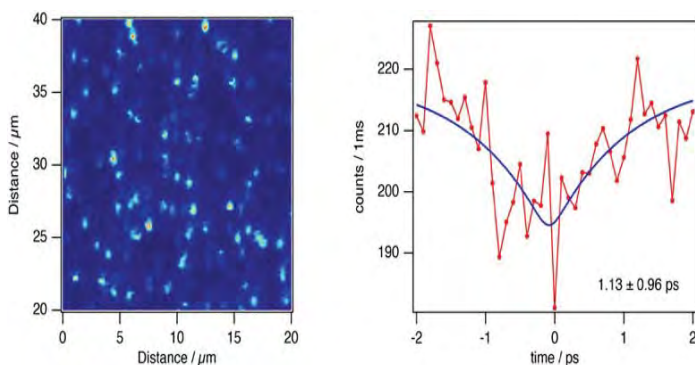


**Figure 3.** Single-molecule ultrafast spectroscopy and microscopic imaging analysis of interfacial electron transfer on dye-TiO<sub>2</sub> nanoparticle interfaces. Single-molecule imaging (Left) and interfacial electron transfer rate detection (right) of 2,3,7-Trihydroxy-9-phenyl-6-fluorone (PF) on TiO<sub>2</sub> nanoparticles. The single-molecule excited state lifetime is measured to be 1.13 ps

**Probing Single-Molecule Ultrafast Interfacial ET Dynamics: Analyzing the donor-acceptor electronic coupling effect on the interfacial electron transfer dynamics.** The photosensitized interfacial ET dynamics of Zn(II)-5,10,15,20-tetra (3-carboxyphenyl) porphyrin (*m*-ZnTCPP)-TiO<sub>2</sub> nanoparticle (NP) system has been studied using time-correlated single photon counting coupled with scanning confocal fluorescence microscopy. Comparing our results obtained with *p*-ZnTCPP-TiO<sub>2</sub> nanoparticle (NP) system, we show the effect of anchoring group binding geometry (*meta* or *para*), hence electronic coupling of sensitizer (*m/p*-ZnTCPP) and TiO<sub>2</sub> substrate, on interfacial ET dynamics. Compared to *p*-ZnTCPP on TiO<sub>2</sub> NP surface, with *m*-ZnTCPP, dark states are observed to dominate in single-molecule fluorescence intensity trajectories.<sup>7</sup> This observation coupled with the large difference in lifetime derived from bright and dark states of *m*-ZnTCPP demonstrate higher charge injection efficiency of *m*-ZnTCPP than *p*-ZnTCPP. The nonexponential autocorrelation function decay and the power-law distribution of the dark-time probability density provide a detailed characterization of the

inhomogeneous interfacial ET dynamics. The distribution of autocorrelation function decay times ( $\tau$ ) and power-law exponents ( $m_{\text{dark}}$ ) for *m*-ZnTCPP are found to be different from those for *p*-ZnTCPP, which indicates the sensitivity of  $\tau$  and  $m_{\text{dark}}$  on the molecular structure, molecular environment, and molecule-substrate electronic coupling of the interfacial electron transfer dynamics. Overall, our results strongly suggest that the fluctuation and even intermittency of excited-state chemical reactivity are intrinsic and general properties of molecular systems that involve strong molecule-substrate interactions.

### **Probing Back Electron Transfer (BET) Dynamics from TiO<sub>2</sub> nanoparticles to the dye molecules.**

Comprehensive introspection of interfacial ET dynamics and associated intermittency of excited-state chemical reactivity requires molecular-level understanding of all related and regulating parameters: for example, adsorbate/semiconductor interactions, Franck-Condon factor, distribution of crystal surfaces and trap states, vibronic coupling, structures and energetics of both the adsorbate and the substrate surfaces, solvation, and local environment thermal fluctuations. There are two major processes involved in the photoinduced interfacial ET at a dye/semiconductor interface: forward electron transfer (FET) from an excited state of dye molecule to the conduction band or energetically accessible surface states of semiconductor, and backward electron transfer (BET) of the excess electron which recombines with the parent oxidized dye molecule. Extensive studies of interfacial ET dynamics have shown that FET kinetics are rather insensitive to variations in experimental condition; whereas, BET kinetics exhibit greater sensitivity to experimental condition.<sup>5</sup> Designing an efficient solar energy harvesting system entails controlling the rate of BET process in order to generate long-lived charge-separated states so that the excess electron can diffuse away to generate photovoltaic potential energy. Despite the greater significance of BET dynamics, it has not been studied in great details, while FET dynamics has been well characterized. BET dynamics have been studied on an ensemble level using transient absorption spectroscopy and fluorescence measurements, but the underlying trapping and de-trapping processes have not been directly probed. Ensemble-average measurements are not necessarily specific to resolve heterogeneity in local environment involving inhomogeneous substrate-dye molecule interactions. Detailed understanding of the molecular mechanics of interfacial ET dynamics requires studying the system at a single molecular level.

### **Probing Driving Force and Electron Accepting State Density Dependent Interfacial Electron Transfer Dynamics: Suppressed Fluorescence Blinking of Single-Molecules on Doped Semiconductors.**

Photo-induced, interfacial electron transfer (ET) dynamics between *m*-ZnTCPP and Sn-doped In<sub>2</sub>O<sub>3</sub> (ITO) film has been studied using single-molecule photon-stamping spectroscopy.<sup>2,4,5</sup> The observed ET dynamics of single *m*-ZnTCPP adsorbed on ITO was compared with that of *m*-ZnTCPP adsorbed on TiO<sub>2</sub> NPs with and without applied electric potential. Compared to *m*-ZnTCPP on TiO<sub>2</sub> NP surface, *m*-ZnTCPP on ITO surface shows reduced lifetime as well as suppressed blinking and quasi-continuous distribution of fluorescence intensities, presumably due to higher electron density in ITO. The higher electron density leads to the occupancy of CB acceptor states/trap states, which supports a higher backward electron transfer (BET) rate that results in quasi-continuous distribution of fluorescence intensities. The dependence of BET rate on electron density and charge trapping is consistent with our previous observations of quasi-continuous distribution of fluorescence intensities of *m*-ZnTCPP on TiO<sub>2</sub> NPs with applied negative potential across the dye-TiO<sub>2</sub> interface. The quasi-continuous distribution of fluorescence intensities in both case of *m*-ZnTCPP on ITO surface and *m*-ZnTCPP on TiO<sub>2</sub> NPs with applied negative potential indicates that the electron density/occupancy in the semiconductor plays a dominant role in dictating the changes in rates of charge transfer in our system, rather than the relative energetics between electron in semiconductor and the oxidized sensitizer.

### **Future Research Plans**

One of the most significant characteristics of our approach is that we will interrogate the complex interfacial electron transfer dynamics by actively pin-point energetic manipulation of the surface interaction and electronic couplings, beyond the conventional excitation and observation. We plan to study the FET and BET dynamics by manipulating the electric field distribution at the interface and the energetic trapping state distributions in the TiO<sub>2</sub> materials. Furthermore, in the wrapping up phase of this project, we will also work on completing our studies of excess electron injection from the excited state of the molecule to the conduction band of the

semiconductor or energetically assessable surface states, the excess electron thermalization, solvation, and the geminate recombination of the excess electron and the parent cation at interface. In this study, we will probe the excess electron diffusion and scattering at interfaces as well as in bulk of the wide-band gap semiconductor. A model of the excess electron diffusion associated with trapping and detrapping under the columbic field of the cation within the Onsager distance will be developed. To achieve femtosecond time resolution and molecular spatial resolution, we will use a combined approach utilizing single- molecule ultrafast spectroscopy, E-chem-AFM, and STM. Ultrafast, spectroscopic, and structural information will be directly correlated for the same individual sites and molecules. Using this approach, correlated information on the adsorption-site structure, molecular orientation, electronic structure, and single-molecule interfacial electron transfer dynamics will be obtained for the forward and backward (FET and BET) electron transfer reactions.

#### **Publications of DOE sponsored research (FY2015-2016)**

- 1 Yufan He, Vishal G. Rao, Jin Cao, H. Peter Lu, "Simultaneous Spectroscopic and Topographic Imaging of Single-Molecule Interfacial Electron Transfer Reactivity and Local Nanoscale Environment," *J. Phys. Chem. Lett.*, **7**, 2221-2227 (2016).
- 2 Bharat Dhital, Vishal G. Rao, H. Peter Lu, "Electronic Coupling-Decoupling Dependent Single-Molecule Interfacial Electron Transfer Dynamics in Electrostatically-Attached Porphyrin on TiO<sub>2</sub> Nanoparticles," *J. Phys. Chem. C*, **120**, 12313-12324 (2016).
- 3 Papatya Sevinc, Bharat Dhital, Vishal G. Rao, Yuanmin Wang, H. Peter Lu, "Probing Electric Field Effect on Covalent Interactions at a Molecule-Semiconductor Interface" *J. Am. Chem. Soc.*, **138**,1536-1542 (2016).
- 4 Vishal G. Rao, Bharat Dhital, H. Peter Lu, "Probing Driving Force and Electron Accepting State Density Dependent Interfacial Electron Transfer Dynamics: Suppressed Fluorescence Blinking of Single-Molecules on Indium Tin Oxide Semiconductors," *J. Phys. Chem. B.*, **120**,1685-1697 (2016).
- 5 Vishal G. Rao, H. Peter Lu, invited review article, "Inhomogeneous and Complex Interfacial Electron Transfer Dynamics: A Single-Molecule Perspective," ACS Energy Letter, in press (2016).
- 6 Arthur Yu, Shaowei Li, Bharat Dhital, H. Peter Lu, Wilson Ho, "Tunneling Electron Induced Charging and Light Emission of Single Porphyrin Molecules," *J. Phys. Chem. C*, in press (2016).
- 7 Vishal G. Rao, Bharat Dhital, H. Peter Lu, "Single-Molecule Interfacial Electron Transfer Dynamics of Porphyrin on TiO<sub>2</sub> Nanoparticles: Dissecting Interfacial Electric Field and Electron Accepting State Density Dependent Dynamics," *Chem. Commun.*, **51**,16821-16824 (2015).

## ***Ab initio* approach to interfacial processes in hydrogen bonded fluids**

Christopher J. Mundy  
Physical Sciences Division  
Pacific Northwest National Laboratory  
902 Battelle Blvd, Mail Stop K1-83  
Richland, WA 99352  
[chris.mundy@pnnl.gov](mailto:chris.mundy@pnnl.gov)

### **Program Scope**

The long-term objective of this research is to develop a fundamental understanding of processes, such as transport mechanisms and chemical transformations, at interfaces of hydrogen-bonded liquids. Liquid surfaces and interfaces play a central role in many chemical, physical, and biological processes. Many important processes occur at the interface between water and a hydrophobic liquid. Separation techniques are possible because of the hydrophobic/hydrophilic properties of liquid/liquid interfaces. Reactions that proceed at interfaces are also highly dependent on the interactions between the interfacial solvent and solute molecules. The interfacial structure and properties of molecules at interfaces are generally very different from those in the bulk liquid. Therefore, an understanding of the chemical and physical properties of these systems is dependent on an understanding of the interfacial molecular structure. The adsorption and distribution of ions at aqueous liquid interfaces are fundamental processes encountered in a wide range of physical systems. In particular, the manner in which solvent molecules solvate ions at the interface is relevant to problems in a variety of areas. Another major focus lies in the development of models of molecular interaction of water and ions that can be parameterized from high-level first principles electronic structure calculations and benchmarked by experimental measurements. These models will be used with appropriate simulation techniques for sampling statistical mechanical ensembles to obtain the desired properties.

### **Progress Report**

#### Intrinsic to collective properties of ions in solution

***Solvation Free Energies:*** Ionic solvation free energies are one of the most fundamental and important properties in physical chemistry and yet there is still debate and uncertainty about what they are. In particular, the contribution from the surface potential of the air-water interface is poorly understood. Our research is aimed at providing clear and rigorous definition of single ion solvation free energies (see **Figure 1**). Starting with model systems we calculate solvation free energies for positive and negative charged hard spheres using interaction potentials based in quantum density functional theory (DFT). For charged hard spheres we show that DFT water responds linearly (see **Figure 2**) to the charge in the center of the cavity but exhibits a very large charge hydration asymmetry (see **Figure 3**) that is much larger than experimental estimates for real ions. This indicates that real ions, particularly anions, are significantly more complex than the simple charged hard spheres they are often considered to be.

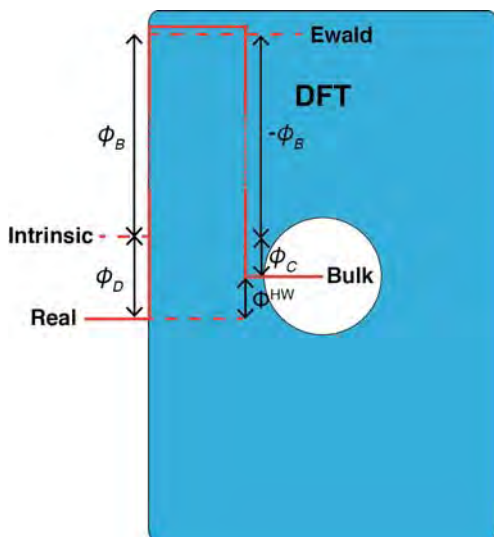


**Figure 1:** Four different definitions of the electrostatic contributions to the solvation free energies: **Real**, **Intrinsic**, **Ewald** (inherently unphysical because they contain the Bethe potential  $-\phi_B$ ), and **Bulk**. The conversion between each of the definitions is denoted schematically by the addition/subtraction of well-defined potentials, namely the Bethe potential  $-\phi_B$ , the dipole potential due to the presence of an interface  $-\phi_D$ , the cavity potential  $-\phi_C$ . Note, for the case of quantum based potentials such as DFT,  $\phi_B$  is large and positive. See Remsing *et al. J. Phys. Chem. Lett.* **5**, 2767 (2014) for details.

determining solvation free energies. It is widely believed that water will interact more strongly with an anion than with a cation of the same size. Remarkably we find that the electrostatic response and the dispersion interaction, as determined from quantum mechanics, that favor anions are cancelled by the exchange energy and the local water structuring, which favor cations. As a result the intrinsic solvation energies based in quantum mechanics show no net preference for anions. The protocols developed in this research will also allow for the application of AIMD techniques to a whole new class of problems that depend on free energy changes.

**A microscopic picture of collective properties of ions in solution** [1-3]: In current and previous funding periods we have studied both the structure and solvation free energetics of single ions in solution. We have demonstrated that the accuracy of the ion-water and water-water interaction afforded by DFT are good enough to reproduce the local aqueous structure of anions as determined by extended x-ray fine structure spectroscopy (EXAFS). Nevertheless questions pertaining to the collective nature of concentrated electrolyte solutions still remain. Moreover, producing well converged ensembles of trajectories of electrolyte solutions at finite

The solvation free energies of “real” ions are crucial targets for models of electrolyte solutions to reproduce.<sup>1</sup> There are two contributions to these free energies, one from the local interaction with the surrounding water molecules, (moving the ion across the electrostatic potential difference created by the dipolar orientation of water molecules at the bulk air-water interface<sup>2</sup> (see **Figure 1**). Until now, we have not known the sizes of these two contributions for single ions in water (the dipole contribution from the presence of an interface cancels for cation-anion pairs.) Using DFT in conjunction with the Potential Distribution Theorem we can accurately calculate these two contributions. Our research thus far suggests how that the quantum mechanical nature of the ion is essential in

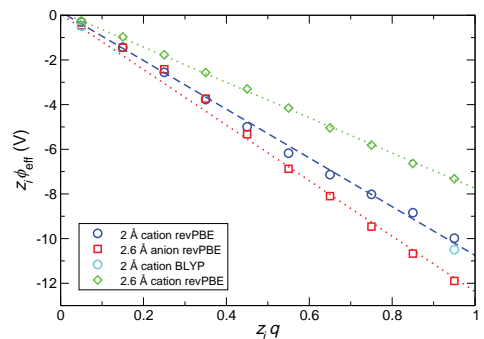


**Figure 2:** Effective potentials as a function of charge,  $q$  of the center of a charged hard sphere cavity,  $z_i$  of a particular radius and charge of the hard using different representations of the DFT exchange and correlation functional. The linearity in the effective potential allows one to make direct contact with simpler theories such as the Born theory of solvation.

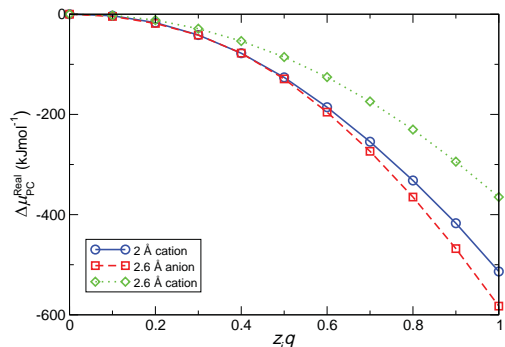


**Figure 3:** Real (see **Figure 1**) ion free energies for charge hard-spheres of particular radius. Note the large asymmetry in the anion and cation solvation free energies for DFT based interaction potentials.

computed with a classical empirical potential that is known to give good agreement with EXAFS. The PMFs are remarkably different.[1] It is well known in the literature that  $\text{CaCl}_2$  does not ion-pair until concentrations above 6M.[1] Although data provided in **Figure 4** provides qualitative evidence of how an accurate description of local structure impacts collective properties such as activity and osmotic coefficients, a more rigorous connection is needed.

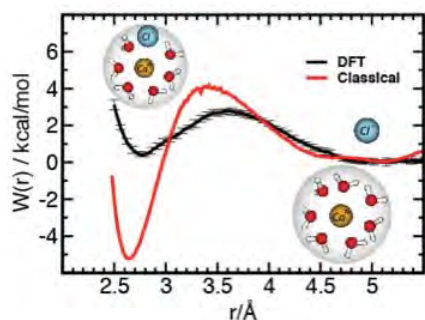


**Figure 4:** PMF for ion pairing of  $\text{CaCl}_2$  using different levels of molecular interaction. The DFT is consistent with a picture little ion pairing in agreement with experiment.[1] The classical force field would suggest that  $\text{CaCl}_2$  forms strong ion pairs.

can efficiently access the osmotic coefficients at finite concentration.[2] The result, as shown in **Figure 6** shows that the coarse grained two-body interaction potential indeed yields reasonable osmotic coefficients up to concentrations of 1 M. Using the ideas of the intrinsic PMF from accurate representations of interaction based in quantum mechanics to inform our understanding of collective properties such as clustering in solution up to moderate concentrations will be the focus of future studies. Specifically, it

concentrations using DFT based interaction potentials remains a challenge. Questions pertaining to the extent of an accurate representation of the short-ranged structure is necessary to predict the long-range collective response of a concentrated electrolyte solution remains. We have shown that DFT based interaction potentials reproduce the local aqueous solvation structure as determined by EXAFS of both isolated  $\text{Ca}^{2+}$  and  $\text{Cl}^-$  ions reproduce.[1] Having established this notionally “intrinsic” measure of accuracy with DFT interaction potentials, we can compute the PMF between two ions in water. **Figure 4** depicts the potential of mean force (PMF) as computed from DFT interaction potentials and classical empirical potential. Also shown in **Figure 4** is the same PMF

**Figure 5** demonstrates schematically how our research is making connections between “intrinsic” properties at infinite dilutions and collective properties at finite concentration.[2] To this end we provided a model for ion pairing of  $\text{NaCl}$  using the short-range (SR) interaction as determined by DFT and the long-range (LR) interaction being determined by simple Coulomb form as shown in **Figure 6**. Using this simple two-body potential for the ion-ion interaction as the input in an integral equations with the hypernetted-chain closure, we

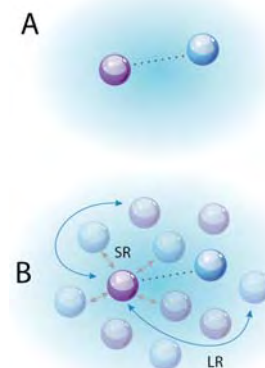


**Figure 5:** A schematic of a PMF of ion-pairing in the dilute limit (A) that was computed in **Figure 4**. (B) how the dilute limit PMF informs collective behavior. This will require the delicate interplay between the slowly varying long-range (LR) interaction and the complex short-range (SR) interaction.

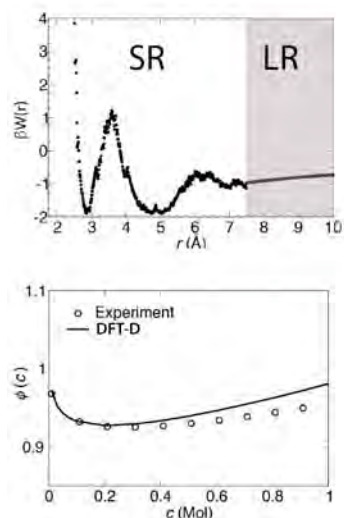


**Figure 5:** (top) the potential of mean force for an isolated  $\text{Na}^+ \text{--} \text{Cl}^-$ . The SR is determined by DFT. The LR is a simple electrostatic term. (bottom) The computed and experimentally determined osmotic coefficients for NaCl as a function of oncentration.

will be the differences in the SR component between quantum versus classical empirical interaction potentials that will drive much of the interesting phenomena.[3]

**Acknowledgements.** This work was performed with Mirza Galib (PNNL), Santanu Roy (PNNL), Tim Duignan (PNNL), John D. Weeks (U. Maryland), Rick Remsing (Temple), Ilja Siepmann (U. Minn.), Greg Schenter (PNNL), Marcel D. Baer (PNNL), Shawn M. Kathmann (PNNL), Greg Kimmel (PNNL), and John Fulton (PNNL). We also acknowledge computer resources from NERSC. Battelle operates Pacific Northwest National Laboratory for the US Department of Energy.

### Publications with BES support (2015-present):

1. Marcel D. Baer and **CJM**, “Local aqueous solvation structure around  $\text{Ca}^{2+}$  during  $\text{Ca}^{2+} \text{--} \text{Cl}^-$  pair formation” *Journal of Physical Chemistry B* **120**, 1885, (2016)
2. Duignan, T.; Baer, M.D.; **CJM**, “Ions Interacting in Solution: Moving from Intrinsic to Collective Properties” *Current Opinion in Colloid & Interface Science* **23**, 58 (2016)
3. Daily M.; Baer, Marcel, **CJM**, “Divalent Ion Parameterization Strongly Affects Conformation and Interactions of an Anionic Biomimetic Polymer” *The Journal of Physical Chemistry B* **120**, 2198 (2016)
4. L. B. Skinner, L.B.; Galib, M.; Fulton, J.L. **CJM**; Parise, J. B.; Pham, V.-T.; Schenter, G.K. and Benmore, C.J., “The structure of liquid water up to 360 MPa from x-ray diffraction measurements using a high Q-range and from molecular simulation, *The Journal of Chemical Physics* **144**, 134504 (2016)
5. Roy, S; Baer, M.D.; **CJM**; Schenter, G.K., “Reaction Rate Theory in Coordination Number Space: An Application to Ion Solvation” *The Journal of Physical Chemistry C* **120**, 7597 (2016)
6. Lei, H.; Baker, N.A.; Wu, L.; Schenter, G.K.; **CJM**, and Tartakovsky, A, “Smoothed Dissipative Particle Dynamics model for mesoscopic multiphase flows in the presence of thermal fluctuations,” *Physical Review E* **94**, 023304 (2016)
7. Lei, H.; **CJM**; Schenter, GK; Voulgarakis NK, “Modeling nanoscale hydrodynamics by smoothed dissipative particle dynamics,” *Journal of Chemical Physics* **142**, 194504 (2015)
8. Chun, J; Schenter, GK; **CJM**, “The role of solvent heterogeneity in determining the dispersion interaction between nanoassemblies,” *Journal of Physical Chemistry B* **119**, 5873 (2015)

## DYNAMIC STUDIES OF PHOTO- AND ELECTRON-INDUCED REACTIONS ON NANOSTRUCTURED SURFACES - DE-FG02-90ER14104

**Richard Osgood,**

Center for Integrated Science and Engineering, Columbia University, New York, NY 10027, [Osgood@columbia.edu](mailto:Osgood@columbia.edu)

### **Program Scope or Definition:**

Our current research program examines the photon- and electron-initiated reaction mechanisms, half-collision dynamics, and other nonequilibrium-excited dynamics effects, occurring with excitation of adsorbates on well-characterized metal-oxide surfaces, both in single-crystal and in nanocrystalline forms. Our program has previously developed a new synthesis methods for uncapped nanocrystals with specific orientation and atomic structure *in situ* on a substrate in a UHV preparation chamber. In our program, STM-based nanocrystallography is used to identify the atomic structure and orientation of these nanocrystals. In order to explore the dynamics of surface reactions, three types of excitation are applied to the molecular adsorbates on the nanocrystals: (a) thermal excitation in temperature programmed desorption (TPD) experiments, (b) irradiation with monochromated light from a UV lamp, focused on the sample in the STM stage; and (c) excitation with the electric charges, injected from the STM tip. The last method allows single-molecule-resolved studies. The resulting chemistry and surface dynamics are investigated via imaging of the reaction fragments in the vicinity of the reaction sites.

Our most recent experiments have been directed toward light-induced reactions of surface bound molecules, where the focus has been on reactions on a single nanocrystal. Also we have made significant progress in characterization of STM tip-triggered reactions on single crystal TiO<sub>2</sub>(110) surface and in understanding the wavelength dependencies of the surface photoreactions. Most recently we have focused on understanding the effects of mechanical strain-induced changes in adsorbate surface reactions on TiO<sub>2</sub>(110) surfaces. These new findings are enabled by the very high values of strain in a field of a few-atomic-layer nanobubbles as a result of UHV preparation of the surface.

### **Recent Progress:**

#### ***STM studies of photoreactions on supported single-crystal & nanocrystal TiO<sub>2</sub>.***

In order to establish the dynamics of light-induced reactions on TiO<sub>2</sub> surfaces of nanocrystals, that could serve as a platform for more complex studies of single-molecule charge-induced reactions, a series of experiments using scanning tunneling microscopy (STM) have been carried out, in which surfaces with adsorbed target molecules were controllably exposed to photon-energy-tuned UV light.

In this section of the report, we summarize this investigation, which began last year but were then reformulated during the early part of this reporting period. In particular, we our work has focused on atomically resolved studies of adsorbate photoreactions on the surface of *a single isolated TiO<sub>2</sub> nanocrystal*. This single-crystal aspect of the experiment is important since DOE has had a long-standing interest in understanding nanocrystal reactions in the face of significant unavoidable spatial dispersion in the dimensions of nanocrystals. Our crystals were grown *in situ* on Au(111) in an ultrahigh-vacuum chamber. The experiments used scanning tunneling microscopy, backed by temperature programmed desorption (TPD) to determine the surface coverage of trimethyl acetic acid

(TMAA) on the nanocrystal surfaces before and after irradiation with monochromated UV light. Trimethyl acetic acid (TMAA) was chosen as a model photoreaction active molecule due to its ease of handling and the existence of numerous prior studies of its photoreactivity, including studies at other DOE Labs (e.g. PNNL). UV doses were administered using a Xe-Hg arc lamp; light from this source was spectrally narrowed, with a monochromator, to a 15 nm bandwidth and focused onto the sample inside our STM stage. A detailed determination of the surface structure of the 1 – 3 nm thick and 10 – 30 nm wide nanocrystals was obtained presented and the importance of moiré effects in controlling the reaction sites shown; **Fig. 1**.

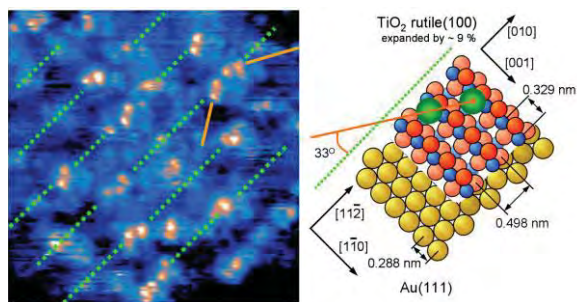


**Fig. 1.** (left)  $25 \times 25$  nm STM image of hexagonal  $\text{TiO}_2$  nanocrystals on a Au(111) surface after a low dose of TMAA. (right) Schematic illustrating the mutual orientation of gold and rutile lattices. Yellow spheres represent gold atoms, blue – Ti atoms, red – O atoms, and two green spheres – positions of TMAA species within a pair.

Our approach is unconventional since we use direct “counting” of molecules before and after irradiation in the case of a single nanocrystal. Since individual TMAA molecules are clearly visible in the STM images, measurement of their areal density can be carried out before and after irradiation. The normalized TMAA photodesorption quantum efficiency from Au-supported  $\text{TiO}_2$  nanocrystals was found to be  $\sim 4$  times lower compared to the same reaction on rutile  $\text{TiO}_2(110)$  surface, a result consistent with the lower fraction of light adsorbed in the nanocrystals. We conclude by noting that this experiment appears to be the first observation of an atomically-resolved study of any photo-induced reaction on the surfaces of  $\text{TiO}_2$  nanocrystals and a full account of this and the succeeding section appears in Publication 5.

### *Wavelength dependent dynamics of TMAA photolysis on $\text{TiO}_2$*

Photolysis of TMAA molecules, adsorbed on  $\text{TiO}_2(110)$  surface, with unfiltered UV light is a relatively well-studied phenomenon – particularly within DOE Labs! In order to gain deeper general insight into the physical phenomena involved in photocatalytic processes, our experimental system has been designed to use monochromated light with a 15 nm bandwidth. The energy output of the optical setup has been calibrated over the whole spectrum to allowing re-calculation of the optical flux in terms of photons per unit area. The experiments consisted of preparation of a  $\text{TiO}_2(110)$  surface with a desired concentration of trimethyl acetate (TMA) and exposure of the surface to controlled doses of UV light. The surfaces were imaged with an STM before and after each exposure. The concentrations of TMA on the surfaces have been estimated from the measured STM images. The example of such series of the STM images is shown in the top section of **Fig. 2**. The lower part of this figure shows the TMA concentration decay curves for UV light at three different wavelengths: 365, 340, and 310 nm.

The first and most obvious observation from the decay curves is that the efficiency of TMA photodesorption is higher for shorter wavelengths (i.e. for higher photon energies). Our calculations have shown that this photon energy-dependent efficiency can be explained by the different characteristic absorption lengths for light with different wave-

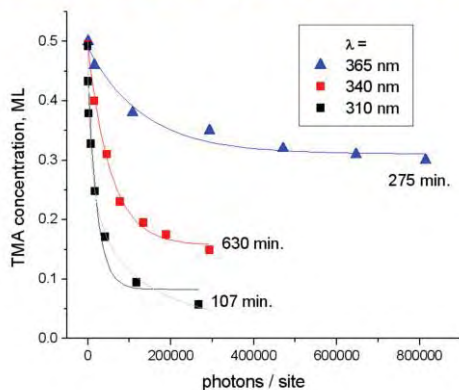
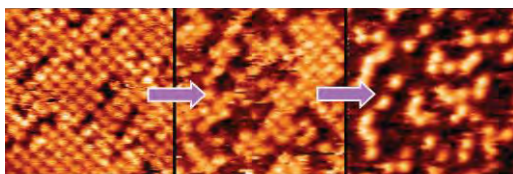


**Fig. 2:** Series of STM images showing the  $10 \times 10$  nm area of TMAA-saturated rutile(110) surface after progressively longer exposures to UV light. Below: surface concentration of TMA groups on the rutile(110) surface as a function of UV exposure at 3 different wavelengths.

lengths. Photons with higher energy are absorbed closer to the surface and the photo-generated holes have higher probability of reaching the surface before recombination with electrons.

In addition, a more detailed analysis of the TMA depletion dynamics has revealed that the efficiency of the photo-desorption decreases by more than an order of magnitude as the photoreaction proceeds to completion. For this reason the data points cannot be fitted well with a simple first-order exponent function (**Fig. 2**). The rates of the efficiency lowering as the function of TMA concentration were found to be nearly identical for 310 and 340 nm light but much higher for 365 nm light. On the basis of such analysis, a number of conclusions can be made about inhibitive influence of the surface-trapped negative charge and about energy position of the reaction-triggering molecular orbital of the adsorbed TMA molecules.

### *Studies of STM tip-induced surface reactions*

As a next step towards understanding dynamics on a single-molecule scale, we have performed a number of experiments, in which surface reactions were triggered by charges, injected from an STM tip. Earlier, we had demonstrated electron-induced chemistry of halo-hydrocarbons on  $\text{TiO}_2$  surface; see Ref 1. Recently, we have explored the possibility of initiation of the TMAA photodesorption reaction on rutile(110) surface by controlled variations of the sample bias voltage. TMAA photodesorption is known to be activated by the electronic holes, generated in the  $\text{TiO}_2$  bulk by UV light. Thus in the case of STM tip-induced experiments, the holes were created by application of negative sample biases. Several experimental protocols have been tested and the result of one such experiment is shown in **Fig. 3**. In this figure the left STM image shows TMAA-saturated rutile(110) surface. After taking the image, a smaller  $20 \times 100$  nm area of the surface was scanned with the sample bias linearly changing from  $V = -3.0$  to  $-4.0$  V with 0.05 V step. Then the original  $40 \times$

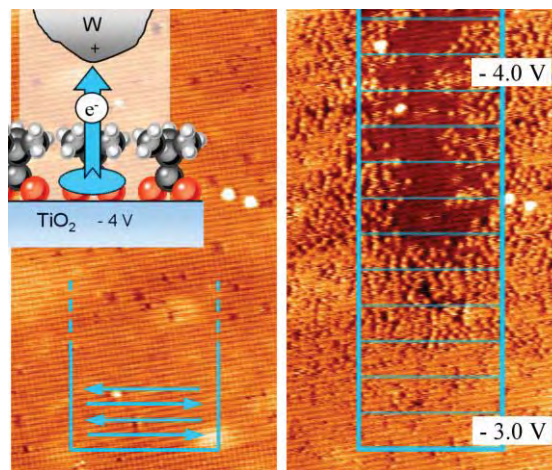


**Fig. 3:** Two STM images showing the same  $40 \times 100$  nm area of TMAA-saturated rutile(110) surface before (left) and after (right) the smaller area, marked with the cyan rectangle, had been scanned with changing negative sample bias.

120 nm area was imaged again at the normal +1.5 V bias. It can be seen from the right image in **Fig. 3** that a fraction of TMA surface species have desorbed as a result of the negative bias application. Also it can be seen that the degree of the tip-induced depletion is clearly bias-dependent with lower (i.e. more negative) biases causing greater extent of TMA desorption. This tip-induced reaction exhibits a clear energy threshold; thus in our experiments  $V = -3.5$  V bias causes about 50% depletion of the initial saturation TMA surface concentration.

We have also explored the influence of other parameters on the tip-induced TMA desorption. In particular we found that the desorption efficiency is almost independent of the tunneling current over the range of 1 – 20 pA, while at currents of 50 pA and higher, the TMA depletion extent increases at fixed negative biases. This later observation may indicate field-induced desorption at the higher tunneling currents that correspond to a shorter tip-surface gap. The collected data suggests that the desorption of TMA species at  $< 20$  pA proceeds through tunneling of an electron from the molecular orbital of TMA species in analogy with the same electron being removed through interaction with an electronic hole in  $\text{TiO}_2$  bulk. The experiments allow us to identify the energy position of this reactive molecular orbital.

### ***Stress-Induced Reactivity on Oxide Surfaces***

Our Group has recently demonstrated the use of nanoscale local strain to control surface reactions on oxide surfaces; see Refs. 3 and 4. As a result, we have used UHV STM imaging to show that such strain locally alters the surface reactivity, thus allowing study of the role of strain in controlling reaction dynamics on a strained surface. Our experiments used a nanoscale template of 5 – 25 nm wide and up to 1 nm high strained areas caused by subsurface Ar filled cavities several nanometer below the surface, as shown in **Fig. 4**. These buried Ar clusters were prepared by a low-energy (i.e. 1 - 2 kV) ion beam in combination with high-temperature annealing. In the vicinity of the buried Ar blister, the crystal lattice layers are deformed upward and a local strain field is established. These strained areas appear as protrusions in the STM images.

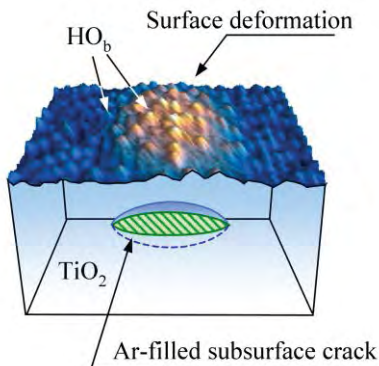


**Fig. 4:** STM image of rutile(110) surface with a protrusion and with  $\text{OH}_b$  groups, combined with a schematic explaining the origin of the protrusion.

Our experiments used a nanoscale template of 5 – 25 nm wide and up to 1 nm high strained areas caused by subsurface Ar filled cavities several nanometer below the surface, as shown in **Fig. 4**. These buried Ar clusters were prepared by a low-energy (i.e. 1 - 2 kV) ion beam in combination with high-temperature annealing. In the vicinity of the buried Ar blister, the crystal lattice layers are deformed upward and a local strain field is established. These strained areas appear as protrusions in the STM images.

We have now used an STM to obtain a statistical aerial distribution of bridge-bonded hydroxyl groups ( $\text{HO}_b$ ) on our rutile sample with a well-defined nanoscale strain field. Our STM images show that the local surface concentration of  $\text{OH}_b$  groups is lower on the protrusions. This lowering of concentration has been interpreted as a reduction in the local O-H bond energy,  $\Delta E_{\text{OH}}$ . An analysis of the reduction in the O-H bond energy across the surface showed a strong correlation between  $\Delta E_{\text{OH}}$  and the characteristic surface strain value,  $S$ . Importantly, the correlations of this  $\Delta E_{\text{OH}}$  value with other geometrical parameters, such as the height of the protrusion, are significantly lower. This result allows us to differentiate between the two hypotheses of the origin of O-H bond lowering: strain-induced versus buried charge-induced effect. Our results strongly support strain-induced modulation

of the surface reactivity. The empirical linear relation between the O-H bond energy and the surface strain, reflected in Fig. 5, has been estimated to be  $\Delta E_{\text{OH}} \text{ (meV)} \approx 11 \cdot S \text{ (\%)}$ .

The  $\Delta E_{\text{OH}}$  values have been calculated through a subtraction of the contribution of the repulsive dipole-dipole interaction between  $\text{OH}_b$  groups. As the quantitative parameters of this interaction are not available from literature, we conducted comprehensive study based on statistical analysis of the radial distribution of  $\text{OH}_b$  pairs in the STM images of flat (protrusion-free)  $\text{TiO}_2(110)$  surface. The data clearly favors the dipole-dipole interaction. The effective dipole moment of an  $\text{OH}_b$  group was found to be  $0.095 \text{ e} \cdot \text{nm} = 1.5 \cdot 10^{-29} \text{ C} \cdot \text{m}$ .

### Future Plans

Our most recent experiments have showed that local (i.e. atomic scale) strain in  $\text{TiO}_2$  layers results in a change in the reactivity of that surface and, in particular, in change of the binding energy of hydrogen atoms, which are the simplest adsorbates on the rutile(110) surface.[5] *Our goal is now to understand the relationship between photo- and tip-reaction dynamics and surface strain.* The O-H bond energy deviations due to surface strain have been deduced by collecting local OH concentration data on the surface protrusions of different dimensions and using the statistical physics to process this data; this work has now been published in JPCC. Our plans for the coming year are to examine tip-induced surface fragment dynamics on  $\text{TiO}_2$ . To this end, we have recently rebuilt our mass spectrometer capability so as to enable more facile measurement.

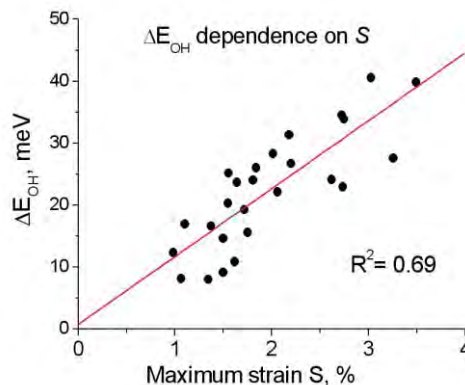


**Fig. 5:** Plot of calculated O-H bond energy as a function of the maximum-strain value  $S$ . The red line shows the best linear fit to the data.

### Recent Grant-Sponsored Publications

1. D. V. Potapenko, Z. Li, R. Osgood, "Dissociation of single 2-chloroanthracene molecules by STM-tip electron injection." *J. Chem. Phys.* **116**, 4679 (2012)
2. D.V. Potapenko, Z.Li, Y. Lou, R. M. Osgood Jr., "2-Propanol reactivity on *in situ* prepared Au(111)-supported  $\text{TiO}_2$  nanocrystals." *J. Catal.* **297**, 281-288 (2012)
3. D.V. Potapenko, Z. Li, J.W. Kysar, R.M. Osgood, "Nanoscale strain engineering on the surface of a bulk  $\text{TiO}_2$  crystal" *Nano Lett.* **14**, 6185 (2014)
4. Z. Li, D.V. Potapenko, R.M. Osgood, "Controlling surface reactions with nanopatterned surface elastic strain" *ASC Nano* **9**, 82 (2015)
5. D.V. Potapenko, Z. Li, R.M. Osgood, "Photoreactions on a single isolated  $\text{TiO}_2$  nanocrystal on Au(111): Photodecomposition of TMAA" *J. Phys. Chem. C* **119**, 28946 (2015).
6. Z. Li, D.V. Potapenko, K.T. Rim, M. Flytzani-Stephanopoulos, G.W. Flynn, R.M. Osgood, X.-D. Wen, and E.R. Batista, "Reactions of deuterated methanol ( $\text{CD}_3\text{OD}$ ) on  $\text{Fe}_3\text{O}_4(111)$ " *J. Phys. Chem. C* **119**, 1113 (2015)
7. D.V. Potapenko, G.T. Gomes, R.M. Osgood, "Correlation of H adsorption energy and nanoscale elastic surface strain on rutile  $\text{TiO}_2(110)$ " *J. Phys. Chem. C*, DOI 10.1021/acs.jpcc.6b05129.
8. D.V. Potapenko and R.M. Osgood, "Diffusion in crystalline solids: Temperature programmed out-diffusion from Ar in  $\text{TiO}_2$  surface layers." (in final preparation)

## Studies of surface adsorbate electronic structure and femtochemistry at the fundamental length and time scales

*Hrvoje Petek*

*Department of Physics and Astronomy and Chemistry  
University of Pittsburgh*

We study the dynamical properties of solid surfaces on the femtosecond temporal and nanometer spatial scales by time-resolved photoemission and scanning tunneling microscopy methods. The chemical and physical properties at molecule-solid interfaces are fundamentally important to solar energy conversion processes. Here we report on the recent results on the first experimental detection of excitons in metals and CO<sub>2</sub> Capture by metal-organic chains on Au surfaces.

**Transient excitons at Ag(111) surface.** In the field-theoretic description of light-matter interaction, the absorption of a photon creating an electron-hole pair is an instantaneous process. At the instant of interaction, a photon induces a nonadiabatic transition in a metal to create an electron-hole pair interacting via the bare Coulomb interaction. This primary transition causes fast deviations from the initial charge density equilibrium of the system, which in turn couples to the dynamical polarization or screening response of the surrounding electronic density within a few lattice sites from the disturbance. The excitation evolves from this *transient excitonic* state, where a bound state of the electron-hole pair exists, to the fully screened state of the system, where a metal does not support a locally bound state of the Coulomb potential, on the time scale of formation of the screening charge density through the virtual single-particle and collective plasma excitations. In the case of a metal surface, the self-consistent linear response to creation of an external charge has the classical analog of perfect screening in the image charge. The image charge through the associated image potential supports a Rydberg series of image potential states. The transient exciton created by the interaction of a surface state electron with a photon can recombine to regenerate the coherent field (reflection), undergo a second-order scattering process with overall energy and momentum conservation (Drude absorption), or evolve into energy conserving asymptotic states such as the image potential states. In a nonlinear multiphoton photoemission experiment, additional absorption of photon can excite the electron above the vacuum level, with the resulting photoemission spectrum capturing the dynamics of the transient exciton evolving into the fully screened image potential state.

In order to study the coherent interaction of light with metals, we developed a coherent three-dimensional multi-photon photoemission (3D-*mPP*) spectroscopy technique. In the case of Ag(111), we employ 3D-*mPP* to resolve for the first time the transient excitonic response of a metal. With single color, broadly tunable <15 fs pulse excitation in the visible spectrum, we excite *mPP* from Ag(111) surfaces, and image the resulting energy *vs.* parallel momentum distributions. The *mPP* spectra exhibit features, which cannot be attributed to single particle excitations among the well-known surface and bulk bands of Ag. In the case of 3PP from Ag(111) surface, a nondispersive feature, which dominates the spectra, appears when the laser is tuned near the two-photon resonant excitation from the Shockley surface state (SS) to the image potential state. The nondispersive character of the spectrum and the momentum range corresponding to the

SS attribute this feature to a localized state that is created by exciting an electron from the SS, namely the transient exciton.

In order to obtain further information on this newly discovered transient exciton, we perform time-resolved *m*PP measurements with interferometric scanning of identical pump-probe pulses. Interferometric time-resolved photoemission movies with different excitation wavelengths identify the coherent pathways and timescales for 3PP via the transient exciton resonance of Ag(111) surface. Interferograms, such as in Fig. 1 for the normal emission from Ag(111) surface, contain information on the coherent interactions leading to the 3PP process. Fourier transforming the interferograms obtains 2D photoelectron spectra, which correlate the components of the coherent polarization excited in the sample with the final state energies in the 3PP spectra. The 2D spectra manifest the evolution of the transient exciton into the fully screened image potential state on the time scale of dephasing of the surface plasmon of Ag. Remarkably, at higher excitation fluences it is possible to drive high-order processes up to 9PP via the excitation of the transient exciton in Ag. In parallel with these experimental studies, we are developing the many-body theory of the ultrafast excitonic response of metals.

The transient exciton at Ag(111) surface can be observed with 15 fs laser pulses due to the unusual screening properties at Ag surfaces. We plan to explore the transient exciton response on adsorbate modified Ag surfaces and on thin metal films on semiconductor surfaces. The transient excitons and polaritonic responses of Ag and Cu surfaces are representative of the ultrafast optical responses of solid-state materials. Thus, similar coherent responses are likely to have a role in the conversion of solar to electrical and chemical energy in organic and inorganic semiconducting materials.

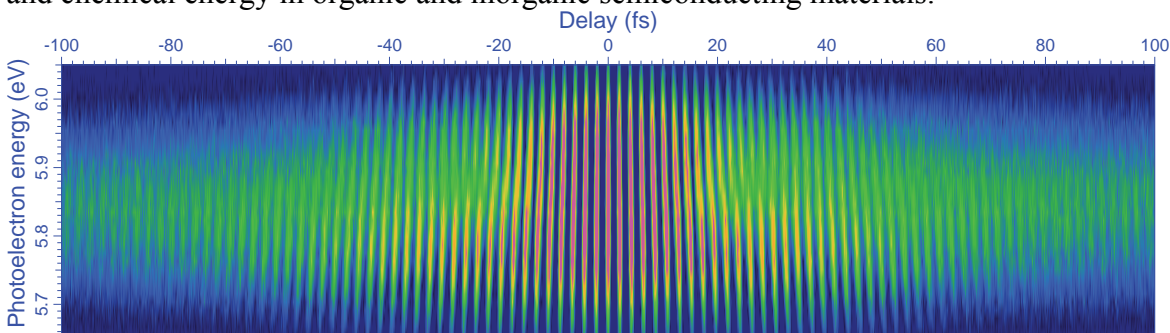


**Fig. 1.** A cross-section through a 3D movie of photoelectron counts vs. energy, momentum, and pump-probe delay time for normal emission from Ag(111) surface excited with 2.04 eV light. Fourier transform of such interferograms provides 2D spectra that correlate the induced linear and nonlinear polarization excited in the sample with specific features in the *m*PP spectra.

**CO<sub>2</sub> capture by metal-organic chains.** Efficient capture of CO<sub>2</sub> by chemical means requires a microscopic understanding of the interactions of the molecule-substrate bonding and adsorption-induced collective phenomena. By molecule-resolved imaging with scanning tunneling microscopy (STM), we investigate self-catalyzed CO<sub>2</sub> adsorption on one-dimensional (1D) substrates composed of self-assembled metal-organic chains (MOCs) supported on gold surfaces. Exposing Au(100) and Au(111) surfaces to 1,4-phenylene diisocyanide (PDI) molecules under UHV conditions leads to self-assembly of one-molecule wide chains that uniformly cover the exposed Au surfaces, with a minimum

interchain separation of  $\sim 1.4$  nm. The chains are composed of alternating 1.1 nm long units of Au adatoms forming covalent bonds to  $-\text{NC}$  functional groups of flat lying PDI molecules. The chains order into uniform grating structures even at lower coverages through long-range dipole-dipole repulsion.

Exposing MOCs to  $\text{CO}_2$  at 77 K causes their large-scale redistribution, namely they gather into close-packed structures where  $\text{CO}_2$  molecules are sandwiched in one-molecule wide ranks between the adjacent chains. We attribute the  $\text{CO}_2$  molecule-induced coalescence to a charge redistribution from the chains to the molecules, which transforms the chain interactions from repulsive to attractive. Implicit in this mechanism is charge transfer to  $\text{CO}_2$  molecules, i.e., the first step in  $\text{CO}_2$  reduction.

By mediating the interchain attraction  $\text{CO}_2$  molecules create more favorable adsorption sites for further  $\text{CO}_2$  adsorption thereby self-catalyzing their capture. The release of  $\text{CO}_2$  molecules by thermal desorption returns the MOCs to their original structure, indicating that the  $\text{CO}_2$  capture and release are reversible processes.

To understand more deeply the interactions that lead to the self-catalyzed  $\text{CO}_2$  capture, we employ low temperature scanning tunneling microscopy (LT-STM), X-ray photoelectron spectroscopy (XPS), infrared reflection absorption spectroscopy (IRAS), temperature programmed desorption (TPD), and dispersion corrected density functional theory (DFT) to characterize chemisorption and physisorption of  $\text{CO}_2$  molecules on Au surface supported Au-PDI metal-organic chains. The STM imaging reveals that Au-PDI chains activate the normally inert Au surfaces by promoting  $\text{CO}_2$  chemisorption at the Au adatom sites even at  $<20$  K. The  $\text{CO}_2^{\delta-}$  species at low coverage are imaged as single molecules attached to either or both sides of Au adatoms with a characteristic two-lobed structure (Fig. 2a). As the  $\text{CO}_2$  coverage is increased, additional molecules cluster in highly ordered two-dimensional (2D) physisorbed clusters, which grow into a full monolayer on Au crystal terraces (Fig. 2b, c). The chemisorption-induced physisorption by the “anchoring”  $\text{CO}_2^{\delta-}$  enable unprecedented imaging of single  $\text{CO}_2$  molecules from single molecules to full monolayers. The dispersion interactions with the substrates cause the monolayer films to assume a rhombic structure similar to a high-pressure  $\text{CO}_2$  crystalline solid. The IRAS, XPS, and TPD measurements support the coexistence of the chemisorbed and physisorbed  $\text{CO}_2$  molecules up to 120 K.

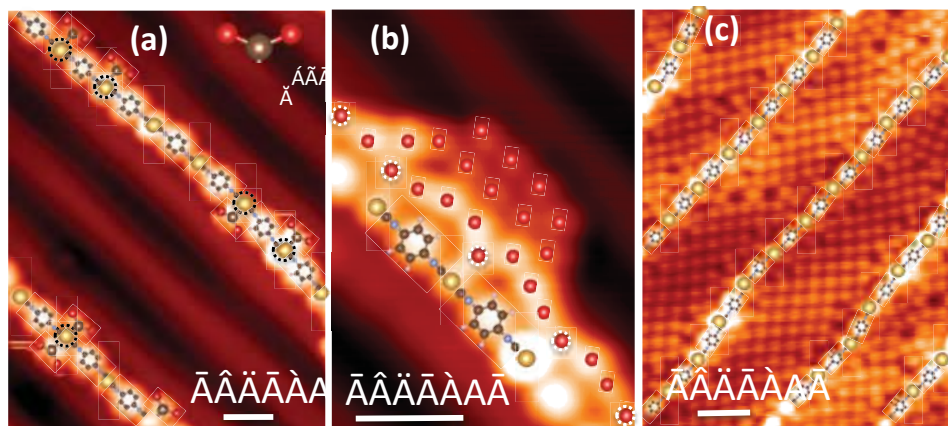


**Fig. 2.** (a) Au-PDI chains at low  $\text{CO}_2$  coverage. Single chemisorbed  $\text{CO}_2^{\delta-}$  species are found aside of Au adatoms. (b) The  $\text{CO}_2^{\delta-}$  species seed and anchor  $\text{CO}_2$  physisorption in larger cluster as the coverage is increased. (c) At full monolayer coverage  $\text{CO}_2$  molecules form a rhombic structure that is characteristic of a high-pressure  $\text{CO}_2$  phase.

The Au surface supported Au-PDI chains provide a platform for investigating the physical and chemical interactions involved in CO<sub>2</sub> capture and reduction. Au-PDI chains and Au substrates exhibit characteristics of both the homogeneous and heterogeneous catalysis, but it is not clear to what extent are the observed activity due to the Au-PDI chains, the substrate, or a cooperative interaction among them. In future experiments we plan to investigate whether similar self-assembly of metal-organic constructs occurs on other noble and transition metal substrates, and to what extent are the observed interactions enabled by the metal-organic constructs in the absence of the metallic substrate. Such metal-organic constructs are an interesting interfacial species with yet unknown chemical properties, because they appear to exist mainly on metal surfaces and not independently in other environments. Other experiments will probe the unoccupied electronic structure of Au-PDI chains by time-resolved two-photon photoemission with and without decoration of CO<sub>2</sub> molecules, to investigate the possibility of photoinduced reduction of CO<sub>2</sub>. Coadsorption with proton donating molecules may enable further reduction through proton-coupled electron transfer.

### DOE Sponsored Publications 2013-2015<sup>1-9</sup>

- <sup>1</sup> Feng, M., Shi, Y., Lin, C., Zhao, J., Liu, F., Yang, S., & Petek, H. Energy stabilization of the s-symmetry superatom molecular orbital by endohedral doping of C<sub>82</sub> fullerene with a lanthanum atom. *Phys. Rev. B* **88**, 075417 (2013).
- <sup>2</sup> Winkelmann, A., Tusche, C., Ünal, A.A., Chiang, C.-T., Kubo, A., Wang, L., & Petek, H., Ultrafast multiphoton photoemission microscopy of solid surfaces in real and reciprocal space in *Dynamics of interfacial electron and excitation transfer in solar energy conversion: theory and experiment*, edited by P. Piotrowiak (Royal Society of Chemistry, Cambridge, 2013).
- <sup>3</sup> Cui, X., Wang, C., Argondizzo, A., Garrett-Roe, S., Gumhalter, B., & Petek, H. Transient excitons at metal surfaces. *Nat Phys* **10**, 505-509 (2014).
- <sup>4</sup> Feng, M., Sun, H., Zhao, J., & Petek, H. Self-Catalyzed Carbon Dioxide Adsorption by Metal–Organic Chains on Gold Surfaces. *ACS Nano* **8**, 8644-8652 (2014).
- <sup>5</sup> Petek, H. Single-Molecule Femtochemistry: Molecular Imaging at the Space-Time Limit. *ACS Nano* **8**, 5-13 (2014).
- <sup>6</sup> Zhao, J., Feng, M., Dougherty, D.B., Sun, H., & Petek, H. Molecular Electronic Level Alignment at Weakly Coupled Organic Film/Metal Interfaces. *ACS Nano* **8**, 10988-10997 (2014).
- <sup>7</sup> Silkin, V.M., Lazić, P., Došlić, N., Petek, H., & Gumhalter, B. Ultrafast electronic response of Ag(111) and Cu(111) surfaces: From early excitonic transients to saturated image potential. *Phys. Rev. B* **92**, 155405 (2015).
- <sup>8</sup> Feng, M., Petek, H., Shi, Y., Sun, H., Zhao, J., Calaza, F., Sterrer, M., & Freund, H.-J. Cooperative Chemisorption Induced Physisorption of CO<sub>2</sub> Molecules by Metal–Organic Chains. *ACS Nano* (in press).
- <sup>9</sup> Feng, M. & Petek, H., Scrutinizing the Endohedral Space: Superatom States and Molecular Machines in *Endohedral Fullerenes: electron transfer and spin*, edited by A. Popov (Springer, in press).

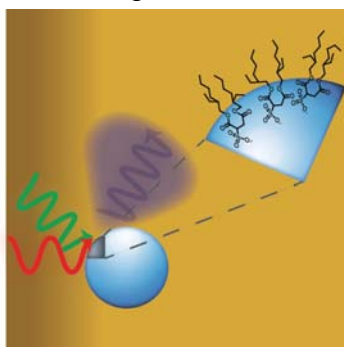
# MOLECULAR STRUCTURE, BONDING AND ASSEMBLY AT NANOEMULSION AND LIPOSOME SURFACES

PI: Geraldine Richmond, University of Oregon

Email: richmond@uoregon.edu

## Program Scope and Definition

Nanoemulsions are kinetically stable dispersions of oil, water, and surfactants that are advantageous because of their small size, and enhanced stability<sup>1</sup> compared to larger macroemulsions. Reverse nanoemulsions are water droplets suspended in oil and are gaining increasing interest for emulsified fuel technologies, reactors for nanoparticle synthesis, carriers for slow drug release, and models for confined water environments.<sup>2</sup> With time, nanoemulsions will destabilize and eventually separate into their separate phases with the process initialized by either coalescence or Ostwald ripening mechanisms.<sup>3</sup> Molecular species, such as surfactants adsorbed to the droplet interface play a significant role in nanoemulsion stability by increasing the steric hindrance or electrostatic repulsions between droplets and lowering the interfacial tension between the oil and water phases.<sup>1</sup> Although there have been many studies of nanoemulsion stability,<sup>3</sup> there is a lack of understanding of the role the interface plays in their macroscopic behavior and stability.



The objective of these studies is just that: *to advance our understanding of the molecular structure, orientation and bonding of surfactants at the surface of nanoemulsions and liposomes, and the bonding characteristics of interfacial water that is either confined or surrounding the surfactant coated soft particle surfaces.* Our approach involves measuring the surface vibrational spectroscopy of the surfactant coated particle surfaces in-situ using vibrational sum frequency scattering spectroscopy (VSFSS), with related complementary studies of these surfactant systems examined at the more well-defined planar oil/water interface by vibrational

sum frequency spectroscopy (VSFS). Classical molecular dynamics (MD) calculations coupled with density functional theory (DFT) methods are employed to assist in spectral assignments and understanding solvation effects. Other experimental techniques such as dynamic light scattering (DLS), zeta potential and interfacial tensiometry are being used.

## Recent Progress

Over the past year we have focused our studies on two nanoemulsion systems, those formed with sodium di-2-ethylhexylsulfocinate (AOT) and the alkyl amine cetyltrimethylammonium bromide (CTAB). The molecular structure of AOT micelles have been extensively studied when it assembles to form smaller micellar structures but little is known about the molecular features of AOT stabilized nanoemulsions. Little is also known about CTAB nanoemulsion structuring. Both have also been selected because they form both regular and reverse micelles, allowing us to compare the surfactant and water interfacial structure at both the spherical interfaces and the planar oil/water interface. Also of importance in these studies is to understand the strengths and limitations of this new nonlinear scattering technique, VSFSS.

**AOT Studies:** AOT has been one of the most well studied surfactant systems and continues to generate interest due to its ability to effectively form reverse micelles in organic solvents, and to form a myriad of structures, such as micellar, vesicular, lamellar and liquid crystalline phases, in

aqueous systems.<sup>4</sup> Due to the efficacy of AOT to assemble in both aqueous and non-aqueous solvents, it is widely used as a commercial surfactant to stabilize oil-water interfaces. The AOT molecule is made up of a sulfonate head group with a sodium counterion with two nearby ester groups that preferentially solubilize in the aqueous phase and two branched alkyl chains that solubilize in the oil phase. The unique wedge like shape of AOT has been cited as one of the major reasons why it is so efficient at forming reverse micellar systems in organics and forming lamellar systems in water.<sup>5</sup> The molecular structure of AOT at the oil-water interface of nanoemulsions has not yet been explored due to the inherent challenge of probing nanoemulsion droplet interfaces. In our spectroscopic studies AOT surfactant vibrational spectra are measured at the regular (o/w) and reverse (w/o) nanoemulsion interface *in situ* using VSFS. Our goal is to elucidate the structure of AOT alkyl chains and head group at the nanoemulsion interface to determine the differences in its assembly at regular and reverse nanoemulsion interfaces. The vibrational spectrum of AOT at the CCl<sub>4</sub>-D<sub>2</sub>O w/o droplet and at the D<sub>2</sub>O-hexadecane-d<sub>34</sub> o/w droplet (~200 nm) interfaces were measured in the C-H stretching region, using a femtosecond broadband laser system in a scattering geometry. Some results are shown in Figure 1 below.

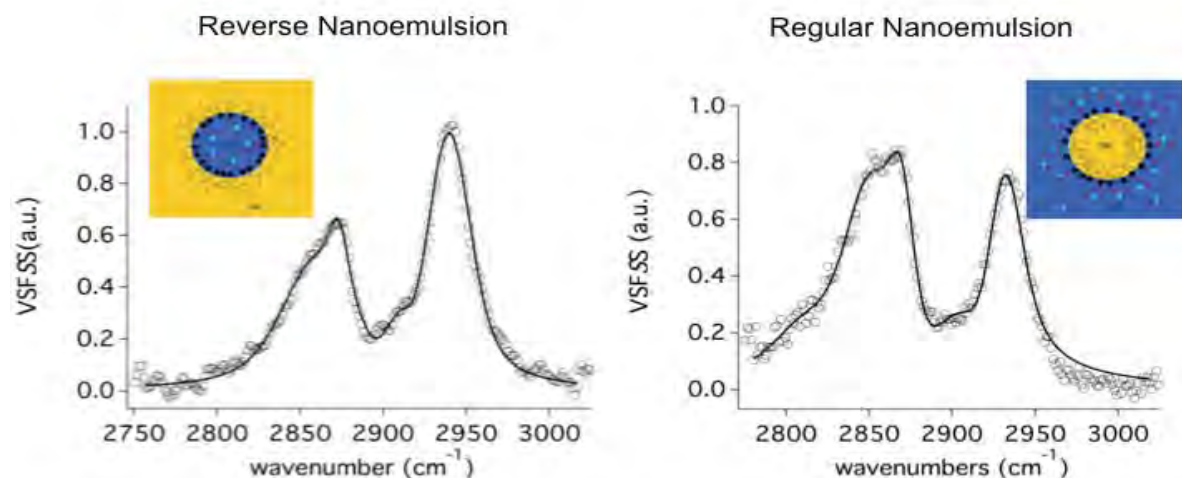


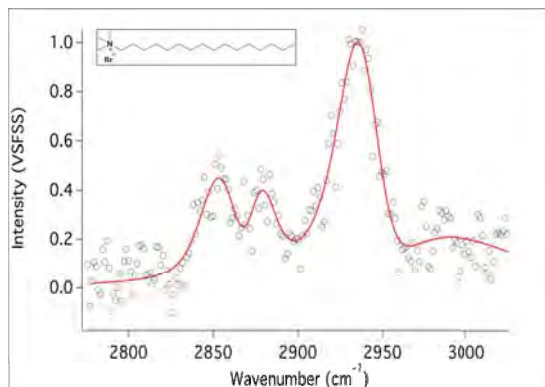
**Figure 1.** VSFS spectra of AOT at the reverse CCl<sub>4</sub>-D<sub>2</sub>O nanoemulsions (shown on the left) and at the regular D<sub>2</sub>O-hexadecane-d<sub>34</sub> nanoemulsions (shown on the right).

The spectra have been fit to four peaks aiding in the spectral assignment of normal C-H vibrational modes, which include the following: symmetric methylene and methyl, the methine stretch and the Fermi resonance splitting of the methyl symmetric stretch and the bending mode. By comparing the two spectral fits, both spectra show an equal number of vibrational modes with similar peak positions and spectral widths. In reverse micellar systems, the unique branching of the AOT alkyl chains has been suggested to be the reason why AOT is so efficient at stabilizing these systems. The similarity in spectral shapes in Figure 1 between these two systems has indicated that the structure of AOT is nearly identical between these two different nanoemulsion systems. The nanoemulsion interface can be assumed to be nearly planar considering the molecular dimensions of AOT compared to the large size of the nanoemulsion. With that in mind, AOT was investigated at the planar oil-water interface with complementary techniques such as VSFS and surface tensiometry. Surface pressure data (not shown here) shows that at an

AOT concentration of 0.6-0.7 mM, the surface pressure starts to level off with subsequent additions of AOT. When measuring the VSFS spectra of AOT at the  $\text{CCl}_4\text{-D}_2\text{O}$  interface at varying concentrations below and above this concentration (0.01-2 mM), there is very little spectral change besides an increase in overall intensity. This indicates that with increasing AOT population at the planar oil-water interface, there is no substantial change in its alkyl chain structure. AOT molecules are not very well packed at these interfaces and this is corroborated with the large AOT head group area of  $97 \text{ \AA}^2$  determined from surface tension analysis. The similar structure of alkyl chains of AOT at the regular and reverse nanoemulsion interfaces indicates that at these interfaces AOT cannot tightly pack due to the increased sterics of the branched alkyl chains. This is more similar to the behavior seen in lamellar structures compared to reverse micellar systems. We have also measured the S-O and C=O modes of the AOT head group on the reverse nanoemulsion and planar oil-water interfaces, which we plan to explore in further detail to learn how the head group aids surface stabilization of nanoemulsions.

### CTAB Studies

CTAB nanoemulsions have been chosen for study for several reasons, one with the potential to help us elucidate finer details of the adsorbed surfactant monolayer as well as to optimize experimental parameters. CTAB has garnered interest due to its use in DNA condensation, liposome stabilization with polyelectrolytes, nanomaterial synthesis and drug delivery. We are interested in CTAB as it is a good model system due to its ability to form stable nanoemulsions,



to the regular hexadecane- $\text{D}_2\text{O}$  nanoemulsion interface. The red line is the fit from which our ratios are derived from.

its single chain structure, simplifying the vibrational spectrum, and its variety of commercially available deuterated species allowing us to selectively probe either the head group or aliphatic chain. This past year our focus with CTAB has been on establishing our experimental and computational protocols. On the experimental side this has been no easy task, as these VSFS experiments are very sensitive to a large number of different experimental parameters. However, we have recently succeeded in measuring CTAB (1 mM) adsorbed to the interface of regular oil-in-water nanoemulsions (Figure 2), characterized by dynamic light scattering to have a diameter of  $\sim 200 \text{ nm}$ . We look for the contributions of the methylene ( $d^+$ ) and methyl ( $r^+$ ) modes to our vibrational spectrum, as the ratio between the two can provide insight into the conformational disorder of the aliphatic chains. For CTAB adsorbed to the regular nanoemulsion interface we calculate  $d^+/r^+$  to be  $1.1 \pm 0.3$ , compared to  $0.6 \pm 0.2$  at the planar oil-water interface. The data shows that surfactant monolayer at the regular nanoemulsion interface is orientationally ordered, yet somewhat conformationally more disordered compared to a planar oil-water interface. We are currently working to improve the S/N ratio of our CTAB scattering experiments, which can be affected both by scattering experiment details as well as the surfactant system itself to enable us to draw stronger conclusions.

Our computational work is oriented at helping us understand the effects that conformational disorder, i.e. the presence of gauche defects, has on our sum-frequency spectra. In our lab we perform MD simulations to generate an “experimental” oil-water interface, which we couple with DFT calculations to calculate a sum-frequency spectra. Previously, our methodology has been utilized at both the air-water interface<sup>6</sup> and the oil-water interface.<sup>7</sup> This past year we have been working on identifying the most probable CTAB conformers, to reduce our conformational space from ten’s of thousands. This is crucial for several reasons, in particular for the set-up of our MD simulations as well as the fact that VSFSS is sensitive to the molecular conformation. Thus, we have taken great care to make sure we are accurately representing the conformational space of CTAB. Through a series of dihedral potential energy scans following Berkowitz<sup>8</sup> we have reduced the conformer library from ten’s of thousands to ~150 necessary conformers.

### ***Future Studies***

**AOT:** We are currently completing our manuscript for publication of the above-described AOT studies. However our initial work into understanding is assembly at the regular and reverse nanoemulsion interfaces<sup>9</sup> opens up questions as to whether the surface population is lower than the planar, or if there are some interactions between surfactant head groups causing the more disordered assemblies. To address these we have a series of ion studies planned to understand how the surfactant head groups interact, both with neighboring head groups and their counter-ions. We have already performed a number of counter-ion exchanges, replacing the original sodium counter-ion with potassium, magnesium, and zinc ions. We are planning on taking VSFSS spectra of both the carbonyl moieties and the sulfonate moieties under varied concentrations and ion identities, observing how the vibrational responses change.

**CTAB:** Now that we have had success with measuring CTAB at the oil-in-water nanoemulsions, we turn our attention to water-in-oil nanoemulsions. Like with AOT, we want to be able to compare CTAB at the regular and reverse nanoemulsion interfaces. The advantage with CTAB is we can draw firmer conclusions as to surfactant conformational disorder at each interface by using the  $d^+/r^+$  ratio and computational work. We also are pursuing concentration studies to observe changes in surface packing, and the effect that has on the nanoemulsion interface. These experiments coupled with our continued computational efforts should elucidate some of the details of surfactant behavior at the curved nanoemulsion interface, including the effects of having a particular phase confined and the manner in which the monolayers assemble.

- (1) Bouchemal, K.; Briançon, S.; Perrier, E.; Fessi, H. *International Journal of Pharmaceutics* **2004**, *280*, 241.
- (2) Fayer, M. D.; Levinger, N. E. *Annual Review of Analytical Chemistry* **2010**, *3*, 89.
- (3) Tadros, T.; Izquierdo, P.; Esquena, J.; Solans, C. *Advances in Colloid and Interface Science* **2004**, *108-109*, 303.
- (4) Nave, S.; Eastoe, J.; Penfold, J. *Langmuir* **2000**, *16*, 8733.
- (5) Moilanen, D. E.; Fenn, E. E.; Wong, D.; Fayer, M. D. *Journal of the American Chemical Society* **2009**, *131*, 8318.
- (6) Valley, N. A.; Blower, P. G.; Wood, S. R.; Plath, K. L.; McWilliams, L. E.; Richmond, G. L. *The Journal of Physical Chemistry A* **2014**, *118*, 4778.
- (7) Valley, N. A.; Robertson, E. J.; Richmond, G. L. *Langmuir* **2014**, *30*, 14226.
- (8) Dominguez, H.; Berkowitz, M. L. *The Journal of Physical Chemistry B* **2000**, *104*, 5302.
- (9) Hensel, J., Kittredge, C., Carpenter, A., Ciszewski, R., manuscript in preparation.

## Sampling Rare Events In Aqueous Systems Using Molecular Simulations

Ryan DeFever<sup>1</sup>, Walter Hanger<sup>2</sup>, Amy Apon<sup>3</sup>, Linh Ngo<sup>4</sup>, and Sapna Sarupria<sup>1</sup>

<sup>1</sup>Chemical and Biomolecular Engineering

<sup>2</sup>Electrical and Computer Engineering

<sup>3</sup>School of Computing

<sup>4</sup>Cyberinfrastructure Technology Integration

Clemson University, Clemson SC

Rare events correspond to events that occur with low frequency. These events usually have potentially widespread impact and are therefore, events of considerable interest. At the molecular level, important transitions such as self-assembly and phase transitions in aqueous systems are rare events – meaning that the waiting time involved to observe even a single event is larger than the typical timescales accessible to molecular simulations. This hinders the ability to calculate the kinetics of these transitions. In our proposed research we focus on developing novel methods and the software infrastructure that implements these methods effectively on high performance computing systems to enable the studies of rare events in molecular simulations. While we motivate our work through studies of heterogeneous ice nucleation, the methods and software infrastructure developed here is applicable to any system.

**Proposed work:** In our proposed research, we combine state-of-the-art tools in molecular simulations, BigData and multitasking handling systems, and visualization techniques to develop a robust infrastructure for performing rare event simulations. We specifically build on a method called forward flux sampling (FFS). We propose to develop a multidimensional FFS method (nDFFS) that will enable us to address the issue of finding appropriate order parameters for any given transition on-the-fly. This methodology has the potential of addressing the major knowledge gap – lack of an ability to find reaction coordinates on-the-fly – in simulations of rare events.

**Previous Results:** In our previous work, we have developed a software program called Scalable Forward Flux Sampling (ScaFFS) to perform large scale forward flux sampling (FFS) calculations efficiently and effectively in high performance computing (HPC) infrastructure. In FFS, transitions from state A to state B are sampled through several intermediate transitions by dividing the phase space between A and B into interfaces. Several simulations are initiated at a given interface and configurations from those which reach the next interface are harvested. Then several simulations are initiated from the harvested configurations at the “new” interface to obtain configurations for the next interface. This process is continued until the final state is reached. While the process is straightforward, the application of the method to realistic systems can result in large number of simulation jobs and huge amount of data. To handle these large jobs and amounts of data effectively, we have developed ScaFFS.

ScaFFS represents a collaboration of state-of-the-art techniques in molecular simulations with those from Big Data to enable rare event simulations at massive scales. ScaFFS is designed to be adaptive, data-intensive, high-performance, elastic, and resilient. ScaFFS uses Hadoop in a novel manner to handle the millions of simulations performed and files generated in FFS calculations. Through this approach we have been able to address all the challenges listed above. In addition, we do this in such a manner that the user only deals with the details of their FFS simulation. This is analogous to the MD software programs, where you only feed the details of the simulation system and parameters without worrying about how the parallelization would occur or what format the files can be written as. We use a similar approach here.

Advantages of ScaFFS (also summarized in Fig. 1):

- Able to decide interfaces on-the-fly based on user specified criteria.
- There is no need for modification to the source codes for simulation i.e. if MD is being performed then no source code modification of GROMACS/LAMMPS or any other software is required.
- The status of each job is tracked and if needed, failed jobs are automatically re-run.
- Each file is tracked and intermediate data is not stored. However, if needed, the user can specify to retrieve it.
- The jobs are distributed over the nodes efficiently.
- ScaFFS is capable of restarting the FFS simulation in case the calculations run over wall-time such that no data is lost.
- The biggest advantage from a user perspective is that the user needs to only modify one file that specifies all details about the FFS parameters and details of file storage etc.
- ScaFFS has been tested extensively in both the institutional shared HPC environment at Clemson University as well as the publicly available HPC resources at XSEDE.



Figure 1:User friendly features of ScaFFS

**Specific goals of proposed research:**

- Integration of nDFFS into ScaFFS: We will develop and integrate nDFFS method into ScaFFS thereby enabling us to run large scale simulations required to validate nDFFS on realistic systems.
- Validation of nDFFS method based on simulations of crystallization of Lennard Jones liquid: This system has been studied widely and the appropriate reaction coordinates for this transition have been determined based on other techniques.
- Heterogeneous ice nucleation: Specifically, we will study the nucleation of ice near silver iodide surfaces. This provides a “realistic” system for testing the nDFFS method. Finding the appropriate reaction coordinate will improve the efficiency of FFS significantly and will become an important aspect as the systems and processes get more complex.

The successful completion of our work will enable simulations to study the kinetics of complex processes -- an aspect that has greatly lagged behind so far. While our work is motivated by phase transitions and assembly processes in aqueous systems, rare events are relevant to a broad span of fields including telecommunications, finance, insurance, physics, chemistry, and biology. The techniques and software program developed here can easily be adapted to these systems. Therefore, our methodology and the simultaneous development of the software infrastructure to implement these methods will provide the broad scientific community with powerful tools to study previous inaccessible processes through molecular simulations.

**Grant Number and Title:**

DE-SC0015448 Sampling Rare Events In Aqueous Systems Using Molecular Simulations

**Students:** Ryan DeFever (PhD student)

## Solvation

Richard Saykally (saykally@berkeley.edu), Musahid Ahmed (mahmed@lbl.gov), Phillip L. Geissler (plgeissler@lbl.gov) and Teresa Head-Gordon (thg@berkeley.edu)

Lawrence Berkeley National Laboratory, Chemical Sciences Division,  
1 Cyclotron Road, Berkeley, CA 94720

### Program Scope

It is widely recognized that the solvation properties of ions and molecules influence, or even actually determine vital phenomena and processes, like electrochemical transport, bubble formation, ion pair formation and crystallization, protein folding, corrosion, as well as chemical reactions in solutions and at interfaces. The goal of this work is to develop predictive models of bulk electrolyte behavior and interfacial phenomena.

### Progress Report

Geissler performs theoretical studies of solvation at interfaces. The equilibrium statistical mechanics of small ions in liquid water highlight significant shortcomings of classic solvation theories such as dielectric continuum theory (DCT). Perhaps the most striking example is the failure of DCT to predict the observed asymmetry between cations and anions, in which the latter are much more favorably solvated in bulk water than positively charged species of the same size. Moreover, as first emphasized in computer simulations by Tobias and Jungwirth, such solutes can counterintuitively adsorb to the interfacial region, where they would seem to sacrifice the very favorable polarization energy underlying their high solubility. Computational work has shown that the molecular origins of these phenomena are varied, with discrepancies in bulk solvation explained by molecular reorganization in the solute's coordination shell, and the solute's influence on capillary fluctuations determining the interfacial behavior. Understanding these phenomena in microscopic physical detail has formed a central goal of our work, both for its relevance for atmospheric and electrochemistry and also for the basic gaps in chemical theory that it reveals.

Building on insight from our work on this problem, we have aimed to address the general question: What reduced description of microscopic fluctuations in liquid water will allow efficient, transparent, and accurate treatment of the diverse solute chemistries pertinent to energy sciences? To this end, we have developed a field theory based on the molecular quadrupole moment of water that accurately captures the hydration free energy of small ions in bulk water. One of the key ingredients in this theory is the relationship between the symmetries of the quadrupole and dipole moments, which allows us to describe the molecular reorganization in the first coordination shell simply in terms of the solvent's dipole field. We have also started to investigate the adsorption of ions to interfaces other than liquid-vapor. In particular, SHG experiments by Saykally's group show that the free energies of adsorption of small anions to the liquid-graphene interface are similar to liquid-vapor. Our molecular simulations have shown that this similarity is due to a cancelation of effects that arise from the fact that the graphene suppresses capillary fluctuations: On the one hand this suppression mitigates the entropic cost associated with ion adsorption to the interface, while on the other hand the enthalpic gain is reduced as fewer hydrogen bonds are transferred to the bulk solvent.

Saykally seeks to develop, and apply novel methodologies for atom-specific characterization of hydration in liquids, solutions and their interfaces, employing combinations of liquid microjet

technology with synchrotron X-ray and ultrafast nonlinear optical spectroscopy in close connection with state-of-the-art theory.

X-ray spectroscopy of liquid microjets of water/alcohol solutions were investigated to ascertain the level of molecular-scale heterogeneity, suggesting that the measured negative excess entropy of isopropanol is a result of clustering or micro-immiscibility. Since their introduction into the commercial marketplace in 1991, lithium ion batteries have become increasingly ubiquitous in portable technology. X-ray absorption spectroscopy of solutions of  $\text{LiBF}_4$  in propylene carbonate (PC), interpreted using first-principles electronic structure calculations within the eXcited electron and Core Hole (XCH) approximation yields new insight into the solvation structure of the  $\text{Li}^+$  ion in this model electrolyte, suggesting that computational models of lithium ion battery electrolytes need to move beyond tetrahedral coordination structures. As a route to further clarifying the mechanism that selectively drives ions to and away from the air/water interface, we have developed a new experiment (Deep UV Sum Frequency Generation) for measuring the complete charge transfer to solvent (CTTS) spectrum of interfacial anions, and have applied it to the prototypical case of the iodide anion. The spectrum shows significant differences from the bulk CTTS spectrum, and provides a new variable for constructing general models to explain interfacial ion behavior, which is underway in the Geissler group. Experiments to extend our studies of ion adsorption to solid-liquid interfaces were initiated in a study of aqueous ion adsorption to the water-graphene interface, using our UV-SHG approach. Interpretation of the spectra via theoretical modeling by the Geissler group indicates but subtle differences from the ion behavior at air-water interfaces.

Ahmed studies clusters as a route to definitive characterization of solvation that is amenable to detailed theoretical interpretation and comparison. He has recently developed an experimental strategy for characterizing neutral versus ion-induced growth using in-source ionization of molecular-beam species with tunable VUV synchrotron radiation. Molecular dynamic processes in hydrocarbon clusters, and excitonic energy transfer have been studied experimentally, augmented by theoretical calculations from Martin Head-Gordon. Guided by these methods, a barrier-less pathway to covalent benzene ring formation from linear van-der-Waals acetylene clusters has been demonstrated following single-photon ionization. Using VUV photoionization mass spectrometry complimented by DFT calculations, it has been demonstrated that a single water molecule enhances the stability of symmetric acetaldehyde water clusters, and acts as a bridge for the transport of a proton between two acetaldehyde molecules. A newly commissioned apparatus has been used to perform Velocity Map Imaging- X-Ray Photoelectron spectroscopy on aqueous nanoparticle systems, and site-specific proton transfer mapped in solvated amino acid systems. These results are being modelled (electronic structure calculations of core levels in solvated amino acids) by Anna Krylov's group at USC.

Head-Gordon performs theoretical studies on solvation. We have made significant progress in multiple areas of CPIMS research including solvation and chemical transformations. Here we highlight one example of work on solvation. THz spectroscopy has proven to be a sensitive tool in order to probe solvation shell dynamics around a variety of solutes, from simple single monovalent ions to complex biological systems like proteins and enzymes. But in order to understand the experimentally observed spectra in molecular detail, theoretical methods are required. For small model systems, *ab initio* molecular dynamics (AIMD) simulations have proven to give a very accurate description of the THz experimental observable, and hence can be relied upon to decompose the motions of solvation shell dynamics. But for larger systems we need a more

tractable but still accurate model to understand the THz observable. We have tested the AMOEBA polarizable model for its ability to reproduce the accuracy realized by AIMD on the water solvent motions near the zwitterionic form of single glycine and valine peptides. It is noteworthy that the signature of the intermolecular vibrations of the water network in the 6 THz region is captured by the direct polarization and full mutual polarization AMOEBA models, whereas if we turn-off the many-body polarization component, this feature is lost from the simulated THz spectrum. In recently reported methodological work, we have shown that AMOEBA reproduces the THz spectral features and their mode decompositions as well as the AIMD studies, thereby setting up more advanced studies of larger systems studied by THz spectroscopy.

### **Future Plans**

Geissler plans to extend his approach to describe multiple ion effects in bulk solvation contexts. Energy applications such as desalination often involve sufficiently concentrated electrolyte solutions that the correlations between solutes cannot be neglected. As the number and size of solutes increase, the physics of interface formation will also become important. He also plans to continue investigations into ion solvation at different interfaces by quantifying the effects of different surface species on capillary fluctuations and electrostatic potential distributions. Preliminary results indicate that potential fluctuations favoring anionic solvation are suppressed to a greater extent, relative to the bulk, than those that favor the cation, suggesting that the coupling between the dipole/quadrupole field and capillary wave fluctuations may be important.

Saykally will extend the studies described above to other proposed lithium battery solvents and other counterions. Application of the new DUV-SHG experiment described above to measure CTTS spectra of other surface-enhanced ions will be pursued, including the study of counterion effects on the spectra. The goal is to develop a more complete model of ion adsorption to liquid interface, with the Geissler group. Saykally will also extend the studies of ion adsorption to graphene surfaces, seeking to extract entropy and enthalpy effects, which will be used to develop a model with the Geissler group.

Ahmed plans to use synchrotron radiation based VUV mass spectroscopy and X-Ray photoelectron spectroscopy in an integrated approach to move seamlessly from gas-phase systems to solution-phase chemistry mediated via clusters and nanoparticles. Ahmed proposes to advance the molecular-level understanding of metal ion solvation by integrating size-selected clusters in an ion trap mass spectrometer with X-Ray and IR spectroscopy. In conjunction with theory, those measurements can provide direct information on electrostatic and covalent bonding, and intermolecular forces. Liquid surfaces will be probed by means of mass spectrometry and X-ray photoelectron spectroscopy in collaboration with Xiao-Ying Yu (PNNL). IR spectroscopy of neutral clusters will be performed at the Dalian VUV-FEL in collaboration with Ling Jiang (DICP, China).

Head-Gordon will continue work that will decompose solvation dynamics of more complex systems using classical polarizable force fields. Furthermore THz and mode analyses are quite useful to understanding biocatalysis, to understand the interplay of non-equilibrium effects on the standard Michaelis-Menten view of catalytic mechanisms, and the homogenous catalysis systems we have planned using confinement.

### **Publications Acknowledging DOE support:**

- L. E. Felberg, A. Doshi, G. L. Hura, J. Sly, V. A. Plunova, R. Miller, J. E. Rice, W. C. Swope, T. Head-Gordon (2016). Controlling the structural transition of polymers with pH using chemical composition and star polymer architecture. *Mol. Phys. In press*.
- A. Bhowmick, S. Sharma, T. Head-Gordon (2016). The role of side chain entropy and mutual information for improving the de novo design of Kemp Eliminases KE07 and KE70. *Phys. Chem. Chem. Phys.* In press
- S. Vaikuntanathan and P.L. Geissler, "Putting water on a lattice: The importance of long wavelength density fluctuations in theories of hydrophobic and interfacial phenomena" *Phys. Rev. Lett.*, 112, 020603, 1-5 (2014).
- N. Schwierz, R. K. Lam, Z. Gamlieli, J. J. Tills, A. Leung, P. L. Geissler, and R. J. Saykally, "Hydrogen and electric power generation from liquid microjets: Design principles for optimizing conversion efficiency", *J. Phys. Chem. C* doi: 10.1021/acs.jpcc.6b03788 (2016).
- S. Vaikuntanathan, G. M. Rotskoff, A. Hudson, P. L. Geissler, "Necessity of capillary modes in a minimal model of nanoscale hydrophobic solvation", *Proc. Natl. Acad. Sci. U.S.A.* 113, E2224 (2016).
- Lam, R. K., Smith, J. W., Saykally, R. J. "Communication: Hydrogen bonding interactions in water-alcohol mixtures from X-ray absorption spectroscopy" *J. Chem. Phys.*, **144**, 191103 (2016).
- Smith, J. W., Lam, R. K., Sheardy, A. T., Shih, O., Rizzuto, A. M., Borodin, O., Harris, S. J., Prendergast, D., Saykally, R. J., "X-Ray absorption spectroscopy of LiBF<sub>4</sub> in propylene carbonate: a model lithium ion battery electrolyte" *Phys. Chem. Chem. Phys.*, **2014**, 16 (23), 23496-24110
- Otten, D. E., Saykally, R. J. "Spectroscopy and modeling of aqueous interfaces" in *Proceedings of the International School of Physics "Enrico Fermi", Course 187 "Water: Fundamentals as the Basis for Understanding the Environment and Promoting Technology,"* edited by P. G. Debenedetti, M. A. Ricci, and F. Bruni (IOS Press, Amsterdam; SIF, Bologna) 2015.
- Smith, J. W., Lam, R. K., Shih, O., Rizzuto, A. M., Prendergast, D., Saykally, R. J. "Properties of aqueous nitrate and nitrite from x-ray absorption spectroscopy" *J. Chem. Phys.*, **2015**, 143, 084503.
- O. Kostko, B. Bandyopadhyay, T.P. Troy and M. Ahmed. *Proton transfer in acetaldehyde–water clusters mediated by a single water molecule*, PCCP (In press)
- B. Bandyopadhyay, T. Stein, Y. Fang, O. Kostko, A. White, M. Head-Gordon, and M. Ahmed, "Probing Ionic Complexes of Ethylene and Acetylene with Vacuum Ultraviolet Radiation," *J. Phys. Chem. A.* (2016) **120**, 5053, DOI: 10.1021/acs.jpca.6b00107
- O. Kostko, B. Bandyopadhyay, and M. Ahmed, "Vacuum Ultraviolet Photoionization of complex chemical systems," *Ann. Rev. Phys. Chem.* (2016) Vol. 67, 19, DOI: 10.1146/annurev-physchem-040215-112553
- B. Bandyopadhyay, O. Kostko, Y. Fang, and M. Ahmed, "Probing Methanol Cluster Growth by Vacuum Ultraviolet Ionization," *J. Phys. Chem. A.* (2015) **119**, 4083.
- M. Perera, K. M. Roenitz, R. B. Metz, O. Kostko, and M. Ahmed, "VUV photoionization measurements and electronic structure calculations of the ionization energies of gas-phase tantalum oxides TaO<sub>x</sub> (x=3-6)," *J. Spectrosc. Dyn.* (2014) **4**, 21

## **Molecular Theory & Modeling**

*Development of Statistical Mechanical Techniques for Complex Condensed-Phase Systems*

Gregory K. Schenter  
Physical Sciences Division  
Pacific Northwest National Laboratory  
902 Battelle Blvd.  
Mail Stop K1-83  
Richland, WA 99352  
[greg.schenter@pnnl.gov](mailto:greg.schenter@pnnl.gov)

The long-term objective of this project is to advance the development of molecular simulation techniques to better understand fundamental properties and processes of molecular and nanoscale systems in complex environments, such as condensed phases and interfaces. We have focused on complexity associated with broken symmetries corresponding to vacuum/liquid, liquid/solid, and liquid/liquid interfaces or highly concentrated electrolytes. The characterization of these systems requires a description of molecular interaction that is more robust than what is required to describe bulk, homogeneous systems. Understanding the balance between descriptions of molecular interaction and complexity will continue to be the focus of future research efforts. We will continue to develop a systematic connection between models of molecular interactions and collective behavior of molecular systems. This will lead to an improved knowledge of complex collective behavior on a macroscopic scale. It involves the investigation of representations of molecular interaction as well as statistical mechanical sampling techniques and finding the balance between efficiency and accuracy in the description of molecular interaction.

To better understand collective many-body phenomena we are exploring the connection between: 1) the many-body decomposition of atom based potentials, 2) the partitioning of a system into an explicit sub-system and a bath and 3) transport and fluctuations of macroscopic mass, charge, and energy field densities, as well as electrostatic and electrodynamic fields. Each of these frameworks have a long history of development. We expect that the relation between these frameworks will need to be better understood in order to impact understanding of more complex phenomena.

In current work we focus on the water exchange process about ions, comparing and contrasting the dependence on the descriptions of molecular interaction. In studying these exchange processes it is necessary to find the proper balance between the ion-water and water-water interaction. In our studies we search for the appropriate amount of explicit treatment of electronic structure that allows for efficient sampling of a statistical mechanical ensemble of a system of interest. We have established that a Density Functional Theory (DFT) description of molecular interaction provides a quantitative representation of the short-range interaction and structure when compared to Extended X-ray Absorption Fine Structure (EXAFS) measurements. To do this we continue to develop our MD-EXAFS approach.[6] This direct comparison to experimental measurement gives us the confidence that the short range molecular phenomena is effectively and accurately described by DFT electronic structure coupled to statistical mechanical sampling. Much of our future efforts will concentrate on characterizing fluctuations,

taking advantage of effective potentials of mean force and linear response kernels from density, charge and electromagnetic fluctuations.

In Ref. [3] we explored the dynamics of  $\text{Li}^+ - \text{F}^-$  ion pairing in aqueous solvent, focusing on the transition from a contact ion-pair to a solvent separated ion pair. We constructed a generalized Langevin equation framework to compare DFT and empirical potential descriptions of molecular interaction. A key result of this study was the identification of high frequency coupling associated with “geometrically-frustrated charge pairing”[a] that occurs in some empirical potentials but not in the DFT description of molecular interaction. As a result, the enhanced coupling of the solute motion to the solvent through a frictional term results in a lowering of the rate constant by a factor of two. In Figure 1, we show the spectral density of the coupling of the solute to the solvent. This is the Fourier transform of the friction kernel. Empirical potentials [OPLS and DANG] contain structure around  $250 \text{ cm}^{-1}$  that is not present in the DFT response, a signature of this spurious coupling. Future work will explore the features in empirical potentials responsible for such behavior.

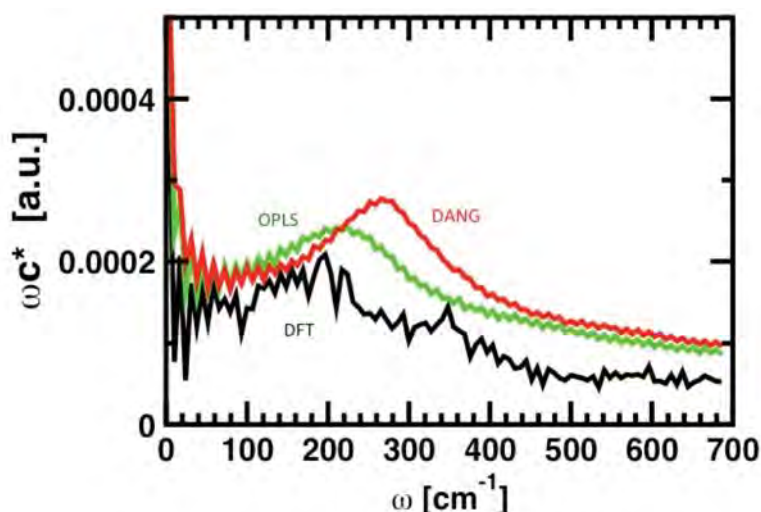


Figure 1. Spectral density of the coupling of the solute to the solvent, showing enhancement in empirical potentials [OPLS (green) and DANG (red)] compared to DFT (black).

In Ref. [4] we explored the use of the coordination number as a reaction coordinate to describe water exchange rates about solvated ions. We developed a consistent transition state theory (TST) in this coordinate. This allows us to more effectively characterize the important collective motions that lead to the rare event processes. Typical potentials of mean force in this coordinate are displayed in Figure 2. Future work will involve extending these concepts to combinations of distance based reaction coordinates (distance between ions) and coordination number. In Figure 3 we display preliminary two-dimensional potential of mean force results associated with the  $\text{Li}^+ - \text{F}^-$  and  $\text{Li}^+ - \text{I}^-$  ion pairing in aqueous solvent. We are exploring TST in terms of these coordinates, developing reduced descriptions of dynamics using generalized Langevin equations.

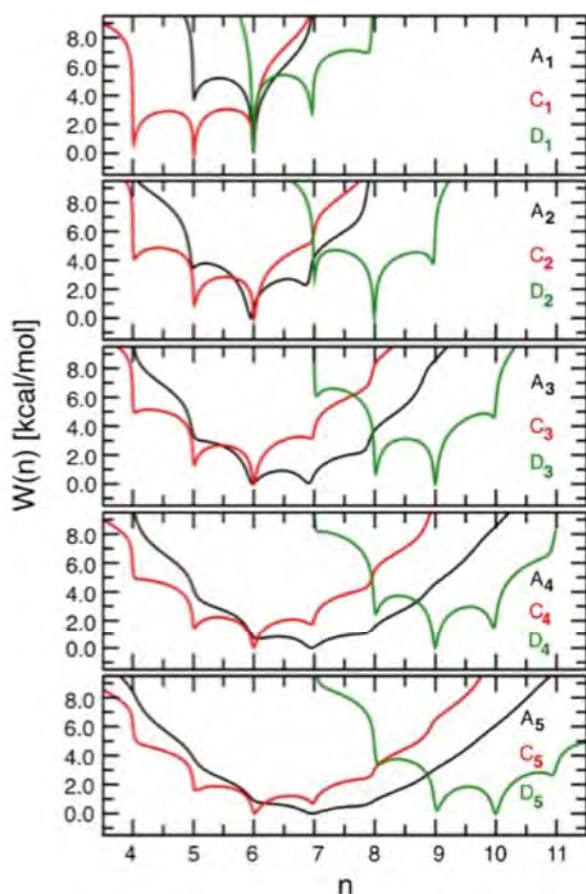


Figure 2. The potential of mean force  $W(n)$  as a function of coordination number for a series of anions (A), singly charged cations (C) and doubly charged cations (D). The subscript 1 through 5 indicates increasing size of the ion (from top to bottom). With the increase in ionic size, higher coordination states become accessible along with barrier reduction between the states. Cations are more stable and structured than comparable sized anions.

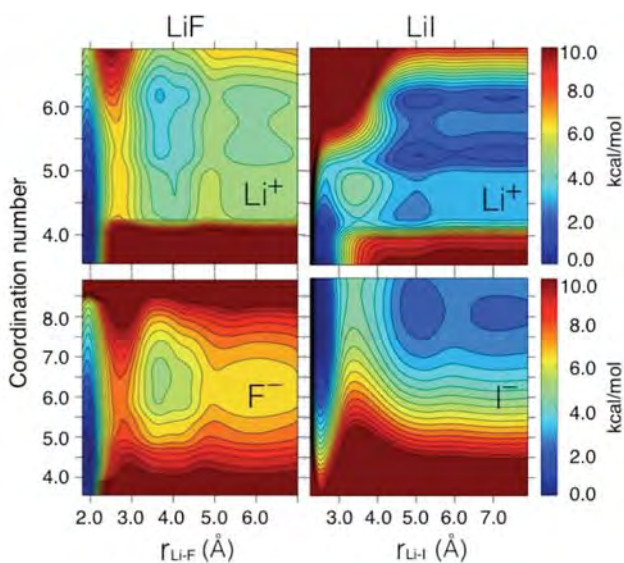


Figure 3. An example of the rich structure in a two-dimensional potential of mean force,  $W(n,r)$  where  $n$  is a water coordination number and  $r$  is an ion-ion distance.

With our improved understanding of the balance between ion-ion, ion-water, and water-water interaction, we plan to extend our developments in the description of Dynamical Nucleation Theory [b,c,d,e] to the condensed phase. We have initiated studies of the nucleation pathways of CaCO<sub>3</sub> formation, comparing empirical potential and electronic structure descriptions of molecular interaction.

*Acknowledgements:* Direct collaborators on this project include C. J. Mundy, M. Baer, S. Roy S. M. Kathmann and J. Fulton. Valuable interactions with S. S. Xantheas, L. X. Dang and M. Valiev have influenced the course of this work. Battelle operates Pacific Northwest National Laboratory for the US Department of Energy.

## **References**

- a. R. C. Remsing, J. M. Rodgers, and J. D. Weeks, "Desconstructing Classical Water Models at Interfaces and in Bulk," *J. Stat. Phys.* **145**, 313 (2011).
- b. Schenter, G. K.; Kathmann, S. M.; Garrett, B. C., "Dynamical benchmarks of the nucleation kinetics of water," *J. Chem. Phys.* **116**, 4275-4280 (2002).
- c. Schenter, G. K.; Kathmann, S. M.; Garrett, B. C., "Variational transition state theory of vapor phase nucleation," *J. Chem. Phys.* **110**, 7951-7959 (1999).
- d. Schenter, G. K.; Kathmann, S. M.; Garrett, B. C., "Dynamical nucleation theory: A new molecular approach to vapor-liquid nucleation," *Phys. Rev. Lett.* **82**, 3484-3487 (1999).
- e. Kathmann, S. M.; Schenter, G. K.; Garrett, B. C., "Dynamical nucleation theory: Calculation of condensation rate constants for small water clusters," *J. Chem. Phys.* **111**, 4688-4697 (1999).

## **References to publications of CPIMS sponsored research (2015-2016)**

1. Chun, J. H.; Mundy, C. J.; Schenter, G. K., "The Role of Solvent Heterogeneity in Determining the Dispersion Interaction between Nanoassemblies," *J. Phys. Chem. B* **119**, 5873-5881 (2015) DOI: 10.1021/jp512550c.
2. Dang, L. X.; Schenter, G. K., "Solvent exchange in liquid methanol and rate theory," *Chem. Phys. Lett.* **643**, 142-148 (2016). DOI: 10.1016/j.cplett.2015.10.045.
3. Pluharova, E.; Baer, M. D.; Schenter, G. K.; Jungwirth, P.; Mundy, C. J., "Dependence of the Rate of LiF Ion-Pairing on the Description of Molecular Interaction," *J. Phys. Chem. B* **120**, 1749-1758 (2016). DOI: 10.1021/acs.jpcc.5b09344.
4. Roy, S.; Baer, M. D.; Mundy, C. J.; Schenter, G. K., "Reaction Rate Theory in Coordination Number Space: An Application to Ion Solvation," *J. Phys. Chem. C* **120**, 7597-7605 (2016). DOI: 10.1021/acs.jpcc.6b00443.
5. Skinner, L. B.; Galib, M.; Fulton, J. L.; Mundy, C. J.; Parise, J. B.; Pham, V. T.; Schenter, G. K.; Benmore, C. J., "The structure of liquid water up to 360 MPa from x-ray diffraction measurements using a high Q-range and from molecular simulation," *J. Chem. Phys.* **144**, 10 (2016). DOI: 10.1063/1.4944935.
6. Schenter, G. K.; Fulton, J. L.; "Molecular Dynamics Simulations and XAFS (MD-XAFS)", In "XAFS Techniques for Catalysts, Nanomaterials, and Surfaces", Yasuhiro Iwasawa, Kiyotaka Asakura, and Mizuki Tada, editors, Springer, New York, (2017). ISBN 978-3-319-43866-5.

# **An Atomic-scale Approach for Understanding and Controlling Chemical Reactivity and Selectivity on Metal Alloys**

E. Charles H. Sykes (charles.sykes@tufts.edu)

Department of Chemistry, Tufts University, 62 Talbot Ave, Medford, MA 02155

## **Program Scope:**

Catalytic hydrogenations are critical steps in many industries including agricultural, chemicals, foods and pharmaceuticals. In the petroleum refining industry, for instance, catalytic hydrogenations are performed to produce light, hydrogen rich products like gasoline. Hydrogen activation, uptake, and reaction are also important phenomena in fuel cells, hydrogen storage devices, materials processing, and sensing. Typical heterogeneous hydrogenation catalysts involve nanoparticles composed of expensive noble metals or alloys based on metals like Pt, Pd, and Rh. Our goal is to alloy these reactive metals, at the single atom limit, with more inert and often much cheaper hosts (which we term *single atom alloys*, SAAs) and to understand how the local atomic geometry affects reactivity. We have focused on understanding the adsorption, diffusion, spillover and reactivity of hydrogen in a number of these types of systems. We designed well-defined alloy surfaces using combinations of Pd, Co, Pt, Au, and Cu that are amenable to high resolution scanning probe studies, X-ray photoelectron spectroscopy, and chemical analysis of adsorbate binding, spillover and reaction.

These types of alloy systems allow us to address previously unobtainable structures, densities and phases of hydrogen due to the limitations of single crystal work in ultra-high vacuum. By understanding the energy landscape for hydrogen activation, adsorption and spillover we have been able to generate catalytically relevant high coverage hydrogen phases, design efficient and selective hydrogenation sites, and trap hydrogen on surfaces beyond its normal desorption point yielding novel catalytic intermediates.

## **Recent Progress:**

### **Controlling Hydrogen Activation, Spillover, and Desorption with Pd-Au Single Atom Alloys**

A key requirement in the efficient use of heterogeneous catalysts, fuel cells and hydrogen storage devices is the ability of the material to activate, uptake and release hydrogen. The addition of Pd into Au is known to change the catalytic activity of the surface, but the atomic geometry of the active sites and the adsorption energies of key molecules are unknown. In this study, we used an atomically resolvable model system of dilute Pd-Au surface alloys and density functional theory (DFT) calculations to elucidate the energetics of H<sub>2</sub> activation, diffusion, and desorption from Pd monomers in Au(111). We experimentally demonstrated that Pd monomers in a Au(111) surface can activate H<sub>2</sub>, a process suggested by other experiments to require two contiguous Pd atoms. We clearly show by coupling high resolution scanning tunneling microscopy (STM) with temperature programmed desorption (TPD), that low concentrations of individual, isolated Pd atoms can dissociate H<sub>2</sub> since the concentration of adsorbed H atoms is proportional to the surface concentration of Pd atoms in Au. Combining TPD with DFT calculations, we elucidated the energetic landscape for H<sub>2</sub> adsorption, activation, and desorption from isolated Pd atoms revealing a low temperature pathway for H<sub>2</sub> activation and release through the Pd atoms with minimal spillover to Au (Figure 1). The co-adsorption of H<sub>2</sub> and D<sub>2</sub> leads to complete scrambling of H and D supporting the dissociation of H<sub>2</sub> and the transient existence of H atoms on Au. Additionally, Pd-Au SAAs bind CO significantly more weakly than Pd(111) (270 K vs. 450 K) which

can potentially improve the CO tolerance of the catalysts. The competitive adsorption of CO and H on the Pd atoms forces H atoms to spillover onto the Au surface altering the desorption pathway to an even lower temperature through Au (110 K vs. 175 K). Our work demonstrates that individual, isolated Pd atoms in Au allow for facile H<sub>2</sub> activation and weak adsorption of H atoms, a key requirement for efficient and selective hydrogenation catalysis.

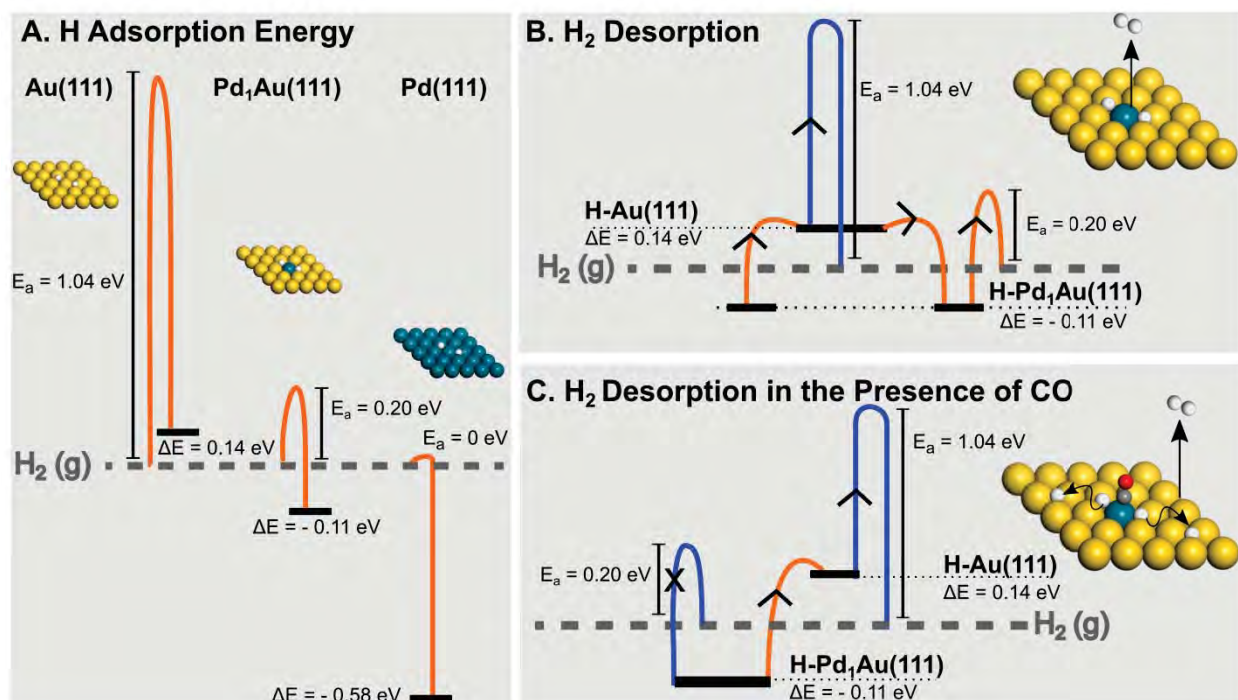


**Figure 1.** Schematics of the energy landscapes for H<sub>2</sub> adsorption and desorption on Pd-Au SAAs. (A) H<sub>2</sub> activation energy ( $E_a$ ) per H<sub>2</sub> molecule, and H adsorption energy ( $\Delta E$ ) per H atom on monometallic Au, Pd and Pd-Au SAA. Energetics of H<sub>2</sub> desorption for Pd-Au SAA (B) without and (C) with CO. Schematic illustrates the preferred active sites for H<sub>2</sub> dissociation as well as preferred adsorption sites for H and CO. Preferred and minor desorption pathways are displayed in orange and blue, respectively. In (B) the preferred pathway for H<sub>2</sub> desorption is via the Pd site. In (C) the Pd site is blocked by CO, so H atoms spillover to Au and then desorb from there. All energies are reported relative to H<sub>2</sub> in the gas phase, as noted by the dashed horizontal lines. Note that  $E_a$  for H<sub>2</sub> on Au(111) calculated by DFT (which doesn't account for quantum nuclear effects) may in fact be a large overestimate of the barrier, as experimentally H<sub>2</sub> desorbs from Au(111) at 110 K.

### A Microscopic View of the Active Sites for Selective Dehydrogenation of Formic Acid on Cu(111)

Formic acid is an important molecule due to its potential for hydrogen storage. Formic acid decomposes on metal surfaces through either dehydrogenation to produce CO<sub>2</sub> and H<sub>2</sub> or via dehydration to produce CO and H<sub>2</sub>O. High selectivity to dehydrogenation is necessary for energy and hydrogen storage applications, and the dehydration route can poison catalysts through strong binding of reactively formed CO. However, these two mechanisms are linked via the water-gas shift reaction (WGS) making them hard to understand. It is well accepted that Cu catalysts have high selectivity towards dehydrogenation. While there is extensive research examining the reaction of formic acid on Cu(110), little work has been performed on Cu(111) despite the fact that this is the dominant facet on many nanoparticles. There were, to the very best of our knowledge, no temperature programmed reaction (TPR) studies of formic acid on Cu(111) reported in the literature.

Using TPD/R and STM, we have probed key steps in the decomposition of formic acid on Cu(111) at the atomic-scale, observing intact adsorption and surface intermediates, as well as the surface after product desorption (Figure 2). Our model system allowed us to investigate the reaction under conditions where WGS is inactive. We found that Cu(111) decomposes formic acid 100% selectively through dehydrogenation. At 85 K, formic acid adsorbs molecularly on Cu(111), forming hydrogen bonded chains in the  $\beta$  configuration. The acid loses a H atom by 160 K producing the formate intermediate and surface bound H atoms, both of which are visualized by STM. All molecules at surface step edges react to formate, but on the Cu(111) terraces desorption of formic acid competes with formate production which limits formate production to  $\sim 5\%$  on the terraces. H atoms formed by deprotonation recombine to form  $H_2$  in a desorption rate limited process by 360 K.  $CO_2$  and  $H_2$  desorb from the surface in a reaction rate limited processes at 400 and 450 K due to formate decomposition on terraces and steps respectively. The surface is left clean following the dehydrogenation of formate. Our results indicate that while the Cu(111) surface is significantly less reactive than the well-studied Cu(110) facet, roughening the Cu(111) surface leads to a significant increase in reactivity with no drop in selectivity to  $CO_2$  and  $H_2$ .

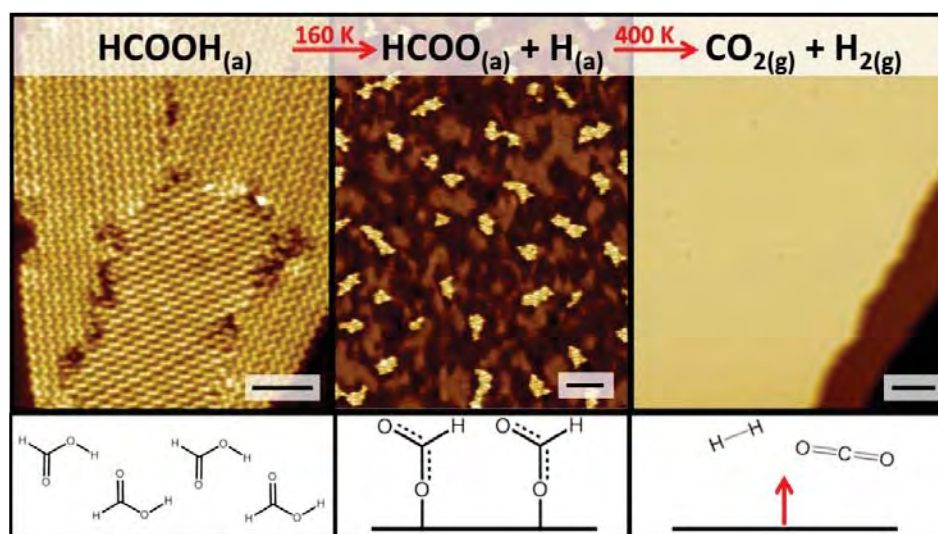


**Figure 2. Reaction Pathway for Formic Acid Dehydrogenation on Cu(111).** Summary of the key reaction steps illustrated with STM images and schematics of the corresponding species. Initially, between 80–160 K intact formic acid forms hydrogen bonded chains on the surface. Scale bar = 3 nm. At 160 K formic acid deprotonates to yield formate. Scale bar = 5 nm. Between 400–500 K formate decomposes to yield  $H_2$  and  $CO_2$ , which desorb instantaneously in a reaction rate limited process leaving a clean Cu surface. Scale bar = 5 nm.

### Future Plans:

Our approach offers the opportunity to study the atomic-scale composition and structure of active sites and relate this information to their ability to activate, spillover and react industrially relevant small molecules. We will use these guiding principles to examine catalytic metal alloys from a new perspective and discover new processes. Future work is aimed at:

- 1) Extending our single atom alloy (SAA) approach to understanding hydrogenations on PdAg
- 2) Using the “molecular cork” effect to control the activity and selectivity of surface catalyzed hydrogenation reactions
- 3) Elucidating the optimal atomic geometry of AgCu for oxygen activation

These model systems will allow us a fundamental understanding of many important elementary steps in surface catalyzed chemistry. The atomic-scale structure of the active sites in metal alloy catalysts is hard, if not impossible, to characterize by conventional methods. Our surface science approach that includes scanning probes offers methods to characterize the structure, stoichiometry, and reactivity, and provides an atomic-scale view of local structure and adsorbate binding/diffusion. However, when working on well-defined model systems it is imperative to work with the same elements, structures and ensembles that are present in the real catalysts under working conditions. Implementation of the SAA approach to the design of real catalysts requires consideration of the effect of higher reaction temperature and pressure, which may cause the minority active element to segregate into the bulk of the more inert host and hence cause a loss in activity. Understanding and controlling surface segregation under reaction conditions will also be crucial for the efficient use of the costly elements of the alloy by keeping them in active sites on or near the surface. Promisingly, there are now many experimental and theoretical examples of metal alloys under realistic conditions in which the more active element is stabilized at the surface by adsorbates.

All our proposed systems have been chosen with these considerations in mind. Active elements will be alloyed into more inert Cu, Ag, and Au surfaces. The (111) facet is chosen, as it is often the most commonly exposed facet on metal nanoparticles. While minority structures like step edges or defects often dominate the reactivity of metal surfaces, the chemistry of our alloyed systems is expected to be driven at the added metal atom sites and this will be checked with control experiments of the reactivity before and after alloying.

#### **DOE-Sponsored Research Publications in the Last Two Years:**

- 1) "Tackling CO Poisoning with Single Atom Alloy Catalysts" J. Liu, F. R. Lucci, M. Yang, S. Lee, M. D. Marcinkowski, A. J. Therrien, C. T. Williams, E. C. H. Sykes, and M. Flytzani-Stephanopoulos *Journal of the American Chemical Society* **2016**, 138, 6396-6399 [Cover Story]
- 2) "Controlling Hydrogen Activation, Spillover, and Desorption with Pd-Au Single Atom Alloys" F. R. Lucci, M. T. Darby, M. F. G. Mattera, C. J. Ivimey, A. J. Therrien, A. Michaelides, M. Stamatakis, and E. C. H. Sykes *The Journal of Physical Chemistry Letters* **2016**, 7, 480-485
- 3) "A Microscopic View of the Active Sites for Selective Dehydrogenation of Formic Acid on Cu(111)" M. D. Marcinkowski, C. J. Murphy, M. L. Liriano, N. Wasio, F. R. Lucci, and E. C. H. Sykes *ACS Catalysis* **2015**, 5, 7371-7378
- 4) "Collective Effects in Physisorbed Molecular Hydrogen on Ni/Au(111)" A. J. Therrien, A. Pronschinske, C. J. Murphy, E. A. Lewis, M. L. Liriano, M. D. Marcinkowski, and E. C. H. Sykes *Physical Review B* **2015**, 92, 161407(R)
- 5) "Squeezing and Stretching Pd Thin Films: A High-Resolution STM Study of Pd/Au(111) and Pd/Cu(111) Bimetallics" M. E. Blecher, E. A. Lewis, A. Pronschinske, C. J. Murphy, M. F. G. Mattera, M. L. Liriano, and E. C. H. Sykes *Surface Science* **2015**, 646, 1-4
- 6) "Spin Modified Catalysis" R. Choudhary, P. Manchanda, A. Enders, B. Balamurugan, A. Kashyap, D. J. Sellmyer, E. C. H. Sykes, and R. Skomski - *The Journal of Applied Physics* **2015**, 117, 17D720
- 7) "Enhancement of Low-Energy Electron Emission in 2D Radioactive Films" A. Pronschinske, P. Pedevilla, C. J. Murphy, E. A. Lewis, F. R. Lucci, G. Brown, G. Pappas, A. Michaelides, and E. C. H. Sykes - *Nature Materials* **2015**, 14, 904-907

# Solvation Dynamics in Nanoconfined and Interfacial Liquids

Ward H. Thompson

*Department of Chemistry, University of Kansas, Lawrence, KS 66045*

*wthompson@ku.edu*

## Program Scope

There is currently significant interest in nanostructured materials that can confine liquids in nanoscale pores, due to both the appearance of new fundamental phenomena in these systems and their wide range of potential applications, including catalysis, sensing, separations, electrochemistry, and optical materials. However, the design principles are still lacking for the development of such mesoporous ( $2 \text{ nm} \leq \text{diameter} \leq 50 \text{ nm}$ ) materials for practical applications that take advantage of their large surface area-to-volume ratio and their high degree of tunability through pore size, shape, roughness, and chemical functionality. At the same time, this gap points to the need to improve our fundamental understanding of how complex liquid dynamics can arise from nanoscale confinement and vary strongly with the confining environment properties.

We are addressing some of the outstanding questions regarding these nanoconfined liquid dynamics and the implications for chemical reactions – *i.e.*, *How does a chemical reaction occur differently in a nanoconfined solvent than in a bulk solvent?* – in multiple ways, as described below.

## Recent Progress & Future Plans

### *Solvation Dynamics.*

We have continued our work on solvation dynamics in confining silica frameworks and extended it to behavior at planar silica interfaces. Solvation dynamics is closely related to the reaction coordinate for charge transfer reactions such as electron or proton transfer reactions and is often dramatically affected by nanoconfinement. It is by now well established that liquid layering and orientational ordering at interfaces produces an underlying free energy surface that affects the behavior of solutes, *e.g.* reactants or chromophores. We have previously proposed that this should affect chemical reactivity and spectroscopy.

We have completed non-equilibrium simulations of the time-dependent fluorescence signal of the C153 dye molecule dissolved in ethanol confined within  $\sim 2.4$  diameter hydrophilic, amorphous silica pores. Initial conditions were sampled from replica exchange MD simulations with C153 in the ground electronic state.<sup>1,2</sup> The results for the dynamic Stokes shift,  $S(t) = [E_{fl}(t) - E_{fl}(\infty)]/[E_{fl}(0) - E_{fl}(\infty)]$  where  $E_{fl}$  is the fluorescence energy, can be fit with a tri-exponential that gives the longest timescale (the one most strongly influenced by confinement) as 86 ps, in good agreement with the 102.7 ps reported by Baumann *et al.*<sup>3</sup> Analysis of the nonequilibrium trajectories indicates that the slowed dynamics primarily originates from interfacial ethanol molecules, consistent with the canonical two-state, or core-shell, model. However, this model does not provide a complete picture, *e.g.*, a relatively small number of ethanol molecules ( $< 10$ ) account for the vast majority of the solvation response.

We are now also carrying out simulations of liquids at planar silica interfaces. We have developed atomistic models of hydrophilic (OH-terminated) amorphous silica interfaces for simulations with various liquids, including methanol, water, and acetonitrile. We are investigating the structure and dynamics of these liquids with a particular focus on comparing these properties at an amorphous interface with the corresponding results at a crystalline one, *e.g.*,  $\beta$ -cristobalite. The latter aims to investigate the effect of silica surface structure – while a majority of experiments use (amorphous) fused silica, most simulations are based on crystalline silica surface models – that we have found to be important in our previous simulations of mesoporous silica.

*Vibrational Spectroscopy.*

We have recently simulated the vibrational (IR, Raman, and 2D-IR photon echo) spectra of water (specifically HOD in D<sub>2</sub>O) confined in a  $\sim 2.4$  nm diameter silica pore.<sup>4</sup> The OH frequency is obtained using the empirical map approach of Skinner and co-workers.<sup>5</sup> Our simulations indicate that confined water exhibits an IR spectrum that is only slightly perturbed from the bulk; this result is quite surprising in light of the dramatic effects on reorientation and spectral diffusion dynamics of the confined water,<sup>6,7</sup> but is in agreement with previously reported experimental spectra.<sup>8</sup> In contrast, the Raman spectrum is principally changed by the addition of a larger shoulder at higher frequencies – also in agreement with measurements<sup>9</sup> – due to weaker hydrogen bonding near the silica interface that leads to blue-shifted OH frequencies. (These same OH groups do not contribute significantly to the IR spectrum due to their smaller transition dipole moments.) The results indicate that the IR spectrum is insensitive to the interfacial waters which are better probed by Raman spectroscopy.

We have also predicted the 2D-IR spectra for this system<sup>4</sup> which have not yet been measured (our simulations thus represent the first prediction of their behavior). The simulated spectra indicate that it should be possible to probe the slower spectral diffusion of confined water compared to the bulk liquid by analysis of the 2D-IR spectra. This is illustrated in Fig. 1 where the center-line-slope (CLS) obtained from the 2D-IR spectra, and representative of the spectral dynamics, are shown for both confined and bulk HOD in D<sub>2</sub>O. The corresponding frequency autocorrelation functions are also shown and are in excellent agreement with the CLS results.

The relative insensitivity of vibrational spectroscopy to the confinement of water has motivated us to begin simulations of the vibrational sum-frequency generation (SFG) spectrum of the water/silica planar interface. The simulations also make use of the empirical mapping approach<sup>5</sup> and the planar amorphous silica models discussed above. The simulations are of HOD in D<sub>2</sub>O with no deprotonation of the surface silanol groups (a situation realized experimentally at low *pH*). There are a number of measurements of the SFG spectra in the literature that will provide critical

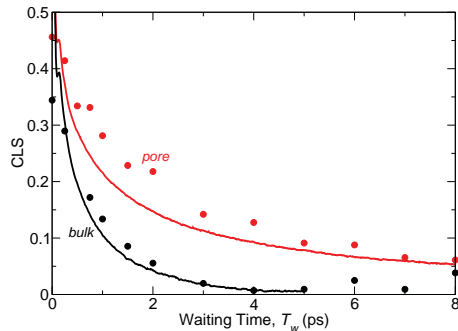


Figure 1: CLS (circles) is shown as a function of waiting time and compared to the frequency autocorrelation function (solid lines) for bulk (black) and confined (red) water.

validation of the amorphous silica surface models. Because the spectra probe only waters in the interfacial region, it is anticipated that the SFG spectra will represent a more quantitative test of the simulations (which, as noted above, have so far been able to reproduce the features observed in measured IR and Raman spectra of mesoporous silica-confined water).

We have also studied the reorientational and hydrogen-bond (H-bond) dynamics along with the vibrational spectroscopy of water confined within phospholipid reverse micelles in collaboration with two research groups in France. These systems provide an interesting comparison to the more widely studied AOT reverse micelles as well as the nanoscale silica pores discussed above. The validation and characterization of the models used to describe the reverse micelles has been completed along with the first examination of the reorientational dynamics and infrared spectroscopy.<sup>10</sup> A full, molecular-level analysis of the dynamics, including a critical examination of the two-state model and simulations of the 2D-IR spectra, is in progress.

#### *Reaction Rate Theory.*

We recently presented a general approach for directly calculating the activation energy for a chemical reaction from a simulation at a single temperature.<sup>11</sup> The methods are applicable to both classical and quantum systems. The activation energy is obtained from a correlation function that can be evaluated from the same trajectories or quantum dynamics used to evaluate the rate constant itself and thus requires essentially no extra computational work. These approaches can be implemented in the context of nearly any method for calculating a rate constant. We successfully applied the methods to determining the activation energy of the one-dimensional Eckart barrier, described in terms of both classical and quantum mechanics, and the classical H-bond exchange dynamics in liquid water.

#### *Dynamics and Spectroscopy of Alcohols.*

We are continuing our work aimed at understanding the H-bond dynamics of alcohols by developing models for simulating their vibrational spectra. Specifically, we are parametrizing empirical maps for the transition frequencies and dipoles of the OH stretch of linear alcohols from methanol through butanol using electronic structure calculations of clusters extracted from MD simulations. We have already obtained results for methanol and ethanol that are in good agreement with reported IR spectra. This work is motivated in part by our previous examination of the OH reorientation and H-bond dynamics of isomeric butanols to understand how the dynamics in alcohols vary with the arrangement of the steric bulk.<sup>12</sup> For many alcohol systems, including the isomeric butanols, there is limited experimental data on the dynamics. The present work will address this issue by enabling comparisons between simulations and (comparatively plentiful) measured IR spectra, and will also facilitate extensions of our simulations of vibrational spectra to alcohol/silica interfaces.

#### *Nonlinear Response and Gaussian Statistics.*

Linear response theory, in which perturbations are described by fluctuations in the equilibrium state, is the dominant theory for describing nonequilibrium dynamics. In this approximation, the perturbation is assumed to be weak – on the order of thermal energies ( $k_B T$ ). Linear response has been remarkably successful at predicting nonequilibrium dynamical properties for weak perturba-

tions and even for perturbations much larger than those on the order of the thermal energy. We have previously shown, in the context of solvation dynamics, that the (static) linear-response approximation actually represents the assumption that the relevant variable – the energy gap between the electronic ground- and excited-states – obeys Gaussian statistics.<sup>13</sup>

Recently, we have addressed some of the fundamental questions about nonequilibrium chemical dynamics and the Gaussian statistics approximation in the context of the “dipole-flip” model.<sup>14</sup> First, *Can non-Gaussian statistics be predicted by relying only on equilibrium simulations?* We showed that the answer to this question is yes, by comparing higher-order time correlation functions with their Gaussian statistics approximations. Second, *What is the origin of the non-Gaussian statistics?* We developed tools for isolating the degrees-of-freedom responsible for non-Gaussian (nonlinear) behavior by decomposing the total correlation function and testing for Gaussian behavior in the resulting subset of coordinates. Third, *Can the Gaussian statistics approximation be corrected to describe nonlinear response without resorting to full nonequilibrium simulations?* We have shown that this can be accomplished to a limited degree, but this issue requires additional work. We are currently applying the same approach to understand nonlinear response in reactions of the solvated electron.<sup>15</sup>

## References

- [1] †J.A. Harvey and W.H. Thompson, *J. Phys. Chem. B* **119**, 9150-9159 (2015). “Thermodynamic Driving Forces for Dye Molecule Position and Orientation in Nanoconfined Solvents”
- [2] †J.A. Harvey and W.H. Thompson, *J. Chem. Phys.* **143**, 044701 (2015). “Solute Location in a Nanoconfined Liquid Depends on Charge Distribution”
- [3] R. Baumann, C. Ferrante, E. Kneuper, F.-W. Deeg, and C. Bräuchle, *J. Phys. Chem. A* **107**, 2422-2430 (2003).
- [4] †P.C. Burris, D. Laage, and W.H. Thompson, *J. Chem. Phys.* **144**, 194709 (2016). “Simulations of the Infrared, Raman, and 2D-IR Photon Echo Spectra of Water in Nanoscale Silica Pores”
- [5] B.M. Auer and J.L. Skinner, *J. Chem. Phys.* **128**, 224511 (2008).
- [6] D. Laage and W.H. Thompson, *J. Chem. Phys.* **136**, 044513 (2012).
- [7] †A.C. Fogarty, E. Duboué-Dijon, D. Laage, and W.H. Thompson, *J. Chem. Phys.* **141**, 18C523 (2014). “Origins of the Non-exponential Reorientation Dynamics of Nanoconfined Water”
- [8] R. Musat, J.P. Renault, M. Candelaresi, D.J. Palmer, D. S. Le Caër, R. Righini, and S. Pommeret, *S. Angew. Chem. Intl. Ed.* **47**, 8033-8035 (2008).
- [9] X.F. Huang, Q. Wang, X.X. Liu, S.H. Yang, C.X. Li, G. Sun, L.Q. Pan, K.Q. Lu, *J. Phys. Chem. C* **113**, 18768-18771 (2009).
- [10] †S. Abel, N. Galamba, E. Karakas, M. Marchi, W.H. Thompson, and D. Laage, *Langmuir* (submitted). “On the Structural and Dynamical Properties of DOPC Reverse Micelles”
- [11] †O.O. Mesele and W.H. Thompson, *J. Chem. Phys.* (submitted). “Removing the Barrier to the Calculation of Activation Energies”
- [12] †O.O. Mesele, A.A. Vartia, D. Laage, and W.H. Thompson, *J. Phys. Chem. B* **120**, 1546-1559 (2016). “Reorientation of Isomeric Butanols: Exploring the Role of Steric Bulk on Hydrogen Bond Dynamics”
- [13] B.B. Laird and W.H. Thompson, *J. Chem. Phys.* **126**, 211104 (2007); **135** 084511 (2011).
- [14] M.S. Skaf and B.M. Ladanyi, *J. Chem. Phys.* **100**, 18258 (1996).
- [15] K. Kanjana, B. Courtin, A. MacCormell, and D.M. Bartels, *J. Phys. Chem. A* **119**, 11094-11104 (2015).

†DOE-sponsored publication in past 2 years

# Imaging Interfacial Electric Fields on Ultrafast Timescales

William A. Tisdale

*Department of Chemical Engineering  
Massachusetts Institute of Technology, Cambridge, MA 02139  
tisdale@mit.edu*

## Program Scope

The objective of this project is to explore a novel methodology for visualization of ultrafast electronic processes at interfaces. The method, which is based on optical stimulation, builds upon previous success using spontaneous second-order nonlinear optical probes to track the temporal evolution of interfacial electric fields resulting from charge separation across an interface. A goal is to speed signal acquisition by orders of magnitude so that laser scanning ultrafast microscopy becomes feasible. The ultimate aim is to generate movies of interfacial electronic phenomena occurring on femtosecond timescales and submicron length scales, thereby informing our understanding of disorder, heterogeneity, and morphology, and how these factors affect ensemble behavior in photovoltaic, electrochemical, and optoelectronic systems.

## Recent Progress I: Stimulated SHG

Second harmonic generation (SHG) is a second order nonlinear optical process in which two photons at a fundamental frequency  $\omega$  combine to form a single photon at frequency  $2\omega$ . Like any even-ordered nonlinear optical process, SHG is dipole-forbidden in the bulk of centrosymmetric media such as many crystal structures, amorphous solids, liquids, and gases; observed SHG signals in these media originate from materials' interfaces. SHG experiments selectively probe interfaces and are sensitive to the interfacial environment. SHG is an inefficient process, and high incident fundamental fluences are necessary to produce measurable signals. The incident fundamental fluence is often limited by the sample's optical damage threshold, and signals are usually very weak. Even with an optimal detection system, the signal to noise ratio (SNR) in SHG experiments is limited by the presence of shot noise. It is desirable to amplify the weak spontaneous SHG signal allowing high quality measurements to be taken in a shorter period of time. Such an advance would enable SHG measurements with time and spatial resolution, which are currently infeasible due to intractably long acquisition times resulting from spontaneous SHG's notoriously low SNR.

In Year 2 of the project, we published a successful amplification of weak spontaneous SHG signals by optical stimulation in an idealized proof-of-principle demonstration (Goodman & Tisdale, *Phys. Rev. Lett.* **2015**).<sup>2</sup> Though the initial demonstration showed an improvement in SHG signal generation by a factor of  $10^4$  compared to the spontaneous signal, the signal suffered from large fluctuations due to optical phase instability. As we showed in the initial paper, the stimulated SHG signal is highly sensitive to the relative optical phase between the incident fundamental and second harmonic fields. While this sensitivity caused undesired signal fluctuations in the original intensity modulation scheme, we soon realized that we could use the phase sensitivity to our advantage by modulating the optical phase of the stimulating field rather than modulating its intensity. This approach has the added benefit of removing artifacts associated with intensity modulation of the second harmonic field, such as third-order phenomena and two-photon fluorescence.

Our first successful implementation of phase-modulation stimulated SHG is shown schematically in Fig. 1(a). A common optical path is employed to reduce phase noise, as demonstrated in Fig. 1(b). Modulation of the relative optical phase between the fundamental and stimulating fields is accomplished using an electro-optic modulator (EOM) operated at 1 MHz. Numerical simulations and later experimental confirmation (Fig. 1(c)) revealed requirements for both the depth of the modulation (exactly  $2\pi$ ) and the modulation waveform (sawtooth) needed for long-term stability of the stimulated SHG signal. While we have not yet reached the shot noise limit, the signal now has sufficient stability (Fig. 1(b,d)) to begin imaging studies.

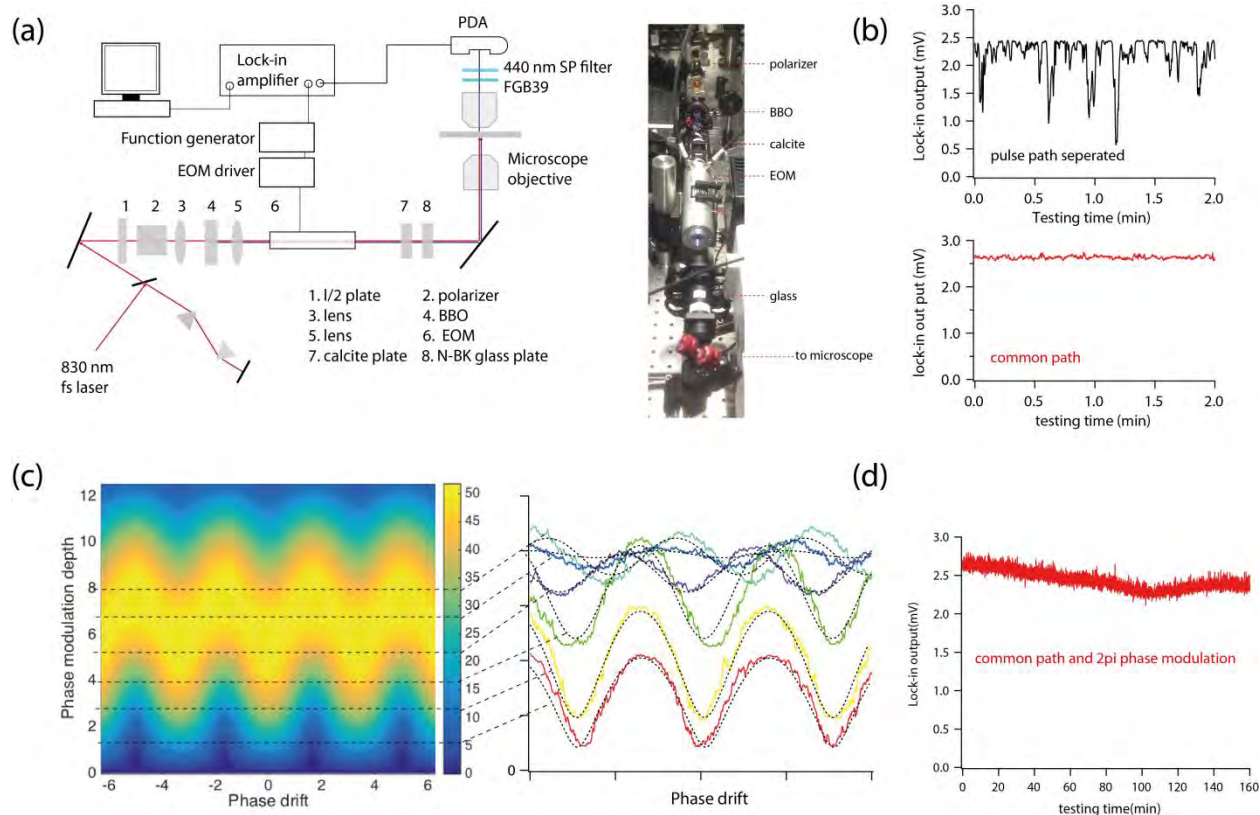


**Figure 1.** Phase-modulation stimulated SHG. (a) Schematic of the common path design and a photo of the common path modulation scheme. (b) Comparison of the stability of the stimulated SHG signal before (black, upper panel) and after (red, lower panel) introduction of the common path phase modulation scheme. (c) Numerical simulation (left) and experimental confirmation (right) of the effect of phase modulation depth and phase drift on the lock-in detected SSHG signal. (d) Long-time stability of the SSHG signal.

### Recent Progress II: Charge Carrier Dynamics in Homogeneously Broadened PbS Quantum Dot Solids

Lead sulfide (PbS) quantum dots (QDs) are solution-processed semiconductors in which the size of the QD determines the band gap. The band gap can be tuned across the near infrared region of the electromagnetic spectrum, making PbS QDs useful for telecommunications applications and a variety of optoelectronic devices including solar cells, IR light-emitting diodes, and photodetectors. In Year 1 of the project we developed methods to synthesize highly monodisperse PbS QDs over a broad size range, and to control the polydispersity by adjusting the Pb to S precursor ratio (Weidman *et al.*, *ACS Nano* **2014**).<sup>1</sup> We have found that monodisperse PbS QDs self-assemble into highly ordered BCC superlattices, and that some long-range order remains even after exchanging the long hydrocarbon ligands required for colloidal stability in solution for short ligands that promote charge carrier transport.

Energetic disorder in quantum dot solids adversely impacts charge carrier transport in quantum dot solar cells and electronic devices. Recently (*unpublished*), we used ultrafast transient absorption spectroscopy (Fig. 2) to show that homogeneously broadened PbS quantum dot arrays ( $\sigma_{hom}^2 : \sigma_{inh}^2 > 30:1$ ,  $\sigma_{inh}/kT < 0.3$ ) can be realized if quantum dot batches are sufficiently monodisperse ( $\delta \lesssim 3.3\%$ ). Homogeneous linewidth was found to be an inverse function of quantum dot size, monotonically increasing from  $\sim 30$  meV for the largest quantum dots (5.8 nm diameter/0.92 eV energy) to  $\sim 60$  meV for the smallest (4.1 nm/1.3 eV energy). Furthermore, we showed that intrinsic charge carrier hopping rates are faster for smaller quantum dots. This finding is opposite the mobility trend commonly observed in device measurements, but is consistent with theoretical predictions. Fitting our data to a

kinetic Monte Carlo model, we extracted charge carrier hopping times ranging from 40 ps for the smallest quantum dots to over 1 ns for the largest, with the same ethanethiol ligand treatment. Additionally, we made the surprising observation that in slightly polydisperse ( $\delta \lesssim 4\%$ ) quantum dot solids, structural disorder has a greater impact than energetic disorder in inhibiting charge carrier transport. These findings emphasize how small improvements in batch size dispersity can have a dramatic impact on intrinsic charge carrier hopping behavior, and will stimulate further improvements in quantum dot device performance.

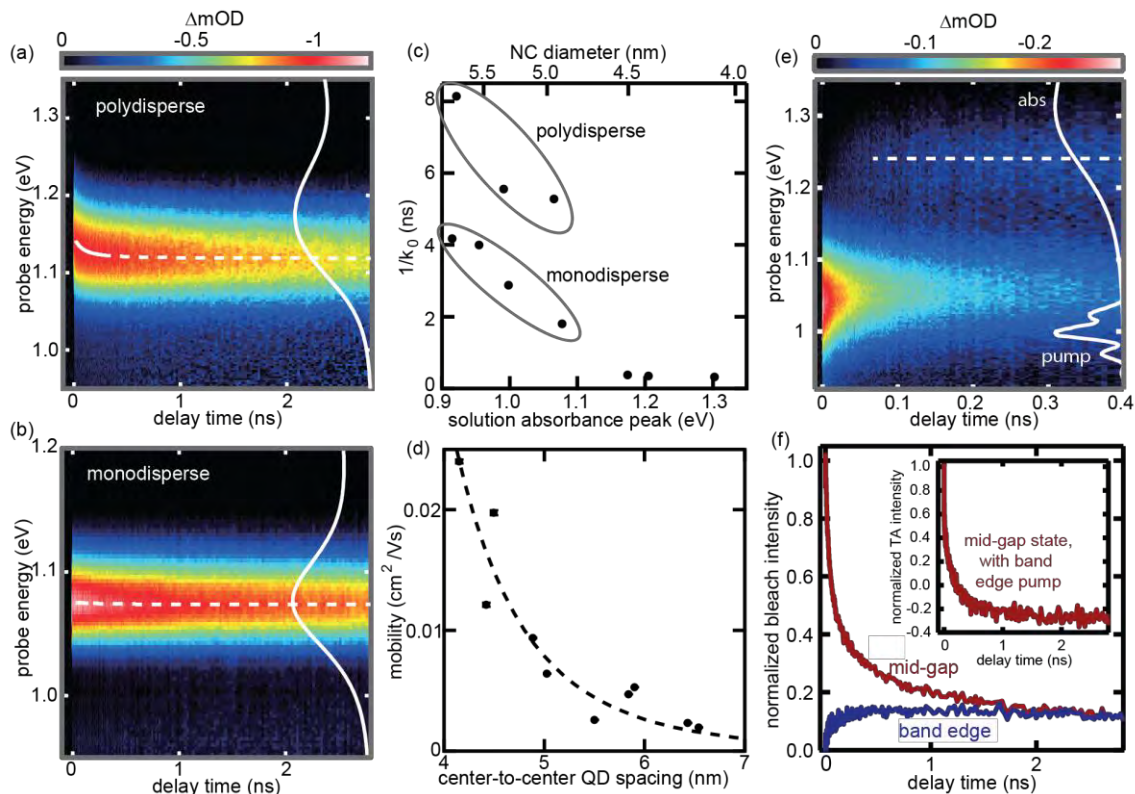


**Figure 2.** Charge carrier dynamics in PbS QD solids. (a,b) Transient absorption data on PbS QD solids showing the redshift of the band edge bleach following uniform excitation. Dashed lines show the peak position and solid lines show linear absorption spectra. (c) Reciprocal of the fitted prefactor from the KMC model as a function of QD solution absorbance peak. (d) Expected free carrier mobility as a function of center-to-center spacing. The dashed line shows the expected  $1/r^6$  dependence. (e) Transient absorption data on a coupled PbS QD solid following mid-gap state excitation. (f) Normalized bleach intensity for the mid-band gap state and band edge states, calculated from (e). Inset shows the bleach at the mid-gap state energy following band edge excitation. They dynamics are the same in all cases, indicating equilibrium between the two states. Data collected at Brookhaven Center for Functional Nanomaterials.

### Future Plans

We are now turning our attention to using the new time-resolved micro-SHG instrument to investigate interfaces of fundamental interest. Our initial efforts are focused on interfaces between QDs and bulk semiconductor surfaces, which have previously exhibited interesting ultrafast coherent dynamics. These efforts will leverage both the spectroscopy instrument development and synthetic materials progress over the first two years of the project.

CPIMS-Supported Publications (2014-2016)

1. M.C. Weidman, M.E. Beck, R.S. Hoffman, F. Prins, W.A. Tisdale; "Monodisperse, Air-Stable PbS Nanocrystals *via* Precursor Stoichiometry Control," *ACS Nano* **8**, 6363-6371 (2014).
2. A.J. Goodman & W.A. Tisdale; "Enhancement of Second-Order Nonlinear-Optical Signals by Optical Stimulation," *Phys. Rev. Lett.* **114**, 183902 (2015).
3. P. Tyagi, S.M. Arveson, W.A. Tisdale; "Colloidal Organohalide Perovskite Nanoplatelets Exhibiting Quantum Confinement," *J. Phys. Chem. Lett.* **6**, 1911-1916 (2015).
4. A.J. Goodman & W.A. Tisdale; "Replay to Comment on Enhancement of Second-Order Nonlinear-Optical Signals by Optical Stimulation," *Phys. Rev. Lett.* **116**, 059402 (2016).

# Structural Dynamics in Complex Liquids Studied with Multidimensional Vibrational Spectroscopy

Andrei Tokmakoff

*Department of Chemistry, James Franck Institute, and Institute for Biophysical Dynamics  
The University of Chicago, Chicago, IL 60637  
E-mail: tokmakoff@uchicago.edu*

The ability of water to integrate charged species into its hydrogen bond (H-bond) network and the rapid transport of this charge, in particular the proton, has made aqueous systems attractive candidates for alternative energy sources such as fuel cells, water oxidation catalysis, and new battery technology. These unique properties of water are derived from its intricate H-bond network which results in strong intra- and intermolecular coupling that span many water molecules, leading to energy transport and dissipation on ultrafast timescales. It has been our aim to develop a molecular-level description of these collective, ultrafast processes in aqueous systems in order to gain a more fundamental understanding of how water stores, converts, and transports electrical, chemical, and thermal energy.

The research conducted over the past year has continued to be driven by the development of new ultrafast laser sources, specifically our plasma-based broadband infrared (BBIR) source which allows us to probe the entire mid-IR in our two-dimensional infrared (2D IR) experiments with sub-70 fs pulses, which is critical for covering the extremely broad IR features and fast dynamics in liquid water. After our successful implementation of this BBIR technology in studying the ultrafast solvation structure and transport dynamics of protons in aqueous acids (*Science*, 2015) and hydroxide (*J. Chem. Phys.*, 2016), our efforts have focused on three main areas: (1) The continued work on understanding water's ultrafast dynamics and coupled motions, and comparison to D<sub>2</sub>O where the strong anharmonic couplings that plague H<sub>2</sub>O are suppressed. (2) The direct observation of how water responds to solute excitation allowing for new insight into the nature of solute-water interactions in both acid and salt solutions. These experimental studies were made possible by using a commercial optical parametric amplifier (*Topas*) with difference frequency generation (DFG) to generate high-intensity, short pulses tunable from 1300-3000 cm<sup>-1</sup>. (3) The development of new theoretical methods in collaboration with Greg Voth (UChicago) to more accurately model and predict the spectroscopic behavior of proton transport in solution.

By expanding the capabilities of our spectrometer, we have been able to probe the dynamics of liquid water more deeply than was previously possible. Essentially, the ability to rapidly collect high signal-to-noise 2D IR spectra has enabled systematic studies of liquid H<sub>2</sub>O, and allowed us to refine our understanding of its molecular dynamics. In particular, we observe almost no temperature dependence of water's dynamical observables which is at odds with intuition. We interpret this in terms of the strong coupling induced by the H-bonding interaction, which significantly distorts the nuclear potential energy surface of the O—H bond and results in motion that is delocalized over multiple molecules. In an effort to comprehend the nature of this delocalization, we have conducted 2D IR depolarization experiments which give spectrally resolved orientational correlations. We interpret frequencies at which the O—H stretch does not depolarize quickly as arising due to less delocalization. Our experiments are consistent with previous theoretical calculations of the delocalization, and we observe more localized behavior for both extremely strong and weak hydrogen bonds. This work was recently selected as a Feature and Cover Article in *J. Chem. Phys.*

To probe the nuclear potential energy surface directly, we have undertaken experiments on the heavier isotopologue of water, D<sub>2</sub>O. We have found that D<sub>2</sub>O is qualitatively different from H<sub>2</sub>O in its molecular dynamics with the former having a behavior that is more in line with a weakly anharmonic system. This is evidenced by a number of factors, with the most notable being the presence of residual symmetric and anti-symmetric stretching in D<sub>2</sub>O, which is not observed in H<sub>2</sub>O. This difference in molecular dynamics guides our understanding of the nuclear potential energy surface, and places a significant constraint on theoretical models. Any theoretical model that can describe liquid water should be able to capture this difference between light and heavy water.

Our previous work on aqueous acids have opened up new avenues for directly measuring the structure and dynamics of proton solvation in water. We have collected 2D IR spectra of 4M HCl pumped at 6  $\mu\text{m}$ , directly exciting both the water bend and the acid bend at 1760  $\text{cm}^{-1}$ . While the acid peak appears as a shoulder on the water bend peak in a linear FTIR spectrum, the acid peak appears distinct from the H<sub>2</sub>O bend and with stronger intensity in 2D IR spectra. The acid bend peak is broad in both  $\omega_1$  and  $\omega_3$ , with no diagonal elongation visible, which means the breadth is dominated by homogeneous broadening. Moreover, the peak shows long-lived anisotropy decay, which can be modeled biexponentially with timescales of 300 fs and 3 ps.

To further characterize the excess proton species, we will be planning experiments with pump pulses tuned to new features in the acid infrared spectrum. First, we plan to tune to 4  $\mu\text{m}$  to pump acid species that contribute to the “continuum” between 1800 and 3000  $\text{cm}^{-1}$ . These vibrations are thought to originate from acidic OH stretches in a wide distribution of local electric fields. Exciting these frequencies will elucidate the nature of the stretching modes in acid species. Finally, we are currently developing methods to improve excitation and detection at lower frequencies, particularly the 1200  $\text{cm}^{-1}$  feature thought to arise from the proton oscillation mode of the Zundel species. The ability to measure the ultrafast properties of this feature will be crucial for directly measuring Grotthuss proton diffusion in liquid water.

Working with Greg Voth to assign the vibrational spectral features for different proton-water complexes in isotopically dilute acid, a mixed quantum-classical spectroscopic model has been developed using the latest multi-state empirical valence bond (MS-EVB 3.2) proton model. We have developed a semi-empirical single oscillator spectroscopic map by constructing the potential energy surface (PES) along the O—H stretch coordinate using DFT calculations on the frozen instantaneous proton-water clusters taken from different timeframes of reactive MS-EVB simulation trajectories. During the proton transfer events the PES changes drastically which results in large fluctuations in the instantaneous transition frequencies. By decomposition of the spectral response into geometrically different sub-ensembles, we have found that the Zundel and Eigen solvation behaves distinctly different. Since the excess charge is more delocalized in the Zundel arrangement, we have observed a continuous frequency red-shift while approaching Zundel-like configurations from Eigen solvation structures. We have also studied the effects of an excess proton in different solvation shells and observed that the excess charge largely modifies the response of the first solvation shell. The contributions to the broad acid continuum to different solvation structures have also been demonstrated.

In order to understand the correlations of vibrational degrees of freedom with transiently solvated proton-water clusters in the case of isotopically pure solution, we have performed mixed quantum-classical harmonic normal mode analysis on the frozen instantaneous proton-water clusters taken from the MS-EVB 3.2 trajectory. We find that with increasing hydrogen bond strength the transition frequency shows a significant red shift. The in-phase stretching mode of the four flanking water molecules in the

Zundel-like species is associated with the excess proton bend response and the proton oscillation band is strongly coupled with the symmetric bend mode of the central  $\text{H}_5\text{O}_2^+$  moiety.

Finally, we have begun to investigate the intermolecular couplings between ions and water in solution. We have focused on aqueous nitrate and carbonate, two isoelectronic ions that are on opposite ends of the Hofmeister series. Key to this work was the ability to pump and probe both the water OH stretch at 3  $\mu\text{m}$  and the ion asymmetric stretches at 7  $\mu\text{m}$ , in particular, following the spectral changes and dynamics of the two cross-peak regions in the 2D IR spectra. Using these cross-peak dynamics, we have found that the strong H-bonding between carbonate and its first hydration shell results in direct mixing of the ion and water vibrational modes yielding highly coupled and correlated intermolecular motion that spans beyond the first shell, as evidenced by the appearance of strong ion-to-water and water-to-ion cross peaks at the earliest waiting times. In contrast, aqueous nitrate displays very weak ion-water cross peaks. In fact, the cross-peak line shapes and dynamics do not point to direct OH stretch-nitrate stretch mixing, but rather to coupling with low-frequency water librational and H-bond distortion modes. This is evidenced by the immediate narrowing of the nitrate stretch distribution upon OH stretch excitation, indicating that a homogenous environment around the ion rapidly forms as fluctuations in the first or second shell waters increase. Moreover, due to the excitonic and delocalized nature of the OH stretch discussed above, we observe that the influence of both these ions on the water H-bond network extends at least into the second hydration shell. This work was recently published in *J. Am. Chem. Soc.* We are beginning to develop a clearer understanding of how the sensitive balance between intra- and intermolecular couplings influence the solvation structure and dynamics of molecular ions. Future work will aim to more definitively answer the controversial question of how ions influence the water H-bond network beyond the first solvation shell, and further investigating the role that coupling to librational and H-bond modes have in the ultrafast processes that distribute energy in aqueous systems.

### DOE Supported Publications 2015–2016

1. “Ultrafast 2D IR spectroscopy of the excess proton in liquid water,” M. Thämer, L. De Marco, K. Ramasesha, A. Mandal and A. Tokmakoff, *Science* **350**, 78–82 (2015).
2. “Vibrational dynamics of aqueous hydroxide solutions probed using broadband 2DIR spectroscopy,” A. Mandal and A. Tokmakoff, *J. Chem. Phys.* **143**, 194501 (2015).
3. “Role of presolvation and anharmonicity in aqueous phase hydrated proton solvation and transport,” R. Biswas, Y.-L. S. Tse, A. Tokmakoff and G. A. Voth, *J. Phys. Chem. B* **120**, 1793–1804 (2016).
4. “Differences in the vibrational dynamics of  $\text{H}_2\text{O}$  and  $\text{D}_2\text{O}$ : Observation of symmetric and antisymmetric stretching vibrations in heavy water,” L. De Marco, W. Carpenter, H. Liu, R. Biswas, J. M. Bowman and A. Tokmakoff, *J. Phys. Chem. Lett.* **7**, 1769–1774 (2016).
5. “Interplay of ion–water and water–water interactions within the hydration shells of nitrate and carbonate directly probed with 2D IR spectroscopy,” J. A. Fournier, W. Carpenter, L. De Marco and A. Tokmakoff, *J. Am. Chem. Soc.* **138**, 9634–9645 (2016).
6. “Anharmonic exciton dynamics and energy dissipation in liquid water from two-dimensional infrared spectroscopy,” L. De Marco, J. A. Fournier, M. Thämer, W. Carpenter and A. Tokmakoff, *J. Chem. Phys.* **145**, 094501 (2016).

# Chemistry of Ionic Species in Aqueous Systems

Marat Valiev

Environmental Molecular Sciences Laboratory and  
Pacific Northwest National Laboratory

902 Battelle Blvd.

Mail Stop K9-90

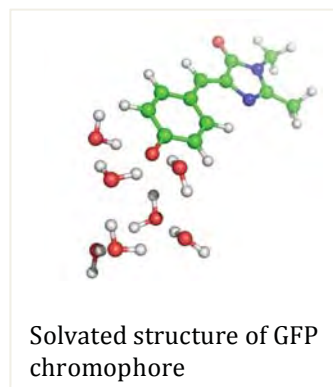
Richland, WA 99352

[marat.valiev@pnl.gov](mailto:marat.valiev@pnl.gov)

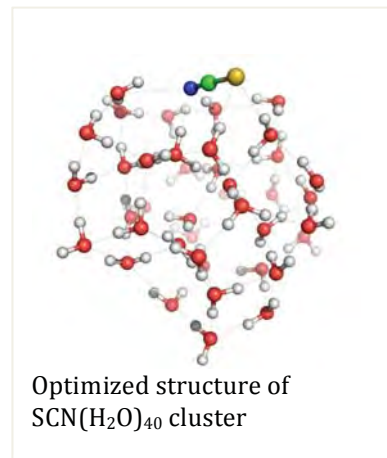
The main goal of our research is to provide molecular based understanding of chemical processes that occur in aqueous solutions, including cluster, bulk, and interfacial environments. Majority of our research activities revolves around ionic and radical molecular complexes. One of our objectives is to understand how electronic structure properties of these solute molecules are affected by the aqueous phase. This is accomplished by performing accurate ab-initio calculations in conjunction with spectroscopy measurements of gas phase, cluster, and bulk systems. This information is then used to gain insight into more complex problems involving combined solute-solvent systems. There, the main challenge lies in identifying proper collective variables that expose the essential properties of the system and ultimately provide predictive and reliable approaches to understand chemistry of ionic solutions.

In this period we have continued our investigation of Green Fluorescent Protein (GFP) chromophore focusing on cluster solvation properties as well as its excited states in bulk solution. Despite extensive experimental and computational studies, there remain many open questions regarding the key fundamental variables that govern the photochemistry of GFP. The analysis of GFP in gas phase, cluster, and bulk aqueous environments provides a unique way to isolate intrinsic chemical properties of the chromophore and track the impact of the environment in a controlled manner. Through selective generation of microsolvated structures of GFP of predetermined size and subsequent analysis of experimental photoelectron spectra by high level ab-initio methods we were able to precisely identify the structure of the system, establish the accuracy of theoretical data, and provide a reliable description of the auto-ionization process as a function of the hydrogen-bonding environment. Our study clearly illustrated that the first few water molecules progressively stabilize the excited state of the chromophore anion against the autodetached neutral state, which should be an important trait for crystallographic water molecules in GFPs that has not been fully explored to date.

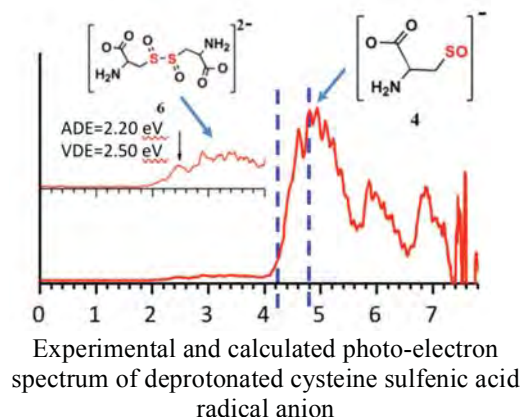
We are continuing our investigation of molecular specific effects in cluster solvation studies. Our main hypothesis is that solute specific effects observed in the bulk environment should be amplified in clusters and thereby provide important insight into relevant collective variables that govern the solvation process. Our methodology is based on the combined theoretical and experimental analysis of electron binding energy as a function of cluster size. Such analysis proved instrumental in understanding solvation



patterns of  $\text{IO}_3^-$  and  $\text{SCN}^-$  molecules. One of the research directions here involves analysis of increasingly larger water clusters, based on newly obtained experimental PES data for  $\text{SCN}^-$  with solvation clusters up to 40 waters. At this size of solvation region we have a unique opportunity to gain insight how cluster solvation transitions into the bulk environment. Our results indicate that in large water clusters  $\text{SCN}^-$  is located on the surface, which confirms as our prior assignment of  $\text{SCN}^-$  as chaotrope species. In addition to rigid anion poly-atomic species, we are also investigating more complex cases involving cation-anion pairs. Cation-anion interactions in aqueous phase are highly specific, i.e. depend on the molecular level of detail, and this specificity results in rich and complex chemistry. One of the systems that we are currently investigating is alkali-carboxylate complex. We have previously studied these systems in gas phase, and this study is focused on the effects of aqueous cluster solvation.



A new research direction we have recently initiated is focused on chemistry sulfur-oxide species. The two classes of systems that we are currently investigating are iodine-sulfur oxides and cysteine sulfenic acid. In the first case, we are focused on  $\text{ISO}_3^-$ ,  $\text{IS}_2\text{O}_3^-$ , and  $\text{IS}_2\text{O}_4^-$  - short-lived intermediates which have been detected interfacial reactions involving aqueous charged droplets of iodine/sulfur oxides. Our results suggests that these anions may be viewed as  $[\text{X}-\text{SO}_3]^-$  complexes with  $\text{X} = \text{I}$ ,  $\text{IS}$ , and  $\text{ISO}$ , respectively, linked by I-S or S-S bonds. In the second case, we are interested in understanding chemistry of disulfide bonds.



Collaborators on this project include Xue-Bin Wang(PNNL), C. J. Mundy (PNNL), S. M. Kathmann(PNNL), G. K. Schenter(PNNL), S. S. Xantheas (PNNL), Sergei Lyman (BNL)

#### Publications:

Valiev, M.; Deng, S. H. M.; Wang, X.-B., How Anion Chaotrope Changes the Local Structure of Water: Insights from Photoelectron Spectroscopy and Theoretical Modeling of  $\text{SCN}^-$  Water Clusters, *Journal of Physical Chemistry B* 2015.

Bhaskaran-Nair, K.; Valiev, M.; Deng, S. H. M.; Shelton, W. A.; Kowalski, K.; Wang, X.-B., Probing microhydration effect on the electronic structure of the GFP chromophore anion: Photoelectron spectroscopy and theoretical investigations. *Journal of Chemical Physics* 2015, 143 (22), 224301.

# Chemical Kinetics and Dynamics at Interfaces

## Cluster Model Investigation of Condensed Phase Phenomena

Xue-Bin Wang

Physical Sciences Division, Pacific Northwest National Laboratory, P.O. Box 999, MS K8-88, Richland, WA 99352. E-mail: [xuebin.wang@pnnl.gov](mailto:xuebin.wang@pnnl.gov)

Additional collaborators include: SHM Deng, GL Hou, WT Borden, SR Kass, CC Cummins, SH Strauss, OV Boltalina, CEH Dessent, ZR Sun, M Valiev, SS Xantheas, K Kowalski

### Program Scope

We aim at obtaining a molecular-level understanding of solution chemistry and condensed phase phenomena using gas phase clusters as model systems. Clusters occupy an intermediate region between gas phase molecules and the condensed states of matter and play an important role in heterogeneous catalysis, aerosol chemistry, and biological processes. We use electrospray ionization (ESI) to generate a wide variety of molecular and ionic clusters to simulate key species involved in the condensed phase reactions and transformations, and characterize them using low temperature, and temperature-controlled negative ion photoelectron spectroscopy (NIPES). Inter- and intra-molecular interactions and their variation as function of size and composition, important to understand complex chemical reactions and nucleation processes in condensed and interfacial phases can be directly obtained. Experiments and *ab initio* calculations are synergistically combined to (1) obtain a molecular-level understanding of the solvation and stabilization of complex singly- and multiply-charged anions important in condensed phases; (2) probe solute specific effects in hydrated anion and neutral clusters; (3) study temperature-dependent conformation changes and isomer populations of complex solvated clusters; (4) quantify thermodynamic driving forces resulting from hydrogen-bonded networks formed in aerosol nucleation processes and enzymatic catalytic reactions; (5) investigate intrinsic electronic structures of environmentally and catalytically important species and reactive diradicals; and (6) understand the molecular processes and initial steps of dissolution of salt molecules in polar solvents. The central theme of this research program lies at obtaining a fundamental understanding of environmental materials and solution chemistry important to many primary DOE missions (waste storage, subsurface and atmospheric contaminant transport, catalysis, etc.), and enhances scientific synergies between experimental and theoretical studies towards achieving such goals.

### Recent Progress

**Molecular Level Probe of Anion- $\pi$  Specific Interactions.** Proposed in theory and confirmed to exist, anion- $\pi$  interactions have been recognized as new and important non-covalent binding forces. Despite extensive theoretical studies, numerous crystal structure identifications, and a plethora of solution phase investigations, anion- $\pi$  interaction strengths that are free from complications of condensed phase environments, have not been directly measured. We conducted a joint photoelectron spectroscopic and theoretical study on this subject, in which *tetraoxacalix[2]arene[2]triazine* **1**, an electron-deficient and cavity self-tunable macrocyclic molecule was used as a charge-neutral host to probe its interactions with a series of anions with distinctly different shapes and charge states (spherical halides  $\text{Cl}^-$ ,  $\text{Br}^-$ ,  $\text{I}^-$ , linear thiocyanate  $\text{SCN}^-$ , trigonal planar nitrate  $\text{NO}_3^-$ , pyramidal iodate  $\text{IO}_3^-$ , and tetrahedral sulfate  $\text{SO}_4^{2-}$ ). The electron binding energies of the resultant gaseous 1:1 complexes (**1**· $\text{Cl}^-$ , **1**· $\text{Br}^-$ , **1**· $\text{I}^-$ , **1**· $\text{SCN}^-$ , **1**· $\text{NO}_3^-$ , **1**· $\text{IO}_3^-$  and **1**· $\text{SO}_4^{2-}$ ) were directly measured experimentally, exhibiting substantial non-covalent interactions with pronounced anion specific effects. The binding strengths between  $\text{Cl}^-$ ,  $\text{NO}_3^-$ ,  $\text{IO}_3^-$  and **1** are found to be strongest among all singly charged anions, amounting to *ca.* 30 kcal/mol, but only about 40% of that between **1** and  $\text{SO}_4^{2-}$ . Quantum chemical calculations reveal that all anions reside in the center of the cavity of **1** with anion- $\pi$  binding motif in the complexes' optimized structures, where **1** is

seen to be able to self-regulate its cavity structure to accommodate anions of different geometries and three-dimensional shapes. Electron density surface and charge distribution analyses further support anion- $\pi$  binding. The calculated binding energies of the anions and **1** nicely reproduce the experimentally estimated electron binding energy increase. This work illustrates that size-selective photoelectron spectroscopy combined with theoretical calculations represent a powerful technique to probe anion- $\pi$  interactions and has potential to provide quantitative guest-host molecular binding strengths and unravel fundamental insights in specific anion recognition (J Zhang, B Zhou, ZR Sun, and XB Wang. *Phys. Chem. Chem. Phys.* 2015, 17, 3131-3141).

**Photoelectron Spectroscopic Studies of the Green Fluorescent Protein (GFP) Chromophore and Microhydration Effect on its Electronic Structure:** We reported a NIPES study of the model green fluorescent protein (GFP) chromophore anion. Despite the considerable size and low symmetry of the molecule, well resolved vibrational structures were obtained with the 0-0 transition being the most intense peak, from which the adiabatic (ADE) and vertical detachment energy (VDE) were determined, both higher than the energy level of the bright excited  $S_1$  state of the chromophore anion. Hence our study reveals unambiguously the excited  $S_1$  state being a true bound state, a key parameter that determines fluorescence efficiency and the photoresponse of GFP (SHM Deng, XY Kong, GX Zhang, Y Yang, WJ Zheng, ZR Sun, DQ Zhang, and XB Wang, *J. Phys. Chem. Lett.* 2014, 5, 2155-2159). The photophysics of the GFP chromophore is also critically dependent on its local structure and environment. In spite of extensive experimental and computational studies, there remain many open questions regarding the key fundamental variables that govern the photoresponse of GFP. One outstanding problem is the role of autoionization as a possible relaxation pathway of the excited state under different environmental conditions. This issue was considered in our recent work through combined experimental and theoretical studies of microsolvated clusters of the GFP chromophore anion. Through selective generation of microsolvated structures of predetermined size and subsequent analysis of experimental photoelectron spectra by high level ab initio methods we are able to precisely identify the structure of the system, establish the accuracy of theoretical calculations, and provide a reliable description of the auto-ionization process as a function of the hydrogen-bonding environment. Our study clearly illustrates that the first few water molecules progressively stabilize the excited state of the chromophore anion against the autodetached neutral state, which should be an important trait for crystallographic water molecules in GFPs that has not been fully explored to date (K Bhaskaran-Nair, M Valiev, SH Deng, WA Shelton, K Kowalski, and XB Wang. *J. Chem. Phys.* 2015, 143, 224301-1-6, 2015).

**Probe Electronic Structures and Electron Affinities of Environmentally Important Species – the  $CO_3$  Radical Anion ( $CO_3^{\cdot-}$ ):** Carbon trioxide,  $CO_3$ , is an unusual molecule with a long history. It is important in both atmospheric chemistry and astrochemistry as an intermediate in the photoreaction of  $O_3$  with  $CO_2$  and as a reactive intermediate in the photoreaction of  $CO_2$  with itself. Despite extensive experimental and theoretical studies, surprisingly, fundamental information about the electronic structure and electron affinity of  $CO_3$  has not yet been directly measured. We report the first NIPE spectrum of  $CO_3^{\cdot-}$ . The  $CO_3$  radical anion ( $CO_3^{\cdot-}$ ) has been formed by electrospraying carbonate dianion ( $CO_3^{2-}$ ) into the gas phase. The NIPE spectrum of  $CO_3^{\cdot-}$  shows that, unlike the isoelectronic trimethylenemethane [ $C(CH_2)_3$ ],  $D_{3h}$  carbon trioxide ( $CO_3$ ) has a singlet ground state. From the NIPE spectrum, the electron affinity of  $D_{3h}$  singlet  $CO_3$  was, for the first time, directly determined to be  $EA = 4.06 \pm 0.03$  eV, and the energy difference between the  $D_{3h}$  singlet and the lowest triplet was measured as  $\Delta E_{ST} = -17.8 \pm 0.9$  kcal/mol. The obtained electronic structure information and electron affinity may help to understand the critical roles of  $CO_3$  in  $CO_2$  chemical transformations for long term sequestration (DA Hrovat, GL Hou, B Chen, XB Wang, and WT Borden, *Chem. Sci.* 2016, 7, 1142-1150).

## Future Directions

The main thrust of our BES program will continue to be on cluster model studies of condensed phase phenomena in the gas phase. The experimental capabilities that we have developed give us the

opportunity to attack a broad range of fundamental chemical physics problems pertinent to ionic solvation, solution chemistry, homogeneous / heterogeneous catalysis, aerosol chemistry, biological processes, and material synthesis. The ability to cool and control ion temperature enables us to study different isomer populations and conformation changes of environmentally important hydrated clusters. Another major direction is to use gaseous clusters to model ion-specific interactions in solutions, ion transport, and ion-receptor interactions in biological systems, and initial nucleation processes relevant to atmospheric aerosol formation.

### References to Publications of DOE CPIMS Sponsored Research (2014 - present)

1. J Zhang, P Yang, ZR Sun, and XB Wang, "Covalently Bound Tetracoordinated Organoborons as Superhalogens: A Combined Negative Ion Photoelectron Spectroscopy and Theoretical Study", *J. Phys. Chem. A* 118, 8074-8080 (2014).
2. A Shokri, SHM Deng, XB Wang, and SR Kass, "Molecular Recognition: Preparation and Characterization of Two Tripodal Anion Receptors", *Organic Chemistry Frontiers* 1, 54-61 (2014).
3. B Chen, DA Hrovat, SHM Deng, J Zhang, XB Wang, and WT Borden, "The Negative Ion Photoelectron Spectrum of meta-Benzoquinone Radical Anion (MBQ<sup>-</sup>): A Joint Experimental and Computational Study", *J. Am. Chem. Soc.* 136, 3589-3596 (2014).
4. TT Clikeman, EV Bukovsky, IV Kuvychko, LK San, SH M Deng, XB Wang, YS Chen, SH Strauss, and OV Boltalina, "Poly(trifluoromethyl)azulenes: Structures and Acceptor Properties" *Chem. Comm.* 50, 6263-6266 (2014).
5. SHM Deng, XY Kong, GX Zhang, Y Yang, WJ Zheng, ZR Sun, DQ Zhang, and XB Wang, "Vibrationally Resolved Photoelectron Spectroscopy of the Model GFP Chromophore Anion Revealing the Photoexcited S<sub>1</sub> State Being Both Vertically and Adiabatically Bound against the Photodetached D<sub>0</sub> Continuum" *J. Phys. Chem. Lett.* 5, 2155-2159 (2014).
6. SHM Deng, GL Hou, XY Kong, M Valiev, and XB Wang, "Examining the Amine Functionalization in Dicarboxylates: Photoelectron Spectroscopy and Theoretical Studies of Aspartate and Glutamate" *J. Phys. Chem. A* 118, 5256-5262 (2014).
7. M Samet, XB Wang, and SR Kass, "A Preorganized Hydrogen Bond Network and Its Effect on Anion Stability" *J. Phys. Chem. A* 118, 5989-5993 (2014).
8. B Chen, DA Hrovat, R West, SHM Deng, XB Wang, and WT Borden, "The Negative Ion Photoelectron Spectrum of Cyclopropane-1,2,3-Trione Radical Anion, (CO)<sub>3</sub><sup>-</sup> – A Joint Experimental and Computational Study" *J. Am. Chem. Soc.* 136, 12345-12354 (2014).
9. XB Wang and Steven R. Kass, "Anion A<sup>-</sup> • HX Clusters with Reduced Electron Binding Energies: Proton vs Hydrogen Atom Relocation upon Electron Detachment", *J. Am. Chem. Soc.* 136, 17332-17336 (2014).
10. TT Clikeman, SHM Deng, AA Popov, XB Wang, SH Strauss and OV Boltalina. "Fullerene Cyanation does not Always Increase Electron Affinity: An Experimental and Theoretical Study". *Phys. Chem. Chem. Phys.* 17, 551-556 (2015).
11. J Zhang, B Zhou, ZR Sun, and XB Wang. "Photoelectron Spectroscopy and Theoretical Studies of Anion- $\pi$  Interactions: Binding Strength and Anion Specificity". *Phys. Chem. Chem. Phys.* 17, 3131-3141 (2015).
12. LK San, EV Bukovsky, BW Larson, JB Whitaker, SHM Deng, N Kopidakis, G Rumbles, AA Popov, YS Chen, XB Wang, OV Boltalina and SH Strauss. "A Faux Hawk Fullerene with PCBM-like Properties" *Chem. Sci.* 6, 1801-1815 (2015).
13. SHM Deng, XY Kong, and XB Wang. "Probing the Early Stages of Salt Nucleation – Experimental and Theoretical Investigations of Sodium/Potassium Thiocyanate Cluster Anions", *J. Chem. Phys.* 142, 024313-1-9 (2015).
14. J Zhang, ZR Sun, and XB Wang. "Examining the Critical Roles of Protons in Facilitating Oxidation of Chloride Ions by Permanganates: A Cluster Model Study", *J. Phys. Chem. A* 119, 6244-6251 (2015).
15. DA Hrovat, GL Hou, XB Wang, and WT Borden. "Negative Ion Photoelectron Spectroscopy Confirms the Prediction that 1,2,4,5-Tetraoxatetramethylenebenzene Has a Single Ground State", *J. Am. Chem. Soc.* 137, 9094-9099 (2015).
16. A Sen, GL Hou, XB Wang, C Dessent. "Electron Detachment as a Probe of Intrinsic Nucleobase Dynamics in Dianion-Nucleobase Clusters: Photoelectron Spectroscopy of the Platinum II Cyanide Dianion Bound to Uracil, Thymine, Cytosine and Adenine", *J. Phys. Chem. B.* 119, 11626-11631 (2015).

17. TT Clikeman, EV Bukovsky, XB Wang, YS Chen, G Rumbles, SH Strauss, OV Boltalina. "Core Perylene Diimide Designs via Direct Bay and Ortho (Poly)trifluoromethylation: Synthesis, Isolation, X-ray Structures, Optical and Electronic Properties", *Eur. J. Org. Chem.* 6641-6654 (2015).
18. WL Li, Y Li, CQ Xu, XB Wang, E Vorpagel, and J Li. "Periodicity, Electronic Structures, and Bonding of Gold Tetrahalides  $[\text{AuX}_4]^-$  ( $X = \text{F}, \text{Cl}, \text{Br}, \text{I}, \text{At}, \text{Uus}$ )", *Inorg. Chem.* 54, 11157-11167 (2015).
19. A Sen, EM. Matthews, GL Hou, XB Wang, and CEH Dessent. "Photoelectron Spectroscopy of Hexachloroplatinate-nucleobase Complexes: Nucleobase Excited State Decay Observed via Delayed Electron Emission", *J. Chem. Phys.* 143, 184307-1-8 (2015).
20. K Bhaskaran-Nair, M Valiev, SH Deng, WA Shelton, K Kowalski, and XB Wang. "Probing Microhydration Effect on the Electronic Structure of the GFP Chromophore Anion: Photoelectron Spectroscopy and Theoretical Investigations" *J. Chem. Phys.* 143, 224301-1-6, 2015 (**Featured on Cover, Dec. 14, 2015 Issue**).
21. M Valiev, SH Deng, and XB Wang. "How Anion Chaotrope Changes the Local Structure of Water: Insights from Photoelectron Spectroscopy and Theoretical Modeling of  $\text{SCN}^-$  – Water Clusters", *J. Phys. Chem. B.* 120, 1518-1525 (2016).
22. KC Rippy, EV Bukovsky, TT Clikeman, YS Chen, GL Hou, XB Wang, AA Popov, OV Boltalina, and SH Strauss. "Copper Causes Regiospecific Formation of  $\text{C}_4\text{F}_8$ -Containing Six-Membered Rings and their Defluorination/Aromatization to  $\text{C}_4\text{F}_4$ -Containing Rings in Triphenylene/1,4- $\text{C}_4\text{F}_8\text{I}_2$  Reactions" *Chem. Eur. J.* 22, 874-877 (2016).
23. KP Castro, TT Clikeman, NJ DeWeerd, EV Bukovsky, KC Rippy, IV Kuvychko, GL Hou, YS Chen, XB Wang, SH Strauss, and OV Boltalina. "Incremental Tuning Up of Fluorous Phenazine Acceptors" *Chem. Eur. J.* 22, 3930-3936 (2016).
24. DA Hrovat, GL Hou, B Chen, XB Wang, and WT Borden. "Negative Ion Photoelectron Spectroscopy Confirms the Prediction that  $D_{3h}$  Carbon Trioxide ( $\text{CO}_3$ ) Has a Singlet Ground State", *Chem. Sci.* 7, 1142-1150 (2016).
25. GL Hou, XT Kong, M Valiev, L Jiang and XB Wang, "Probing the Early Stages of Solvation of cis-Pinate Dianions by Water, Acetonitrile, and Methanol: a Photoelectron Spectroscopy and Theoretical Study" *Phys. Chem. Chem. Phys.* 18, 3628-3637 (2016).
26. A Shokri, XB Wang, Y Wang, GA O'Doherty, and SR Kass. "Flexible Acyclic Polyol-Chloride Anion Complexes and their Characterization by Photoelectron Spectroscopy and Variable Temperature Binding Constant Determinations", *J. Phys. Chem. A* 120, 1661-1668 (2016).
27. GL Hou, M Valiev, and XB Wang. "Deprotonated dicarboxylic acid homodimers: hydrogen bonds and atmospheric implications", *J. Phys. Chem. A* 120, 2342-2349 (2016).
28. GL Hou, B Chen, WJ Transue, DA Hrovat, CC Cummins, WT Borden, and XB Wang. "Negative Ion Photoelectron Spectroscopy of  $\text{P}_2\text{N}_3^-$ : Electron Affinity and Electronic Structures of  $\text{P}_2\text{N}_3^-$ ", *Chem. Sci.* 7, 4667-4675 (2016).
29. X Liu, GL Hou, XF Wang, and XB Wang. "Negative Ion Photoelectron Spectroscopy Reveals Remarkable Noninnocence of Ligands in Nickel Bis(dithiolene) Complexes  $[\text{Ni}(\text{dddt})_2]^-$  and  $[\text{Ni}(\text{edo})_2]^-$ ", *J. Phys. Chem. A* 120, 2854-2862 (2016).
30. WJ Transue, A Velian, M Nava, MA Martin-Drumel, CC Womack, J Jiang, GL Hou, XB Wang, MC McCarthy, RW Field, CC Cummins. "A Molecular Precursor to Phosphaethyne and Its Application in Synthesis of the Aromatic 1,2,3,4-Phosphatriazololate Anion." *J. Am. Chem. Soc.* 138, 6731-6734 (2016).
31. H Wen, GL Hou, YR Liu, XB Wang, W Huang. "Examining the Structural Evolution of Bicarbonate-Water Clusters: Insights from Photoelectron Spectroscopy, Basin-Hopping Structural Search, and Comparison with Available IR Spectral Studies." *Phys. Chem. Chem. Phys.* 18, 17470-17482 (2016).
32. GL Hou, LJ Li, SH Li, ZM Sun, X Gao, XB Wang. "Regioisomer-Specific Electron Affinities and Electronic Structures of  $\text{C}_{70}$  para-Adducts at Polar and Equatorial Positions with (Bromo)Benzyl Radicals: Photoelectron Spectroscopy and Theoretical Study." *Phys. Chem. Chem. Phys.* 18, 18683-18686 (2016).
33. GL Hou, B Chen, WJ Transue, DA Hrovat, CC Cummins, WT Borden, XB Wang. "A Joint Experimental and Computational Study of the Negative Ion Photoelectron Spectroscopy of the 1-Phospha-2,3,4-triazololate Anion,  $\text{HCPN}_3^-$ " *J. Phys. Chem. A* 120, 6228-6235 (2016).

## Free Radical Reactions of Hydrocarbons at Aqueous Interfaces

Principal Investigator: Kevin R. Wilson

Lawrence Berkeley National Laboratory, 1 Cyclotron Road, MS 6R2100, Berkeley, CA 94720

Email: [krwilson@lbl.gov](mailto:krwilson@lbl.gov)

**Program Scope and Long Term Objectives:** This project will probe the surface chemistry of organic molecules residing on nanometer and micron-sized aqueous droplets exposed to gas phase hydroxyl radicals using atmospheric pressure surface sensitive mass spectrometry and ambient pressure photoelectron spectroscopy. This program aims to:

*Quantify the link between molecular structure, phase and surface reactivity at aqueous and organic interfaces using aerosols of nanoparticles and micron-sized droplets.*

This work broadly supports the Department of Energy's Basic Energy Sciences program to better assess, mitigate and control the efficiency, utilization, and environmental impacts of energy use. This work seeks a rigorous molecular understanding of how heterogeneous reaction pathways lead to either bulk solvation of a surface active organic molecule or its removal from the interface through decomposition into gas phase products. Understanding these fundamental processes are critical for predicting the chemical fate of hydrocarbon byproducts of energy use and consumption.

**Recent Progress:** During the last funding period we have focused on the completing our work on the elucidating the interfacial chemistry of cloud droplet formation on organic aerosols. We have completed our measurements and analysis. We observed unexpectedly that droplet sizes measured at cloud activation conditions were 40-60% larger than predicted by theory assuming that the organic material is dissolved inside the droplet bulk. Our model analysis of the experimental results revealed a new interfacial mechanism for cloud droplet formation on organic rich aerosols. We incorporated a monolayer equation of state and isotherm (known in previous literature as the compressed film model) into Köhler Theory (an established approach to predict cloud droplet formation). This model explains the larger cloud droplets that form at activation, and showed how interfacial molecules can depress surface tension and fundamentally alter the relationship between the quantity of water vapor in the gas phase and the resulting droplet size. In fact the role of interfacial organic molecules is somewhat subtle, in that surface tension by these molecules doesn't appreciable enhance cloud droplet formation, but rather increases the hygroscopicity (i.e. water content) of the aerosol by allowing it to grow larger than the simple case of bulk dissolution. This work shows that current cloud droplet formation parameterizations (which neglect surface chemistry) used in climate and region models is based, for many aerosol types, on incorrect physics. In our manuscript we show how parameterizations based on this new mechanism (compressed film model of cloud droplet activation) could be implemented in such models.

We have completed and published our first results from our aerosol optical tweezer instrument. In this work we develop a new approach that combines single droplets confined in an optical trap with isotopic exchange ( $D_2O/H_2O$ ). This approach allows us to measure the water diffusion

coefficient over a broad range ( $D_w \sim 10^{-12} - 10^{-17} \text{ m}^2 \text{ s}^{-1}$ ) for viscous organic liquids (citric acid, sucrose and shikimic acid) and inorganic gels (magnesium sulfate,  $\text{MgSO}_4$ ). This approach is integral to our larger effort to understand the coupling and feedbacks between surface reactions and diffusive transport in ultra-viscous, glassy and amorphous gel phases.

We have also continued our work into how the structure of an organic molecule, in particular in the presence of hydroxyl groups, controls the heterogeneous reaction mechanism of oxygenated organic compounds. This work investigates the OH-radical initiated oxidation of aqueous tartaric acid ( $\text{C}_4\text{H}_6\text{O}_6$ ) droplets using an aerosol flow tube reactor. The aerosol mass spectra reveal that four major reaction products are formed: a single  $\text{C}_4$  functionalization product ( $\text{C}_4\text{H}_4\text{O}_6$ ) and three  $\text{C}_3$  fragmentation products ( $\text{C}_3\text{H}_4\text{O}_4$ ,  $\text{C}_3\text{H}_2\text{O}_4$ , and  $\text{C}_3\text{H}_2\text{O}_5$ ). The  $\text{C}_4$  functionalization product does not originate from peroxy radical self-reactions, but instead forms via a  $\alpha$ -hydroxylperoxy radical intermediate produced from the OH abstraction at the tertiary carbon site. The proximity of a hydroxyl group to the peroxy moiety enhances the unimolecular  $\text{HO}_2$  elimination from the  $\alpha$ -hydroxylperoxy intermediate to form the reaction products we observe. These results are in contrast with our previous work on two structurally related dicarboxylic acids which lack a hydroxyl group (succinic acid and 2,3-dimethylsuccinic acid). Together these results will provide a more comprehensive picture as to how the identity and location of functional groups (i.e. methyl vs. hydroxyl groups) alters heterogeneous OH reaction mechanisms.

Finally, we have made progress on building and coupling a two ring electrodynamic balance (EDB) with atmospheric pressure extractive electrospray ionization mass spectrometry. The EDB is designed to trap “clouds” of micron-sized droplets for long periods of time (seconds to days). The ability to trap droplets of these long time scales (hours to days) allows us to access heterogeneous reaction mechanisms that are not dominated by peroxy + peroxy radical reactions. Key science questions that we will address is how unimolecular peroxy radical reactions compete with bimolecular reactions at aqueous interfaces. To accomplish this requires coupling the EDB to our existing Orbitrap mass spectrometer to obtain single droplet mass spectra. We have developed such an interface in which we can simultaneously store 10-20 droplets for hours in the trap and then eject them on demand from the trap into an extractive electrospray ionization source. We have measured single droplet mass spectra for a test reaction (oleic acid droplets + ozone) over many hours and succeeded in observing the correct products of the reaction as well as the correct heterogeneous reaction rate.

**Future Plans:** Moving beyond our prototype two ring EDB we will design and build a more sophisticated version based upon a linear quadrupole design. This quad design has superior particle stability enabling in addition to mass spectrometry, spectroscopic (i.e. Raman and dynamic light scattering) probing of single droplet arrays (100's of droplets). The approach will utilize the same mass spectrometry interface described above. The science objectives of this instrument will again be focused on understanding how unimolecular reaction of free radical intermediates formed at droplet surfaces compete with bimolecular reactions and depend upon the water content of the droplet. Water can participate directly or catalytically in free radical reaction

mechanisms as well as controlling the transport properties in the aerosol (glassy vs. fluid droplets.) In this respect we hope to obtain a detailed molecular picture of the complex coupling between surface reactions and the availability and mobility of interfacial organic reactants.

We have also begun detailed measurements of heterogeneous reacto-diffusive lengths. The depth below the surface that a gas phase species (OH or ozone) can travel before it reacts is an elementary step in all multiphase chemical reactions. To measure these nanometer sized reacto-diffusive lengths we will create core shell aerosols. The dimensions of the core and shell can be precisely controlled with nanometer resolution using differential mobility analysis. Using a combination of reactive and unreactive shells and selecting a core material that is reactive to OH or ozone we will measure the transmission probability of OH and ozone as a function of shell thickness. Simple Fickian models of reaction + diffusion will be used to interpret the data measured for a variety of systems providing value data necessary to constrain larger scale 3-D reaction diffusion simulations of multiphase chemistry.

#### **Publications Acknowledging Support of the DOE Office of Science Early Career Award:**

1. L. Lee and K.R. Wilson, “*The Reactive–Diffusive Length of OH and Ozone in Model Organic Aerosols*”, J. Phys. Chem. A, **120**, 6800 (2016)
2. C. T. Cheng, M. Chan, and K. R. Wilson, “*Importance of Unimolecular HO<sub>2</sub> Elimination in the Heterogeneous OH Reaction of Highly Oxygenated Tartaric Acid Aerosol*,” J. Phys. Chem. A., **120**, 5887, DOI: 10.1021/acs.jpca.6b05289 (2016)
3. C. R. Ruehl, J. Davies and K. R. Wilson, “*An interfacial mechanism for cloud droplet formation on organic aerosols*,” Science, **351**, 1447, DOI: 10.1126/science.aad4889 (2016)
4. N. K. Richards-Henderson, A. H. Goldstein, and K. R. Wilson, “*Sulfur Dioxide Accelerates the Heterogeneous Oxidation Rate of Organic Aerosol by Hydroxyl Radicals*,” Environ. Sci. Technol., DOI: 10.1021/acs.est.5b05369 (2016, accepted)
5. J. Davies and K. R. Wilson, “*Raman Spectroscopy of Isotopic Water Diffusion in Ultraviscous, Glassy, and Gel States in Aerosol by Use of Optical Tweezers*,” Anal. Chem., **88**, 2361, DOI: 10.1021/acs.analchem.5b04315 (2016)
6. J. Davies and K. R. Wilson, “*Nanoscale interfacial gradients formed by the reactive uptake of OH radicals onto viscous aerosol surfaces*,” Chem. Sci., **6**, 7020, DOI: 10.1039/C5SC02326B (2015)
7. J. H. Kroll, C. Y. Lim, S. H. Kessler, and K. R. Wilson, “*Heterogeneous Oxidation of Atmospheric Organic Aerosol: Kinetics of Changes to the Amount and Oxidation State of Particle Phase Carbon*,” J. Phys. Chem. A., **119**, 10767, DOI: 10.1021/acs.jpca.5b06946 (2015)
8. N. Richards-Henderson, A. H. Goldstein, and K. R. Wilson, “*Large Enhancement in the Heterogeneous Oxidation Rate of Organic Aerosols by Hydroxyl Radicals in the Presence of Nitric Oxide*,” J. Phys. Chem. Lett., **6**, 4451, DOI: 10.1021/acs.jpcllett.5b02121 (2015)
9. C. T. Cheng, M. N. Chan, and K. R. Wilson, “*The Role of Alkoxy Radicals in the*

*Heterogeneous Reaction of Two Structural Isomers of Dimethylsuccinic Acid,*” Phys. Chem. Chem. Phys., **17**, 25309, DOI: 10.1039/C5CP03791C (2015)

10. H. Zhang, D. Worton, S. Shen, T. Nah, G. Isaacman-VanWertz, K.R. Wilson, and A.H. Goldstein, "*Fundamental Timescales Governing Organic Aerosol Multiphase Partitioning and Oxidative Aging*", submitted, 2015.

11. M. R. Canagaratna, P. Massoli, E. C. Browne, J. P. Franklin, K. R. Wilson, T. B. Onasch, T. W. Kirchstetter, E. C. Fortner, C. E. Kolb, J. T. Jayne, J. H. Kroll, and D. R. Worsnop, "*Chemical Compositions of Black Carbon Particle Cores and Coatings via Soot Particle Aerosol Mass Spectrometry with Photoionization and Electron Ionization,*" J. Chem. Phys. A., DOI: 10.1021/jp510711u (2015)

12. F. A. Houle, W. D. Hinsberg and K. R. Wilson, "*Oxidation of a model alkane aerosol by OH radical: the emergent nature of reactive uptake,*" Phys. Chem. Chem. Phys., DOI: 10.1039/C4CP05093B (2015).

13. A. A. Wiegel, K. R. Wilson, W. D. Hinsberg and F. A. Houle, "*Stochastic methods for aerosol chemistry: a compact molecular description of functionalization and fragmentation in the heterogeneous oxidation of squalane aerosol by OH radicals,*" Phys. Chem. Chem. Phys., DOI: 10.1039/C4CP04927F (2015).

14. T. Nah, H. Zhang, D. R. Worton, C. Ruehl, B. B. Kirk, A. Goldstein, S. R. Leone, and K. R. Wilson, "*Isomeric Product Detection in the Heterogeneous Reaction of Hydroxyl Radicals with Aerosol Composed of Branched and Linear Unsaturated Organic Molecules,*" J. Phys. Chem. A, DOI: 10.1021/jp508378z (2014).

15. M.N. Chan, H. Zhang, A. H. Goldstein, and K. R. Wilson, "*The Role of Water and Phase in the Heterogeneous Oxidation of Solid and Aqueous Succinic Acid Aerosol by Hydroxyl Radicals,*" J. Phys. Chem. C, DOI: 10.1021/jp5012022 (2014).

16. C. Ruehl and K.R. Wilson, "*Surface Organic Monolayers Control the Hygroscopic Growth of Submicron Particles at High Relative Humidity*", J. Phys. Chem. A, **118**, 3952, DOI: 10.1021/jp502844g (2014).

# Non-Empirical and Self-Interaction Corrections for DFTB: Towards Accurate Quantum Simulations for Large Mesoscale Systems

Bryan M. Wong

Department of Chemical & Environmental Engineering and Materials Science & Engineering Program, University of California-Riverside, Riverside, CA 92521

[bryan.wong@ucr.edu](mailto:bryan.wong@ucr.edu)

## 1. Program Scope

Mesoscale science has garnered significant attention as it builds even further on the enormous foundation of nanoscience created by the scientific community over the last decade. At mesoscale dimensions, the emergence of collective behavior naturally arises as interactions between disparate degrees of freedom (electronic, mechanical, and chemical phenomena all acting in concert) become dominant. While classical molecular dynamics can handle hundreds of thousands of atoms, it cannot provide a first-principles based description of mesoscale systems at the quantum level. At the other extreme, conventional Kohn-Sham DFT methods can probe the true quantum nature of chemical systems; however, these methods cannot tackle the large sizes relevant to mesoscale phenomena. The density functional tight binding (DFTB) formalism utilized in this project provides a viable approach for probing these mesoscale systems at a quantum mechanical level of detail. Moreover, the new non-empirical corrections and GPU enhancements implemented in this project will enable a detailed assessment of the importance of quantum effects in mesoscale processes, creating an exciting opportunity for BES leadership in these large, complex systems.

To address these complex mesoscale systems, this project has two complementary but parallel thrusts: (1) introducing self-interaction corrections for improving the accuracy of DFTB and (2) implementing massively-parallelized GPUs for calculating the electron dynamics of these large systems. Improving the accuracy of DFTB is vital since exchange-correlation effects can still remain very strong in mesoscale systems, and it is crucial to incorporate *quantum-based non-empirical corrections* in DFTB to treat these large, complex systems. At the same time, enhancing the computational efficiency of DFTB is also essential since optimal computational performance is required for addressing the large size scales associated with mesoscale processes. Within the broader computational objectives of DOE-BES, the DFTB enhancements proposed in this project will also lay the computational groundwork for addressing electron dynamics in mesoscale materials and processes. The DOE has specifically identified electron dynamics in mesoscale systems as a “*Grand Challenge in Basic Energy Sciences*” and have called for a deeper understanding of mesoscale dynamics in complex systems. To further our understanding of these large mesoscale structures, this project will implement two different (but complementary) non-empirical corrections *and* GPU enhancements to the DFTB formalism described further below.

## 2. Recent Progress

The start date of this project was 08/15/2016, and during the past month we have focused our initial efforts on the second thrust of this project, specifically GPU parallelization for calculating the electron dynamics of large systems. The specific material systems we have chosen are large metallic nanocluster-molecule systems and nanocluster arrays. In particular, we are harnessing GPUs and implementing new computational routines to understand plasmonic interactions and collective many-body excitations in these metallic nanoparticles on an atomistic scale with DFTB. We have chosen metallic nanoparticles as an ideal system for GPU parallelization since our

understanding of the detailed quantum-mechanical mechanisms in these collective excitations is severely limited due to the sheer size and complexity of plasmonic nanostructure-molecule interfaces. Specifically, while classical electrodynamics methods can handle metallic nanostructures at a continuum level, they cannot provide a first-principles based description of plasmonic systems at the quantum level, which is *absolutely crucial for describing electron tunneling processes at sub-nanometer gaps*. At the other extreme, conventional linear-response time-dependent methods can probe the true quantum nature of chemical systems; however, these methods cannot tackle the large sizes relevant to *collective excitations* in plasmonic materials. Recently, using real-time time-dependent DFTB (TDDFTB), we have shown that collective plasmonic excitations produce large electric fields on metallic surfaces, leading to dramatic enhancements in the optical response. In particular, the largest electric field enhancements occur on regions of highest local curvature (i.e., at the corners of the structure), yielding “hot spots” on the surface of the metal nanoparticle (cf. **Figure 1**). As such,

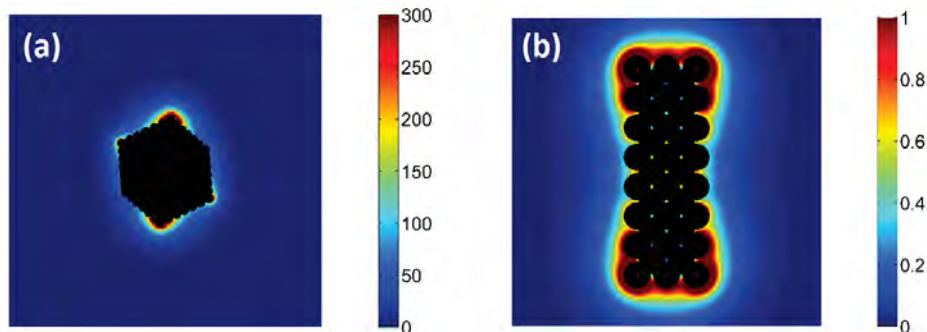


**Figure 1.** Electric field enhancement obtained from RT-TDDFTB for (a) an icosahedral-shaped sodium nanoparticle and (b) a rod-shaped sodium nanoparticle.

the development of GPU-enhanced electron dynamics methods that can resolve these features for large systems plays an important step in predicting and understanding the dynamics in these complex plasmonic systems.

To probe the dynamics of these large systems using massively-parallelized GPUs, we calculate the time evolution of the density matrix from a numerical integration of the Liouville-Von Neumann equation of motion:

$$\frac{\partial \hat{P}}{\partial t} = -\frac{i}{\hbar} (S^{-1} \cdot \hat{H}(\hat{P}, t) \cdot \hat{P} - \hat{P} \cdot \hat{H}(\hat{P}, t) \cdot S^{-1}), \quad (1)$$

where  $\hat{P}$  is the DFTB density matrix, and  $S$  is the overlap matrix, which is required due to the non-orthogonal DFTB basis functions. For extremely large systems, the memory requirements for storing the DFTB density matrices exceeds the GPU global memory, which severely limits the types of systems that can be studied. Currently, we are implementing and evaluating three custom algorithms for out-of-core matrix-matrix multiplication designed to address this problem for larger systems. Within these three different algorithms, we split the multiplicands into block matrices and perform the multiplication as follows:

$$[A][B] = \begin{bmatrix} A_1 \\ A_2 \end{bmatrix} [B_1 \quad B_2] = \begin{bmatrix} A_1 B_1 & A_1 B_2 \\ A_2 B_1 & A_2 B_2 \end{bmatrix}. \quad (2)$$

In **Algorithm 1**, memory is allocated for one submatrix of the first multiplicand and one submatrix of the second. The single multiply is performed, and memory is copied back to the product matrix before moving on to the next computation. Of the three algorithms tested, this uses the least memory of the algorithms, but generates the most memory transfer operations as we split the matrix into more submatrices. In **Algorithm 2**, memory is allocated for one submatrix of the first multiplicand and the entire second multiplicand. Using this additional memory, we are able

to launch all of the kernels for one row group at once. This allows for better performance at the cost of additional memory requirements. Finally, for **Algorithm 3**, we modified the first algorithm and pipelined it with CUDA streams, with each thread in the operation having a corresponding CUDA stream. This increases the performance of the first algorithm in most cases when the number of threads and streams is optimal for the number of submatrices and the size of the problem. A downside of this approach is that this algorithm uses more memory than the first on both the host and the GPU, because each thread or stream needs a context to work in.

Using these custom GPU algorithms, we have calculated the absorption spectrum of extremely large gold nanoparticles obtained from the Fourier transform of the time-dependent dipole moment after deconvolution of the applied electric field (cf. **Figure 2**). It is worth mentioning that it is computationally prohibitive to obtain these results with conventional Casida-type TDDFT methods due to the immense size of these systems, whereas the entire spectrum can be directly obtained with the RT-TDDFTB approach. Most importantly, as opposed to frequency-domain calculations common in linear-response TD-DFT, it is relatively straightforward to parallelize the time-propagation steps on GPUs. We are still evaluating the efficiencies in each of the three different algorithms, and our preliminary assessment is as follows: Algorithm 1, though a naive approach, works very well, and actually outperforms the other two algorithms in certain cases. However, as the matrices get very large, it becomes prohibitive to perform the multiplication with a small number of submatrices, and the algorithm's performance subsequently suffers. Algorithm 2 exhibits the best performance for multiplications where it can store one of the multiplicands in GPU memory; however, once that size is exceeded, algorithm 2 is less useful. Algorithm 3 serves as a pipelined version of Algorithm 1 which puts the amount of memory it uses on a sliding measure between algorithm 1 and 2. Accordingly, it exhibits the best performance of all three algorithms for all matrix sizes tested in this project.

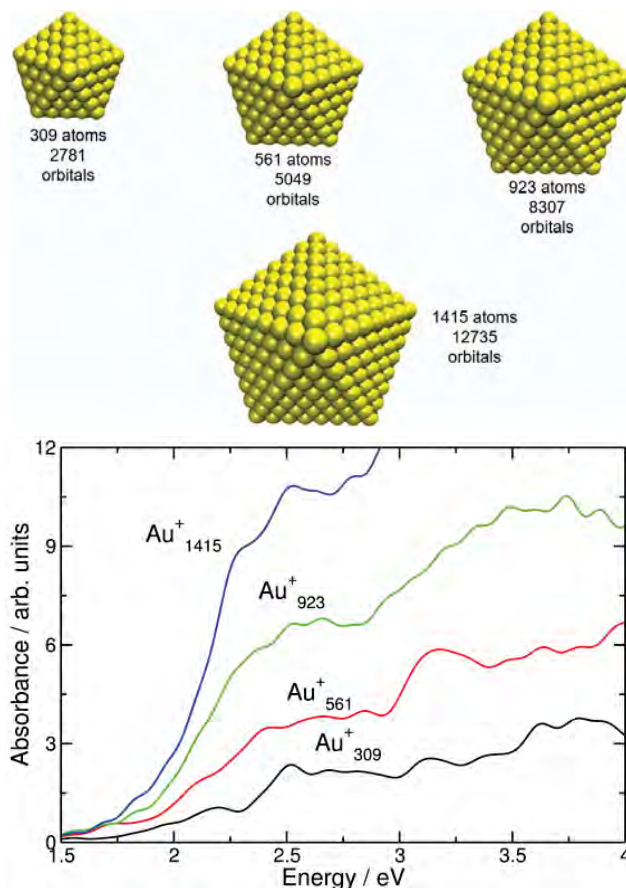


**Figure 2. Top:** Large, icosahedral-shaped gold nanoparticles containing up to 12,735 orbitals; **Bottom:** Absorption spectra of gold nanoparticles obtained from the GPU-enhanced RT-TDDFTB approach.

### 3. Future Plans

As mentioned in the Program Scope, this project has two parallel thrusts: (1) introducing self-interaction corrections to DFTB and (2) implementing new GPU algorithms in DFTB for efficiently calculating the electron dynamics of these large systems. Starting in late 2016, we intend to focus strongly on thrust (1) by implementing unitarily-invariant self-interaction

corrections (SICs) to DFTB using Fermi Orbitals (FOs) as described by Pederson and coworkers (Pederson, M.R.; Ruzsinszky, A.; Perdew, J. P. *J. Chem. Phys.* **2014**, *140*, 121103). The specific procedure for implementing the DFTB FO-SIC approach in this project is summarized in **Figure 3** and given as follows: (1) For a set of DFTB orbitals,  $\{\psi_\alpha\}$ ,  $N$  centroid positions  $\{\mathbf{a}_1, \mathbf{a}_1, \dots, \mathbf{a}_N\}$  will be found which provides a set of  $N$  normalized linearly independent (but not orthogonal) FOs,  $\{F_1, F_2, \dots, F_N\}$ ; (2) Löwdin's method of symmetric orthonormalization will then be used to construct a set of localized orthonormal orbitals,  $\{\phi_1, \phi_2, \dots, \phi_N\}$  and construct the SIC-DFTB energy in Eq. (6) from the set of FOs; (3) the SIC-DFTB energy will be minimized as a function of the DFTB orbitals and the FO centroids. In summary, this procedure will allow us to construct  $N$  localized DFTB orbitals from  $N$  quasi-classical electronic positions  $\{\mathbf{a}_1, \mathbf{a}_1, \dots, \mathbf{a}_N\}$  for calculating the SIC energy. Again, *the key advantage of this approach is that it leads to localized orbitals that retain size-extensivity of the DFTB Hamiltonian.* Most importantly, this approach circumvents the original Perdew-Zunger localization equations which scale as  $O(N^6)$  for a small number of electrons. In a recent publication, Pederson also presented closed-form expressions for derivatives of the FO centroid positions required for efficient minimization of the SIC energy (Pederson, M. R. *J. Chem. Phys.* **2015**, *142*, 064112). These derivatives vanish when the energy is minimized and will also be used in this project to efficiently navigate to the minimum energy. As such, the simple procedure for solving the FO-SIC equations can easily scale as favorably as DFTB itself, and even further efficiency may be obtained by accounting for the sparsity inherent to the DFTB approach. To validate the SIC-DFTB approach and to mitigate errors in this thrust, detailed comparisons between DFTB-FOs and standard DFT-FOs will be analyzed. For example, the FOs account for all the density at a given point in space and are, therefore, very localized orbitals. For example, the DFTB FO centroids for CO<sub>2</sub>, C<sub>2</sub>, and N<sub>2</sub> will be directly compared to the centroids computed by Pederson et al. to confirm that the DFTB FO centroids form vertices on distorted tetrahedral similar to their previous work. Finally, to further mitigate any errors in this task, several tests of the proposed DFTB code against high-level benchmark calculations will be carried out. Specifically, fundamental gaps and quasiparticle orbital energies generated from the modified DFTB code will be compared to rigorous GW and experimental values. With the DFTB FO-SIC approach properly benchmarked, it is anticipated that these corrections to DFTB will significantly improve the description of *other electronic properties* such as quasiparticle energy levels and excited state properties, which will be coupled with the GPU enhancements mentioned previously to probe the electronic structure and dynamics of large systems in this project.

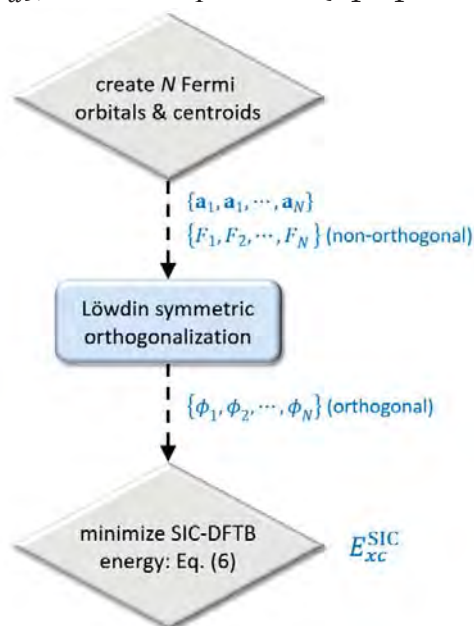


**Figure 3.** Algorithmic flowchart for implementing the DFTB FO-SIC approach. The computed outputs of each block are listed next to the dotted arrows, which are later used in subsequent blocks.

#### 4. Recent Progress

Due to the recent start date of 08/15/2016, no publications have been produced under this award.

## Intermolecular interactions in the gas and condensed phases

Sotiris S. Xantheas

Physical Sciences Division, Pacific Northwest National Laboratory  
902 Battelle Blvd., Mail Stop K1-83, Richland, WA 99352

[sotiris.xantheas@pnnl.gov](mailto:sotiris.xantheas@pnnl.gov)

**Program Scope:** The objective of this research effort aims at developing a comprehensive, molecular-level understanding of the collective phenomena associated with intermolecular interactions occurring in the gas phase, in guest/host molecular systems and in aqueous environments. The motivation of the present work stems from the desire to establish the key elements that describe the structural and associated spectral features of solutes in a variety of hydrogen bonded environments such as bulk water, aqueous interfaces and aqueous hydrates. Simple model systems including small molecules of complex electronic structure as well as aqueous clusters offer a starting point in this process by providing the test bed for validating new approaches for analyzing the electronic structure as well as the nature of interactions and the magnitude of collective phenomena at the molecular level. For instance, high level first-principles calculations of the structures, energetics, and vibrational spectra of aqueous neutral and ionic clusters provide useful information needed to assess the accuracy of reduced representations of intermolecular interactions, such as classical potentials used to model the macroscopic structural and thermodynamic properties of those systems. The database of accurate cluster structures, binding energies, and vibrational spectra can, furthermore, aid in the development of new density functionals, which are appropriate for studying the underlying interactions. Representative applications include the development of novel descriptions of the electronic structure of simple molecules, the modeling of liquid water and ice, the quantitative description of aqueous ion solvation, the structure of clathrate hydrates and the interaction of host molecules with those guest networks. The detailed molecular-scale account of aqueous systems provided by these studies is relevant to Department of Energy programs in contaminant fate and transport and waste processing as well as hydrogen storage.

**Recent progress:** We have reported the first optimum geometries and harmonic vibrational frequencies for the water ring pentamer and several hexamer clusters (prism, cage, cyclic and two book) at the CCSD(T)/aug-cc-pVDZ level of theory. The CCSD(T) results confirm the cooperative effect of the homodromic ring networks (systematic contraction of the nearest-neighbor (*nn*) intermolecular separations with cluster size) previously reported by MP2, albeit with O-O distances shorter by  $\sim 0.02$  Å, indicating that MP2 overcorrects this effect. The harmonic frequencies at the minimum geometries were obtained

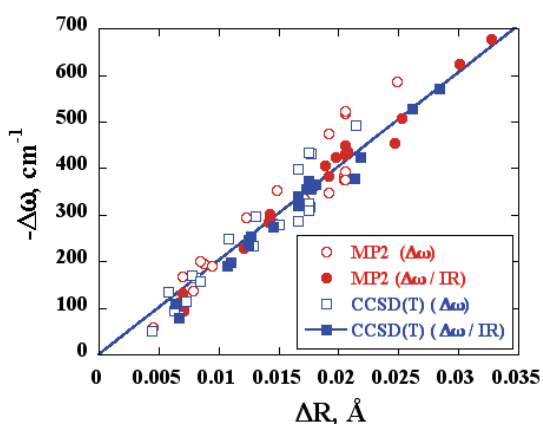


**Fig. 1.** Red shift of the hydrogen bonded frequencies ( $-\Delta\omega$ ,  $\text{cm}^{-1}$ ) from the monomer's average of symmetric and antisymmetric OH vibrations as a function of the elongation of the hydrogen bonded OH bond with respect to the monomer's value ( $\Delta R$ , Å) for the  $n = 2 - 6$  clusters. Blue [red] colors correspond to the CCSD(T) [MP2] results. Filled (open) symbols denote the IR active (inactive) frequencies.

by the double differentiation of the CCSD(T) energy using an efficient scheme based on internal coordinates that reduces the number of required single point energy evaluations by  $\sim 15\%$  when compared to the corresponding double differentiation using Cartesian coordinates. Negligible differences between MP2 and CCSD(T) were found for the librational modes, while uniform increases of  $\sim 15$  and  $\sim 25$   $\text{cm}^{-1}$  were observed for the bending and “free” OH harmonic frequencies. The largest differences between CCSD(T) and MP2 are observed for the harmonic hydrogen bonded frequencies for which the former produces larger absolute values than the latter. Their CCSD(T) red shifts from the monomer values ( $\Delta\omega$ ) are smaller than the MP2 ones, due to the fact that CCSD(T) produces shorter elongations ( $\Delta R$ ) of the respective hydrogen bonded OH lengths from the monomer value with respect to MP2. Both the MP2 and CCSD(T) results for the hydrogen bonded frequencies were found to closely follow the relation  $-\Delta\omega = s \cdot \Delta R$ , with  $s = 20.2$   $\text{cm}^{-1} / 0.001$   $\text{\AA}$  for hydrogen bonded frequencies with IR intensities  $> 400$   $\text{km/mol}$ . The CCSD(T) harmonic frequencies, when corrected using the MP2 anharmonicities obtained from second order vibrational perturbation theory (VPT2), produce anharmonic CCSD(T) estimates that are within  $< 60$   $\text{cm}^{-1}$  from the measured infrared (IR) active bands of the  $n=2-6$  clusters. The energetic order between the various hexamer isomers on the PES (prism has the lowest energy) previously reported at MP2 was found to be preserved at the CCSD(T) level, whereas the inclusion of anharmonic corrections further stabilizes the cage hexamer isomer.

We have furthermore established a computational protocol for the accurate estimation of the MP2 and CCSD(T) Complete Basis Set (CBS) limits from calculations with smaller basis sets of triple and even double zeta quality. Our best CCSD(T)/CBS estimates are  $-4.99 \pm 0.04$   $\text{kcal/mol}$  (dimer),  $-15.8 \pm 0.1$   $\text{kcal/mol}$  (trimer),  $-27.4 \pm 0.1$   $\text{kcal/mol}$  (tetramer),  $-35.9 \pm 0.3$   $\text{kcal/mol}$  (pentamer),  $-46.2 \pm 0.3$   $\text{kcal/mol}$  (prism hexamer),  $-45.9 \pm 0.3$   $\text{kcal/mol}$  (cage hexamer),  $-45.4 \pm 0.3$   $\text{kcal/mol}$  (book hexamer),  $-44.3 \pm 0.3$   $\text{kcal/mol}$  (ring hexamer),  $-73.0 \pm 0.5$   $\text{kcal/mol}$  ( $D_{2d}$  octamer) and  $-72.9 \pm 0.5$   $\text{kcal/mol}$  ( $S_4$  octamer). We have found that the percentage of both the uncorrected ( $D_e$ ) and BSSE-corrected ( $D_e^{\text{CP}}$ ) binding energies recovered with respect to the CBS limit falls into a narrow range on either side of the CBS limit for each basis set for all clusters. In addition, this range decreases upon increasing the basis set. Relatively accurate estimates (within  $< 0.5\%$ ) of the CBS limits can be obtained when using the “ $\frac{2}{3}$ ,  $\frac{1}{3}$ ” (for the AVDZ set) or the “ $\frac{1}{2}$ ,  $\frac{1}{2}$ ” (for the AVTZ, AVQZ and AV5Z sets) mixing ratio between  $D_e$  and  $D_e^{\text{CP}}$ . These mixing ratios are determined via a least-mean-squares approach from a dataset that encompasses clusters of various sizes. This protocol can be used to estimate accurate binding energies of clusters containing up to 30 molecules (for CCSD(T)) and up to 100 molecules (for MP2).

Interest in water clusters in the  $>15$  molecule range stems from the fact that clusters with internally solvated water molecules are widespread models that mimic the local environment of the condensed phase. The appearance of stable  $(\text{H}_2\text{O})_n$  cluster isomers having a fully coordinated

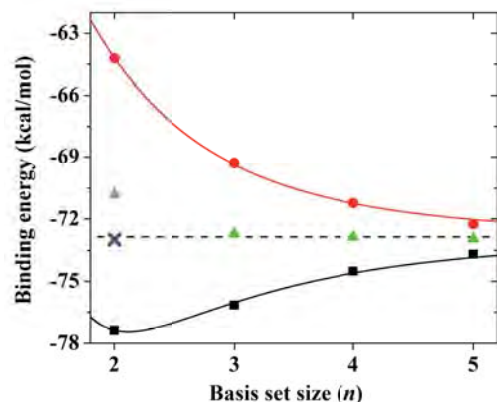


**Fig. 2.** Binding energy of the  $D_{2d}$  isomer of the  $(\text{H}_2\text{O})_8$  cluster for the MP2/AV $n$ Z series as a function of the cardinal number  $n$  of the basis set. The dashed line indicates the MP2/ $D_e^{\text{CBS}}$  limit. Black (red) symbols and curves correspond to the uncorrected (BSSE-corrected) binding energies,  $D_e$  ( $D_e^{\text{CP}}$ ). Green triangles trace their average values ( $D_e^{\text{ave}}$ ), while the blue cross marks the value corresponding to  $2/3 \cdot D_e(\text{AVDZ}) + 1/3 \cdot D_e^{\text{CP}}(\text{AVDZ})$ .

interior molecule has been theoretically predicted to occur around the  $n=17$  size range. However, our current knowledge about their structures has remained hypothetical from simulations in lieu of the absence of precisely size-resolved experimental measurements. In collaboration with the Buck and Zeuch groups at the Max Planck Institute and the University of Gottingen, Germany, we have identified a fully solvated isomer of  $(\text{H}_2\text{O})_{20}$  via a joint experimental isomer selective infrared (IR) excitation modulated photoionization spectroscopy and high level electronic structure calculations. The observed absorption patterns in the OH stretching region are consistent with the theoretically predicted spectra of two structurally distinct isomers of exceptional stability: A drop-like cluster with a fully coordinated (interior) water molecule and an edge-sharing pentagonal prism cluster in which all atoms are on the surface. The drop-like structure is the first experimentally detected water cluster exhibiting the local connectivity (two donor and two acceptor ligands to a central water) found in liquid water.

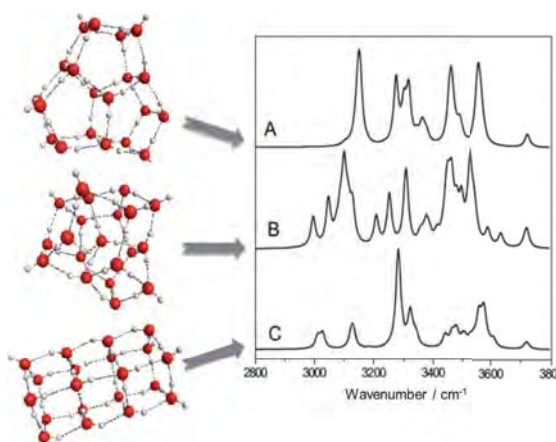


**Fig. 3.** The most stable isomers of  $(\text{H}_2\text{O})_{20}$  and their predicted IR spectra in the OH stretch region. (A) Edge-sharing pentagonal prism, (B) drop-like, (C) face-sharing pentagonal prism.

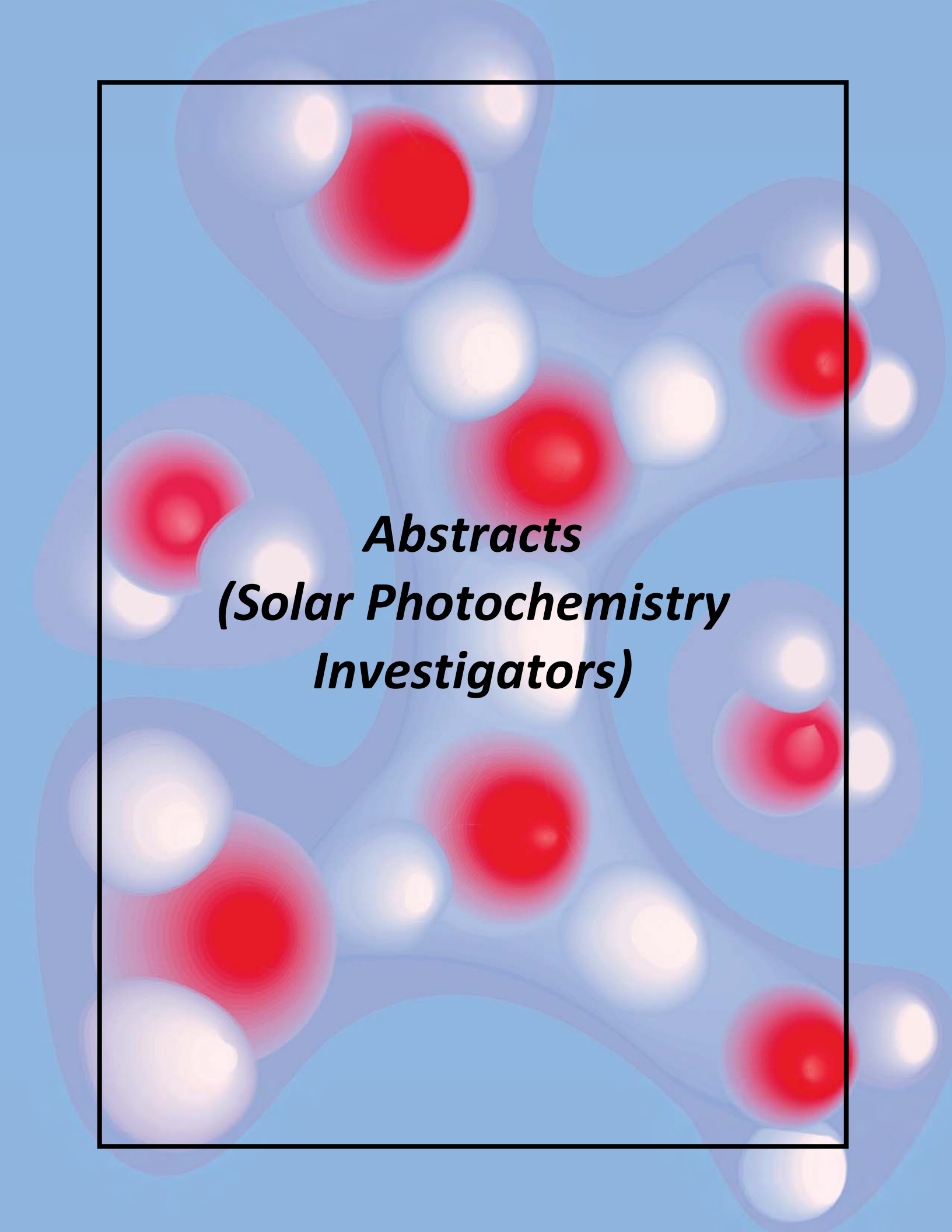
**Future Plans:** The developed protocol for the accurate determination of the CBS limit for the interaction energies of weak interactions opens up a plethora of opportunities for establishing reliable benchmarks for weak intermolecular interactions. The protocol will be further validated using published results for very weak interactions (i.e. rare gas dimers), aromatic and anti-aromatic  $\pi$ - $\pi$  interactions as well as the interaction of guest molecules with host hydrate lattices. The latter are required for the construction of interaction potentials to study macroscopic processes related to the encapsulation and exchange of hosts such as  $\text{H}_2$ ,  $\text{CH}_4$  and  $\text{CO}_2$  that are pertinent to energy production, energy storage and Carbon sequestration.

**Acknowledgments:** This research used the resources of the National Energy Research Scientific Computing Center (NERSC), which is supported by the Office of Science of the U.S. Department of Energy under Contract No. DE-AC02-05CH11231, under a NERSC Initiative for Scientific Exploration (NISE) Award and the Molecular Science Computing Facility (MSCF) in EMSL, a national scientific user facility sponsored by the Department of Energy's Office of Biological and Environmental Research located at PNNL. Battelle operates Pacific Northwest National Laboratory for the US Department of Energy.

#### References to publications of DOE sponsored research (2015 - 2016)

1. J. C. Werhahn, E. Miliordos and S. S. Xantheas, "A new variation of the Buckingham exponential-6 potential with a tunable, singularity-free short-range repulsion and an adjustable long-range attraction", *Chemical Physics Letters* **619**, 133 (2015)
2. E. Miliordos and S. S. Xantheas, "On the validity of the basis set superposition error and complete basis set limit extrapolations for the binding energy of the formic acid dimer", *Journal of Chemical Physics* **142**, 094311 (2015)

3. E. Miliordos and S. S. Xantheas, "Ground and excited states of the  $[\text{Fe}(\text{H}_2\text{O})_6]^{2+}$  and  $[\text{Fe}(\text{H}_2\text{O})_6]^{3+}$  clusters: Insights into the electronic structure of the  $[\text{Fe}(\text{H}_2\text{O})_6]^{2+}$  –  $[\text{Fe}(\text{H}_2\text{O})_6]^{3+}$  complex", *Journal of Chemical Theory and Computation* **11**, 1549 (2015)
4. E. Miliordos and S. S. Xantheas, "An accurate and efficient computational protocol for obtaining the Complete Basis Set (CBS) limits of the binding energies of water clusters at the MP2 and CCSD(T) levels of theory: Application to  $(\text{H}_2\text{O})_m$ ,  $m = 2 - 6, 8, 11, 16$  and  $17$ ", *Journal of Chemical Physics* **142**, 234303 (2015)
5. S. Imoto, S. S. Xantheas and S. Saito, "Ultrafast dynamics of liquid water: Energy relaxation and transfer processes of the OH stretch and the HOH bend", B. Bagchi Special issue (invited), *Journal of Physical Chemistry B* **119**, 11068 (2015)
6. J. A. Fournier, C. T. Wolke, and M. A. Johnson, T. T. Odbadrakh and K. D. Jordan, S. M. Kathmann and S. S. Xantheas, "Snapshots of Proton Accommodation at a Microscopic Water Surface: Vibrational Spectral Signatures of the Charge Defect in Cryogenically Cooled  $\text{H}^+(\text{H}_2\text{O})_{n=2-28}$  Clusters", Feature Article (invited), *Journal of Physical Chemistry A* **119**, 9425 (2015). Journal cover
7. K. R. Brorsen, S. Y. Willow, S. S. Xantheas, and M. S. Gordon, "The melting temperature of liquid water with the effective fragment potential", *Journal of Physical Chemistry Letters* **6**, 3555 (2015)
8. J. S. Moore, S. S. Xantheas, J. W. Grate, T. W. Wietsma, E. Gratton, A. E. Vasdekis, "Modular Polymer Biosensors by Solvent Immersion Imprint Lithography", *Journal of Polymer Science, Part B: Polymer Physics* **54**, 98 (2016)
9. E. Miliordos and S. S. Xantheas, "The origin of the reactivity of the Criegee intermediate: implications for atmospheric particle growth", Communication to the Editor, *Angewandte Chemie International Edition* **55**, 1015 (2016). Hot paper
10. S. Yoo Willow, X. Cheng Zeng, S. S. Xantheas, K. S. Kim and S. Hirata, "Why is MP2-Water 'Cooler' and 'Denser' than DFT-Water?", *Journal of Physical Chemistry Letters* **7**, 680 (2016)
11. C. T. Wolke, J. A. Fournier, E. Miliordos, S. M. Kathmann, S. S. Xantheas, and M. A. Johnson, "Isotopomer-selective spectra of a single intact  $\text{H}_2\text{O}$  molecule in the  $\text{Cs}^+[(\text{D}_2\text{O})_5 \cdot \text{H}_2\text{O}]$  isotopologue: Going beyond pattern recognition to harvest the structural information encoded in vibrational spectra", *Journal of Chemical Physics* **144**, 074305 (2016)
12. S. Iwata, D. Akase, M. Aida and S. S. Xantheas, "Hydrogen-Bonded Networks in Polyhedral Water Clusters  $(\text{H}_2\text{O})_n$ ,  $n = 8, 20$  and  $24$ " *Physical Chemistry Chemical Physics* **18**, 19746 (2016)
13. E. Miliordos, E. Aprà and S. S. Xantheas, "A New, Dispersion - Driven Intermolecular Arrangement for the Benzene – Water Octamer Complex: Isomers and Analysis of their Vibrational Spectra", *Journal of Chemical Theory and Computation* **12**, 4004 (2016)
14. T.-M. Chang and S. S. Xantheas, A. E. Vasdekis, "Mesoscale Polymer Dissolution probed by Raman Spectroscopy and Molecular Simulations" *Journal of Physical Chemistry B* (under revision)



***Abstracts  
(Solar Photochemistry  
Investigators)***

## FUNDAMENTAL ADVANCES IN RADIATION CHEMISTRY

Principal Investigators:

DM Bartels ([bartels.5@nd.edu](mailto:bartels.5@nd.edu)), I Carmichael, I Janik, JA LaVerne, S Ptasińska  
Notre Dame Radiation Laboratory, University of Notre Dame, Notre Dame, IN 46556

### SCOPE

*Research in fundamental advances in radiation chemistry is organized around two themes. First, energy deposition and transport seeks to describe how energetic charged particles and photons interact with matter to produce tracks of highly reactive transients, whose recombination and escape ultimately determine the chemical effect of the impinging radiation. The work described in this part is focused on fundamental problems specific to the action of ionizing radiation. Particular projects include investigation of neutron radiolysis in high temperature water, experimental and theoretical investigation of the VUV spectra of liquids up to supercritical conditions, chemistry of highly excited states in spur and track recombination in aromatic hydrocarbon liquids, and investigation of a novel radiation source, the atmospheric pressure plasma jet. The second thrust deals with structure, properties and reactions of free radicals in condensed phases. Challenges being addressed include the experimental and theoretical investigation of solvated electron reaction rates, measurement of radical reaction rates in high temperature water, determination of the redox potentials of hyper-reduced transition metal ions, and investigation of the structure and reactivity of OH radical adducts.*

### PROGRESS AND PLANS

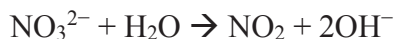
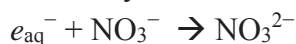
Quantum diffusion of atomic hydrogen isotopes in water was studied in a combined experimental and simulation study. Relative diffusion coefficients were determined in water for the D, H, and Mu isotopes of atomic hydrogen, by measuring their diffusion-limited spin exchange rate constants with  $\text{Ni}^{2+}$  as a function of temperature. H and D atoms were generated by pulse radiolysis of water and measured by time resolved pulsed EPR. Mu atoms are detected by muonium spin resonance. To isolate the atomic mass effect from solvent isotope effect, all three spin exchange rates were measured in 90%  $\text{D}_2\text{O}$ . The diffusion depends on the atomic mass, demonstrating breakdown of Stokes-Einstein behavior. The diffusion can be understood using a combination of water "cavity diffusion" and "hopping" mechanisms, as has been proposed in the literature. The H/D isotope effect agrees with previous modeling using Ring Polymer Molecular Dynamics (RPMD). The "quantum swelling" effect on muonium due to its larger de Broglie wavelength does not seem to slow its "hopping" diffusion as much as predicted in previous work. Quantum effects of both the atom mass and the water librations have been modeled using RPMD and a qTIP4P/f quantized flexible water model. These results suggest that the muonium diffusion is very sensitive to the muonium vs. water potential used.

Molecular hydrogen is a primary product of the interaction of low-LET ( $\gamma$ ,  $\beta$ ) radiation with water, and previous measurements have shown that its initial yield increases at elevated temperature. This has been the subject of controversy because more atomic H and  $e_{\text{aq}}^-$  free radicals escape recombination at elevated temperature, and the corresponding  $\text{H}_2$  product should decrease. Room temperature experiments have demonstrated that a large fraction of  $\text{H}_2$  also comes from early physico-chemical processes (presumably electron-hole charge recombination and/or dissociative electron attachment) which can be suppressed by scavenging pre-solvated electrons. We extended these scavenging measurements up to 350 °C to investigate why the overall  $\text{H}_2$  yield increases. It is found that most of the  $\text{H}_2$  yield increase is due to the presolvation processes. Relatively small changes in the scavenging efficiency vs. LET, and a significant effect of temperature depending on the (positive or negative) charge of the scavenger, indicate that the

presolvation H<sub>2</sub> is dominated by electron-hole charge recombination rather than dissociative electron attachment at all temperatures. This means that virtually all popular water radiolysis modeling codes incorporate the wrong mechanism (DEA) for H<sub>2</sub> production.

Reactions of the hydrated electron with divalent aqueous transition-metal ions: Cd<sup>2+</sup>, Zn<sup>2+</sup>, Ni<sup>2+</sup>, Cu<sup>2+</sup>, Co<sup>2+</sup>, Fe<sup>2+</sup> and Mn<sup>2+</sup> were studied using a pulse radiolysis technique up to 300°C. The activation energies obtained from the Arrhenius plots are in the range of 14.5 to 40.6 kJ/mol. Pre-exponential factors are quite large, between  $1 \times 10^{13}$  and  $7 \times 10^{15} \text{ M}^{-1} \text{ s}^{-1}$ . There appears to be a large degree of entropy-enthalpy compensation in the activation of Zn<sup>2+</sup>, Ni<sup>2+</sup>, Co<sup>2+</sup> and Cu<sup>2+</sup>, as the larger pre-exponential factors strongly correlate with higher activation energy. Saturation of the ionic strength effect suggests that these reactions could be long-range nonadiabatic electron "jumps", but Marcus theory is incompatible with direct formation of ground state (M<sup>+</sup>)<sub>aq</sub> ions. A self-consistent explanation is that electron transfer occurs to excited states derived from the metal 4s orbitals. Ionic strength effect in the Mn<sup>2+</sup> and Fe<sup>2+</sup> reactions suggests that these proceed by short-range adiabatic electron attachment involving breakdown of the water coordination shell.

Waste separations are generally based on the extraction of isotopes from aqueous nitric acid solutions into a solid or liquid organic phase. Nitrate is known to be a good scavenger for the hydrated electron and its precursor, but little is known about the overall chemistry of these systems at the very high nitrate concentrations (6M) used in separations and for various types of LET. The initial focus of our study has been on nitrite production and later studies will incorporate H<sub>2</sub> production and modeling. Reduction of the nitrate is generally initiated by the reaction of the hydrated electron (or presolvated electron at high NO<sub>3</sub><sup>-</sup> concentrations).



The oxidizing OH radical will undergo a wide variety of reactions, one of which will reduce the nitrite ion concentration in the following reaction.



Measured nitrite ion yields are due to the competition between oxidizing and reducing processes. Irradiations have been performed with both  $\gamma$ -rays and 5 MeV He ions, the latter to mimic  $\alpha$ -particle radiolysis. Nitrate concentrations have been varied from 1 mM to 6 M in order to reproduce conditions in separation streams. Nitrite yields are found to increase with increasing nitrate concentration as expected from scavenging of the hydrated electron and its precursor in the  $\gamma$ -ray spur or He ion track. At nitrate concentrations above 1 M, direct effects begin to occur and one observes direct decomposition of the nitrate ion itself. This process will obviously be rather important in actual separation conditions. A very strong dose effect was observed in these systems at certain nitrate concentrations suggesting complex long-time chemistry as well. Further studies will vary LET over a wider range and include high acid concentrations. Track diffusion kinetic models will be applied in order to fully understand these systems.

Reactive species present in a helium atmospheric pressure plasma jet (He-APPJ) were recently characterized by optical emission spectroscopy (OES). In addition, OES was used to study the relative emission intensities of various species produced when oxygen was added to He. The emission spectra were obtained from two regions of our plasma system: one between the high voltage and ground electrodes (core region) and the other a few cm away from the nozzle into the air (jet region). The emission spectrum obtained in the core region of the APPJ in He

was composed of lines from metastable He, He<sub>2</sub>, N<sub>2</sub>, N<sub>2</sub><sup>+</sup>, H, OH, and O. The emission spectra of the jet region of the APPJ in He and a He/O<sub>2</sub> mixture were significantly different from the those measured in the core region. The intense N<sub>2</sub> emission lines observed in the jet region are typical of plasma ignited in atmospheric conditions and are produced by the interaction of the plasma jet with the surrounding air. A 2D numerical model that described the gas dynamics and the afterglow chemistry in an APPJ operating in He with humid air impurity complemented the experimental work. The model consisted of two parts, that of the background gas dynamics, and of the afterglow chemistry. The former describes the gas flow and mixing of the He/air mixture inside and outside the plasma jet, while the latter describes the chemistry outside the plasma jet. Presently, we are developing novel and complementary diagnostics, such as interferometry and Schlieren photography, necessary to probe physical properties of APPJs which have strong spatial gradients, reduced time scales, and an enormous number of processes.

High-resolution VUV supercritical water absorption spectra were acquired for the first time at 381°C at 15 different pressures ranging from 4 to 300 bar, with corresponding densities ranging from 0.0013 to 0.529 g cm<sup>-3</sup>. At the lowest pressures, the SCW data mimic gas-phase results for the water monomer. The calculated  $\tilde{A}$  state monomer surface is purely repulsive with respect to extension of either O-H bond, and Franck-Condon excitation to this PES accesses the saddle point above and between the two equivalent dissociation channels. The diffuse structure in the measured absorption spectrum has been assigned to motion in this saddle point region perpendicular to the dissociation co-ordinate, corresponding to the symmetric stretch. The diffuse nature of the structure reflects the short-lived nature of the stretching resonances. Upon increase of the pressure up to 300 bar, two main effects are observed: (i) a 0.28 eV blue shift, related to the rise in the population of water dimers and trimers and (ii) disappearance of the vibrational coherence feature. We suppose that the coherence only exists in isolated monomer species, and its disappearance corresponds to perturbation of the C<sub>2v</sub> monomer electronic symmetry. Detailed analysis of the spectra allowed us to determine the threshold intermolecular distances needed to extinguish the coherence feature, resulting in surprisingly large distances on the order of 4.5Å.

Time-resolved resonance Raman (TRRR) spectroscopy was applied to characterize primary intermediates produced at the early stages of OH induced oxidation of metal cations (Tl<sup>+</sup>, Ag<sup>+</sup>, Cu<sup>2+</sup>, Sn<sup>2+</sup>) in aqueous solutions. It has been suggested in the past that these intermediates having characteristic transient absorption spectra located in the UV region, originate from OH adducts to the respective metal aquo cations. Yet the nature of the bonding between metal and oxygen of electrophilic OH radicals has never been examined. We were able to observe vibrational spectroscopic signatures of the intermediates produced by oxidation of Tl<sup>+</sup> and Ag<sup>+</sup> by Raman scattering in resonance with their transient absorptions at 350 nm and 295 nm, respectively. TRRR spectra of both intermediates resemble pseudo-diatom OH adducts to halides or sulfides, where only one fundamental vibration with a progression of overtones was observed. The fundamental signal in the TlOH<sup>+</sup> and AgOH<sup>+</sup> intermediate spectra have been assigned to X-O (X=Tl, Ag) bond symmetric stretch and had 383 and 483 cm<sup>-1</sup> Raman shifts, respectively. Exchange of the solvent from light water to heavy water caused the fundamental Raman shifts to decrease by several wavenumbers indicating that both adducts are protonated. From the progression of the observable overtones, the harmonic frequency, anharmonicity constant, and bond dissociation energies of TlOH<sup>+</sup> and AgOH<sup>+</sup> were estimated. Based on the spectroscopic parameters it seems that the character of metal-oxygen bond differs significantly between the two. The bond nature in AgOH<sup>+</sup> resembles a single covalent bond,

whereas in TlOH<sup>+</sup> the data imply weak hemibonding with large anharmonicity (~8.8 cm<sup>-1</sup>) and very low dissociation energy (0.6 eV).

#### **PUBLICATIONS WITH BES SUPPORT SINCE 2014**

- Kosno K.; Janik I.; Celuch M.; Mirkowski J.; Kisała, J.; Pogocki, D. *Isr. J. Chem.* **2014**, **54**, 302-315 The role of pH in the mechanism of •OH radical induced oxidation of nicotine.
- Han X., Cantrell W.A., Escobar E.E., Ptasińska S. *Eur. Phys. J* **2014**, **D68**, 46. Plasmid DNA Damage Induced by Helium Atmospheric Pressure Plasma Jet.
- Zhang X., Ptasińska S. *J. Phys. D.* **2014**, **47**, 145202. Growth of Silicon Oxynitride Films by Atmospheric Pressure Plasma Jet.
- Bahnev B., Bowden M.D., Stypczyńska A., Ptasińska S., Mason N.J.; Braithwaite N.St.J. *Eur. Phys. J D* **2014**, **68**, 140-1-5 A novel method for the detection of plasma jet boundaries by exploring DNA damage.
- Han X., Liu Y, Stack M.S., Ptasińska S. *J. Phys: Conf. Ser.* **2014**, **565**, 012011-1-6 3D Mapping of plasma effective areas via detection of cancer cell damage induced by atmospheric pressure plasma jets.
- Kanjana K.; Walker J.A.; Bartels D.M. *J. Phys. Chem. A* **2015**, **119**, 1830-7 Hydroxymethyl Radical Self-Recombination in High-Temperature Water.
- Rumbach P.; Bartels D.M.; Sankaran R.M.; Go D.B. *Nat Commun* **2015**, 6 The solvation of electrons by an atmospheric-pressure plasma.
- Rumbach P.; Bartels D.M.; Sankaran R.M.; Go D.B. *J. Phys. D: Appl. Phys.* **2015**, **48** The effect of air on solvated electron chemistry at a plasma/liquid interface.
- Kumar A., Walker J.A., Bartels D.M., Sevilla M.D. *J. Phys. Chem. A* **2015**, **119** A Simple ab initio Model for the Hydrated Electron that Matches Experiment
- Janik I., Marin T.W. *Rev Sci Inst.*, **2015**, **86**, 015102. Design of an ultrashort optical transmission cell for vacuum ultraviolet spectroscopy of supercritical fluids.
- Arjunan K.P., Sharma V.K., Ptasińska S. *Int. J. Mol. Sci.* **2015**, **16**, 2971-3016 Effects of atmospheric pressure plasmas on isolated and cellular DNA – a review.
- Kanjana K.; Courtin B.; MacConnell A.; Bartels D.M. *J. Phys. Chem. A* **2015**, **119**, 11094-104 Reactions of Hexa-aquo Transition Metal Ions with the Hydrated Electron up to 300 degrees C.
- Dawley M.M.; Tanzer K.; Carmichael I.; Denifl S.; Ptasińska S. *J. Chem. Phys.* **2015**, **142**, 21501. Dissociative electron attachment to the gas-phase nucleobase hypoxanthine
- Sterniczuk M.; Bartels D.M. *J. Phys. Chem. A* **2016**, **120**, 200-9 Source of Molecular Hydrogen in High-Temperature Water Radiolysis.
- Sterniczuk M.; Yakabuskie P.A.; Wren J.C.; Jacob J.A.; Bartels D.M. *Radiat. Phys. Chem.* **2016**, **121**, 35-42 Low LET radiolysis escape yields for reducing radicals and H<sub>2</sub> in pressurized high temperature water.
- Walker J.A.; Mezyk S.P.; Roduner E.; Bartels D.M. *The Journal of Physical Chemistry B* **2016**, **120**, 1771-9 Isotope Dependence and Quantum Effects on Atomic Hydrogen Diffusion in Liquid Water.
- Janik I.; Tripathi G.N.R. *J. Chem. Phys.* **2016**, **144**, 154307-7 The nature of CO<sub>2</sub><sup>-</sup> radical anion in water.
- Huang W.; Ptasińska S. *Appl. Surf. Sci.* **2016**, **367**, 160-6. Functionalization of Graphene by Atmospheric Pressure Plasma Jet in Air or H<sub>2</sub>O<sub>2</sub> environments.
- Adhikari E.; Ptasińska S. *Eur. Phys. J. D* **2016**, **70**, 180-7. Correlation between plasma induced DNA damage level and helium atmospheric pressure plasma jet (APPJ) variables.
- Arjunan K.; Obrusnik A.; Jones B.; Zajickova L.; Ptasińska S. *Plasma Proc. and Polym.* **2016** Effect of additive oxygen on the reactive species profile and microbicidal property of a helium atmospheric pressure plasma jet. 10.1002/ppap.201600058

## Exceptionally rapid capture of radical cations made by pulse radiolysis

Principal Investigators: Andrew R. Cook and John R. Miller  
*Department of Chemistry, Brookhaven National Laboratory, Upton, NY, 11973 USA*  
acook@bnl.gov, jrmiller@bnl.gov

### Program Scope:

This program applies both photoexcitation and ionization by short pulses of fast electrons to investigate fundamental chemical problems relevant to the production and efficient use of energy and thus obtain unique insights not attainable with other techniques. These studies may play an important role in the development of safer, more effective, and environmentally beneficial processes for the chemical conversion of solar energy. Picosecond pulse radiolysis at the Laser Electron Accelerator Facility (LEAF) is employed to generate and study reactive chemical intermediates or other non-equilibrium states of matter in ways that are complementary to photolysis and electrochemistry and often uniquely accessible by radiolysis. This program also develops new tools for such investigations, applies them to chemical questions, and makes them available to the research community. Advanced experimental capabilities, such as Optical Fiber Single-Shot detection system (OFSS), allow us to work on fascinating systems with 5-10 ps time-resolution that were previously prohibitive for technical reasons.

### Recent Progress:

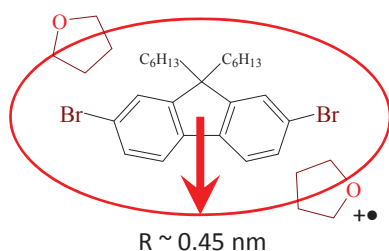
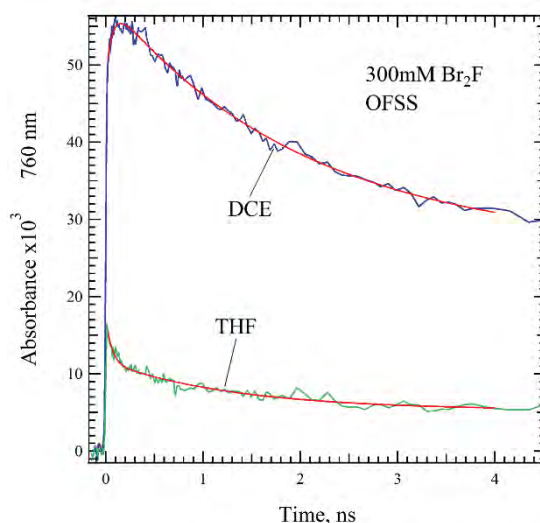
**Rapid cation capture** The radiation chemistry of non-aqueous media is much less understood than that of water, but is an enabling science that makes important contributions to many areas of research in our group. Non-aqueous solvents are often better solvents for dissolving molecules. Low polarity organic solvents allow minimization of energy losses due to electrostatic environment relaxation, which is particularly important for our investigations of charge transport in conjugated polymers relevant to OPV.

An important question is whether it is possible to rapidly and in high yield oxidize solutes using organic solvent radical cations formed by pulse-radiolysis? The literature is full of reports of solute oxidation at near (or below) diffusion limited rates in a variety of solvents. Even at modest solute concentration, this means oxidation of solutes can take many nanoseconds. Capture of electrons, which can have mobilities as large as  $100 \text{ cm}^2/\text{Vs}$  in some non-polar liquids, can be far faster. In addition, electrons are known to be captured in good yield prior to solvation on timescales  $\ll 10 \text{ ps}$ . Such mechanisms are not known for solute oxidation. The “hole” from ionization is usually found to be a solvent molecular cation, which requires mass transport and thus diffuses slowly. Examples of electronic transport in molecular liquids are rare. An additional complication with organic solvent radical cations is that in many cases they can be short lived, fragmenting by proton transfer or C-C bond scission to make more stable cations and radicals, both of which may be unable to oxidize solutes. All of these factors lead to an expectation of low solute cation yield and slow oxidation in most solvents of interest.

Previous results in chloroform found very different results. As a function of concentration, experiments showed unknown and unexpectedly rapid and high yield capture of holes in chloroform, observed in OFSS experiments as “Step” increases in absorption within the experimental time resolution of  $\sim 15 \text{ ps}$ . A radiochemical yield of up to  $G=1.7$  cations/100eV absorbed could be captured in  $\text{CHCl}_3$  in under 15 ps; essentially all of the capturable solvent radical cations. This rather startling result was best fit by the same exponential dependence on

concentration used for capture of electrons prior to solvation. The main conclusion of this work was that these solvent holes were not diffusing molecular ions, but being captured prior to solvation, implying some sort of electronic mechanism without mass transport. We considered the hypothesis that holes could initially be delocalized over many solvent molecules, and be captured at significant distances away from the center of the ionization if the wavefunction of the hole overlapped with a solute. An intriguing possibility is that these delocalized holes might also propagate rapidly through the solvent to find solutes. Data supported oxidation of solutes as far as 2.3 nm away from the center of the ionization in  $< 15$  ps. The results represent the first observations of this remarkable process.

Recent work has been exploring how general this phenomena might be. Is it something particular to  $\text{CHCl}_3$  or chlorinated solvents? To what extent does it occur in other media? A strong test is provided by solvents where solvent radical cations formed by pulse radiolysis are not known to oxidize solutes. As noted above, these are solvents termed as “fragmenting”, where the initial solvent radical cation is known to rapidly undergo chemistry to degrade its oxidizing power. An example is THF, which is often used in our group as it is a great solvent for conjugated polymers. It has been shown that the lifetime of the solvent radical cation is  $\sim 0.5$  ps, rapidly transferring a proton to a neighboring THF molecule to make largely unreactive solvated protons and radicals, which are unable to oxidize almost all solutes. The preferred probe molecules are brominated aryls, such as 2,7-dibromo-9,9-dihexyl-9H-fluorene ( $\text{Br}_2\text{F}$ ); chosen for its high solubility in many solvents, and a special feature that its anion rapidly dissociates to make non-absorbing  $\text{Br}^-$  and a radical upon electron attachment. In this way, the only species we detect is  $\text{Br}_2\text{F}^{+\bullet}$ . The figure to the right compares signals detected in OFSS experiments ( $\sim 15$  ps time resolution) at the maximum of the  $\text{Br}_2\text{F}^{+\bullet}$  absorption band for a 300mM sample in dichloroethane, which is well known to produce a large yield of solute radical cations, to THF. The data clearly show a significant yield of  $\text{Br}_2\text{F}^{+\bullet}$  in THF. An important question is how much of this yield is due to direct ionization of  $\text{Br}_2\text{F}$ , and how much may be due to capture of pre-solvated

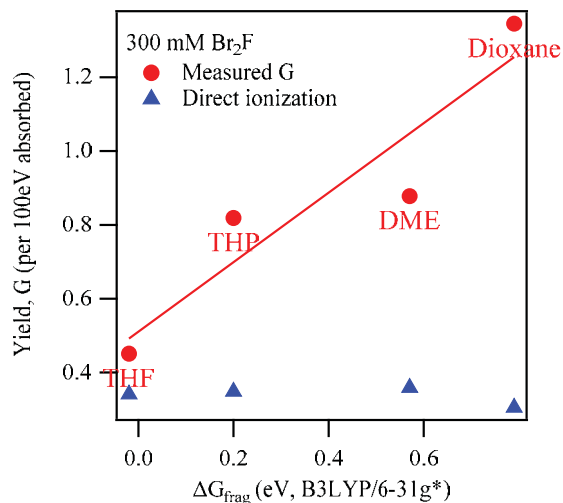


holes? Using the signal in DCE as the maximum yield possible ( $G_{\text{max}} \sim 3.6$ ), we find that the yield in THF is  $\sim 2$ x that expected for the direct ionization. As in  $\text{CHCl}_3$ , the yield of  $\text{Br}_2\text{F}^{+\bullet}$  in THF as a function of  $c = [\text{Br}_2\text{F}]$  is well described by:  $G = G_{\text{max}}(1 - e^{-qc})$ , where  $q = 1/C_{37}$ , and  $C_{37} = 1.5$  M. While this is a large value, it can be used to determine the maximum average distance for capture, 0.45nm. This implies that pre-solvated hole capture is occurring

when the THF radical cation is a nearest neighbor to a  $\text{Br}_2\text{F}$  molecule.

We have made similar measurements in other fragmenting ethers, including tetrahydropyran (THP), 1,2-dimethoxyethane (DME) and 1,4-dioxane. We find higher yields of  $\text{Br}_2\text{F}^{+\bullet}$  production in all, as well as correspondingly larger capture distances. Our hypothesis in

this series is that the yield of pre-solvated hole capture is related to the lifetime of the solvent radical cation. While this lifetime is known for THF,  $\sim 0.5$  ps, it is not known for the others. As a proxy for the solvent hole lifetime, we have calculated the free energy of fragmentation,  $\Delta G_{\text{frag}}$ , defined as a proton transfer from the solvent radical cation to a neighboring molecule. We find a fair correlation between the observed yield and  $\Delta G_{\text{frag}}$ , seen to the right. A similar correlation with C-H dissociation barrier is also found. It should be noted that the figure to the right only considers proton transfer; in some molecules other fragmentation mechanisms may dominate or occur simultaneously, such as C-C bond scission suggested in the literature for  $\text{DME}^{+\bullet}$ , will also effect lifetime – possibly explaining the slightly low yield in DME.



An important conclusion that can be drawn from this work is that the timescale for pre-solvated hole capture in such media is likely slower than 2 ps. If it were faster, the yield in THF would have been larger. Additionally, pre-solvated hole capture provides a way to make an unexpected yield of solute radical cations, even in solvents where cations are not normally expected. This can lead to unanticipated chemistry. It also points to a way where solute radical cations may be studied in useful media where previously not thought possible.

**Polyfluorene triplets** Pulse radiolysis is an excellent way to produce triplet excited states of solutes. This technique has been applied to determine  $T_1 \rightarrow T_n$  spectra and extinction coefficients ( $\epsilon$ ) in a series of oligomers (oFn) and polymers (pFn) of length n repeat units of fluorene. An expectation was that  $\epsilon$  would increase with oF length until a maximum defined by delocalization in the  $T_1$  and  $T_n$  states, then remain constant. We find instead that it increases to a length of  $n=3$ , then decreases out to the longest length pF tested, with  $n=84$ . This is combined with a spectrum that red-shifts until a length of 6 units, along with an oscillator strength that does the same. Conjugated polymer spectra and  $\epsilon$  as a function of length are interpreted in terms of a fixed polaron, with conjugation length determined by the balancing of energy and changes in angles and bond lengths. The current data are suggesting a different picture, where motion of the polaron on the polymer chain makes for smaller changes in band angles and lengths, as it only resides in each part of the chain for a short time, before moving to another part. Put another way, exciton motion may be faster than geometric relaxation.

**Chain length dependence on energetic properties of oligofluorenes** Redox potentials and excited state energies determined as functions of length for conjugated oligomers provide an insight to understand the electron and energy transfer in the conjugated polymers. Because charges and excitons are thought to form delocalized polarons of certain lengths, an expectation is that their energies would become constant once the length of the oligomer exceeds the delocalization length of the polaron. Despite this, redox potentials have been reported to continue to decrease slowly past this length. This phenomena has been described empirically as a particle in the box, giving a redox potential that varies linearly with  $1/n$ . We propose an alternate picture, in which the energy of the polaron becomes constant for the chain lengths greater than the delocalization length, while the free energy continues to slowly change due to the positional entropy arising because the polaron can reside at varied positions along the chain. Using pulse radiolysis at LEAF, we have measured reduction potentials and triplet free energies of fluorene oligomers and a polymer with

lengths of 1-10 and 57 repeat units. We have shown that this alternate model works well to describe the measured free energies as a function of length beyond the delocalization length, reinforcing the view that charges and triplet excitons in conjugated chains exist as polarons and that positional entropy can replace a popular empirical model of the energetics.

### Future Plans:

Work will explore other media, spanning alkanes, ethers, nitriles, and possibly alcohols for the rapid production of solute radical cations due to pre-solvated solvent cations. A key goal will be to seek trends to shed additional light on the mechanism. Data above suggest that pre-solvated hole capture may be possible on solids. This may provide a way to study transport on conjugated polymers in dilute solid matrices, and make comparisons to measurements in solution. Another question will focus on energetics – can step captured holes produce radical cations of solutes with higher IP than can diffusion of solvated holes? A consequence of “Step” capture of holes in certain cases appears to be large amounts of solute excited states produced by rapid recombination. This will be further explored.

### Publications of DOE sponsored research that have appeared in the last 2 years:

1. Mani, T.; Miller, J. R. "Role of Bad Dihedral Angles: Methylfluorenes Act as Energy Barriers for Excitons and Polarons of Oligofluorenes" *J. Phys. Chem. A* **2014**, *118*, 9451-9459.
2. Busby, E.; Xia, J. L.; Wu, Q.; Low, J. Z.; Song, R.; Miller, J. R.; Zhu, X. Y.; Campos, L. M.; Sfeir, M. Y. "A design strategy for intramolecular singlet fission mediated by charge-transfer states in donor-acceptor organic materials" *Nat. Mater.* **2015**, *14*, 426-433.
3. Li, X.; Bird, M.; Mauro, G.; Asaoka, S.; Cook, A. R.; Chen, H. C.; Miller, J. R. "Transport of Triplet Excitons along Continuous 100 nm Polyfluorene Chains" *J. Phys. Chem. B* **2015**, *119*, 7210-7218.
4. Mani, T.; Grills, D. C.; Miller, J. R. "Vibrational Stark Effects To Identify Ion Pairing and Determine Reduction Potentials in Electrolyte-Free Environments" *J. Am. Chem. Soc.* **2015**, *137*, 1136-1140.
5. Mani, T.; Grills, D. C.; Newton, M. D.; Miller, J. R. "Electron Localization of Anions Probed by Nitrile Vibrations" *J. Am. Chem. Soc.* **2015**, *137*, 10979-10991.
6. Sanders, S. N.; Kumarasamy, E.; Pun, A. B.; Trinh, M. T.; Choi, B.; Xia, J. L.; Taffet, E. J.; Low, J. Z.; Miller, J. R.; Roy, X.; et al. "Quantitative Intramolecular Singlet Fission in Bipentacenes" *J. Am. Chem. Soc.* **2015**, *137*, 8965-8972.
7. Zaikowski, L.; Mauro, G.; Bird, M.; Karten, B.; Asaoka, S.; Wu, Q.; Cook, A. R.; Miller, J. R. "Charge Transfer Fluorescence and 34 nm Exciton Diffusion Length in Polymers with Electron Acceptor End Traps" *J. Phys. Chem. B* **2015**, *119*, 7231-7241.
8. Zarzana, C. A.; Groenewold, G. S.; Mincher, B. J.; Mezyk, S. P.; Wilden, A.; Schmidt, H.; Modolo, G.; Wishart, J. F.; Cook, A. R. "A Comparison of the gamma-Radiolysis of TODGA and T(EH)DGA Using UHPLC-ESI-MS Analysis" *Solvent Extr. Ion Exch.* **2015**, *33*, 431-447.
9. Craig, P. R.; Havlas, Z.; Trujillo, M.; Rempala, P.; Kirby, J. P.; Miller, J. R.; Noll, B. C.; Michl, J. "Electronic Spectra of the Tetraphenylcyclobutadienecyclopentadienylnickel(II) Cation and Radical" *J. Phys. Chem. A* **2016**, *120*, 3456-3462.
10. Hack, J.; Grills, D. C.; Miller, J. R.; Mani, T. "Identification of Ion-Pair Structures in Solution by Vibrational Stark Effects" *J. Phys. Chem. B* **2016**, *120*, 1149-1157.

## Interfacial Radiation Sciences

Jay A. LaVerne, David M. Bartels, Ian Carmichael, Sylwia Ptasinska  
Notre Dame Radiation Laboratory, University of Notre Dame, Notre Dame, IN 46556  
[laverne.1@nd.edu](mailto:laverne.1@nd.edu), [bartels.5@nd.edu](mailto:bartels.5@nd.edu), [carmichael.1@nd.edu](mailto:carmichael.1@nd.edu), [sylwia.ptasinska.1@nd.edu](mailto:sylwia.ptasinska.1@nd.edu)

### Program Scope

*Fundamental processes induced by radiation at interfaces are being probed using a wide variety of innovative techniques and a multidisciplinary approach. Understanding radiation induced processes at interfaces on the molecular scale is an immense challenge because of the transport of mass, charge and energy along and through the interface. Many of these interfaces are not well characterized and are directly or indirectly modified by the radiation. This program is an extension of studies on fundamental radiation chemical effects in homogeneous media that have been and continue to be a major effort at the NDRL. Heterogeneous systems are applicable to a wide variety of scenarios throughout the nuclear power and solar industries. This work extends our extensive knowledge on the radiolysis of water and aqueous solutions to include the effects due to an added interface. Another active area of research involves probing the precise interactions occurring at gas – solid interfaces using advanced X-ray photoelectron spectroscopy techniques. In particular, emphasis has been given to gases at GaN and perovskites because of their use in photoelectrochemical devices.*

### Recent Progress and Future Plans

Silicon carbide is a relatively inert ceramic that has been proposed for use in the nuclear power industry as a replacement for the zircaloy cladding material currently being used. Most of the reactor systems proposed with SiC will not have water as a coolant, but almost all materials have dissociated chemisorbed water associated with their surface. Accidents may also introduce water so the radiolysis of water-SiC interfaces is extremely important. Silicon carbide  $\alpha$ -phase and  $\beta$ -phase nanoparticles with associated water were irradiated with  $\gamma$ -rays and 5 MeV  $^4\text{He}$  ions followed by the determination of the production of molecular hydrogen,  $\text{H}_2$ , and characterization of changes in the particle surface. The yields of  $\text{H}_2$  from SiC – water slurries were always greater than expected from a simple mixture rule indicating that the presence of SiC was influencing the production of  $\text{H}_2$  from water. The increase in  $\text{H}_2$  yields was rather modest compared to other oxides including zirconia, and it probably occurs through an energy transfer from the solid to liquid phase. Decreasing the relative water mass relative to that of the SiC led to an increase in  $\text{H}_2$  yields, which indicates a significant surface effect of adsorbed water. As expected for these types of materials, little change in the SiC surface was observed following radiolysis except for some conversion of  $\beta$ -phase SiC to the  $\alpha$ -phase and the formation of a  $\text{SiO}_2$  oxide with He ion radiolysis. The latter could be due to infusion of  $\text{O}_2$  into the system and the production of ozone. A variety of other proposed cladding materials including SiN and graphite will be examined for changes to their surface as well as for any influence to the water chemistry.<sup>1</sup>

The radiolysis of aluminum interfaces associated with water occurs in a variety of scenarios related to nuclear power including in reactor construction in waste storage. Nanoparticles of  $\text{Al}_2\text{O}_3$  with water were irradiated with  $\gamma$ -rays and 5 MeV He ions followed by the determination of the production of  $\text{H}_2$  and characterization of changes in the particle surface. Any variation in the water chemistry to the presence of the  $\text{Al}_2\text{O}_3$  interface should lead to a variation in the yield of  $\text{H}_2$  as

compared to that in pure water. For  $\text{Al}_2\text{O}_3$  samples with adsorbed water, the radiation chemical yield of  $\text{H}_2$  was found to be  $79.8 \pm 15.4$  molecules/100 eV (1 molecule/100 eV =  $1.04 \times 10^{-7}$  mol/J). This value is to be compared with the 0.45 molecules/100 eV for pure water. Such a large difference shows the high degree of energy migration in this system. In slurries, the yield of  $\text{H}_2$  was observed to decrease as the amount of water present increased relative to the  $\text{Al}_2\text{O}_3$ . As with many of the other oxides examined, surface interactions have a large effect on the radiolysis of water on or near to the interface. Surface studies indicated that the  $\pm$ -phase  $\text{Al}_2\text{O}_3$  samples changed phase following irradiation by He ions. The surface was found to have an oxyhydroxide layer present on the pristine sample, which is removed by irradiation. Future endeavors in the examination of the radiolysis of water-oxide surfaces will more thoroughly examine the water chemistry, especially the interactions of  $\text{Al}_2\text{O}_3$  surfaces with  $\text{H}_2\text{O}_2$  as described next.

Decomposition of water leads to the formation of  $\text{H}_2\text{O}_2$ , which is a problem in the nuclear power industry because of its oxidizing nature. The addition of  $\text{H}_2$  to water in reactors is a common procedure to prevent the formation of  $\text{H}_2\text{O}_2$  by scavenging the precursor OH radicals before they can recombine. The mechanism for this scavenging reaction is due to a chain reaction that was first isolated years ago by A. O. Allen and co-workers and essentially converts  $\text{H}_2$  and  $\text{H}_2\text{O}_2$  back to water. Chain processes are easily influenced by impurities and other external factors such as an interface so the details of this process are still not understood. Long time radiation chemical studies of pure water will lead to a steady state concentration of  $\text{H}_2\text{O}_2$  of about  $1 \mu\text{M}$ .<sup>2</sup> Solutions containing various amount of initial  $\text{H}_2\text{O}_2$  will show a gradual decrease in its concentration until a steady state is reached. Radiolysis of aqueous  $\text{H}_2\text{O}_2$  solutions with  $\gamma$ -rays and added alumina and/or  $\text{H}_2$  were performed. The concentration of  $\text{H}_2\text{O}_2$  was varied from 50 to 250 micromole and was found to decrease to a steady state value with increasing dose. The addition of  $\text{H}_2$  was found to increase the rate of loss of  $\text{H}_2\text{O}_2$  with dose and a lower steady state value was reached. Addition of  $\text{Al}_2\text{O}_3$  with  $\text{H}_2$  led to an even greater increase in the rate of decrease in  $\text{H}_2\text{O}_2$  concentration with increasing dose and a lower steady state value. Continuing studies will examine the variations in the amount of  $\text{Al}_2\text{O}_3$  and the  $\text{H}_2$  concentrations to map out their influence on  $\text{H}_2\text{O}_2$  decay. Previous studies have suggested that the decomposition of  $\text{H}_2\text{O}_2$  involves its adsorption onto the surface followed by decomposition.<sup>3</sup> Model studies were unable to show that a simple adsorption of the  $\text{H}_2\text{O}_2$  on the alumina surface was sufficient to account for the observed kinetics. Other experiments using a tris buffer were unable to show if the  $\text{H}_2\text{O}_2$  actually did adsorb on the alumina surface. Further experiments in combination with model studies will try to identify  $\text{H}_2\text{O}_2$  adsorption and its consequences as well as elucidate the overall mechanism.

Recently, we conducted fundamental investigations of water adsorption and dissociation onto surfaces of Ga-based photoelectrodes (GaAs, GaP, and Ga-N), which can be incorporated into PEC solar cells, in order to elucidate the water effects on surfaces upon water splitting. Our latest study on water interactions with GaN showed a correlation between chemical and electronic structures of the  $\text{H}_2\text{O}/\text{GaN}$  interface under ambient conditions.<sup>4</sup> III-N semiconductors possess many favorable properties that make them promising candidates as photocathode materials in future PEC solar cells. By varying the elemental stoichiometry or with the application of co-catalysts to these semiconductors, various properties, such as bandgap, lattice constant, and refractive index can be tuned precisely to satisfy a specific system, which also makes them electronically and architecturally flexible. Considerable attention has been focused recently on GaN as a material for photoelectrodes, thus, the  $\text{H}_2\text{O}/\text{GaN}$  interfacial properties have been investigated both theoretically and experimentally, primarily under ultra-high vacuum conditions.

These studies indicated that there was detectable band bending and surface photovoltage effects on a pristine surface and a surface exposed to H<sub>2</sub>O. However, the interfacial chemistry and electronic properties of H<sub>2</sub>O/GaN under operational conditions can differ significantly.

We employed ambient pressure AP-XPS) to investigate the electronic and chemical properties of the H<sub>2</sub>O/GaN(0001) interface under elevated pressures and/or temperatures. A pristine GaN(0001) surface exhibited upward band bending, which was partially flattened when exposed to H<sub>2</sub>O at room temperature. However, the GaN surface work function was slightly reduced due to the adsorption of molecular H<sub>2</sub>O and its dissociation products. At elevated temperatures a negative charge generated on the surface by a vigorous H<sub>2</sub>O/GaN interfacial chemistry induced an increase in both the surface work function and upward band bending. We tracked the dissociative adsorption of H<sub>2</sub>O onto the GaN(0001) surface by recording the core-level photoemission spectra and obtained the electronic and chemical properties at the H<sub>2</sub>O/GaN interface under ambient conditions. Our results suggest a strong correlation between the electronic and chemical properties of the material surface. The evolution of these properties will lead to significantly different behavior at the electrolyte/electrode interface in a working PEC solar cell. Therefore, there is an urgent need to investigate the relationships between semiconductor electronic properties with local interfacial chemistry of other III-V semiconductors (e.g., GaP, GaAsP, InAsP and other binary and ternary systems), which we plan to investigate in a near future.

In addition to III-V semiconductors other type of materials were studied, namely perovskites.<sup>5,6</sup> To elucidate both the chemical changes and the influence of these compositional changes on solar cell performance, we analyzed the results of X-ray photoelectron spectroscopy (XPS), scanning electron microscopy (SEM), and X-ray diffraction (XRD) of perovskite films exposed to ambient conditions. Chemical analysis revealed the loss of CH<sub>3</sub>NH<sub>3</sub><sup>+</sup> and I<sup>≠</sup> species from CH<sub>3</sub>NH<sub>3</sub>PbI<sub>3</sub> and its subsequent decomposition into lead carbonate, lead hydroxide, and lead oxide. After long-term storage under ambient conditions, morphological analysis revealed the transformation of randomly distributed defects and cracks, initially present in the densely packed crystalline structure, into relatively small grains. In contrast to a PbI<sub>2</sub> powder, CH<sub>3</sub>NH<sub>3</sub>PbI<sub>3</sub> exhibited a different degradation trend under ambient conditions. Therefore, we proposed a plausible CH<sub>3</sub>NH<sub>3</sub>PbI<sub>3</sub> decomposition pathway that explains the changes in the chemical composition of CH<sub>3</sub>NH<sub>3</sub>PbI<sub>3</sub> under ambient conditions. In addition, films stored under such conditions were incorporated into photovoltaic cells, and their performances were examined. The chemical changes in the decomposed films were found to cause a significant decrease in the photovoltaic efficiency of CH<sub>3</sub>NH<sub>3</sub>PbI<sub>3</sub>. Moreover, low-energy electrons can also affect structural and chemical properties of CH<sub>3</sub>NH<sub>3</sub>PbI<sub>3</sub>, leading to transformations of the organic part of the material, i.e., methylammonium cation.

## References

- (1) Schofield, J.; Reiff, S. C.; Pimblott, S. M.; La Verne, J. A. Radiolytic Hydrogen Generation at Silicon Carbide - Water Interfaces. *J. Nucl. Mater.* **2016**, *469*, 43-50.
- (2) Daub, K.; Zhang, X.; Noel, J. J.; Wren, J. C. Effects of Gamma-Radiation versus H<sub>2</sub>O<sub>2</sub> on Carbon Steel Corrosion. *Electrochem. Acta* **2010**, *55*, 2767-2776.
- (3) Lousada, C. M.; La Verne, J. A.; Jonsson, M. Enhanced Hydrogen Formation During the Catalytic Decomposition of H<sub>2</sub>O<sub>2</sub> on Metal Oxide Surfaces in the Presence of HO Radical Scavengers *Phys. Chem. Chem. Phys.* **2013**, *15*, 12674-12679.

- (4) Zhang, X. Q.; Ptasińska, S. Electronic and chemical structure of the H<sub>2</sub>O/GaN(0001) interface under ambient conditions. *Sci Rep* **2016**, *6*.
- (5) Huang, W. X.; Manser, J. S.; Kamat, P. V.; Ptasińska, S. Evolution of Chemical Composition, Morphology, and Photovoltaic Efficiency of CH<sub>3</sub>NH<sub>3</sub>PbI<sub>3</sub> Perovskite under Ambient Conditions. *Chem. Mat.* **2016**, *28*, 303-311.
- (6) Milosavljevic, A. R.; Huang, W. X.; Sadhu, S.; Ptasińska, S. Low-energy Electron-induced Degradation of Organolead Halide Perovskite. *Angew. Chem. Int. Ed.* **2016**, *10.1002/anie.201605013*.

### Publications with BES support (2014-2016)

- Brown, A.R., Wincott, P.L., La Verne, J.A., Small, J.S., Vaughan, D.J., Pimblott, S.M., Lloyd, J.R., 2014. The Impact of  $\gamma$  Radiation on the Bioavailability of Fe(III) Minerals for Microbial Respiration. *Envir. Sci. Tech.* *48*, 10672-10680.
- Dhiman, S.B., Goff, G.S., Runde, W., LaVerne, J.A., 2014. Gamma and Heavy Ion Radiolysis of Ionic Liquids: A Comparative Study. *Journal of Nuclear Materials* *453*, 182-187.
- Huang W.; Manser J.; Kamat P.V.; Ptasińska S. *Chem. Mater.* **2016**, *28*, 303-11. Evolution of chemical composition, morphology, and photovoltaic efficiency of CH<sub>3</sub>NH<sub>3</sub>PbI<sub>3</sub> perovskite under ambient conditions.
- Jiang T.; Zhang X.; Vishwanath S.; Mu X.; Kanzyuba V.; Sokolov D.; Ptasińska S.; Go D.B.; Xing G.; Luo T. *Nanoscale* **2016**, *8* Covalent bonding modulated graphene-metal interfacial thermal transport.
- LaVerne, J.A., Dowling-Medley, J., 2015. Combinations of Aromatic and Aliphatic Radiolysis. *J. Phys. Chem. A* *119*, 10125-10129.
- Milosavljevic A.R.; Huang W.; Sadhu S.; Ptasińska S. *Angew. Chem. Int. Ed.* **2016**. Low-energy electron-induced degradation of organolead halide perovskite. 10.1002/anie.201605013
- Mincher, B.J., Mezyk, S.P., Elias, G., Groenewold, G.S., La Verne, J.A., Nilsson, A.R., Pearson, J., Schmitt, N.C., Tillotson, R.D., Olsen, L.G., 2014. The Radiation Chemistry of CMPO: Part 2. Alpha Radiolysis. *Solv. Extr. Ion Exch.* *32*, 167-178.
- Reiff, S.C., La Verne, J.A., 2015. Gamma and He Ion Radiolysis of Copper Oxides. *J. Phys. Chem. C* *119*, 8821-8828.
- Reiff, S.C., La Verne, J.A., 2015. Radiation-Induced Chemical Changes to Iron Oxides. *J. Phys. Chem. B* *119*, 7358-7365.
- Sayle T.X.T.; Caddeo F.; Zhang X.; Sakthivel T.; Das S.; Seal S.; Ptasińska S.; Sayle D.C. *Chem. Mat.* **2016**, Structure–Activity Map of Ceria Nanoparticles, Nanocubes, and Mesoporous Architectures. 10.1021/acs.chemmater.6b02536
- Schofield, J., Reiff, S.C., Pimblott, S.M., La Verne, J.A., 2016. Radiolytic hydrogen generation at silicon carbide - water interfaces. *Journal of Nuclear Materials* *469*, 43-50.
- Zhang X.; Ptasińska S. *Top. Catal.* **2016**, *59*, 564-73. Heterogeneous oxygen-containing species formed via oxygen or water dissociative adsorption onto a gallium phosphide surface.
- Zhang X.; Ptasińska S. *Sci. Rep.* **2016**, *6*, 24848. Electronic and chemical structure of the H<sub>2</sub>O/GaN(0001) interface under ambient conditions.
- Zhang X.; Ptasińska S. *ChemCatChem* **2016**, *8*, 1632. High pressure induced pseudo-oxidation of copper surface by carbon monoxide.

## Solution Reactivity and Mechanisms through Pulse Radiolysis

Sergei V. Lymar

Chemistry Department, Brookhaven National Laboratory, Upton, NY 11973-5000

e-mail: lymar@bnl.gov

### Scope

This program applies pulse radiolysis and complementary time-resolved techniques for investigating reactive intermediates and inorganic reaction mechanisms. The specific systems are selected based on their fundamental significance or importance in energy and environmental problems.

The first project investigates physical chemistry of nitrogen oxides and their congeneric oxoacids and oxoanions. These species play an essential role in environmental chemistry, particularly in the terrestrial nitrogen cycle, pollution, bioremediation, and ozone depletion. Nitrogen-oxygen intermediates are also central to the radiation-induced reactions that occur in nuclear fuel processing and within attendant nuclear waste. Equally important are the biochemical roles of nitrogen oxides. We apply time-resolved techniques for elucidation of the prospective reactions in terms of their thermodynamics, rates and mechanisms.

The second project deals with radiation chemistry in polar aprotic solvents. Due to their solubilizing properties, low nucleophilicity, and large electrochemical window, these solvents are widely used in mechanistic studies relevant to redox catalysis. Recently, we have shown that pulse radiolysis, particularly combined with time-resolved infrared detection (TRIR), is a powerful technique for gaining mechanistic insights into the dynamics of redox catalysis in polar aprotic solvents through probing normally inaccessible catalysts' oxidation states. However, this research is hampered by insufficient understanding of primary radiolysis species in these solvents and by the deficiency of methods for directing their reactivity toward generating strong reductants or oxidants that can be used for initiating useful redox chemistry. Our current work focuses on acetonitrile, which is our solvent of choice for a number of planned TRIR mechanistic studies.

The goal of the third project has been to gain mechanistic insight into proton coupled electron transfer (PCET). These reactions, which involve an overall transfer of a proton and an electron, play an important role in natural and artificial photosynthetic transformations providing low energy pathways in charge separation, charge transport and redox catalysis. In this project, we apply time-resolved techniques to investigate the reaction rates dependencies upon the driving force. When combined with the computational thermodynamic analysis, such an approach provides information that is critical for distinguishing between alternative stepwise and concerted PCET pathways and evaluating the influence of solvent properties on the PCET mechanisms.

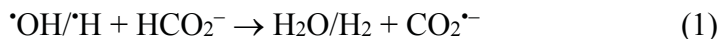
This abstract summarizes recent results from the last two projects; the first project was presented in detail at the 2014 CPIMS meeting.

Collaborators on these projects include M. Valiev (PNNL),<sup>1</sup> J. Hurst (WSU, emeritus),<sup>2-5</sup> D. Polyansky (BNL),<sup>4</sup> M. Ertem (BNL),<sup>6</sup> and D. Grills (BNL).<sup>7</sup>

### Recent progress

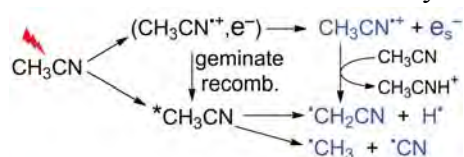
*CO<sub>2</sub><sup>•-</sup> Radical in Acetonitrile.* (with David C. Grills, BNL) Carbon dioxide radical anion (CO<sub>2</sub><sup>•-</sup>) is a powerful reductant ( $E^{\circ}(\text{CO}_2/\text{CO}_2^{\bullet-}) = -1.90 \text{ V vs NHE in H}_2\text{O}^{8-9}$ ). In aqueous pulse radiolysis, a common strategy to generate overall reducing conditions is to add formate anion

( $\text{HCO}_2^-$ ), resulting in the scavenging of  $\cdot\text{OH}$  and  $\cdot\text{H}$  radicals via H-atom transfer and the production of  $\text{CO}_2^{\cdot-}$ ; that is,



Recently, there has been increasing interest in organic solvents as media for pulse radiolysis. We are particularly interested in acetonitrile ( $\text{CH}_3\text{CN}$ ) as a solvent for mechanistic investigations of  $\text{CO}_2$  reduction catalysts using our recently-developed technique of pulse radiolysis combined with nanosecond time-resolved infrared spectroscopy (PR-TRIR).<sup>7</sup> Compared with water, much less is known about the identity and reactivity of the primary radiolysis products in  $\text{CH}_3\text{CN}$ .

However, product analysis studies<sup>10-11</sup> clearly identify fragmentation as the predominant radiation-induced process in MeCN, whereby a variety of solvent-derived radicals are produced as shown in the scheme to the left.

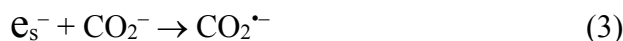


It was previously proposed<sup>12</sup> that the addition of  $\text{HCO}_2^-$  to  $\text{CH}_3\text{CN}$  results in the  $\text{CO}_2^{\cdot-}$  generation through H-atom abstraction from  $\text{HCO}_2^-$  by the radiolytically-generated  $\cdot\text{CH}_2\text{CN}$  radical; that is, a reaction analogous to eq 1



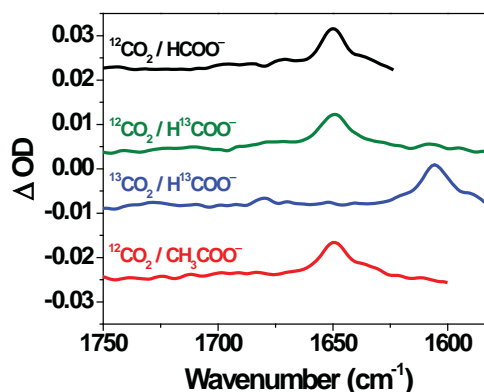
More recently we presented data that could be interpreted as a support for such reactivity.<sup>7</sup>

Another pathway for the radiolytic formation of  $\text{CO}_2^{\cdot-}$  in  $\text{CH}_3\text{CN}$ , which will be important in investigating  $\text{CO}_2$  reduction catalysts, is the direct reduction of dissolved  $\text{CO}_2$  by the solvated electrons; that is,



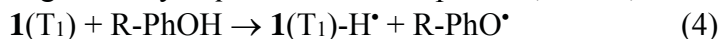
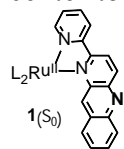
However, to the best of our knowledge, the  $\text{CO}_2^{\cdot-}$  radical has never been spectroscopically characterized or monitored in  $\text{CH}_3\text{CN}$  solution.

We have taken advantage of the structural specificity of the PR-TRIR technique to probe the generation of  $\text{CO}_2^{\cdot-}$  by both of the abovementioned pathways. The  $\text{CO}_2^{\cdot-}$  radical was found to absorb at  $1650 \text{ cm}^{-1}$  (Figure to the right). Experiments with various combinations of unlabeled and  $^{13}\text{C}$ -labeled  $\text{CO}_2$  and  $\text{HCO}_2^-$  allowed us to unravel the contributions of the two pathways (eq. 2 and 3) into  $\text{CO}_2^{\cdot-}$  formation. Our results indicate that formate predominantly acts to boost the yield of  $\text{CO}_2^{\cdot-}$  from  $e_s^-$  (eq. 3). We conjecture that this occurs through  $\text{HCO}_2^-$  serving as a base that scavenges protons released during the solvent ionization, which helps to suppress the electron-proton geminate recombination thereby enhancing the  $e_s^-$  yield. The formation of  $\text{CO}_2^{\cdot-}$  from  $\text{HCO}_2^-$  through H-atom abstraction by solvent radicals is a minor pathway. From literature,<sup>8-9,13</sup> we estimate  $BDE(\text{H}-\text{CO}_2^-) \approx 92 \text{ kcal/mol}$ . Because  $BDE(\text{H}-\text{CH}_2\text{CN})$  is  $\sim 97 \text{ kcal/mol}$ , such a reaction is thermodynamically feasible, but its small driving force makes it rather slow and inefficient.

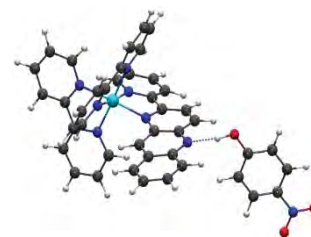


TRIR spectra recorded immediately after pulse radiolysis of  $\text{CD}_3\text{CN}$  containing various combinations of  $^{12}\text{CO}_2$ ,  $^{13}\text{CO}_2$ ,  $\text{HCO}_2^-$ ,  $\text{H}^{13}\text{CO}_2^-$ , and acetate.

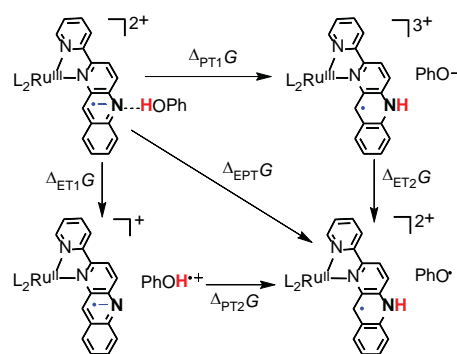
*Proton-Coupled Electron Transfer.*<sup>6</sup> (with Dmitry Polyansky and Mehmed Ertem, BNL) Photoexcitation of the polypyridine Ru(II) complex whose structure is shown to the left (L = bipyridine) leads to the triplet (T<sub>1</sub>) excited state, in which the electron is transferred from the Ru(II) center to the azaacridine ligand. This increases both the complex reduction potential (by 1.70 V) and Brønsted basicity of the ligand (by 4.5 pK<sub>a</sub> units). Through a combination of pulse radiolysis and flash photolysis experiments, we have shown that the complex in its T<sub>1</sub> is capable of oxidizing a variety of *para*-substituted phenols, that is,



Although formally this reaction amounts to hydrogen atom transfer, mechanistically it constitutes PCET because the electron goes to the Ru center and the proton is accepted by the ligand's N atom. This reaction exhibits negative activation energy, which is a clear indication that a precursor complex is formed between **1**(T<sub>1</sub>) and R-PhOH. Computational data strongly suggest that this complex is due to the hydrogen bonding interaction between the ligand's N atom and phenol's OH group, as shown to the right for *para*-nitrophenol. This result emphasizes the critical role that hydrogen bonding plays in PCET reactions in general.



To gain a deeper mechanistic insight into reaction 4, we have employed the in-depth energy analysis of the three possible PCET pathways shown in the Scheme below. Based on this analysis, we have concluded that the nature of a *para* substituent plays a decisive role in the partitioning of reactivity between these pathways. For phenols with more electron-donating substituents (*e.g.*, MeO- or Ph-), reaction 4 occurs entirely through the diagonal, one-step pathway in the Scheme which can be described as a concerted electron-proton transfer (EPT). In contrast, for phenols with electron-donating substituents (*e.g.*, NC- or O<sub>2</sub>N-), the two-step PT1-ET2 pathway consisting of proton transfer followed by electron transfer within the **1**(T<sub>1</sub>)-H/PhO<sup>-</sup> ion pair becomes dominant. The two-step ET1-PT2 pathway that begins with electron transfer does not play any role due to the prohibitively strong endothermicity of this step for all phenols.



MeO- or Ph-), reaction 4 occurs entirely through the diagonal, one-step pathway in the Scheme which can be described as a concerted electron-proton transfer (EPT). In contrast, for phenols with electron-donating substituents (*e.g.*, NC- or O<sub>2</sub>N-), the two-step PT1-ET2 pathway consisting of proton transfer followed by electron transfer within the **1**(T<sub>1</sub>)-H/PhO<sup>-</sup> ion pair becomes dominant. The two-step ET1-PT2 pathway that begins with electron transfer does not play any role due to the prohibitively strong endothermicity of this step for all phenols.

*Planned work will investigate:*

- Nature and radiation yields of primary acetonitrile radiolysis products.
- Techniques for directing primary radiolysis species toward generating strong reductants or oxidants in acetonitrile.
- Novel pathways for generating nitroxyl species (<sup>1</sup>HNO and <sup>3</sup>NO<sup>-</sup>) and their reactivity, including their self-decay and spin-forbidden ground state bond breaking/making reactions.
- Energetics and redox reactivity of trioxodinitrate (HN<sub>2</sub>O<sub>3</sub><sup>-</sup>/N<sub>2</sub>O<sub>3</sub><sup>2-</sup>) species, and their nitroxyl release mechanism.
- Redox and radical chemistry in the nitrite/nitrate system, including: formation pathways and thermodynamics of nitrate radical anion, NO<sub>3</sub><sup>2-</sup>; rates and mechanisms of its acid-catalyzed and redox reactions.
- Kinetic isotope effect and kinetic solvent effect in the PCET reactivity.

**References** (DOE sponsored publications in 2015-present are marked with asterisk)

- (1) Shaikh, N.; Valiev, M.; Lymar, S. V. *J. Inorg. Biochem.* **2014**, *141*, 28-35.
- (2) Cape, J. L.; Lymar, S. V.; Lightbody, T.; Hurst, J. K. *Inorg. Chem.* **2009**, *48*, 4400-4410.
- (3) Stull, J. A.; Britt, R. D.; McHale, J. L.; Knorr, F. J.; Lymar, S. V.; Hurst, J. K. *J. Am. Chem. Soc.* **2012**, *134*, 19973-19976.
- (4) Polyanskiy, D. E.; Hurst, J. K.; Lymar, S. V. *Eur. J. Inorg. Chem.* **2014**, 619-634.
- (5\*) Hurst, J. K.; Roemeling, M. D.; Lymar, S. V. "Mechanistic Insight into Peroxydisulfate Reactivity: Oxidation of the *cis,cis*-[Ru(bpy)<sub>2</sub>(OH<sub>2</sub>)<sub>2</sub>O]<sup>4+</sup> "Blue Dimer"" *J. Phys. Chem. B* **2015**, *119*, 7749-7760.
- (6\*) Polyanskiy, D. E.; Ertem, M.; Lymar, S. V. "Mechanistic Insights into Photoinduced Proton-Coupled Electron Transfer from Phenols to Polypyridine Ru(II) Complexes" *J. Am. Chem. Soc.* **2016**, submitted.
- (7) Grills, D. C.; Farrington, J. A.; Layne, B. H.; Lymar, S. V.; Mello, B. A.; Preses, J. M.; Wishart, J. F. *J. Am. Chem. Soc.* **2014**, *136*, 5563-5566.
- (8) Armstrong, D. A.; Huie, R. E.; Lymar, S.; Koppenol, W. H.; Merényi, G.; Neta, P.; Stanbury, D. M.; Steenken, S.; Wardman, P. *Bioinorg. React. Mech.* **2013**, *9*, 59-61.
- (9\*) Armstrong, D. A.; Huie, R. E.; Lymar, S.; Koppenol, W. H.; Merényi, G.; Neta, P.; Ruscic, B.; Stanbury, D. M.; Steenken, S.; Wardman, P. "Standard Electrode Potentials Involving Radicals in Aqueous Solution: Inorganic Radicals (IUPAC Technical Report)" *Pure Appl. Chem.* **2015**, *87*, 1139-1150.
- (10) Bradley, D.; Wilkinson, J. *J. Chem. Soc. A* **1967**, 531-537.
- (11) Ayscough, P. B.; Drawe, H.; Kohler, P. *Radiation Res.* **1968**, *33*, 263-273.
- (12) Burrows, H. D.; Kosower, E. M. *J. Phys. Chem.* **1974**, *78*, 112-117.
- (13) Wagman, D. D.; Evans, W. H.; Parker, V. B.; Schumm, R. H.; Halow, I.; Bailey, S. M.; Churney, K. L.; Nuttall, R. L. *J. Phys. Chem. Ref. Data* **1982**, *11*, Suppl. 2.

## Ionic Liquids: Radiation Chemistry, Solvation Dynamics and Reactivity Patterns

James F. Wishart

Chemistry Department, Brookhaven National Laboratory, Upton, NY 11973-5000

wishart@bnl.gov

### Program Definition

Ionic liquids (ILs) are a rapidly expanding family of condensed-phase media with important applications in energy production, storage and consumption, including advanced devices and processes and nuclear fuel and waste processing. ILs generally have low volatilities and are combustion-resistant, highly conductive, recyclable and capable of dissolving a wide variety of materials. They are finding new uses in dye-sensitized solar cells, chemical synthesis, catalysis, separations chemistry, batteries, supercapacitors and other areas. Ionic liquids have dramatically different properties compared to conventional molecular solvents, and they provide a new and unusual environment to test our theoretical understanding of primary radiation chemistry, charge transfer and other reactions. We are interested in how IL properties influence physical and dynamical processes that determine the stability and lifetimes of reactive intermediates and thereby affect the courses of reactions and product distributions. We study these issues by characterization of primary radiolysis products and measurements of their yields and reactivity, quantification of electron solvation dynamics and scavenging of electrons in different states of solvation. From this knowledge we wish to learn how to predict radiolytic mechanisms and control them or mitigate their effects on the properties of materials used in nuclear fuel processing, for example, and to apply IL radiation chemistry to answer questions about general chemical reactivity in ionic liquids that will aid in the development of applications listed above.

Soon after our radiolysis studies began it became evident that the slow solvation dynamics of the excess electron in ILs (which vary over a wide viscosity range) increase the importance of pre-solvated electron reactivity and consequently alter product distributions and subsequent chemistry. This difference from conventional solvents has profound effects on predicting and controlling radiolytic yields, which need to be quantified for the successful use under radiolytic conditions. Electron solvation dynamics in ILs are measured directly when possible and estimated using proxies (e.g. coumarin-153 dynamic emission Stokes shifts or benzophenone anion solvation) in other cases. Electron reactivity is measured using ultrafast kinetics techniques for comparison with the solvation process.

A second important aspect of our interest in ionic liquids is how their unusual sets of properties affect charge transfer and charge transport processes. This is important because of the many applications of ionic liquids in devices that operate on the basis of charge transport. While interest in understanding these processes in ionic liquids is growing, the field is still in an early stage of development. We are using donor-bridge-acceptor systems to study electron transfer reactions across variable distances in a series of ionic liquids with a range of structural motifs and whose dynamical time scales vary from moderately fast to extremely slow, and to compare them with conventional solvents.

**Methods.** Picosecond pulse radiolysis studies at BNL's Laser-Electron Accelerator Facility (LEAF) are used to identify reactive species in ionic liquids and measure their solvation and reaction rates. This work is aided greatly by the development of Optical Fiber Single-Shot (OFSS) detection at LEAF by A. Cook (DOI: 10.1063/1.3156048) and its present extension into the NIR regime. LEAF's unique capability in mid-infrared transient absorption detection<sup>3</sup> allows precise identification of radiolytic intermediates and their reaction kinetics. IL solvation and rotational dynamics, and electron transfer reactions, are measured by TCSPC in the laboratory of E. W. Castner, Jr. at Rutgers Univ. Picosecond transient absorption measurements of excited state dynamics and electron transfer reactions are done in our lab at BNL. Diffusion rates of anions, cations and solutes are obtained by PGSE NMR in the S. Suarez and S.

Greenbaum labs at CUNY and by Castner's group at Rutgers. We have extensive collaborations with other major groups in ionic liquid synthesis, physical chemistry, simulations and radiation chemistry.

***Ionic liquid synthesis and characterization.*** Our work often involves novel ILs that we design to the requirements of our radiolysis and solvation dynamics studies and are not commercially available. We have developed robust in-house capabilities and long-standing collaborations (particularly with S. Lall-Ramnarine of Queensborough CC and R. Engel of Queens College) to design, prepare and characterize ILs in support of our research objectives. Cation synthesis is done by several methods, including a CEM microwave reactor, resulting in higher yields of purer products in much shorter time than traditional methods. We have a diverse instrumentation cluster including DSC, TGA, viscometry, AC conductivity, Karl Fischer moisture determination, ion chromatography and ESI-mass spec (for purity analysis and radiolytic product identification). The cluster serves as a resource for a widespread network of collaborations. Our efforts are substantially augmented by student internships from the BNL Office of Educational Programs, particularly the VFP (formerly FaST) program, which brings collaborative faculty members and their students into the lab for ten weeks each summer. Since 2003, a total of 48 undergrads, three graduate students, one pre-service teacher, two high school students and four junior faculty have worked on IL projects in our lab, many of them for more than one summer.

## Recent Progress

***Longer polyether side chains on pyrrolidinium cations show remarkable viscosity behavior in the IL.***<sup>1</sup> Imidazolium and pyrrolidinium bis(trifluoromethylsulfonyl)amide ionic liquids bearing side chains 4 to 10 atoms in length with repeating ether units, and their alkyl analogues, were prepared and characterized for their thermal and transport properties. Remarkably, as the number of ether units in the pyrrolidinium ILs increases there is hardly any increase in the viscosity, in contrast to alkylpyrrolidinium ILs where the viscosity increases steadily with chain length (Fig. 1). Viscosities of imidazolium ether ILs increase with chain length but always remain well below their alkyl congeners. Viscosities were measured over a wide temperature range for each IL and fitted to the Vogel-Tammann-Fulcher equation. The differences between IL families shown in Fig. 1 for a single temperature were reflected consistently over the whole temperature range and the VTF fitting parameters.

While it has been observed for some time that the alkyl-substituted imidazolium NTf<sub>2</sub> ILs are significantly less viscous than their pyrrolidinium NTf<sub>2</sub> counterparts, when oligoether chains are attached, the pyrrolidinium and imidazolium NTf<sub>2</sub> ILs are much closer in viscosity than in the alkyl case, with the pyrrolidinium ILs actually being less viscous when the ether chains get longer. No one had rigorously investigated these longer polyether side chain ILs before, so this effect was a discovery. Structural and molecular dynamics studies on related systems by our collaborators suggest that ether and alkyl side chains distribute themselves differently within the IL, where the alkyl chains tend to self-segregate into non-polar domains while the ether chains do not. These structural differences manifest themselves in the dynamical and transport properties of the ILs. However, the nearly constant viscosities with increasing alkyl chain length observed with the pyrrolidinium series, in comparison with the imidazolium series, was not anticipated by previous work. These results call for further studies using PGSE NMR diffusion measurements, X-ray scattering studies of liquid structure, and molecular dynamics simulations to interpret the observed dynamical behavior. They also suggest a significant new parameter space concerning the choice of starting materials for researchers designing ILs for specific applications.

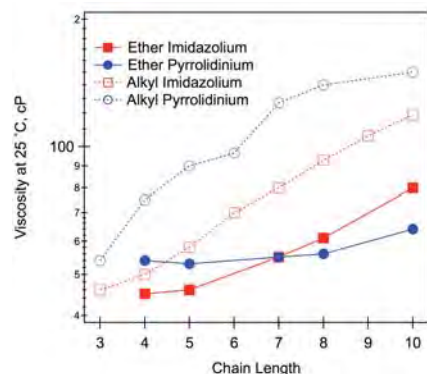


**Figure 1.** Viscosities of the imidazolium and pyrrolidinium ether and alkyl NTf<sub>2</sub> ionic liquids at 25 °C.

## Future Plans

**Scavenging and solvation processes of pre-solvated electrons in ionic liquids.** Our early work in the reactivity of excess electrons in ionic liquids demonstrated the importance of pre-solvated electron scavenging in trying to understand and predict the distributions of early radiolysis products and radiolytic damage accumulation. It was also clear that the slower relaxation dynamics of ILs made them excellent media for the general study of fundamental radiolysis processes without the need to use cryogenic techniques, in combination with the advanced instrumentation of the LEAF Facility. We recently connected our observed electron solvation dynamics to the kinetics of electron scavenging. In other preliminary work we have observed that selected scavengers (e.g., nitrate, benzophenone) in ILs show different reaction profiles towards the various precursor states to the solvated electron. Different scavenger reactivities towards pre-solvated and solvated electrons have been known empirically for many years and cryogenic kinetic work by Jonah and Lewis showed specific mechanistic differences between scavengers similar to what we have seen in ILs. However, the combination of extended IL dynamical time scales and the time resolution of the LEAF OFSS detection system, coupled with the fact that it uses only small amounts of samples that do not have to be flowed, as well as the ability of ILs to dissolve polar and nonpolar scavengers, provides a unique opportunity to characterize the fundamental reactivity of pre-solvated electron species and understand how the properties of scavengers control their reaction profiles. The extension of the LEAF OFSS detection capability to the NIR (900-1700 nm) greatly facilitates the study of dynamical and electron solvation processes in our ILs. This knowledge will permit the design of better systems to control radiation-induced reactivity, for example in the processing of radioactive materials (whether in ionic liquids or not), in systems for radiation processing and sterilization, and during long-term exposure to space, for example. (with A. Cook, BNL)

## Publications

1. *The Effect of Lengthening Cation Ether Tails On Ionic Liquid Properties* S. I. Lall-Ramnarine, C. Rodriguez, R. Fernandez, N. Zmich, E. D. Fernandez, S. B. Dhiman and J. F. Wishart *ECS Trans.*, in press.
2. *Transport Properties of Ionic Liquid Mixtures Containing Heterodications* S. I. Lall-Ramnarine, E. D. Fernandez, C. Rodriguez, S. Wei, S. B. Dhiman and J. F. Wishart *ECS Trans.*, in press.
3. *Development of nanosecond time-resolved infrared detection at the LEAF pulse radiolysis facility* D. C. Grills, J. A. Farrington, B. H. Layne, J. M. Preses, H. J. Bernstein, J. F. Wishart, *Rev. Sci. Instrum.* **86**, 044102 (2015) DOI: 10.1063/1.4918728
4. *Distributed Electron Transfer Dynamics for a Donor-Bridge-Acceptor Complex in Ionic Liquids*, J. A. Devine, M. Labib, M. E. Harries, R. Abdel Malak Rached, J. Issa, J. F. Wishart, E. W. Castner, Jr., *J. Phys. Chem. B* **119**, 11336–11345 (2015). DOI: 10.1021/acs.jpcc.5b03320
5. *What Makes Fluoroethylene Carbonate Different?* I. A. Shkrob, J. F. Wishart, D. P. Abraham, *J. Phys. Chem. C* **119**, 14954-14964 (2015). DOI: 10.1021/acs.jpcc.5b03591
6. *Ultrafast Transient Absorption Spectrum of the Room Temperature Ionic Liquid 1-Hexyl-3-Methylimidazolium Bromide: Confounding Effects of Photo-degradation* R. M. Musat, R. A. Crowell, D. E. Polyanskiy, M. F. Thomas, J. F. Wishart, Y. Katsumura, K. Takahashi, *Radiat. Phys. Chem.*, **117**, 78-82 (2015). DOI: 10.1016/j.radphyschem.2015.07.015
7. *A comparison of the  $\gamma$ -radiolysis of TODGA and T(EH)DGA using UHPLC-ESI-MS analysis* C. A. Zarzana, G. S. Groenewold, B. J. Mincher, S. P. Mezyk, A. Wilden, H. Schmidt, G. Modolo, J. F. Wishart and A. R. Cook, *Solv. Extr. Ion Exch.*, **33**, 431-447 (2015). DOI: 10.1080/07366299.2015.1012885

The background of the entire page is a light blue color. Overlaid on this background is a large, abstract graphic consisting of several interconnected, rounded shapes in a slightly darker shade of blue. Within these shapes are numerous spheres. Some spheres are bright white with a soft glow, while others are a vibrant red, also with a soft glow. The spheres are scattered throughout the composition, creating a dynamic and somewhat organic feel. In the center of this graphic, the text 'List of Participants' is written in a bold, italicized, black font.

***List of Participants***

## LIST OF PARTICIPANTS

Dr. Musahid Ahmed  
Lawrence Berkeley National Laboratory  
<https://sites.google.com/site/musaswebcorner/home>

Professor Heather Allen  
Ohio State University  
<https://research.cbc.osu.edu/allen.697/>

Professor Abraham Badu-Tawiah  
Ohio State University  
<https://research.cbc.osu.edu/badu-tawiah.1/>

Dr. Marcel Baer  
Pacific Northwest National Laboratory  
[http://www.pnnl.gov/science/staff/staff\\_info.asp?staff\\_num=7648](http://www.pnnl.gov/science/staff/staff_info.asp?staff_num=7648)

Professor L. Robert Baker  
Ohio State University  
<https://research.cbc.osu.edu/baker.2364/>

Dr. David Bartels  
Notre Dame Radiation Laboratory  
<http://rad.nd.edu/people/faculty/david-m-bartels/>

Dr. Ali Belkacem  
Lawrence Berkeley National Laboratory  
<http://ultrafast.lbl.gov/amos/dr-ali-belkacem/>

Dr. Hendrik Bluhm  
Lawrence Berkeley National Laboratory  
<https://sites.google.com/a/lbl.gov/hendrik-bluhm/>

Dr. Nicholas Camillone  
Brookhaven National Laboratory  
<http://www.bnl.gov/chemistry/bio/Camillone%20Nicholas.asp>

Professor Ian Carmichael  
Notre Dame Radiation Laboratory  
<http://rad.nd.edu/people/faculty/ian-carmichael/>

Professor Aurora Clark  
Washington State University  
<https://aclark.chem.wsu.edu/>

Dr. Andrew Cook  
Brookhaven National Laboratory  
<https://www.bnl.gov/chemistry/bio/CookAndrew.asp>

Professor Tanja Cuk  
Lawrence Berkeley National Laboratory  
<http://www.cchem.berkeley.edu/tkgrp/>

Dr. Liem Dang  
Pacific Northwest National Laboratory  
[http://www.pnl.gov/science/staff/staff\\_info.asp?staff\\_num=5604](http://www.pnl.gov/science/staff/staff_info.asp?staff_num=5604)

Dr. Patrick El-Khoury  
Pacific Northwest National Laboratory  
[http://www.pnnl.gov/science/staff/staff\\_info.asp?staff\\_num=7868](http://www.pnnl.gov/science/staff/staff_info.asp?staff_num=7868)

Professor Michael Fayer  
Stanford University  
<http://www.stanford.edu/group/fayer/>

Dr. Christopher Fecko  
DOE/Basic Energy Sciences  
<http://science.energy.gov/bes/csgb/about/staff/dr-christopher-fecko/>

Dr. Gregory Fiechtner  
DOE/Basic Energy Sciences  
<http://science.energy.gov/bes/csgb/about/staff/dr-gregory-i-fiechtner/>

Mr. John L. Fulton  
Pacific Northwest National Laboratory  
[http://www.pnl.gov/science/staff/staff\\_info.asp?staff\\_num=5587](http://www.pnl.gov/science/staff/staff_info.asp?staff_num=5587)

Professor Etienne Garand  
University of Wisconsin  
<http://garand.chem.wisc.edu/>

Dr. Bruce Garrett  
Pacific Northwest National Laboratory  
[http://www.pnl.gov/science/staff/staff\\_info.asp?staff\\_num=5496](http://www.pnl.gov/science/staff/staff_info.asp?staff_num=5496)

Dr. Mary K. Gilles  
Lawrence Berkeley National Laboratory  
<https://commons.lbl.gov/display/csd/Mary+K.+Gilles>

Mark Gordon  
Ames Laboratory/Iowa State University  
<https://www.ameslab.gov/amcs/mark>

Dr. Niranjan Govind  
Pacific Northwest National Laboratory  
[http://www.pnl.gov/science/staff/staff\\_info.asp?staff\\_num=8375](http://www.pnl.gov/science/staff/staff_info.asp?staff_num=8375)

Dr. Alexander Harris  
Brookhaven National Laboratory  
<http://www.bnl.gov/chemistry/bio/HarrisAlex.asp>

Professor Teresa Head-Gordon  
Lawrence Berkeley National Laboratory  
<http://thglab.berkeley.edu/>

Dr. Wayne Hess  
Pacific Northwest National Laboratory  
[http://www.pnl.gov/science/staff/staff\\_info.asp?staff\\_num=5505](http://www.pnl.gov/science/staff/staff_info.asp?staff_num=5505)

Professor Wilson Ho  
University of California, Irvine  
<http://www.physics.uci.edu/~wilsonho/whoghp.htm>

Dr. Ireneusz Janik  
Notre Dame Radiation Laboratory  
<http://rad.nd.edu/people/faculty/ireneusz-janik/>

Professor Caroline Chick Jarrold  
Indiana University  
<http://mypage.iu.edu/~ciarrold/index.htm>

Professor Mark Johnson  
Yale University  
<http://ilab.chem.yale.edu/>

Professor Kenneth Jordan  
University of Pittsburgh  
<http://www.pitt.edu/~jordan/>

Dr. Shawn Kathmann  
Pacific Northwest National Laboratory  
[http://www.pnl.gov/science/staff/staff\\_info.asp?staff\\_num=5601](http://www.pnl.gov/science/staff/staff_info.asp?staff_num=5601)

Dr. Bruce Kay  
Pacific Northwest National Laboratory  
[http://www.pnl.gov/science/staff/staff\\_info.asp?staff\\_num=5530](http://www.pnl.gov/science/staff/staff_info.asp?staff_num=5530)

Professor Munira Khalil  
University of Washington  
<https://sites.google.com/a/uw.edu/khalilgroup/>

Dr. Greg Kimmel  
Pacific Northwest National Laboratory  
[http://www.pnl.gov/science/staff/staff\\_info.asp?staff\\_num=5527](http://www.pnl.gov/science/staff/staff_info.asp?staff_num=5527)

Professor Amber Krummel  
Colorado State University  
<http://sites.chem.colostate.edu/krummellab/>

Dr. Jeffrey L. Krause  
DOE/Basic Energy Sciences  
<http://science.energy.gov/bes/csgb/about/staff/dr-jeffrey-l-krause/>

Professor Christy Landes  
Rice University  
<http://www.lrg.rice.edu/>

Dr. Jay LaVerne  
Notre Dame Radiation Laboratory  
<http://rad.nd.edu/people/faculty/jay-a-laverne/>

Professor Stephan Link  
Rice University  
<http://slink.rice.edu/>

Professor H. Peter Lu  
Bowling Green State University  
<https://www.bgsu.edu/arts-and-sciences/chemistry/faculty/peter-lu.html>

Dr. Sergei Lyman  
Brookhaven National Laboratory  
<https://www.bnl.gov/chemistry/bio/LymanSergei.asp>

Diane Marceau  
DOE/Basic Energy Sciences  
<http://science.energy.gov/bes/csgb/about/staff/>

Dr. John Miller  
Brookhaven National Laboratory  
<https://www.bnl.gov/chemistry/bio/MillerJohn.asp>

Dr. Karl Mueller  
Pacific Northwest National Laboratory  
[http://www.pnnl.gov/science/staff/staff\\_info.asp?staff\\_num=8286](http://www.pnnl.gov/science/staff/staff_info.asp?staff_num=8286)

Dr. Christopher Mundy  
Pacific Northwest National Laboratory  
[http://www.pnl.gov/science/staff/staff\\_info.asp?staff\\_num=5981](http://www.pnl.gov/science/staff/staff_info.asp?staff_num=5981)

Dr. Charles (Chuck) Peden  
DOE/Basic Energy Sciences  
<http://science.energy.gov/bes/csgb/about/staff/dr-charles-peden/>

Dr. Mark Pederson  
DOE/Basic Energy Sciences  
<http://science.energy.gov/bes/csgb/about/staff/dr-mark-r-pederson/>

Professor Hrvoje Petek  
University of Pittsburgh  
<http://www.ultrafast.phyast.pitt.edu/Home.html>

Professor Sylwia Ptasinska  
University of Notre Dame  
<http://www3.nd.edu/~sptasins/>

Professor Krishnan Raghavachari  
Indiana University  
<http://php.indiana.edu/~krgroup/>

Professor Geraldine L. Richmond  
University of Oregon  
<http://richmondscience.uoregon.edu/>

Dr. James (Jim) Rustad  
DOE/Basic Energy Sciences  
<http://science.energy.gov/bes/csgb/about/staff/dr-james-rustad/>

Professor Sapna Sarupria  
Clemson University  
<http://www.clemson.edu/ces/molecularsimulations/>

Professor Richard Saykally  
Lawrence Berkeley National Laboratory  
<http://www.cchem.berkeley.edu/risgrp/>

Dr. Gregory Schenter  
Pacific Northwest National Laboratory  
[http://www.pnl.gov/science/staff/staff\\_info.asp?staff\\_num=5615](http://www.pnl.gov/science/staff/staff_info.asp?staff_num=5615)

Dr. Robert Schoenlein  
SLAC National Accelerator Laboratory  
<https://ultrafast.stanford.edu/people/robert-schoenlein>

Dr. Viviane Schwartz  
DOE/Basic Energy Sciences  
<http://science.energy.gov/bes/csgb/about/staff/dr-vivian-schwartz/>

Dr. Thomas Settersten  
DOE/Basic Energy Sciences  
<http://science.energy.gov/bes/csgb/about/staff/dr-thomas-settersten/>

Dr. David K. Shuh  
Lawrence Berkeley National Laboratory  
<http://actinide.lbl.gov/gtsc/Staff/dkshuh/>

Dr. Mark Spitler  
DOE/Basic Energy Sciences  
<http://science.energy.gov/bes/csgb/about/staff/dr-mark-spitler/>

Professor Charles Sykes  
Tufts University  
<http://ase.tufts.edu/chemistry/sykes/Sykes%20Lab%20Research%20Group.html>

Professor Ward Thompson  
University of Kansas  
<http://thompsongroup.ku.edu/>

Professor William A. Tisdale  
Massachusetts Institute of Technology  
<http://web.mit.edu/tisdalelab>

Professor Andrei Tokmakoff  
University of Chicago  
<http://tokmakofflab.uchicago.edu/>

Dr. Marat Valiev  
Pacific Northwest National Laboratory  
[http://www.pnl.gov/science/staff/staff\\_info.asp?staff\\_num=8349](http://www.pnl.gov/science/staff/staff_info.asp?staff_num=8349)

Dr. Xue-Bin Wang  
Pacific Northwest National Laboratory  
[http://www.pnl.gov/science/staff/staff\\_info.asp?staff\\_num=7753](http://www.pnl.gov/science/staff/staff_info.asp?staff_num=7753)

Professor Adam Wasserman  
Purdue University  
[https://www.purdue.edu/dft/?attachment\\_id=551](https://www.purdue.edu/dft/?attachment_id=551)

Professor Michael White  
Brookhaven National Laboratory  
<http://www.bnl.gov/chemistry/bio/WhiteMichael.asp>

Dr Philip A Wilk  
DOE/Basic Energy Sciences  
<http://science.energy.gov/bes/csgb/about/staff/dr-philip-a-wilk/>

Dr. Kevin R. Wilson  
Lawrence Berkeley National Laboratory  
<http://wilsonresearchgroup.lbl.gov/home>

Dr. James Wishart  
Brookhaven National Laboratory  
<http://www.chemistry.bnl.gov/SciandTech/PRC/wishart/wishart.html>

Professor Bryan Wong  
University of California, Riverside  
<http://www.bmwong-group.com/>

Dr. Sotiris Xantheas  
Pacific Northwest National Laboratory  
[http://www.pnl.gov/science/staff/staff\\_info.asp?staff\\_num=5610](http://www.pnl.gov/science/staff/staff_info.asp?staff_num=5610)